Dissertation

Adaptive antennas for mobile radio systems using Time Division CDMA and joint detection

deutscher Titel:

Adaptive Antennen für Mobilfunksysteme mit zeitgeschlitztem CDMA und gemeinsamer Detektion der Teilnehmersignale

von
Dipl.–Ing. Apostolos Papathanassiou

Apostolos Papathanassiou
Ionias Str. 7
17121 Nea Smyrni
Griechenland

Adaptive antennas for mobile radio systems using Time Division CDMA and joint detection

deutscher Titel:

Adaptive Antennen für Mobilfunksysteme mit zeitgeschlitztem CDMA und gemeinsamer Detektion der Teilnehmersignale

Beim Fachbereich Elektrotechnik

der Universität Kaiserslautern

zur Verleihung des akademischen Grades

Doktor–Ingenieur (Dr.–Ing.)

eingereichte Dissertation

von

Dipl.–Ing. Apostolos Papathanassiou

D 386

Tag der Einreichung:	20. Januar 2000
Tag der mündlichen Prüfung:	27. Juni 2000
Dekan des Fachbereichs Elektrotechnik:	Prof. Dr.–Ing. N. Wehn
Vorsitzender der Prüfungskommission:	Prof. Dr.–Ing. habil. L. Litz
1. Berichterstatter:	Prof. Dr.–Ing. habil. P.W. Baier
2. Berichterstatter:	Prof. Dr.techn. J.A. Nossek

Vorwort

Die vorliegende Arbeit entstand in der Zeit von Februar 1997 bis Januar 2000 im Rahmen meiner Tätigkeit als wissenschaftlicher Mitarbeiter von Prof. Dr.–Ing. habil. P.W. Baier am Lehrstuhl für hochfrequente Signalübertragung und –verarbeitung der Universität Kaiserslautern. Ich möchte all jenen danken, die mich bei der Entstehung dieser Arbeit unterstützt haben.

Mein besonderer Dank ergeht an Herrn Prof. P.W. Baier für die Anregung, die Betreuung und die Förderung meiner Arbeit. Durch seine stete Diskussionsbereitschaft sowie durch zahlreiche Ratschläge und Hinweise hat er wesentlich zum Gelingen dieser Arbeit beigetragen.

Herrn Prof. Dr.techn. J.A. Nossek danke ich für zahlreiche sehr hilfreiche Hinweise während meiner Tätigkeit, für die kritisch–kooperative Durchsicht der Dissertation – diese führte zu wesentlichen Verbesserungen – und für die Übernahme des Korreferats. Weiterhin danke ich dem Vorsitzenden der Promotionskommission, Herrn Prof. Dr.–Ing. habil. L. Litz.

Besonderer Dank gilt auch den Herren Professoren J.E. Diamessis und T. Koussiouris von der Nationalen Technischen Universität Athen, für die Anregung zum Durchführen eines Promotionsvorhabens in Deutschland.

Bei der Universität Kaiserslutern möchte ich mich für die Möglichkeit der Benutzung leistungsfähiger Rechnersysteme des Regionalen Hochschulrechenzentrums Kaiserslautern (RHRK) bedanken. Den Mitarbeitern des RHRK danke ich auch für die Beratung und die Hilfestellung in Rechnerfragen.

Die in der vorliegenden Arbeit enthaltenen Ergebnisse entstanden größtenteils im Rahmen von Projekten, die durch die Deutsche Forschungsgemeinschaft gefördert wurden, wofür ich mich bedanken möchte. Im Rahmen dieser Förderung entstand auch eine enge Zusammenarbeit zu den Arbeitsgruppen Prof. Dr.techn. J.A. Nosseks, Prof. Dr.–Ing. J. Eberspächers und Prof. Dr.–Ing. J. Hagenauers, alle Technische Universität München, woraus wichtige Anregungen und Hinweise für meine Arbeit resultierten.

Den jetzigen und den ehemaligen Kollegen am Lehrstuhl für hochfrequente Signalübertragung und –verarbeitung danke ich für die angenehme Arbeitsatmosphäre und für viele fruchtbare Diskussionen, die mir oftmals weitergeholfen haben. Ein besonderer Dank ergeht an Herrn Dr.–Ing. J.J. Blanz für die Unterstützung beim Einarbeiten in das TD–CDMA–Konzept mit adaptiven Antennen und für die freundschaftliche Zusammenarbeit in gemeinsamen Projekten. Weiterhin bedanke ich mich herzlich bei Herrn Dipl.–Ing. M. Meurer für die gute Zusammenarbeit am Ende und auch nach meiner Tätigkeit am Lehrstuhl. Meine Anerkennung gebührt auch der Siemens AG, insbesondere Herrn Dr.–Ing. M. Haardt, für viele fruchtbare Diskussionen.

Ein weiterer Dank ergeht an alle Studenten, die im Rahmen von Studien– und Diplomarbeiten unter meiner Anleitung Beiträge zu dieser Arbeit geleistet haben.

Nicht zuletzt möchte ich mich bei meiner Freundin und meinen Geschwistern bedanken, die mir immer ein großer Rückhalt waren. Ganz besonders herzlich bedanke ich mich bei meiner Mutter und meinem Onkel T.E. Agrafiotis. Sie haben mir das Studium der Elektrotechnik ermöglicht und mich immer nach besten Kräften unterstützt. Ihnen ist diese Arbeit gewidmet.

Kaiserslautern, im August 2000 Apostolos Papathanassiou

Contents

1 Introduction

1.1 Adaptive antennas for mobile radio systems

Due to the constantly increasing demand for mobile radio services, the existing second generation (2G) mobile radio systems will not meet the requirement for increased capacity in the near future [Bai94, Bai96a, Bai96c, ASS98, NTD98]. Moreover, advanced services like multimedia applications, which require higher data rates and higher transmission qualities than voice services mostly offered by 2G mobile radio systems, and flexibility concerning the data rates and the transmission qualities, e.g., coexistence of voice and advanced services, cannot be fulfilled by the existing 2G mobile radio systems [Bai96c, ASS98, NTD98]. Therefore, in the last decade worldwide research activities have aimed at the design and standardization of third generation (3G) mobile radio systems, which, in addition to fulfilling the requirement of capacity, advanced services and flexibility concerning the data rates and the transmission qualities, should also attain a more efficient bandwidth utilization than 2G mobile radio systems [NTD98, Bla98].

In Europe the work towards the third generation standard UMTS (Universal Mobile Telecommunications System) is led by ETSI (European Telecommunications Standards Institute) and has already reached a decision concerning the standard of the multiple access air interface [NTD98], which is one of the most important issues when developing a mobile radio system [Bai96c, Bai96b]. This air interface standard is termed UTRA (UMTS Terrestrial Radio Access) and defines different modes for the duplexing scheme TDD (Time Division Duplex) to be applied in the unpaired UMTS bands, and for the duplexing scheme FDD (Frequency Division Duplex) to be applied in the paired UMTS bands [NTD98]. In the TDD band the multiple access scheme TD–CDMA (Time Division Code Division Multiple Access) and in the FDD band the multiple access scheme W–CDMA (Wideband CDMA) will be applied. The worldwide standardization activities towards a global wideband mobile communications system are directed by ITU (International Telecommunications Union) with the goal of a worldwide 3G mobile radio air interface standard termed IMT–2000 (International Mobile Telecommunications 2000) [ITU97]. The work towards IMT–2000 is substantially supported by the third generation partnership project (3GPP), in which organizational partners, e.g., ETSI, and market representation partners, e.g., UMTS Forum, from all over the world co–operate for the production of technical specifications for a 3G mobile radio system [3GPP]. This system should be based on the evolved core networks of the successful GSM (Global System for Mobile Communications) [MP92, PGH95] and the radio access technologies supported by the organizational partners [3GPP].

Although 3G mobile radio systems will cope with the requirements of high data rates up to 2 Mbit/s, flexibility concerning the data rates and the transmission qualities, and efficient bandwidth utilization [Bai96a, BK95, ASS98, NTD98], they will not fulfill the requirement for capacity, if they exclusively use single antennas [Rap98, BBP97, BBS97, God97a,

God97b] and state of the art equalization and coding techniques [NTD98, ASS98, ITU97]. Therefore, the achievement of increased capacity for 3G mobile radio systems is the subject of worldwide research and standardization activities at present [BBS97, God97a, God97b].

Among the techniques developed for increasing the capacity of 3G mobile radio systems, adaptive antenna concepts are regarded as the most promising candidate [Rap98, God97a, FN94a]. Moreover, adaptive antennas may be incorporated in the existing 2G mobile radio systems, e.g., GSM, for increasing their capacity [God97a, FN94a]. Independently of the target mobile radio system, two different approaches to an adaptive – also called smart or intelligent – antenna may be followed:

- According to the first approach, an adaptive antenna consists of a certain multi–antenna arrangement, e.g., a centro–symmetric array configuration [XRK94, Haa97a], and means for processing the output signals of the antenna elements. This signal processing is performed only in the spatial domain. This means that a signal processing in the temporal domain follows which is applied independently of the spatial signal processing. This approach is, e.g., followed, when the multiple access scheme SDMA (Space Division Multiple Access) is used [FN94a].
- According to the second approach, the adaptive antenna cannot be viewed as a separate unit of the receiver. The signals of the antenna elements of the used multi–antenna arrangement are processed jointly in the temporal and spatial domain. Therefore, the adaptive antenna is considered to be integrated into the receiver. This approach is, e.g., followed, when the multiple access scheme TD–CDMA is used [BBS97, PFBP99].

Therefore, adaptive antennas are more challenging when the second of said approaches is employed, i.e., when the signals are processed jointly in the temporal and spatial domain.

However, regardless of the followed approach, adaptive antennas have gained a considerable worldwide research interest in the last years, since their implementation will enable the required increased system capacity [God97a, Gia99]

- without consuming additional bandwidth, and
- without posing the need for completely new systems, because their implementation goes along only with modifications of the existing mobile radio systems.

Therefore, the incorporation of adaptive antenna concepts into base stations (BSs) is thought to be a promising solution for system capacity increase of the existing 2G and the future 3G mobile radio systems [God97a, God97b, Gia99, FN94a, BBS97].

The general benefits offered by adaptive antennas are discussed in the following. These benefits are relatively independent of the target mobile radio system [God97a, Rap98]. Only the amount of system performance improvement and capacity increase achieved by adaptive antenna concepts is considered to depend on the target system, and not the general benefits briefly analyzed in the following. These benefits have been intensively studied worldwide and can be classified into the categories listed below. According to [God97a, Gia99], adaptive antennas

- increase the capacity of mobile radio systems by
  - reducing interference due to selective reception and transmission, thus allowing frequencies to be reused more often and
  - mitigating the effects of multipath reception caused by the mobile radio propagation properties,
- increase the BS coverage without increasing the total radiated power, which leads to a sparser infrastructure, thus compensating for the increased cost of the additional hardware required for the BSs,
- are able to locate users in a cellular network, e.g., for emergency services,
- allow the use of dynamic channel assignment schemes which explicitly take advantage of the directional characteristics of user signals impinging at the BSs, and
- do not require modifications of
  - the number of BSs,
  - the multiple access method,
  - the subscriber handsets, and
  - the modulation scheme,

  since only the signal processing at the existing BSs has to be adapted [BBS97, BPH00].

It is noted that the last one of the above categories is an important issue concerning the incorporation of adaptive antennas into the existing 2G mobile radio systems [God97a, God97b, FN94a, Pen99].

As mentioned above, the degree of performance improvement achieved by adaptive antenna concepts generally depends on the target mobile radio system. In addition to this dependence, the benefits of adaptive antennas depend on the [God97a, God97b, Gia99, BBS97, BPW99]

- duplexing scheme, i.e., TDD or FDD,

- amount of multipath–induced angular and delay spread of the mobile radio propagation environment,
- Doppler spread,
- power level of co–channel interference,
- spatial separation of co–channel users,
- near–far effect,
- type of antenna configuration used at the BS,
- equalization algorithm, and
- channel estimation techniques.

Finally, one of the main points when dealing with adaptive antenna concepts is the method used for adapting the system behaviour to the instantaneous spatial scenario [God97a, God97b]. In general, this method relies on the use of training sequences in the signal format, or the adaptation of the antenna pattern is performed blindly.

After having discussed the concept of adaptive antennas for mobile radio systems in this section, before jumping into the state of the art on adaptive antennas and the open questions solved by the present thesis, the TD–CDMA mobile radio system, which is the target mobile radio system of the thesis, is briefly described in the following section.

1.2 Time Division CDMA (TD–CDMA)

In the late 1980ies investigations towards novel air interfaces for 3G mobile radio systems began. In the mobile radio air interface considered in this thesis, the combination of the multiple access methods FDMA (Frequency Division Multiple Access) and TDMA (Time Division Multiple Access) known from GSM [MP92, PGH95] is supplemented by a CDMA component [Bai94, BK95, KBJ95, KB93, BKNS94b]. The TD–CDMA air interface concept has been verified by extensive computer simulations [BBNS94, BKNS94b, BJN94, SB96, Kle96] and by field tests performed with a TD–CDMA hardware demonstrator [MSW97b, BEM98a, BEM98b].

TD–CDMA is a time–slotted CDMA mobile radio air interface. In the same frequency band and time slot, the latter termed also burst, K mobile users are active, each using a user specific spreading code, which allows signal separation at the receiver [Naß95, Kle96]. The well–known frame structure of this time-slotted CDMA concept is illustrated in Fig. 1.1, where B, T_{fr}, N_{fr}, and T_{bu} denote the bandwidth of a frequency band, the duration of a TDMA frame, the number of bursts per TDMA frame, and the burst duration, respectively. As shown in Fig. 1.1, the signal transmission in TD–CDMA takes place in bursts. Each burst of user k, $k = 1 \ldots K$, consists of

- two data sections (blocks),
- a user specific midamble inserted between these data sections, which allows channel estimation at the receivers [SK93, Ste95], and
- a guard interval to prevent subsequently transmitted bursts from overlapping at the receiver [BKNS94b].

Each data block of a TDMA burst contains N symbols for each user k, $k = 1 \dots K$, and each symbol is spread by a user specific CDMA code, which is Q chips long, see Fig. 1.2. The midamble and the guard interval contain L_{m} and L_{g} chips, respectively, see Fig. 1.2. The adopted frame and burst structure of TD–CDMA is similar to that used in GSM. This is due to the fact that TD–CDMA has been historically developed as an evolution of GSM by introducing a supplementary CDMA component [BJK96, Bai96a, Bai96c]. Thus, TD–CDMA beneficially facilitates backward compatibility with GSM, which is the de facto world standard of 2G mobile radio systems [Bai94, BK95].

In this thesis the acronym TD–CDMA is used for an air interface concept of a cellular mobile radio system, although in the standardization this acronym is used for an entire system concept. The reliability and the transmission quality of TD–CDMA are determined by the multiple access interference (MAI), i.e., TD–CDMA is interference limited [Cal88, Lee82, Lee89]. The influence of the MAI depends on, among other parameters, the data detection principle. In TD–CDMA the intracell MAI, i.e., the interference from other users assigned to the same BS, is eliminated by the joint detection (JD) algorithm [KB92b, Kle96] at the receivers. Therefore, in contrast to the situation in other CDMA mobile radio systems, e.g., W–CDMA, the intercell MAI, i.e., the interference from users of other cells, plays the most important role on the transmission quality and the reliability of the system. Moreover, in TD–CDMA channel estimation is performed jointly for all users assigned to the same BS and is based on the midamble training sequence inserted in each transmitted burst, see Figs. 1.1 and 1.2 [SK93, Ste95, Naß95, Bla98]. It is noted that joint data detection and joint channel estimation constitute the main characteristics of TD–CDMA receivers.

For single antenna systems, the most important contributions to TD–CDMA from the Research Group for RF Communications, University of Kaiserslautern, are listed in Table 1.1. These contributions cover a very wide spectrum of research activities for TD–CDMA prior to the system standardization [NTD98] and include

- early works on CDMA for 3G mobile radio systems,
- the comprehensive description of the TD–CDMA mobile radio air interface concept,
- the JD principle,
- benefits of JD for CDMA systems,

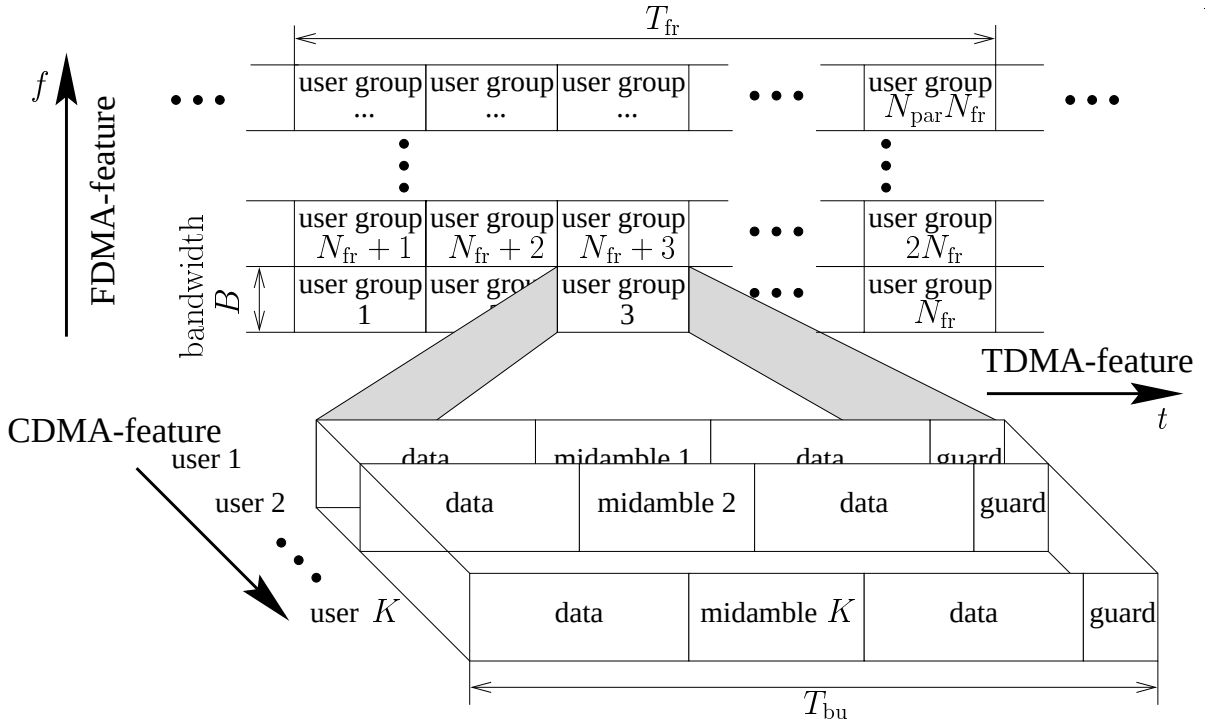

Figure 1.1. Frame and burst structure of TD–CDMA [BHP97, Bla98]

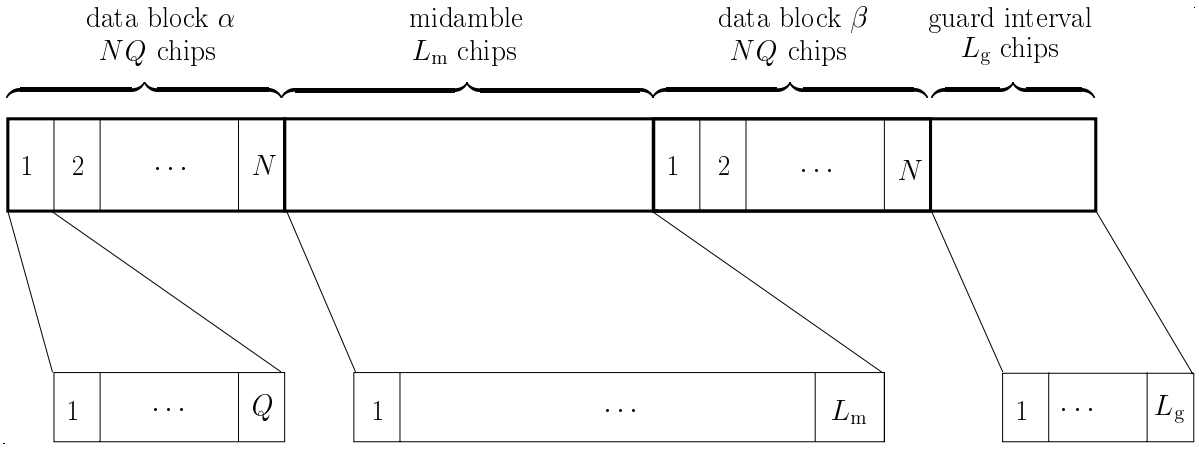

Figure 1.2. Detailed burst structure of TD–CDMA [Naß95, Ste95, Ste96, Bla98]

Table 1.1. Contributions on TD–CDMA with single antennas from the Research Group for RF Communications, University of Kaiserslautern

reference	remarks
[BK91], [Bai94], [BK95], [BJK96]	CDMA for 3G systems
[KB92b], [KB93], [KB92a], [Kle96], [KKB94], [KKB93]	joint data detection principle
[KBJ95], [Naß95], [Kle96]	comprehensive description of the TD–CDMA air interface concept
[BN93]	benefits of JD for CDMA systems
[SK93], [Ste95]	channel estimation
[BBNS94], [BKNS94b], [BJN94], [Naß95]	performance evaluations by realistic simulations
[BKNS94a], [BKNS94c], [SB96]	spectrum efficiency and capacity
[Ste97], [Ste96]	statistics of the C/I
[MSW97a], [MSW98]	protocol and signaling aspects
[MSW97b], [BEM98a], [BEM98b]	realtime hardware feasibility

- the system performance evaluated by realistic simulations,
- the spectrum efficiency and capacity of TD–CDMA,
- statistics of the carrier–to–interference (C/I) ratio,
- protocol and signaling aspects, and
- realtime hardware implementation.

Topics concerning the use of multi–antenna arrangements, including adaptive antennas, in TD–CDMA are considered in detail in the following Section 1.3.

As mentioned in Section 1.1, TD–CDMA forms part of the 3G mobile radio air interface standard for UMTS adopted by ETSI. Moreover, TD–CDMA is intensively studied within the standardization activities of the 3GPP [3GPP], which support the works towards IMT–2000. Since the standardization process has not been finished yet, there is intensive research worldwide concerning the choice of the final parameters of TD–CDMA and, additionally, topics connected with the incorporation of advanced techniques such as adaptive antenna concepts. This fact constitutes the most important motivation for dealing with TD–CDMA, which is an important air interface concept for future mobile radio systems.

1.3 State of the art and open questions

The research field of adaptive antennas has gained a remarkable interest in the last decade, since it has become clear that adaptive antennas will significantly assist the achievement of high user capacity in future wireless communications systems [God97a, Gia99]. In this section, a general view on the state of the art concerning adaptive antenna concepts is provided. It is stressed that this general view aims at demonstrating the importance and the worldwide research interest for adaptive antennas. However, only part of the issues considered in this general view are relevant for the present thesis. The relevant issues for the thesis are explicitely stated in the final part of this section. In this final part, based on the state of the art of adaptive antennas, the open questions treated in the thesis are described in detail.

First, systems other than TD–CDMA are discussed. In what follows, TD–CDMA, which is the mobile radio air interface investigated in the thesis, is considered in detail.

The research activities on adaptive antennas deal with a variety of issues [God97a, God97b]. In order to provide a general view on the state of the art concerning adaptive antennas, the research activities are divided into the following categories:

I: Early works on adaptive antennas,
II: TDMA systems,
III: CDMA systems,
IV: Channel modeling for systems with adaptive antennas,
V: DOA (Direction–Of–Arrival) estimation algorithms,
VI: Influence of errors and perturbations.

In Part I and Part II of Table 1.2 the most important contributions to each category are listed. Category I deals with the first techniques developed for adaptive antennas. Based on these techniques, the research field of adaptive antennas has remarkably expanded in the last decade. As already mentioned in Section 1.1, one of the most important characteristics of adaptive antennas is that they can be integrated into a variety of mobile radio systems mainly distinguished by the multiple access scheme they use. Categories II and III provide a summary of the research activities on adaptive antennas for TDMA and CDMA systems, respectively. In most of the activities of Categories II and III the performance of systems with adaptive antennas is assessed using computer–aided engineering methods like computer simulations. However, the simulation of systems with adaptive antennas requires a profound knowledge of the properties of the mobile radio propagation including its directional characteristics [BBS97, FL96]. Hence, in the last decade extensive worldwide research activities aimed at gaining more insight into the mobile radio propagation in systems utilizing adaptive antennas. Category IV summarizes the most important works on the state of the art of channel modeling including directional information and the channel sounding campaigns which have been useful for the parametrization of the established channel models. Further, because of the importance of

DOA estimation algorithms for adaptive antenna concepts and their independence from the employed multiple access method, a separate category, Category V, on this area is provided. It is noted that the contributions of Categories I to V assume ideal conditions for the used antenna arrays. Unfortunately, these ideal conditions are not met in practice [God97b]. Therefore, research activities aimed at investigating the influence of real world conditions on the performance of systems with adaptive antennas. The most important contributions in this field are listed in Category VI. Before proceeding with a more detailed discussion of the research activities related to each category, it is mentioned that there are numerous other contributions in each category which are not listed in Table 1.2. Thus, the contributions of Table 1.2 should be considered only as a representative reference list for adaptive antennas, illustrating the present state of the art.

The origins of adaptive antennas can be traced back to the research activities on digital signal processing in the 1960ies. Adaptive receiver antennas were formed by combining the output signals of the antenna elements with time varying filters [Rap98]. The papers of Adams [Ada66] and Widrow et al. [WMGG67] are representative of the introductory works made on adaptive antennas, see Category I of Table 1.2. Adams developed an adaptive processor based on maximizing the signal–to–noise ratio (SNR) at its output. This processor can be used in communications systems [MM80]. In [WMGG67] adaptive array configurations were proposed for narrowband and broadband signals. The antenna weights are adjusted by a relatively simple technique based on the least–mean–squares (LMS) algorithm, and the adaptive spatial filtering capability of the developed configurations was illustrated by the results of computer simulations [WMGG67]. The later papers of Gabriel [Gab76] and Applebaum [App76] involve more complex mathematics and illustrate the capability of adaptive arrays for sidelobe cancellation and high–resolution spectral estimation. The early research activities on adaptive antennas are summarized in a tutorial manner in [SIT64] and [SIT76].

In Category II of Table 1.2 the most important contributions on adaptive antennas for TDMA systems are mentioned. These contributions are divided into such on general aspects on adaptive antennas, see Category IIa of Table 1.2, and such on the adaptive antenna algorithms developed for TDMA mobile radio systems, see Category IIb. In [Tan94] a three–step strategy towards the introduction of adaptive antennas in TDMA systems is proposed. The three steps are: Spatial filtering at the uplink only (SFU), spatial filtering for interference reduction (SFIR), and space division multiple access (SDMA). The multiple access method SDMA and its advantages are also presented in detail in [FN94a, FN97a, Far97, Pen99] and [GR94]. Special topics in SDMA like dynamic channel allocation schemes, the spatial separation potential of adaptive antennas, and methods for maximizing the capacity in SDMA are presented in [Har97, GT95, FN96b, FN96a, FN97b]. It is noted that in [Tan94] a significant capacity increase is claimed for TDMA systems applying the SDMA principle compared to single antenna systems. This increase is in the order of $\sqrt{K_{\mathrm{a}}K}$, where K_{a} is the number of antenna elements used at the BS and K is the number of simultaneously active users within the same frequency band and time slot. Further, an overview of adaptive antenna technology is given in [BBA95], and network

Table 1.2. Contributions on adaptive antennas, Part I

category	reference	remarks
I	[Ada66], [WMGG67]	- introduction to adaptive antennas - array configurations for broadband and narrowband signals
	[Gab76], [App76]	capability of sidelobe cancellation and spectral estimation
	[SIT64], [SIT76]	summary of early research activities on adaptive antennas
IIa	[Tan94]	three–step strategy towards adaptive antennas
	[FN94a], [FN97a], [GR94]	advantages of SDMA
	[Har97], [GT95], [FN96b], [FN96a], [FN97b]	special topics associated with SDMA
	[BBA95]	overview of adaptive antenna technology
	[RTVW95]	network aspects in systems with adaptive antennas
IIb	[Fuh97], [Hay91], [Hsu82]	- classification of algorithms for adaptive antennas - TR algorithms based on training sequences: DMI, LS, RLS, SQRLS
	[May93], [MDCM95], [VTP97], [TVP96], [DLDMV96], [MJ96]	blind TR algorithms: CMA, algorithms based on FA and HOS
IIIa	[Vit95], [SOSL85], [ASS98], [TBM97]	design concept and coherent RAKE combining
	[Koh94], [IK96]	joint spatial and temporal signal processing
	[TGM96], [ZS96], [GTB98]	algorithms for adaptive antennas
	[KIH83], [PH94], [KA97], [KA98]	IC techniques
IIIb	[RZ96], [RZ97]	blind space–time RAKE receiver
	[LZ97], [TX97]	blind equalization and channel estimation in CDMA
	[VTP97], [RRPR97]	comparison of different algorithms

aspects in systems with adaptive antennas are covered in [RTVW95].

In Category IIb of Table 1.2 the main contributions concerning the variety of adaptive antenna algorithms for TDMA systems are given. According to [Fuh97] these algorithms

Table 1.2. Contributions on adaptive antennas, Part II

category	reference	remarks
IV	[Hat80], [UHF90], [KCW93a], [Loe92]	propagation prediction models
	[COS89], [BBJ95], [MG96], [Fuh97], [SP97], [SP98b]	models generating channel impulse responses
	[Egg94], [KMT96], [MG96], [FTH99]	channel sounding campaigns useful for the parametrization of channel models
V	[Sch79], [KT82], [KT83], [EJS81]	DOA estimation algorithms originally developed for radar and sonar applications
	[AMVW91], [GR94], [FHNP95], [KS95]	possibility of using DOA estimation algorithms in mobile communications
	[Sch79], [Sch86], [Cap69], [ZW88], [Bur67], [Tho80]	SE algorithms, e.g., MUSIC
	[RK89], [HN95], [Haa97a], [PK89], [VOD92], [VVP97]	PSBE algorithms, e.g., ESPRIT
	[DLR77], [FW88] [FDHT96], [PFM94], [THT98], [FTH99]	DPE algorithms, e.g., SAGE
	[And63], [Sch78], [Aka66], [Ris78], [WK85], [XRK94]	model order estimation
VI	[God97b], [Pen99] [Ste76], [Nit79] [CZO88],	influence of errors and perturbations on adaptive antennas
	[AS84], [DM80], [RS87a], [RS87b], [PN97], [PN98]	array calibration methods
	[KP85], [CZO87], [YU93]	robust beamforming techniques

can be classified into time reference (TR) algorithms, i.e., algorithms which do not explicitely estimate the DOAs of impinging signals, and spatial reference (SR) algorithms, which explicitely determine the DOAs. The class of TR algorithms is further divided into [Fuh97]

- algorithms needing a training sequence for adaptation, and

- blind algorithms which do not rely on training sequences.

One of the most important algorithms relying on training sequences is the DMI (Direct Matrix Inversion) algorithm, which is the generalization of the Wiener filter in the spatial and temporal domain [Hay91]. Other representative algorithms of this class are the LS (Least Squares) [Hay91], the RLS (Recursive Least Squares) [Hay91], and the SQRLS (Square–Root RLS) [Hsu82] algorithms, which exhibit comparable performance in both settling time and output SNR performance [Fuh97]. Concerning the most important blind TR algorithms, which do not rely on training sequences for adapting to the spatial scenario, these algorithms can be classified into algorithms making use of [VTP97]

- the structure of the system matrix, i.e., the matrix formed by the outputs of all antenna elements at different time instances, and
- the signal modulation structure.

In systems with adaptive antennas the system matrix can be factorized into a matrix which depends on the propagation properties of the channel, and a matrix which depends on the transmitted signals [VTP97]. The matrices of this factorization are highly structured: The matrix depending on the channel propagation properties is block Hankel [GvL90], whereas the matrix depending on the transmitted signals is block Toeplitz [GvL90]. Therefore, blind equalization is possible by column or row span methods which aim at finding the unique matrix with the required structural properties [MDCM95, VTP97]. Further, in many wireless systems, the transmitted waveform has a constant modulus (CM), see, e.g., the phase modulated signals in GSM. The CM algorithm (CMA) determines those linear combinations of the antenna outputs which yield signals with the CM property [LT83, May93, TVP96]. Another important structure in digital communications systems is their finite alphabet (FA), see, e.g., BPSK (Binary Phase Shift Keying). As in the CMA, the FA algorithm separates linear combinations of FA signals given a relatively small number of samples [TVP96, Vee97]. Finally, the information about the source distribution makes the signal separation possible by using algebraic methods like the higher–order statistics, which is a relatively new area of research [GM89, DLDMV96, MJ96].

Category III of Table 1.2 deals with adaptive antenna concepts developed for DS–CDMA mobile radio systems. As in TDMA systems, see Category II of Table 1.2, adaptive antenna concepts are categorized for DS–CDMA systems with respect to the use of pilot symbols in the signal format. The most important contributions in the case where pilot symbols are used are shown in Category IIIa, whereas blind CDMA, i.e., CDMA systems which do not use pilot symbols in the signal format, is covered by the contributions listed in Category IIIb. The design concept and the coherent RAKE combining [Vit95, SOSL85, Pro89] applied in W–CDMA are described in detail in [ASS98, TBM97]. The transmitted pilot symbols are associated with each data channel, which makes possible coherent detection in

the uplink [ASS98, TSA97]. The more general approach of joint spatial and temporal signal processing for cellular DS–CDMA mobile radio systems is presented in [Koh94, IK96]. Further, a number of algorithms for DS–CDMA and their performance evaluation are analyzed in detail in [TGM96, ZS96, GTB98]. Finally, interference cancellation (IC) schemes are treated in [KIH83, PH94, KA97, KA98].

Concerning blind CDMA, the most important contributions are listed in Category IIIb. Methods for blind equalization in DS–CDMA with adaptive antennas have gained importance in the last years and, as for the TDMA systems, see Category IIb, these methods take advantage of the structural properties of the system matrix. First works in this area are presented in [NPK94, KPK94], whereas [RZ96, RZ97] deal in detail with the space–time RAKE receiver. Blind equalization and channel estimation techniques for cellular DS–CDMA can be found in [LZ97] and [TX97], respectively. Further, a generalization of the subspace method used in TDMA systems to blind space–time signal processing for CDMA can be found in [VTP97]. Finally, a detailed comparison of the different algorithms for adaptive antennas in blind CDMA systems is reported in [RRPR97].

Category IV deals with the worldwide research activities which have aimed at modeling the mobile radio channel including its directional characteristics [FL96, BBJ95, BKM96, FDHT96, Fuh97, KM96, MG96]. These activities were accompanied and supported by channel sounding campaigns [Egg94, KMT96, MG96, FTH99], the results of which were useful for the parametrization of the established channel models. The established channel models can be divided into two general categories:

- Models for propagation prediction, and
- models generating channel impulse responses, which retain the properties of the mobile radio channel.

Propagation prediction models aim at the development of models which provide an accurate estimate of the mean received power or path loss (PL) based on geographical information about the propagation environment [FL96]. These models are very helpful for mobile radio service providers for planning their networks, because they allow optimization of the cell coverage while minimizing interference effects [FL96]. Within this category three model classes can be identified: Empirical, deterministic, and semi–deterministic models [FL96]. Empirical models consist of diagrams or equations for PL calculation which are obtained from statistical analysis of a large number of measurements. Such models are the Hata empirical model [Hat80] and the COST 231–Hata Model [UHF90]. Deterministic models are established by two approaches. First, a PL equation is provided which is derived based on an idealized environment, retaining some basic features of the physical one in order to make a theoretical treatment possible [FL96]. Such models can be found in [BH94, LWK92]. Second, geographical information about the investigated site supplied by means of digital maps is exploited to predict the dominant propagation paths

and their loss. Some of the models of this kind can be found in [KCW93a, LK94]. Finally, semi–deterministic models result from an empirical modification of deterministic models to improve the agreement with measurements [FL96]. The most well–known model of this class is the COST 231–Walfish–Ikegami semi–deterministic model [Loe92, FL96].

The second category of channel models aim at the generation of channel impulse responses which retain the properties of the mobile radio channel including its directional characteristics [FL96, BBS97]. These channel models describe the small–scale variations of the mobile radio channel [Par92, FL96]. Further, they can be rather easily modified to include the large–scale variations as well [Par92, FL96]. The models of this category can be divided into two classes:

- Algorithmic channel models, and
- geometry-based channel models.

In algorithmic channel models, the mobile radio channel can be represented by tapped delay line arrangements [BBS97]. The well–known COST 207 channel models [COS89] belong to the class of algorithmic channel models. In geometry-based channel models, the model of the wave propagation in the real world mobile radio channel is based on geographical, topographical and morphological data of the considered scenario [KCW93b, BBJ95, Fuh97, MG96]. Such models are the UKL (University of Kaiserslautern) directional channel models presented in [BBJ95, Bla98]. In spite of the advantages offered by the UKL directional channel models, they require an enormous expense of simulation time [Fuh97, SP97, SP98b], and they do not allow the simulation of the movement of an MS (mobile station) within a mobile radio scenario [SP97, SP98b]. These drawbacks of the UKL directional channel models are overcome by the UKL 2 directional channel models [SP97, SP98b] and the moving scatterer models presented in [Fuh97]. These models, on the one hand, considerably reduce the simulation time, and, on the other hand, incorporate methods for simulating the movement of an MS in a scenario. However, a parametrization of the UKL 2 directional channel models is not available, which is a fundamental requirement for investigating adaptive antenna concepts. As a final observation, by using directional channel models the investigation of adaptive antennas in different propagation environments has already been reported in a number of publications, see [Fuh97, Bla98]. However, the specific similarities [BBJ95, Fuh97, Bla98] among the different channel models have not been studied in depth yet.

In Category V of Table 1.2 the most important contributions concerning the important area of DOA estimation techniques are listed. The concept of DOA estimation is independent of the utilized multiple access scheme. It depends only on the presuppositions made for the spatial position of the used antenna elements. DOA estimation algorithms have been originally developed for radar and sonar applications [Sch79, KT82, KT83, EJS81]. The possibility of using DOA estimation algorithms in mobile communications has been

shown in [AMVW91, GR94, FHNP95, KS95]. According to [KV96, FTH99] the DOA estimation algorithms for mobile radio communications can be grouped into three categories:

- Spectral estimation (SE) algorithms,
- parametric subspace–based estimation (PSBE) algorithms, and
- deterministic parametric estimation (DPE) algorithms.

SE algorithms, e.g., MUSIC (MUltiple SIgnal Classification) [Sch79, Sch86], maximum–likelihood (ML) methods [Cap69, ZW88, SS90, WWR94], and the maximum entropy (ME) method of Burg [Bur67, Tho80], were developed for estimating frequencies and, although they have many performance and implementation advantages, they are connected with

- a very high computational cost for searching over the entire parameter space,
- increased storage requirements for the array calibration data, and
- poor separation capability for wavefronts impinging from not significantly separated DOAs.

PSBE algorithms overcome the problem of computational complexity by imposing a constraint on the array structure, e.g., pairwise identical antenna configurations for ESPRIT (Estimation of Signal Parameters via Rotational Invariance Techniques) [RK89] or centro–symmetric array configurations for 1D (one dimensional) and 2D (two dimensional) Unitary ESPRIT [HN95, HZMN95, Haa97a]. Unitary ESPRIT is one of the most important algorithms of this group because it significantly reduces the computational cost compared to the ESPRIT algorithm, since it can be formulated throughout in real computations [HN95, HZMN95]. Further, Unitary ESPRIT offers an increased estimation accuracy by inherently incorporating FBA (Forward–Backward Averaging), which practically doubles the number of available samples, and high resolution capability by spatial smoothing techniques [Haa97a, PK89]. Moreover, the 2D Unitary ESPRIT algorithm is capable of simultaneous azimuth and elevation estimation, which is an important topic in current research studies for mobile radio [Haa97a, ZHM96, PFBP99]. Other subspace–based estimation techniques for jointly estimating azimuth and elevation or azimuth and time delay are presented in [VOD92, VVP97], and they are especially important for blind deterministic beamforming in mobile radio communications [VTP97].

DPE algorithms are the third group of DOA estimation algorithms, and they are based on joint ML vector parameter estimation. The expectation–maximization (EM) algorithm reduces the computational cost of joint ML by implementing K_{d} separate maximization procedures, where K_{d} is the number of plane waves impinging at the antenna array [DLR77, FW88]. The SAGE (Space–Altering Generalized Expectation–maximization)

algorithm replaces the high–dimensional optimization procedure for computing the joint ML parameter estimation by several separate maximization processes performed sequentially [FDHT96, PFM94]. The SAGE algorithm has been successfully applied for joint parameter estimation in real world mobile radio applications, see, e.g., [THT98, FTH99].

One of the most important issues concerning DOA estimation algorithms is the inherent problem of the estimation of the number of DOAs present in the received signal. This problem is the well–known model order estimation problem, which is solved by information theoretic criteria having as their starting point the eigenvalues associated with the signal and the noise subspace [And63, Sch78]. Among the algorithms estimating the number of DOAs, the AIC (Akaike Information Criterion) [Aka66] and the MDL (Minimum Description Length) criterion [Ris78] are the most well–known. The application of these algorithms to realistic wireless communications scenarios has been investigated in [WK85]. In [XRK94] the AIC and the MDL criterion have been modified to include the information about the array configuration used at the receiver.

The contributions on adaptive antennas for mobile radio of Categories I to V assume that the used antenna configurations are free from errors and perturbations. In real systems, though, these ideal conditions are practically not met and the system performance is influenced by the amount the real conditions deviate from the ideal ones [God97a]. Important contributions from this research area are listed in Category VI of Table 1.2. The most important types of errors include [God97b, Pen99, Ste76, Nit79, CZO88]

- deviation in the plane wave assumption,
- uncertainty in the positions and the characteristics of the array elements,
- interelement radiation coupling effects,
- non–linearities of the amplifiers,
- computational errors caused by finite–precision arithmetic,
- errors in adaptive weights, and
- errors in phase and amplitude.

The position of the array elements is determined by calibration processes, which require either auxiliary sources in known locations [AS84, DM80] or only sources in unknown locations [RS87a, RS87b]. Recently developed methods of array calibration designed for mobile radio communications are presented in [PN97, PN98]. Finally, various general schemes have been proposed to overcome parameter errors and perturbations in systems with adaptive antennas. Some of these schemes, known as robust beamforming techniques, may be found in [KP85, CZO87, YU93].

As already mentioned at the beginning of this section, the state of the art of adaptive antennas for TD–CDMA is treated separately, since TD–CDMA is the investigated mobile radio system of the thesis. First, the state of the art of the uplink is discussed. Next, the downlink case is considered. Table 1.3 provides a list of the contributions for both the uplink, see Category I of Table 1.3, and the downlink, see Category II of Table 1.3, of TD–CDMA from the Research Group for RF Communications, University of Kaiserslautern.

In [BBS97, Bla98] it is shown that adaptive antennas can realize spatial micro diversity which is a class of antenna diversity techniques. Other classes of antenna diversity techniques are polarization diversity, field component diversity, spatial macro diversity, and directional diversity [BBS97, Bla98]. The first step of the works for TD–CDMA using multi–antenna arrangements at the BS receiver has been the investigation of antenna diversity techniques [BBNS94, BKNS94b, BJN94, BJSB96, Bla98], see Category I Table 1.3. A comprehensive summary of antenna diversity techniques for the TD–CDMA uplink can be found in [BBS97, Bla98].

As already mentioned in Section 1.2 for the single antenna case, data detection in TD–CDMA is performed according to the JD principle [KB92b, Kle96]. In [BBNS94, BKNS94b, Bla98] the JD principle is generalized to include the use of antenna diversity techniques, which are treated in a unified manner with respect to data detection in TD–CDMA. Further, extensive simulation results are presented in [Bla98], which illustrate the improvement of the bit error ratio (BER) performance achieved by antenna diversity techniques in the TD–CDMA uplink. However, a straightforward approach is not followed in [Bla98] for illustrating the benefits of using JD when antenna diversity techniques are applied in TD–CDMA, compared to the use of single antennas. Moreover, the differences between adaptive and single antennas when applying JD are not presented in a tutorial manner, but only by simulation results.

In contrast to data detection in TD–CDMA, channel estimation is not treated in a unified manner in the published literature, see [Bla98], when applying antenna diversity techniques. When applying spatial macro diversity and directional diversity, channel estimation is performed independently for each antenna, by implementing the Steiner estimator [Ste95], which is the state of the art channel estimation technique for TD–CDMA [BPW99]. In contrast to this situation, when applying spatial micro diversity by using adaptive antennas, advanced channel estimation techniques are required for taking advantage of the directional inhomogeneity of the mobile radio channel. Such an advanced channel estimation technique is presented in [BHP97, Bla98], see Category I Table 1.3. Unfortunately, this technique is only appropriate for rural and typical urban propagation environments. This is due to the fact that the model assumptions adopted in [BHP97, Bla98] collapse in environments where the signals impinge at the BS array from an extended spatial range [BARY95, FL96], as, e.g., in dense urban propagation environments. Further, although simulation results are presented in numerous publications, see [Bla98], for the BER performance of TD–CDMA using the channel estimation

Table 1.3. Contributions on antenna diversity techniques, including adaptive antennas, for TD–CDMA from the Research Group for RF Communications, University of Kaiserslautern

category	reference	remarks
I	[BBNS94] [BJN94] [BJSB96] [BBP97] [Bla98]	- spatial macro diversity - directional diversity - JD principle for TD–CDMA using antenna diversity techniques - simulation results of the BER performance
	[BBS97]	- comprehensive summary of antenna diversity techniques for the uplink
	[BHP97] [Bla98]	- channel estimation technique for adaptive antennas appropriate for rural and typical urban propagation environments - simulation results of the BER performance
	[Bla98]	simulation concept for TD–CDMA, including adaptive antennas
	[Bla98] [WPS99] [WP99a]	- determination of the intercell covariance matrix - technique for estimating the intercell covariance matrix
	[BSPJ97] [BBS97] [BBP97]	- spectrum efficiency of TD–CDMA for spatial macro diversity and directional diversity - spectrum efficiency of TD–CDMA for the adaptive antenna concept of [BHP97, Bla98]
II	[SB97b] [SB97a]	- adaptive antennas for the rural propagation environment - simulation results of the C/I
	[BBS97] [SP98a]	- BER performance - spectrum efficiency of TD–CDMA
	[BBS97]	comprehensive summary of antenna diversity techniques for the downlink

technique of [BHP97, Bla98], no simulation results are available for illustrating the performance of channel estimation independently of the BER performance. Moreover, the simulation results of [Bla98] are made under the assumption that the information about the DOAs of signals impinging at the BS array is perfectly known at the receiver. This assumption is certainly an unrealistic one when the realtime application of TD–CDMA is considered. Finally, the exclusive use of 1D array configurations for the simulation results of [BHP97, Bla98] constitutes another drawback, since the use of 2D array configurations achieve a more efficient exploitation of the directional inhomogeneity of the mobile radio channel in real world mobile radio scenarios [Haa97a].

All simulation results presented for antenna diversity techniques in TD–CDMA, see [Bla98],

are produced by using a generalization of the simulation concept developed in [Naß95] for TD–CDMA with single antennas, see Category I of Table 1.3. Although the developed simulation concept for TD–CDMA offers the advantage of rather cost efficient investigations compared to measurements with realtime experimental hardware setups, simulations are still connected with an enormous expense of time and complexity. Moreover, the simulation concept developed in [Naß95, Bla98] is highly inflexible with respect to the use of coding, interleaving, and modulation schemes: If a new coding, interleaving, and modulation scheme has to be investigated, all simulation steps have to be repeated for evaluating the performance of TD–CDMA under the new conditions. No simulation concept for TD–CDMA has been presented which overcomes the shortcomings of enormous expense of time and inflexibility concerning the use of coding, interleaving, and modulation schemes.

A new research area in TD–CDMA with adaptive antennas is the exploitation of the correlation properties of the intercell MAI for improving the system performance, see Category I of Table 1.3. In [Bla98] the theory for determining and using the covariance matrix of the intercell MAI in TD–CDMA is presented. However, in the simulations of [Bla98] the covariance matrix of the intercell MAI is taken into account neither in channel estimation nor in data detection. In [WPS99, WP99a] a technique for estimating the intercell MAI covariance matrix is presented, and simulation results illustrate the benefits of using the intercell MAI covariance matrix when applying JD in TD–CDMA. However, a straightforward approach for investigating the influence of the intercell MAI covariance matrix on the system behaviour is not reported.

Concerning the efficiency of a mobile radio system with respect to the bandwidth utilization and the available resources, its evaluation should be based on widely accepted performance measures such as the spectrum efficiency and the spectrum capacity [HV99, Bla98, May99]. Concerning the investigated TD–CDMA mobile radio system, in [BSPJ97, Bla98] a three–step simulation concept is presented for determining the spectrum efficiency of TD–CDMA, including the use of adaptive antennas. However, the simulations performed by this simulation concept require an enormous simulation time and complexity, since they are based on the simulation concept of [Naß95, Bla98] for determining the BER. Moreover,

- the movement of users within the simulation scenario is not considered, which is a fundamental characteristic of mobile radio systems,
- a perfect knowledge of the DOAs of signals impinging at the BS array is assumed, which is an unrealistic assumption in real world applications of TD–CDMA, and
- the information about the covariance matrix of the intercell MAI is used neither in channel estimation nor in data detection.

Further, a four–step simulation concept for determining the spectrum capacity of TD–CDMA is presented in [May99]. However, this concept does not rely on the spectrum

efficiency of TD–CDMA, which is an undesired result, since the spectrum efficiency and the spectrum capacity are two closely related performance assessment quantities for mobile radio systems [EHV97]. Moreover, the case of adaptive antennas is not considered at all in the results presented in [May99].

Finally, in [SB97b, SB97a, BBS97] adaptive antenna concepts are presented for the TD–CDMA downlink, see Category II of Table 1.3. In [BBS97] a summary of the developed concepts is provided. The research activities of [SB97b, SB97a] aim at illustrating the improvement of the C/I statistics achieved by adaptive antennas, compared to the single antenna case. Further, in [SP98a] simulation results of the BER performance and the spectrum efficiency of TD–CDMA are presented. However, although the differences between the uplink and the downlink in TD–CDMA are explained theoretically in [SP98a], no measure is provided for illustrating in a straightforward manner the performance differences between the two links.

The overview of the state of the art in the field of adaptive antennas has shown that sophisticated concepts have already been developed. However, there are still several open questions associated with adaptive antennas. These open questions are treated in the following of this section with respect to the TD–CDMA air interface. Nevertheless, most of the open questions encountered in this thesis are also connected directly or under slight modification with the use of other CDMA–based mobile radio air interfaces, e.g., IS–95 and W–CDMA, or other TDMA–based mobile radio system concepts, e.g., GSM. Therefore, the open questions considered in the following are generally valid for other CDMA– or TDMA–based mobile radio systems as well.

Setting out from the state of the art of adaptive antennas for TD–CDMA, the open questions are the following:

- When developing adaptive antenna concepts, a major problem is the investigation of their advantages compared to the use of single antennas. This investigation is associated with the directional information of the signals impinging at the BS array, and it should take place in two steps: In a first step, simple directional channel models are required in order to illustrate the advantages offered by adaptive antennas in a straightforward manner. Such models should
  - first, be based on widely accepted channel models for single antenna systems, and
  - second, incorporate the directional information in a simple way, e.g., by using single DOAs for the signals impinging at the BS array.

  By establishing such models, adaptive antennas can be investigated in a tutorial manner and, moreover, upper bounds for the performance of adaptive antennas can be obtained. In a second step, sophisticated directional channel models should be used which reflect the real world in a more realistic way, thus enabling the

determination of the performance degradation of adaptive antennas, compared to the performance of adaptive antennas in the first step. Such models are the UKL 2 directional channel models [SP98b], which are an evolution of the UKL directional channel models presented in [BBJ95]. As already mentioned during the discussion corresponding to Category IV of Table 1.2, in addition to the advantages offered by the UKL directional channel models, the UKL 2 directional channel models allow the simulation of the movement of an MS in a mobile radio scenario, which is desired in simulations of mobile radio systems. Moreover, the UKL 2 directional channel models reduce considerably the simulation time, compared to the UKL directional channel models. However, a parametrization of the UKL 2 directional channel models for different propagation environments, e.g., rural and urban, is still required in order to use these models for investigating adaptive antennas in a TD–CDMA mobile radio system.

- As already mentioned during the discussion of Category IV of Table 1.2, the investigation of adaptive antennas in different propagation environments has been a major research issue [Fuh97, Bla98]. However, when considering the developed channel models with respect to their directional characteristics, there are specific similarities [BBJ95, Fuh97, Bla98] which have not been exploited yet. Therefore, a unified approach for the different channel models with respect to their directional characteristics is needed, which will also enable the unified treatment of these models, when adaptive antennas are investigated.

- Although the JD principle in TD–CDMA with multi–antenna configurations is presented and investigated by simulations, see Table 1.3, the benefits of using multi–antenna configurations with respect to joint data detection still have to be investigated in a tutorial manner. This investigation should be based on well–known solved mathematical problems, and, moreover, it should clearly state the differences between antenna diversity techniques, including adaptive antennas, and single antennas when JD is applied.

- In spite of the development of a channel estimation technique for adaptive antennas [BHP97, Bla98], see also Table 1.3, this technique is not appropriate for propagation environments where the signals impinge at the BS array from an extended spatial range [BARY95, FL96], see also the discussion corresponding to Table 1.3. Therefore, novel channel estimation techniques should be developed, the model assumptions of which are in accordance with the directional characteristics of the signals in the considered environment. Further, despite the similarities among different propagation environments, there is a lack of a unified approach for all propagation environments concerning channel estimation. Moreover, suitable measures have to be developed for evaluating the performance of channel estimation independently from data detection. Finally, two more issues still have to be considered when channel estimation is investigated for TD–CDMA. The first one is the use of 2D array configurations at the BS receiver, which is expected to increase the performance of adaptive antennas. The second issue is the implementation of well–known DOA

estimation algorithms, e.g., Unitary ESPRIT, with the goal to determine the performance degradation of adaptive antennas, compared to the case where the DOAs are assumed to be known at the BS receiver, see [Bla98].

- Although the developed simulation concepts for TD–CDMA offer the advantage of rather cost efficient investigations compared to measurements with realtime experimental hardware setups, simulations still require an enormous expense of time and inflexibility concerning the use of coding, interleaving and modulation schemes, see also the discussion corresponding to Table 1.3. Therefore, novel simulation concepts are required which, on the one hand, offer a considerable reduction of the simulation time and complexity, and, on the other hand, are flexible with respect to the use of coding, interleaving, and modulation schemes. Certainly, such concepts should retain the accuracy of the original simulation concept developed for TD–CDMA [Naß95, Bla98]. Further, other performance assessment methods should be pursued, which not only reduce the simulation time, but also achieve a more straightforward view of the data detection process in TD–CDMA.

- In addition to the open questions concerning channel modeling, data detection and channel estimation in TD–CDMA with adaptive antennas, there are still three open problems which are not directly related to the development of adaptive antennas, but they are also valid for systems with adaptive antennas. These open problems are described separately as follows:

  - If a single antenna is used at the BS, the information about the CDMA codes of all users and the channel impulse responses for the links between each user and the BS antenna are necessary for applying the JD principle [KB92b, Kle96]. In spite of the extensive research activities on JD, the influence of the correlation properties between the used CDMA codes and the channel impulse responses on the system behaviour still have to be investigated. Unfavourable correlation properties between the used CDMA codes and the channel impulse responses are addressed as the code–channel mismatch problem in the following. Suitable quantities for evaluating the influence of the code–channel mismatch problem have to be sought, as well as techniques for solving the problem in realtime implementations. Finally, a generalization to systems with adaptive antennas would be useful for improving the system behaviour.
  - In air interfaces using TDMA, like the TD–CDMA mobile radio air interface, the information about the DOAs of the users to be assigned in a TDMA frame, see Figure 1.1, may be exploited for applying channel assignment strategies, which explicitely incorporate the information about the DOAs. The development of such channel assignment strategies should be pursued, and their influence on the behaviour of TD–CDMA should be investigated.
  - Although the covariance matrix of the intercell MAI has already been used for improving the behaviour of TD–CDMA [WPS99, WP99a, PW99], a method for explaining in a straightforward manner this improvement is not available for TD–CDMA.

- Concerning the spectrum efficiency of TD–CDMA, the three–step simulation method of [BSPJ97, Bla98] is widely accepted. However, this method is connected with an enormous simulation time and complexity. Methods for reducing the simulation time and complexity of the method presented in [BSPJ97, Bla98] should be sought. Further, the simulations for determining the spectrum efficiency of TD–CDMA should
  - consider the movement of users within the simulation scenario,
  - use well–known DOA estimation algorithms for determining the DOAs of signals impinging at the BS array, and
  - incorporate the covariance matrix of the intercell MAI in both channel estimation and data detection, thus improving the system behaviour when adaptive antennas are used.
- Concerning the spectrum capacity of TD–CDMA, a method should be pursued which explicitely considers the spectrum efficiency of the system during the calculation of its spectrum capacity. Based on this method, the spectrum capacity of TD–CDMA has to be determined for the case of both single and adaptive antennas.
- Finally, although the differences between uplink and downlink in TD–CDMA have been stated [SP98a], a suitable method has to be found for investigating these differences in a more straightforward manner. Then, simulation results should be obtained, where the uplink and downlink of TD–CDMA are compared for both single and adaptive antennas at the BS.

In the following section, the structure of the thesis is presented with respect to the open questions described in this section.

1.4 Structure of the thesis

In addition to the introduction, this thesis consists of nine chapters, the contents of which are outlined in this section. The contents of these chapters provide answers to the open questions described in the last part of Section 1.3. It is noted that the analysis performed in Chapters 2 and 3 is valid for both the uplink and downlink of TD–CDMA. Chapters 4 to 8 are devoted to the investigation of adaptive antennas for the uplink, whereas in Chapter 9 adaptive antennas are considered separately for the downlink and compared to the uplink case.

First, Chapter 2 provides a comprehensive theory of the propagation of electromagnetic waves in mobile radio systems including its directional characteristics according to [BBS97]. This theory describes in a tutorial manner the directional characteristics of the mobile radio channel, which constitute the key issue for the application of adaptive antennas in mobile radio. Moreover, the directional characteristics of the mobile radio

channel are the basis for developing directional channel models, which are used in simulations for assessing the performance of systems with adaptive antennas. Therefore, although this theory is not explicitly related to the rest of the chapter, it is presented because it provides the fundamentals for applying adaptive antennas in TD–CDMA. Then, in order to enable the investigation of adaptive antennas by simulations, two directional channel models are considered in Chapter 2:

- First, in order to investigate adaptive antennas in a tutorial manner, and in order to obtain upper bounds for the performance of adaptive antennas in TD–CDMA, simple directional channel models are presented. These models are addressed as the modified COST 207 channel models. The modified COST 207 channel models are based on the widely accepted COST 207 channel models [COS89], and they incorporate the directional inhomogeneity of the mobile radio channel by using single DOAs for the signals impinging at the BS array. Based on the results of channel sounding campaigns [Egg94, KMT96] and the definition of the COST 207 channel models [COS89, Naß95], three different propagation environments are defined within the modified COST 207 channel models: Rural area (RA), typical urban (TU), and bad urban (BU).
- Second, in order to model the real world effects in a realistic way, the UKL 2 directional channel models are described according to [SP97, SP98b]. Then, a parametrization of the UKL 2 directional channel models for different propagation environments is presented. This parametrization is based on the one proposed in [BBJ95, Bla98] for the UKL directional channel models.

The last part of Chapter 2 is devoted to the investigation of the similarities between the different directional channel models. A novel approach is presented which enables the unified treatment of the different directional channel models with respect to their directional characteristics. According to this approach, a general classification of the different directional channel models into the large cell channel type and the small cell channel type is proposed. These channel types enable the unified treatment of data detection and channel estimation in TD–CDMA with adaptive antennas presented in Chapter 4 and Chapter 5, respectively.

As already mentioned during the discussion corresponding to Table 1.3, adaptive antennas realize spatial micro diversity, which forms a class of antenna diversity techniques. Antenna diversity techniques are treated in a unified manner with respect to the application of JD in TD–CDMA. Therefore, in Chapter 3 a brief summary of antenna diversity techniques is provided based on [BBS97]. Further, the different antenna types used for realizing the different antenna diversity techniques are classified according to [BBS97]. During the discussion of the different antenna types, emphasis is laid on the centro–symmetric array configurations, which are used for applying adaptive antennas in mobile radio. The benefits of using the centro–symmetric array configurations with respect to

data detection and channel estimation in TD–CDMA are investigated in depth in Chapter 4 and Chapter 5, respectively.

In Chapter 4 the problem of data detection in TD–CDMA is treated in detail. Based on the system model of the uplink, a novel approach is presented for illustrating the benefits of antenna diversity techniques in TD–CDMA, compared to the use of a single antenna. Then, the data detection algorithms developed for TD–CDMA are briefly summarized, having the goal to explain the rationale for using the zero forcing block linear equalizer (ZF–BLE) [KB92b, Kle96] as the state of the art equalizer in TD–CDMA. Based on the ZF–BLE, a novel view on the JD process is presented, which enables a straightforward approach for investigating the benefits of adaptive antennas in a theoretical manner, compared to the use of single antennas. This investigation is performed for the large cell channel and the small cell channel types introduced in Chapter 2. Further, simulation results are presented for supporting the theoretical analysis. However, the analysis in Chapter 4 is presented under the assumption of perfectly known channel impulse responses at the receiver. Channel estimation is treated separately in the following Chapter 5. Moreover, in the simulations the modified COST 207 channel models, presented in Chapter 2, are used, which model the directional inhomogeneity of the mobile radio channel in a simple way. Therefore, the results obtained in Chapter 4 should be considered as upper bounds for the performance of TD–CDMA with adaptive antennas.

In Chapter 5 the problem of channel estimation in TD–CDMA is considered. First, the Steiner estimator, which is the state of the art channel estimation technique in TD–CDMA with single antennas, and its generalization to the multi–antenna case are briefly described. Then, based on the large cell and the small cell channel type defined in Chapter 2, channel estimation is treated with respect to adaptive antennas. Concerning the large cell channel type, the channel estimation technique presented in [BHP97, Bla98] is revisited by following a novel approach. This approach is closely related to the novel view on antenna diversity techniques with respect to JD, which is presented in Chapter 4. Concerning the small cell channel type, a novel channel estimation technique is presented, which explicitely conforms to the directional characteristics of the impinging signals in this channel type. Furthermore, in order to enable an evaluation of the channel estimation performance independently of the data detection process, a measure is proposed which is appropriate for mobile radio applications. Finally, based on the proposed measure, simulation results are presented which illustrate the performance of channel estimation techniques for adaptive antennas, compared to the Steiner estimator. In contrast to the state of the art for TD–CDMA, the simulations of Chapter 5 are conducted by considering 2D array configurations at the BS receiver, and by using the well–known 2D Unitary ESPRIT algorithm [HZMN95, Haa97a] for DOA estimation.

In Chapter 6 two performance assessment methods for TD–CDMA are presented. Concerning the first method, based on the novel view on the JD process presented in Chapter 4, a novel simulation concept is introduced, which, on the one hand, offers a considerable reduction of the simulation time and complexity, and, on the other hand, is highly flexi-

ble with respect to the used coding, interleaving, and modulation scheme. Moreover, this novel simulation concept retains the accuracy of the original simulation concept developed for TD–CDMA [Naß95, Bla98]. The novel simulation concept is presented in two steps: In a first step, the channel impulse responses are assumed to be perfectly known at the receiver. In a second step, the concept is extended to include the use of estimated channel impulse responses. Concerning the second performance assessment method, based on the SNR degradation of TD–CDMA receivers defined in [SK93, Kle96], a more adequate definition of the SNR degradation is presented, which is useful in two respects:

- First, based on the SNR degradation, a simplified version of the novel simulation concept presented in the first part of this chapter can be obtained, which achieves an additional reduction of the simulation time and complexity, compared to the original simulation concept for TD–CDMA. This simplified version is also presented in Chapter 6.
- Second, this SNR degradation can be used for evaluating the performance of TD–CDMA in a straightforward manner. Such an evaluation is performed, on the one hand, in Chapter 7, where the code–channel mismatch problem and the influence of the correlation properties of the intercell MAI are studied, and, on the other hand, in Chapter 9, when comparing the uplink with the downlink of TD–CDMA.

Next, the novel simulation concept and its simplified version are compared to the original simulation concept developed for TD–CDMA with respect to simulation time and accuracy. Finally, simulation results obtained by the novel simulation concept are presented, which illustrate the influence of different parameters associated with adaptive antennas on the performance of TD–CDMA. It is noted that these simulation results assess the link level performance of TD–CDMA, i.e., the intercell MAI is modeled as additive white Gaussian noise (AWGN). The evaluation of the system level performance of TD–CDMA, i.e., when the intercell MAI is modeled by real users signals coming from the adjacent cells, is performed in Chapter 8 by determining the spectrum efficiency and capacity of TD–CDMA.

Chapter 7 is devoted to three special techniques which are not directly connected with the development of adaptive antenna concepts, but they can be used in systems with adaptive antennas for enhancing their performance. In the first part of the chapter, the code–channel mismatch problem is treated with respect to JD in TD–CDMA. Based on the SNR degradation defined in Chapter 6, the influence of the code–mismatch problem is explained theoretically and illustrated by simulation results for the single antenna case. Further, a novel technique is presented which leads to an improvement of the system behaviour when code–channel mismatch occurs in TD–CDMA with single antennas. In the second part of the chapter, at first the influence of the user spatial separation on the system performance is considered. This influence constitutes the motivation for developing a novel channel assignment strategy, which explicitely uses the DOAs of all users to

be served in a TDMA frame, see Fig. 1.1. This strategy is verified by simulation results, and is compared to the case where the users are assigned randomly to the time slots of a TDMA frame. Finally, the channel assignment strategy is extended to include the consideration of the code–channel mismatch problem in TD–CDMA with adaptive antennas. In the third part of the chapter, an elementary study of the influence of the intercell MAI on a TD–CDMA mobile radio system is presented. This study is based on a simple spatial scenario of the intercell MAI, and aims at illustrating in a straightforward manner the benefits of using the intercell MAI covariance matrix in the data detection process. As a measure for assessing these benefits, the SNR degradation defined in Chapter 6 is utilized.

In Chapter 8 the spectrum efficiency and capacity of TD–CDMA are determined for both single and adaptive antennas. Concerning the spectrum efficiency of TD–CDMA, the basis of the investigations is the three–step simulation method presented in [BSPJ97, Bla98]. This simulation method is briefly described and, then, the modifications concerning its application for the purpose of this thesis are presented. These modifications reduce the simulation time and complexity, while achieving a more realistic representation of the real world. Concerning the reduction of the simulation time and complexity, the UKL 2 directional channel models, see Chapter 2, are used in the second step of the simulation method, whereas the novel simulation concept presented in Chapter 6 is used in the third step of the simulation method. Concerning the more realistic representation of the real world, the following features are included in the simulations:

- The movement of users within the simulation scenario is considered, since the UKL 2 directional channel models are used in the second step of the simulation method.
- 2D array configurations are used in the third step of the simulation method, when adaptive antennas are investigated.
- The 2D Unitary ESPRIT algorithm is used for estimating the DOAs of signals impinging at the BS array in the third step of the simulation method, when adaptive antennas are investigated.

Moreover, the intercell MAI convariance matrix is used in both channel estimation and data detection, as described in Chapters 5 and 4, respectively. The simulation results for the spectrum efficiency are presented for different operational situations of TD–CDMA, which are defined by the propagation environment, the velocity of the users, and the antenna configuration used at the BS receiver. Concerning the determination of the spectrum capacity of TD–CDMA, based on its definition for mobile radio systems presented in [EHV97, HV99], a novel approach is presented, which explicitely uses the spectrum efficiency of TD–CDMA while calculating its spectrum capacity. Then, the spectrum capacity of TD–CDMA is evaluated for the respective operation situations investigated for the spectrum efficiency, thus enabling a unified treatment of the system level performance of TD–CDMA.

As already mentioned at the beginning of this section, the analyses in Chapters 4 to 8 consider the TD–CDMA uplink. In Chapter 9, the system model of the downlink is briefly described for both single antennas and antenna diversity techniques. In order to enable a straightforward approach for comparing the performance between the uplink and the downlink of TD–CDMA, a novel measure is presented, which is based on the SNR degradation of TD–CDMA receivers defined in Chapter 6. According to this measure, extensive simulation results are presented for illustrating the performance differences between the uplink and the downlink of TD–CDMA mobile radio systems.

Finally, Chapter 10 summarizes the results of Chapters 2 to 8 in English and German and concludes the thesis.

2 Directional mobile radio channels

2.1 Introduction

In Chapter 1 an introduction into the application of adaptive antennas in mobile radio communications is provided. As stated in Chapter 1, the design of systems with adaptive antennas can be considerably supported by computer simulations, which require a profound knowledge of the properties of the mobile radio channel including its directional characteristics [BBS97]. In this chapter, the properties of the mobile radio channel in systems with adaptive antennas are described according to [BBS97]. Although this theory is not explicitly related to the rest of the chapter, it is presented because it provides the fundamentals for applying adaptive antennas in TD–CDMA. Then, the directional channel models used throughout this thesis are considered. Finally, a novel unified approach for treating the different mobile radio propagation environments is presented. This approach is very useful when the benefits of adaptive antennas are investigated, especially when the problem of channel estimation is considered. The benefits of adaptive antennas using the channel models presented in this chapter are illustrated theoretically and by computer simulation results in Chapter 4 to 6.

2.2 Theory of the mobile radio propagation

2.2.1 Relevant conditions for the application of adaptive antennas

In mobile radio communications a part of the electromagnetic energy radiated by the transmitter reaches the receiver by propagating through different paths [Par92, FL96]. In contrast to free space propagation, the line of sight (LOS) path between transmitter and receiver is generally obstructed in mobile radio communications [Par92, BARY95, FL96, BBS97]. Even if the BS antenna is at an elevated location, it usually is not visible from the MS, because the MS is surrounded by buildings, trees, hills, etc. Therefore, the radio connection of an MS to a BS has to rely on physical effects like reflection, refraction, scattering and diffraction by the various objects in the propagation environment [Par92, BARY95]. This means that the electromagnetic waves in a point-to-point connection between a BS and an MS generally propagate along a multitude, or even a continuum, of different paths with each path consisting of several hops [BBS97]. The signals transmitted over these paths are superimposed at the receiver. Because of the movement of the MS and possibly other objects in the propagation environment, these paths are time variant and exist for only a limited life time. In addition, the paths differ more or less from each other in [BBS97]

- delay time,

- attenuation and phase shift,
- launching direction at the transmitter and direction of incidence at the receiver,
- change of the polarization along the path and dependence of the attenuation and phase shift on the starting polarization chosen at the transmitter,
- time dependence of the path characteristics,
- path life time.

The above mentioned differences among paths lead to variations of the received signal, which are divided into small–scale and large–scale variations [BARY95, FL96]. As the MS moves over small distances, e.g., a fraction of the wavelength, the signal at the receiver, which is the sum of many contributions from different directions, exhibits rapid variations due to phase changes of the different contributions. These rapid variations are called small–scale variations and lead to the fast fading of the received signal envelope [Par92]. As the MS moves over larger distances, e.g., some tens of the wavelength, some paths may become partly obstructed or disappear, while new ones may arise. The resulting variations of the received signal averaged over these larger distances are called large–scale variations and lead to the slow fading of the average received signal power [Par92]. The large–scale variations are less rapid than the small–scale variation, but usually they have a larger dynamic range compared to the small–scale variations [BARY95].

In a mobile radio system where a single antenna is used at both the BS and the MS, the channel between the input of the transmitter antenna and the output of the receiver antenna can be described by an impulse response, which originates from a weighted superposition of the impulse responses of a selection of paths, the weighting and selection being determined by the employed antennas [BBS97]. This impulse response exhibits a more or less distinct spread along the delay axis, i.e., delay dispersion occurs, and it is time variant [Par92]. It can be described by its lowpass equivalent $\underline{h}(\tau, t)$, where τ and t denote the delay and the time, respectively. $\underline{h}(\tau, t)$ is related via Fourier transformation to a time variant transfer function [Par92, BBS97]

$$\underline{H}(f, t) = \int_{-\infty}^{\infty} \underline{h}(\tau, t) e^{-j2\pi f\tau}\, d\tau, \tag{2.1}$$

which is frequency selective on account of the delay dispersion of $\underline{h}(\tau, t)$. $\underline{h}(\tau, t)$ and $\underline{H}(f, t)$ are manifestations of the active paths of the propagation environment as seen through the employed antennas [BBS97].

If one is interested in a fundamental understanding of the potential of adaptive antennas in mobile radio communications, the description of the mobile radio channel by the above mentioned functions $\underline{h}(\tau, t)$ and $\underline{H}(f, t)$ is not sufficient. Rather, a more basic and differentiated description is required, which is not a priori biased by the chosen antennas, but

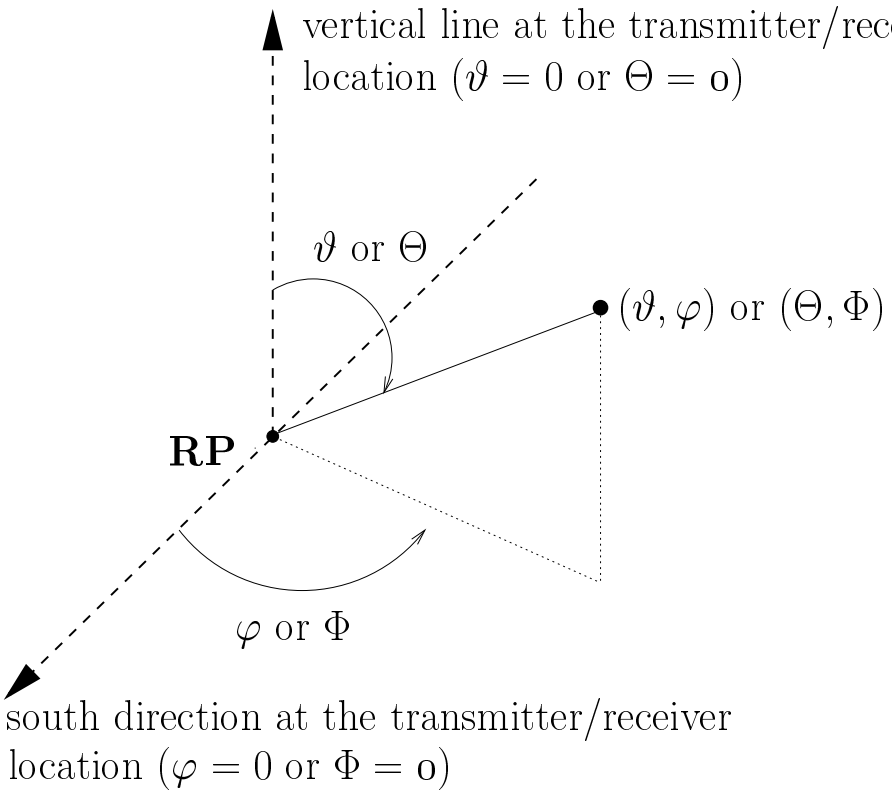

Figure 2.1. Determination of a point with coordinates (ϑ,φ) or (Θ,Φ) at the transmitter or receiver location, respectively

which describes the electromagnetic properties of the propagation environment between the locations of a transmitter and a receiver in such a way that the channel impulse response can be determined depending on the properties of any given pair of antennas. Such a description should, in addition to taking into account delay dispersion and time variance, also tackle the effects of directional dispersion and polarization dispersion [BBS97]. Directional dispersion means that a unidirectionally radiated wave may impinge at a receiver location from a more or less extended angular range, and polarization dispersion means that a wave radiated with a certain polarization may arrive at a receiver location with a set of different polarizations [BBS97]. To obtain such a description, spherical coordinate systems are introduced at the transmitter and receiver locations with the co-elevation angles ϑ and Θ, respectively, and the azimuthal angles φ and Φ, respectively. In order to obtain an unambiguous relation between the angles $\vartheta, \varphi, \Theta, \Phi$ and the four cardinal points at each of the two locations, the following definitions are adopted [BBS97]:

- ϑ equal to zero and Θ equal to zero indicate the vertical directions at the transmitter and receiver locations, respectively, and
- φ equal to zero and Φ equal to zero indicate the south directions at the transmitter and receiver locations, respectively.

Then, a point with coordinates (ϑ,φ) or (Θ,Φ) at the transmitter or receiver location, respectively, is determined as shown in Fig. 2.1. Let us assume that ideal omnidirectional antennas are used at the transmitter and receiver, with the transmitter antenna generating a wave which has an electrical field component only in ϑ-direction, and with the receiver antenna being sensitive only to electrical field components in Φ-direction. The partial impulse response between the ports of the two antennas resulting from illuminating the scenario in the solid angle $\mathrm{d}\,\vartheta \cdot \mathrm{d}\,\varphi \cdot \sin\vartheta$ centered around ϑ, φ and from probing the scenario in the solid angle $\mathrm{d}\,\Theta \cdot \mathrm{d}\,\Phi \cdot \sin\Theta$ centered around Θ, Φ can be represented in the form $\underline{g}_{\mathrm{c}}^{\,(\Phi,\vartheta)}(\vartheta, \varphi, \Theta, \Phi, \tau, t) \cdot \mathrm{d}\,\vartheta \cdot \mathrm{d}\,\varphi \cdot \mathrm{d}\,\Theta \cdot \mathrm{d}\,\Phi \cdot \sin\vartheta \cdot \sin\Theta$, where the delay dispersive and time variant function $\underline{g}_{\mathrm{c}}^{\,(\Phi,\vartheta)}(\vartheta, \varphi, \Theta, \Phi, \tau, t)$ is termed differential directional channel impulse response [BBS97]. In order to obtain a comprehensive description of the propagation environment between the transmitter and receiver locations, which is independent of the antenna characteristics, four differential directional channel impulse responses $\underline{g}_{\mathrm{c}}^{\,(\mu,\nu)}(\vartheta, \varphi, \Theta, \Phi, \tau, t)$, $\mu \in \{\Theta, \Phi\}$, $\nu \in \{\vartheta, \varphi\}$ are needed [BBS97]. Each of these functions describes the transfer characteristics of the scenario for a certain pair of transmitter and receiver polarizations, and these functions cover the dispersions of delay, direction and polarization. Because each of the four functions is constituted by a different set of propagation paths between the transmitter and receiver locations, these functions are more or less independent from each other [BBS97].

However, in order to apply the above introduced differential directional channel impulse responses with the goal to determine the channel impulse response $\underline{h}(\tau, t)$, see (2.1), the transmitter and receiver antennas should not be too closely surrounded by obstacles [BBS97]. Rather, the objects closest to the antennas should lie in the far field regions. Admittedly, this presupposition restricts the applicability of the above theory because, especially in the nearfield regions of the MS, antennas are usually not free from obstacles. Nevertheless, this theory may be helpful in developing a basic understanding of the physical effects being relevant in adaptive antenna design and application [BBS97].

Once the four differential directional channel impulse responses $\underline{g}_{\mathrm{c}}^{\,(\mu,\nu)}(\vartheta, \varphi, \Theta, \Phi, \tau, t)$, $\mu \in \{\Theta, \Phi\}$, $\nu \in \{\vartheta, \varphi\}$, are known for a pair of locations, the channel impulse response $\underline{h}(\tau, t)$, cf. (2.1), between the ports of any transmitter antenna and any receiver antenna being situated at these locations can be determined depending on the antenna characteristics, as described in the following. First, for each antenna two characteristics are required, one for the ϑ- and Θ-components, respectively, and the other for the φ- and Φ-components, respectively, of the electrical fields. These two characteristics are termed $\underline{f}_{\mathrm{t}}^{(\vartheta)}(\vartheta, \varphi)$ and $\underline{f}_{\mathrm{t}}^{(\varphi)}(\vartheta, \varphi)$ for the transmitter antenna and $\underline{f}_{\mathrm{r}}^{(\Theta)}(\Theta, \Phi)$ and $\underline{f}_{\mathrm{r}}^{(\Phi)}(\Theta, \Phi)$ for the receiver antenna [BBS97]. Then, with these four antenna characteristics and the above introduced four differential directional channel impulse responses, the time variant impulse response $\underline{h}(\tau, t)$ between the input of the transmitter antenna and the output of the receiver antenna can be determined. To this purpose, the vectors [BBS97]

$$\underline{\mathbf{f}}_{\mathrm{t}}(\vartheta, \varphi) = \left[\underline{f}_{\mathrm{t}}^{(\vartheta)}(\vartheta, \varphi) \;\; \underline{f}_{\mathrm{t}}^{(\varphi)}(\vartheta, \varphi)\right]^T, \tag{2.2}$$

$$\underline{\mathbf{f}}_{\mathrm{r}}(\Theta,\Phi) = \left[\underline{f}_{\mathrm{r}}^{(\Theta)}(\Theta,\Phi) \;\; \underline{f}_{\mathrm{r}}^{(\Phi)}(\Theta,\Phi)\right]^{T}, \tag{2.3}$$

and the matrix [BBS97]

$$\underline{\mathbf{G}}_{\mathrm{c}}(\vartheta,\varphi,\Theta,\Phi,\tau,t) = \begin{bmatrix} \underline{g}_{\mathrm{c}}^{(\Theta,\vartheta)}(\vartheta,\varphi,\Theta,\Phi,\tau,t) & \underline{g}_{\mathrm{c}}^{(\Theta,\varphi)}(\vartheta,\varphi,\Theta,\Phi,\tau,t) \\ \underline{g}_{\mathrm{c}}^{(\Phi,\vartheta)}(\vartheta,\varphi,\Theta,\Phi,\tau,t) & \underline{g}_{\mathrm{c}}^{(\Phi,\varphi)}(\vartheta,\varphi,\Theta,\Phi,\tau,t) \end{bmatrix} \tag{2.4}$$

are introduced. Then,

$$\begin{aligned} \underline{h}(\tau,t) \;=\; & \int\limits_{\substack{\vartheta,\Theta=0\ldots\pi \\ \varphi,\Phi=0\ldots 2\pi}} \int\int\int \underline{\mathbf{f}}_{\mathrm{r}}^{\mathrm{T}}(\Theta,\Phi)\cdot\underline{\mathbf{G}}_{\mathrm{c}}(\vartheta,\varphi,\Theta,\Phi,\tau,t)\cdot\underline{\mathbf{f}}_{\mathrm{t}}(\vartheta,\varphi)\cdot\sin\vartheta\cdot d\,\vartheta\cdot \\ & \sin\Theta\cdot d\,\Theta\cdot d\,\varphi\cdot d\,\Phi \end{aligned} \tag{2.5}$$

holds [BBS97].

Knowledge of the properties of the mobile radio channel, i.e., ideally about the above introduced differential channel impulse responses, see (2.4), is important in two different respects [BBS97]. On the one hand, such knowledge is required for designing mobile radio systems in an optimum way for the environments in which they have to work, and for comparing different system concepts on a realistic basis. The information required for these purposes is usually obtained by channel sounders (CS) [FBKM93] in expensive measurement campaigns [Egg94, KMT96, MG96] and by evaluation of the measurement results, but also by implementing channel models which imitate the geometrical and electrical conditions of the considered scenario on the computer [KCW93b, Bla98], see also the discussion pertaining to Category IV of Table 1.2 for a detailed analysis of the state of the art of channel modeling for systems with adaptive antennas. On the other hand, when operating a mobile radio network, the valid channel properties have to be estimated continuously in order to be able to adapt the transmitter and/or receiver including their antennas to the channel and, thus, to optimize transmission with the ultimate aim to achieve a large capacity. To solve this task, channel estimation devices are required which work in real time [SK93]. However, it is noted that, usually, not the total knowledge on the channel, i.e., not the above introduced differential channel impulse responses, see (2.4), but rather a knowledge of $\underline{h}(\tau,t)$, see (2.5), becomes available by channel sounders as well as by channel estimation devices. The consideration of channel sounders is beyond the scope of this thesis. For a detailed analysis see [FBKM93, BARY95, BBS97]. However, channel estimation is treated in detail in this thesis, see Chapter 5.

2.2.2 Directional effects in mobile radio channels

In a mobile radio scenario, a multitude of radio links is simultaneously active in the same service area, and a priori no natural isolation between the different links exists [Par92, BBS97]. As a consequence of this lack of isolation, the radiated signals arrive not only at those receivers for which they are intended, which means that part of the radiated

power is wasted, but also at the other receivers where the signal is undesired. The sum of undesired signals impinging at a receiver location from within and from outside their own cell constitutes the intracell and intercell MAI, respectively, see also Section 1.2. In most cases cellular mobile radio systems are interference limited, which means that the factor which limits capacity is not thermal receiver noise but MAI. If the multiple access schemes FDMA and/or TDMA are applied, intracell MAI is a priori avoided in conventional system architectures, where each time slot and frequency band is allocated only to a single user in each cell. This is not true in the case of CDMA, where intracell MAI is unavoidable but may be afterwards eliminated by JD or IC [BBS97]. A vital task of the receivers consists in detecting the desired signals with sufficient quality despite of the presence of MAI. As an essential feature of mobile radio scenarios, the transmitters and receivers are spatially distributed over the service area. For any pair of transmitter and receiver locations, a matrix $\underline{\mathbf{G}}_c(\vartheta, \varphi, \Theta, \Phi, \tau, t)$ of differential directional channel impulse responses exists [BBS97], see (2.4). With respect to the application of adaptive antennas it is important that, in general, the differential directional channel impulse responses of two pairs of locations differ especially with respect to their dependence on their angles $\vartheta, \varphi, \Theta, \Phi$. This is true if at least one location is not the same for the two pairs, i.e., if at least three different locations are involved [BBS97]. Even in the case of LOS propagation such differences would arise. In addition, in the case of real world mobile radio scenarios effects of the following kinds may be observed [BBS97]:

- Signals emitted by two transmitters T_1 and T_2, which appear under the same LOS directions at a certain receiver location R, may impinge with different DOAs at this receiver location, see Fig. 2.2a.
- Signals emitted by two transmitters T_1 and T_2, which appear under different LOS directions at a certain receiver location R, may impinge with the same DOA at this receiver location, see Fig. 2.2b.
- Signals emitted by a transmitter T in two different directions may impinge at two receiver locations R_1 and R_2 appearing under the same LOS direction from this transmitter location, see Fig. 2.2c.
- Signals emitted by a transmitter T in one direction may impinge at two receiver locations R_1 and R_2 appearing under different LOS directions from this transmitter location, see Fig. 2.2d.

Such effects, which result from the spatial distribution of transmitters and receivers, offer the potential to increase the isolation between different radio links in the same service area by adaptive antennas [BBS97]. However, in order to illustrate this potential of adaptive antennas, directional channel models are required, which consider directional effects as the ones discussed in this section. The directional channel models used in this thesis is the subject of the following section.

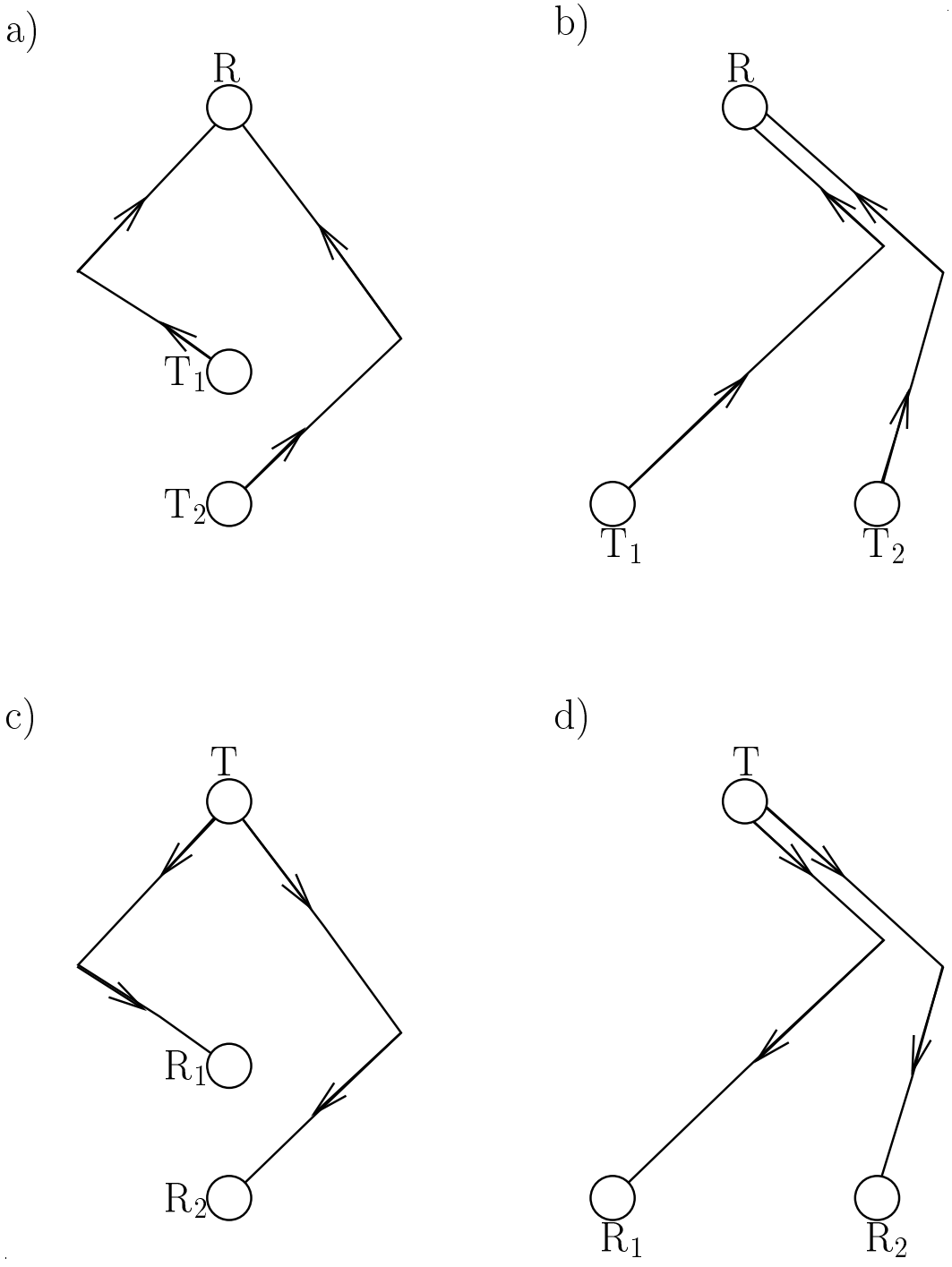

Figure 2.2. Directional effects in mobile radio channels: a) Same LOS direction of T_1 and T_2, b) different LOS direction of T_1 and T_2 c) same LOS direction of R_1 and R_2 d) different LOS direction of R_1 and R_2 (taken from [BBS97])

2.3 Directional channel models used in the thesis

2.3.1 Introduction

In this section, the directional channel models used in the subsequent chapters of this thesis are described. These models include also the directional characteristics of the mobile radio channel, see Section 2.2.2, and are appropriate for investigating the behaviour of mobile radio systems using adaptive antennas at the BS transceiver. First, we set out from the COST 207 channel models [COS89], which do not include directional characteristics of the mobile radio channel. It is possible, though, to incorporate information about the DOAs of impinging signals, e.g., as illustrated in Section 2.2.2, and the resulting directional channel models provide a powerful tool for illustrating in a rather straightforward manner the advantages of adaptive antennas in mobile radio systems [PFBP99, PFB97b]. These channel models are addressed as the modified COST 207 channel models in the following. Second, the geometry-based UKL 2 directional channel models are described [SP97, SP98b]. These models are an evolution of the UKL channel models presented in [BBJ95, Bla98], and they model the directional inhomogeneity of the mobile radio channel in a more realistic way, compared to the modified COST 207 channel models introduced above and presented in the following Section 2.3.2.

2.3.2 Modified COST 207 channel models for systems with adaptive antennas

The COST 207 channel models belong to the category of channel models which generate channel impulse responses retaining the properties of the mobile radio propagation, see Category IV of Table 1.2. They belong to the class of algorithmic channel models defined in [BBS97], see also Section 1.2, and they are described in detail in [COS89, FL96, Naß95]. In [Ste95, Naß95], the COST 207 channel models have been applied to the considered TD–CDMA air interface when a single antenna is used in both the MS and the BS. In this thesis, the models defined in [Ste95, Naß95] for the TD–CDMA air interface using single antennas are modified to include the directional characteristics of the impinging signals in a rather straightforward manner. The resulting modified COST 207 channel models are described in the following.

In [Ste95, Naß95] a created channel impulse response is valid for the link between an MS and a BS, each using a single antenna. Each channel impulse response is the incoherent superposition of P uncorrelated sinusoids, each having a zero phase θ_i, $i = 1 \ldots P$, a Doppler frequency $f_{\mathrm{d},i}$, $i = 1 \ldots P$, and a time delay τ_i, $i = 1 \ldots P$ [COS89, Naß95]. The zero phases θ_i, $i = 1 \ldots P$, are taken from a uniform distribution in the interval $[0, 2\pi]$, and the Doppler frequencies are distributed according to the Jakes or classical Doppler spectrum [Jak74, Naß95]. The P time delays τ_i, $i = 1 \ldots P$, are realizations of a random variable having the probability density function (pdf) determined by one of the power

delay profiles (PDP) defined within COST 207 for the propagation environments rural area (RA), typical urban (TU), bad urban (BU), and hilly terrain (HT) [COS89, Naß95]. Further, the zero phase θ_i, the Doppler frequency $f_{\mathrm{d},i}$ and the time delay τ_i pertaining to each sinusoid i, $i = 1 \ldots P$, are assumed to be independently distributed [Ste95, Naß95]. With $\delta(\cdot)$ designating the Dirac's delta function, the time continuous channel impulse response $\underline{h}(\tau, t)$, see (2.5), is expressed in the form

$$\underline{h}\,(\tau, t) = \frac{1}{\sqrt{P}} \sum_{i=1}^{P} \exp(\mathrm{j}\theta_i)\, \exp(\mathrm{j}2\pi f_{\mathrm{d},i} t)\; \delta(\tau - \tau_i), \tag{2.6}$$

where t denotes the time and τ the delay. When applying the above described COST 207 channel models in TD–CDMA, the system bandwidth can be taken into account by, first, applying an ideal lowpass filter to the contribution of each sinusoid and sampling at the chip rate, after the contributions from each sinusoid are summed up according to (2.6). The bandwidth of the ideal lowpass filter is equal to the inverse of the chip duration [Ste95, Naß95]. Thus, the resulting time discrete channel impulse response in the equivalent lowpass domain can be produced by a tapped delay line, as illustrated in [BBS97]. The channel impulse responses generated according to this scheme exhibit the fast fading characteristics of the mobile radio channel, meaning that variations of the received power due to fast fading are present in the received signal, whereas variations due to path loss or birth and shadowing are supposed to be perfectly eliminated by power control.

The above described COST 207 channel models do not include directional information about the impinging signals. As already mentioned in Section 1.1, adaptive antenna concepts take advantage of the directional inhomogeneity of the mobile radio channel to improve the system behaviour compared to single antenna systems. Thus, a performance evaluation of adaptive antennas should be based on channel models which, besides time variance and frequency selectivity, explicitly incorporate the directional inhomogeneity of the mobile radio channel [BHP97, PFBP99]. When antenna arrays [Haa97a] are used at the BS of a TD–CDMA mobile radio system, the narrowband assumption [RK89] is valid, i.e., time delays of the signal propagation between successive antennas which are smaller than the inverse bandwidth amount only to changes of the argument of the complex signal envelope. These changes depend on the DOA of the impinging signal on the BS array and the array configuration [RK89]. Therefore, it is possible to produce directional channel impulse responses by multiplying the complex channel impulse response created at a reference point of the array configuration according to the COST 207 channel models by a complex exponential which depends only on the DOA and the array configuration [PFB97b, PFBP99]. The number and the distribution of the DOAs depend on the propagation environment, and they should be based on measurement results [Egg94, KMT96, MG96, Bla98], which have been conducted in the considered propagation environments.

In the case of the rural propagation environment the waves impinge at the BS within

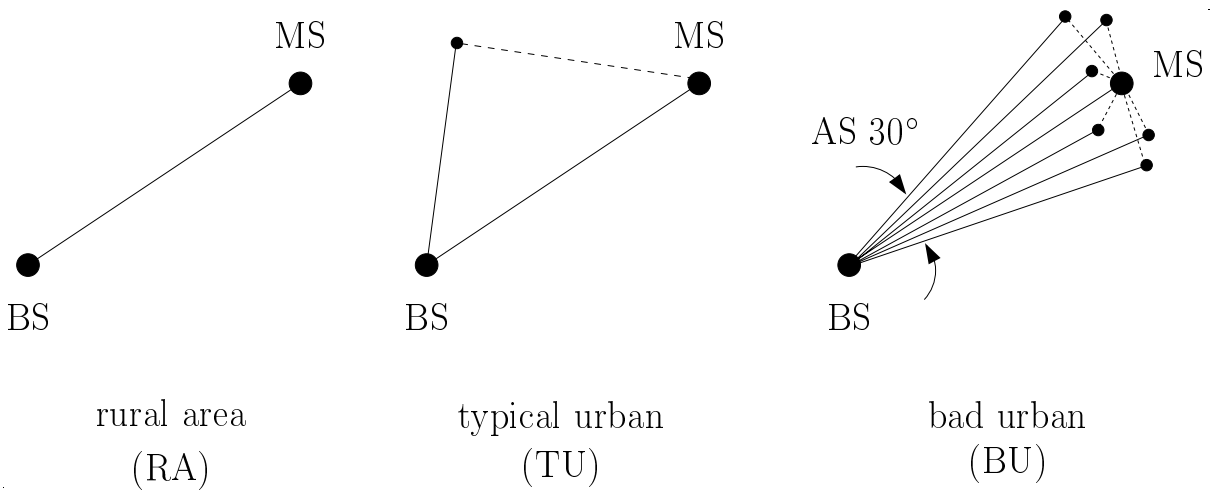

Figure 2.3. Illustration of the modeling of the directional inhomogeneity for the modified COST 207 channel models

a small azimuthal range [KMT96, BHP97], which can be approximated by a single DOA. For this reason, the channel models specified by COST 207 [COS89] for transmission over RA channels are used, with the additional introduction of a single DOA for each user assigned to the considered BS. The resulting channel model is termed modified COST 207 RA channel model. For the urban propagation environment two cases are considered. First, for a non–hilly urban environment, the channel models specified by COST 207 [COS89] for transmission over TU are used by assigning two uniformly and statistically independent DOAs to the P sinusoids mentioned above in this section, see also (2.6), for the directional channel impulse responses of each user. This is a typical situation of the directional inhomogeneity of the mobile radio channel in a non–hilly urban environment [KMT96, PFBP99]. The resulting channel model is termed modified COST 207 TU channel model. Second, for a hilly urban environment, the channel models specified by COST 207 [COS89] for transmission over BU are used by assigning 30 equidistant DOAs in an impinging range of 30°, thus modeling an angular spread (AS), which is a realistic situation in such propagation environment types [KMT96, BBJ95]. The resulting channel model is termed modified COST 207 BU channel model. The directional inhomogeneity adopted for the modified COST 207 channel models is illustrated in Fig. 2.3.

The modified COST 207 channel models presented in this section do not incorporate the directional inhomogeneity of the mobile radio channel in a realistic manner, but they can be used for investigating adaptive antennas in a tutorial manner, compared to the use of single antennas, and obtaining upper bounds for the performance of systems with adaptive antennas. However, when evaluating adaptive antenna concepts for real world

mobile radio applications, more sophisticated directional channel models should be used, which model the real world properties of the mobile radio channel, see Section 2.2.1, in a more realistic way. Such models are the geometry–based UKL 2 directional channel models described in the next section.

2.3.3 UKL 2 directional channel models

In this section the UKL 2 directional channel models are briefly described according to [SP97, SP98b], and a parametrization of the UKL 2 directional channel models for different propagation environments is presented. These models offer a more realistic approach to the directional inhomogeneity of the mobile radio channel, compared to the modified COST 207 channel models of Section 2.3.2. The UKL 2 directional channel models are an evolution of the UKL directional channel models presented in [BBJ95, Bla98]. In addition to the advantages offered by the UKL channel models, the UKL 2 directional channel models

- enable the modeling of the movement of an MS in a mobile radio scenario, and
- reduce considerably the number of necessary scatterers for producing the channel impulse responses on the digital computer.

In the following, the main topics connected with the UKL 2 directional channel models are described and the parameters for three mobile radio propagation environments are established.

The transmission channel between an MS and a BS with single antennas is considered in the following. The channel impulse response at a time instance t is created by a linear superposition of K_e impulse responses, the number K_e of which is much greater than one [Bla98, Höh90, Höh92]. Further, only those impulse responses are considered, which are produced by single reflection, single scattering, or single diffraction [BBJ95, Bla98]. Moreover, a line of sight connection between the MS and the BS is excluded. A time delay $\tau^{(k_\mathrm{e})}$, a Doppler frequency $f_\mathrm{D}^{(k_\mathrm{e})}$, a zero phase $\theta^{(k_\mathrm{e})}$, a direction of departure $\varphi_\mathrm{s}^{(k_\mathrm{e})}$, a DOA $\varphi_\mathrm{e}^{(k_\mathrm{e})}$, and a gain factor $\alpha^{(k_\mathrm{e})}$ are assigned to each impulse response k_e, $k_\mathrm{e} = 1 \ldots K_\mathrm{e}$ [Bla98]. The quantities $\tau^{(k_\mathrm{e})}$, $f_\mathrm{D}^{(k_\mathrm{e})}$, $\varphi_\mathrm{e}^{(k_\mathrm{e})}$, $\varphi_\mathrm{s}^{(k_\mathrm{e})}$, and $\alpha^{(k_\mathrm{e})}$ assigned to each impulse response k_e, $k_\mathrm{e} = 1 \ldots K_\mathrm{e}$, can be directly determined by the position $(x_\mathrm{s}^{(k_\mathrm{e})}, y_\mathrm{s}^{(k_\mathrm{e})})$ of a scatterer (S) relative to the position of the MS and the BS, and the velocity vector $\vec{v}$ of the MS [Bla98], see Fig. 2.4. In Fig. 2.4 d is the distance between the MS and the BS, $r_1^{(k_\mathrm{e})}$ is the distance between the MS and the scatterer k_e, $r_2^{(k_\mathrm{e})}$ is the distance between the scatterer k_e and the BS, $\vec{v}$ is the velocity vector of the MS, and φ_v is the angle characterizing the direction of movement of the MS [Bla98]. Finally, the zero phase $\theta^{(k_\mathrm{e})}$ of the k_e–th impulse response

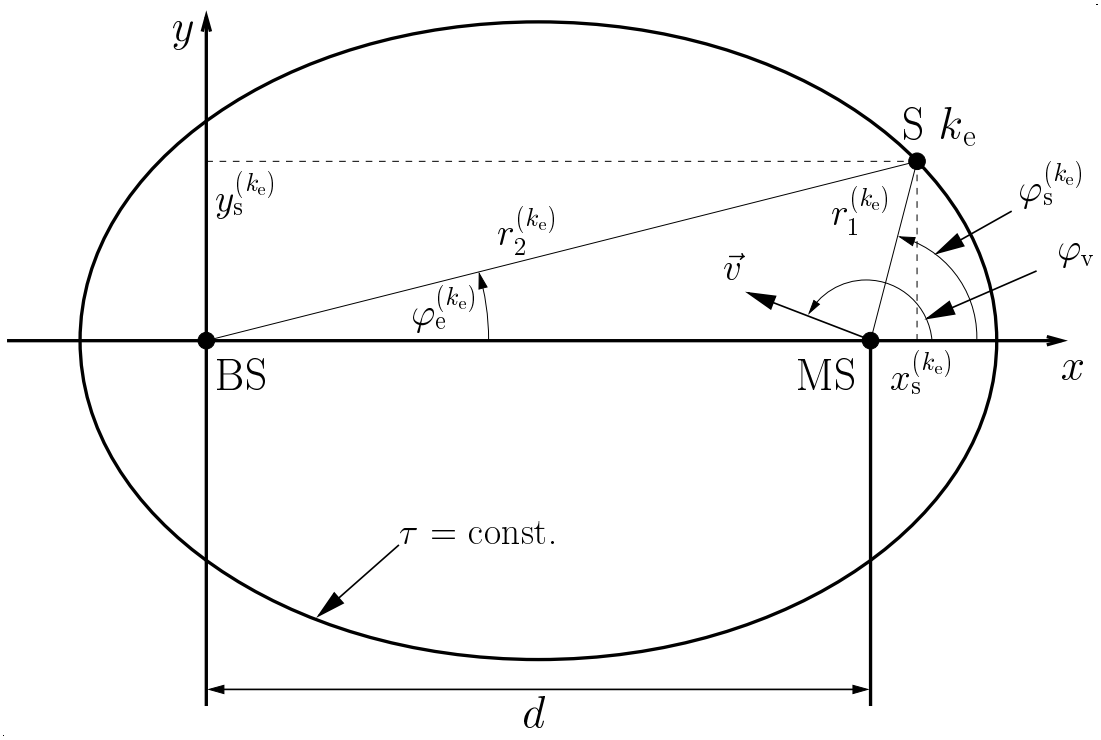

Figure 2.4. Definition of parameters for the UKL 2 directional channel models

is assumed to be generated from a uniform distribution in the interval $[0, 2\pi]$. Then, if the gain factor for each impulse response is given by [Bla98]

$$a^{(k_e)} = \frac{\alpha_0}{\left(r_1^{(k_e)} r_2^{(k_e)}\right)^{\alpha/2}}, \qquad k_e = 1 \ldots K_e, \tag{2.7}$$

i.e., all K_e scattering processes are characterized by the constant factor α_0 [Bla98], the differential directional channel impulse response at a reference point (RP) of the BS is given by [Bla98]

$$\underline{g}_d(\tau, t, \varphi) = \sum_{k_e=1}^{K_e} \frac{a_0}{r_1^{(k_e)} r_2^{(k_e)}} \cdot e^{j\left(2\pi f_D^{(k_e)} t + \theta^{(k_e)}\right)} \cdot \delta\left(\tau - \tau^{(k_e)}\right) \cdot \delta\left(\varphi - \varphi_e^{(k_e)}\right), \tag{2.8}$$

see also the analysis of Section 2.2.1 concerning the differential directional channel impulse responses. In the case that multi–antenna configurations are used at the BS and K users are simultaneously active, a differential directional channel impulse response $\underline{g}_d^{(k,k_a)}(\tau, t, \varphi)$, for each user k, $k = 1 \ldots K$, and each antenna k_a, $k_a = 1 \ldots K_a$, can be defined by taking into account the antenna positions relative to the RP of the BS [Bla98], see also Section 2.3.2.

In order to model the propagation geometrically, a circular area of radius R_s, called

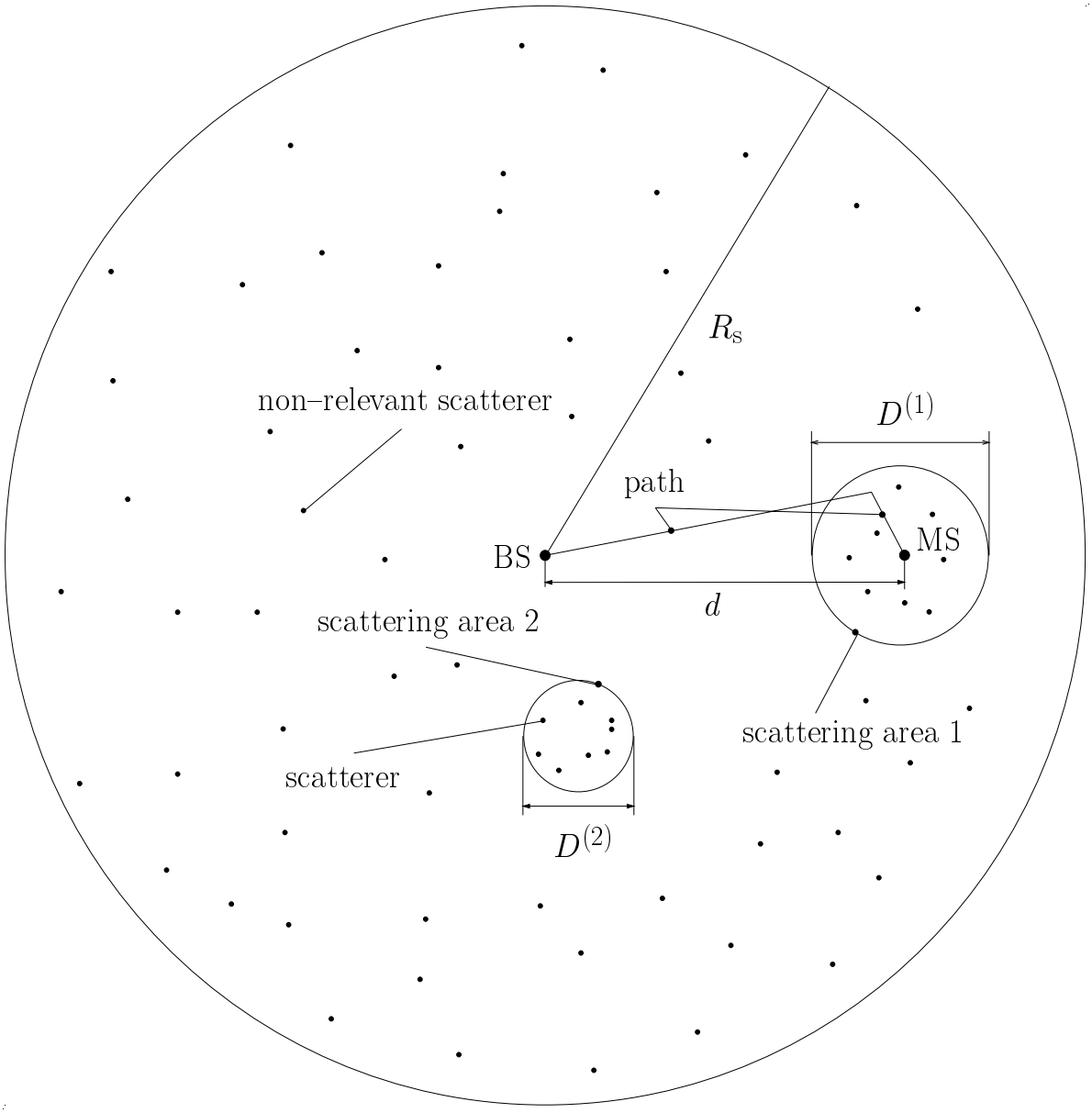

Figure 2.5. Hierarchical division of the scenario area into non–relevant scatterers, scattering areas, and scatterers

scenario area and representing an instantaneous scenario, is covered with scatterers obeying a uniform distribution in the (x, y) plane, see Fig. 2.5. The position of the scatterers within the scenario area is not changed. The BS is placed at the center of the scenario area and the position of an MS is randomly distributed within the scenario area. Then, the scenario area is hierarchically subdivided into

1. Regions with scatterers which are not relevant for the link between the considered MS and the BS.

2. N_z circular scattering areas each of diameter $D^{(n_z)}$, $n_z = 1 \ldots N_z$. The scattering

areas may represent, e.g., urban or suburban ensembles of buildings. The scattering area 1 with diameter $D^{(1)}$ is always placed around the considered MS.

3. ${N_\mathrm{p}}^{(n_\mathrm{z})}$ scatterers which are defined by each circular scattering area n_z, $n_\mathrm{z} = 1 \ldots N_\mathrm{z}$. These scatterers model, e.g., individual buildings or spots on a building from which scattered electromagnetic waves originate.

An example of the hierarchy of the UKL 2 directional channel models is shown in Fig. 2.5 with

$$N_\mathrm{z} = 2, \quad {N_\mathrm{p}}^{(1)} = 9, \quad {N_\mathrm{p}}^{(2)} = 8. \tag{2.9}$$

The above mentioned model allows the movement of the MS by simultaneously moving the scattering area 1 placed around the MS [SP97, SP98b]. As the MS takes another position within the scenario area, the scattering area 1 defines a new number of scatterers ${N_\mathrm{p}}^{(1)}$, which are relevant for the link between the considered MS and the BS. However, if there are additional scattering areas within the scenario area which do not pertain to a certain user, these scattering areas do not change their position as the MS moves within the scenario area [SP97, SP98b]. Compared to the UKL channel models defined in [BBJ95, Bla98], the UKL 2 directional channel models

- allow the modeling of the movement of the MS by defining a scenario area and distinguishing relevant scatterers from non–relevant scatterers for the considered link, and
- do not contain the hierarchy level of circular scatterers of the UKL channel models, thus considerably reducing the number of propagation paths, and consequently the simulation time for producing directional channel impulse responses. Nevertheless, the UKL 2 directional channel models retain the accuracy of the UKL channel models concerning the characteristics of the produced channel impulse responses [SP97, SP98b].

Based on the UKL directional channel models [BBJ95, Bla98], a parametrization for the UKL 2 directional channel models is presented in the rest of this section. The model parameters for three typical macrocellular propagation environments are proposed. These environments are the rural, urban, and dense urban propagation environments. The constellation of the scattering areas for these environments are shown in Fig. 2.6 and correspond to the model types rural, urban 1, and urban 2 of the UKL directional channel models [BBJ95, Bla98]. As already mentioned above in this section, the scattering area 1, which is always centered around the MS, follows the movement of the MS, whereas the position of the additional scattering area 2, if present, remains unchanged while the MS moves. The proposed parameters are shown in Table 2.1, and the resulting model types are addressed as the UKL 2 rural, urban, and dense urban channel models in the rest

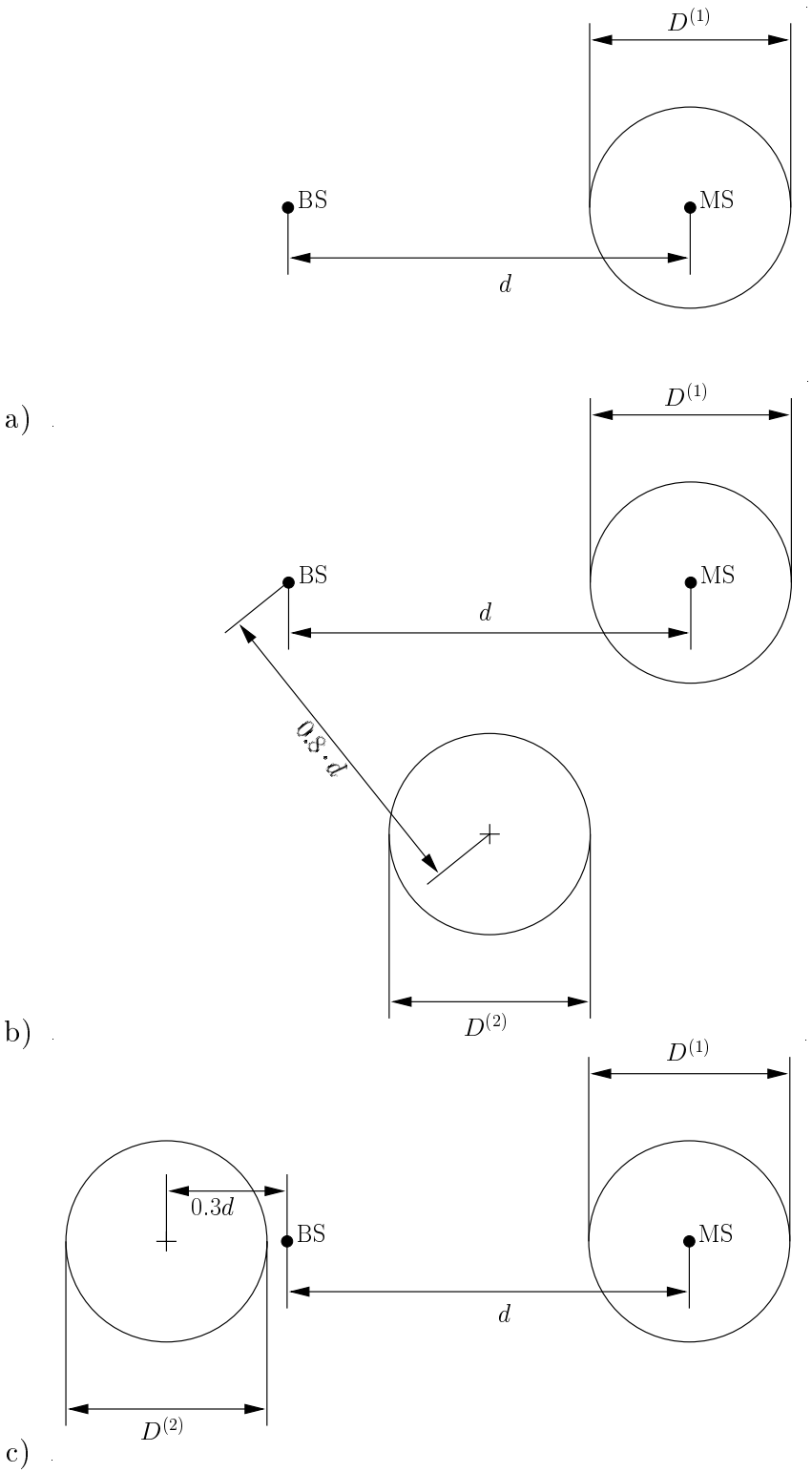

Figure 2.6. Constellation of the scattering areas for the models
a) rural,
b) urban, and
c) dense urban

Table 2.1. Parameters for the models rural, urban and dense urban

	$\frac{R_s}{\text{km}}$	N_z	$\frac{D^{(1)}}{\text{km}}$	$\frac{D^{(2)}}{\text{km}}$	N_p	$\bar{N}_p^{(1)}$	$\bar{N}_p^{(2)}$
rural	5	1	0.1	-	6000	10	-
urban	2	2	0.5	0.25	1500	20	10
dense urban	2	2	0.5	0.25	1500	20	10

of the thesis. In Table 2.1 $\bar{N}_p^{(1)}$ and $\bar{N}_p^{(2)}$ denote the mean number of relevant scatterers for the first and second scattering area, respectively. The averaging has been performed over 10^4 independent scenarios. In the next section of this chapter, a novel approach for a unified treatment of the different mobile radio channel types is presented.

2.4 A novel approach for a unified treatment of the different propagation environments

2.4.1 General

The channel impulse responses are typical of the environment and the mobility scenarios of the MSs [BARY95, FL96, BBS97]. For each mobile radio scenario, which is determined by the topology and the morphology of the considered environment, the cell and cluster sizes, and the distribution of BSs and MSs, these channel impulse responses have typical properties [BBS97]. As shown in Section 2.2.1, a channel impulse response is made up by partial waves leaving the transmitter and impinging at the receiver with a variety of directions at the receiver locations. Moreover, the channel impulse responses can be expressed by time variant differential directional channel impulse responses in combination with the characteristics of the applied antennas, see (2.5). However, in order to investigate the performance of mobile radio systems on the computer, the mobile radio channel including its directional properties is described by directional channel models, see Section 2.3. In this thesis, in order to evaluate adaptive antenna concepts for the considered TD–CDMA mobile radio system, a general classification into large cell and small cell channel types is adopted. In order to define the large cell and the small cell channel type, it is assumed that the full solid angle domain 4π is discretized into $K_s >> 1$ differential elements of size $4\pi/K_s$. Then, a time discrete directional channel impulse response in the equivalent lowpass domain, which is derived by sampling the continuous time directional channel impulse response at time instants equal to the inverse of the bandwidth utilized by the investigated mobile radio system, is characterized in general by $K_s W$ complex elements [BPW99], where W is the total dimension of the time discrete directional channel impulse along the delay axis [Ste95]. In what follows, the characteristics of the large cell and the small channel type are presented.

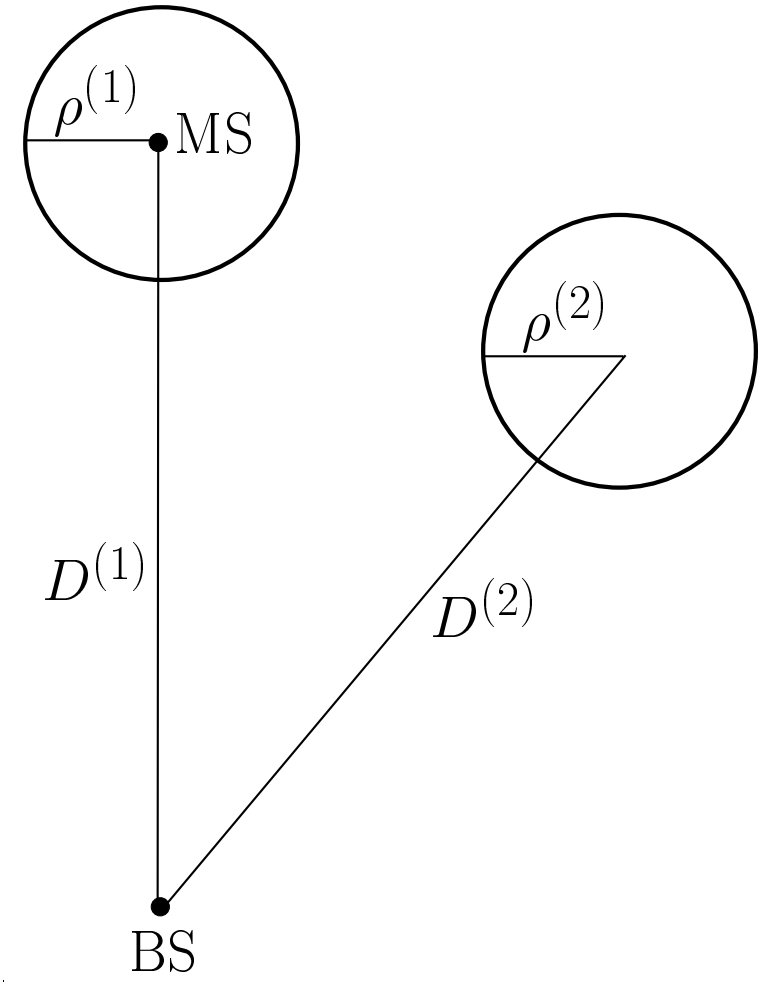

Figure 2.7. Exemplary scenario of a large cell channel type

2.4.2 Large cell channel type

For the large cell channel type it is assumed that the multipath propagation arises due to ${K_{\mathrm{d}}}^{(k)}$ scattering areas for each MS k, $k = 1 \ldots K$. Each scattering area contains uniformly distributed local scatterers and is modeled by a circle of radius $\rho^{(k_{\mathrm{d}})}$, $k_{\mathrm{d}} = 1 \ldots {K_{\mathrm{d}}}^{(k)}$, see also Section 2.3.3. The radius $\rho^{(k_{\mathrm{d}})}$ of each scattering area is assumed to be small compared to the distance $D^{(k_{\mathrm{d}})}$, $k_{\mathrm{d}} = 1 \ldots {K_{\mathrm{d}}}^{(k)}$, of its center to the BS site. Therefore, in the large cell channel type it can be assumed that signals coming from an MS impinge at the BS only from a limited number $K_{\mathrm{d}}^{(k)} << K_{\mathrm{s}}$ of different directions. In this case, a directional channel impulse response is determined by $K_{\mathrm{d}}^{(k)} W$ complex elements. In Fig. 2.7 a scenario with a single MS is depicted where there are ${K_{\mathrm{d}}}^{(k)}$ equal to two scattering areas, i.e., two directional channel impulse responses arise at the BS receiver. The modified COST 207 RA, the modified COST 207 TU, the UKL 2 rural, and the UKL 2 urban channel models belong to this channel type and, as it will be presented in Chapter 5, they can be treated in the same manner with respect to channel estimation in TD–CDMA mobile radio systems.

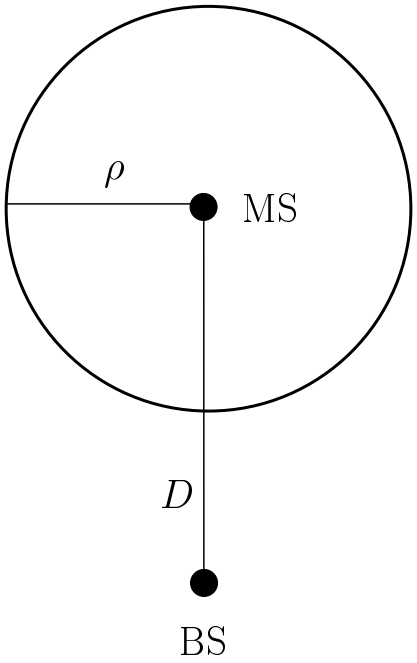

Figure 2.8. Exemplary scenario of a small cell channel type

2.4.3 Small cell channel type

In the small cell channel type it is assumed that the radius $\rho^{(k)}$ of the single scattering area valid for each user k, $k = 1 \ldots K$, see Fig. 2.8, is in the order of the distance between the MS and the BS. Therefore, it is reasonable that each of the W elements of a channel impulse response is associated with only a single direction of incidence, see also [VTP97] for a similar assumption. In this case, a directional channel impulse response is determined by only W complex elements. The modified COST 207 BU and the UKL 2 dense urban channel models belong to the small cell channel type because of the directional characteristics of the produced channel impulse responses [BPW99]. As for the models of the large cell channel type, see Section 2.4.2, the models of the small channel type are treated in the same manner, when channel estimation is performed in TD–CDMA, see Chapter 5 for a detailed analysis. However, before dealing with data detection and channel estimation in TD–CDMA with adaptive antennas, see Chapter 4 and Chapter 5, respectively, antenna diversity techniques and the different antenna types used for applying antenna diversity in mobile radio are briefly treated in the Chapter 3.

3 Antenna diversity and antenna types

3.1 Introduction

In this chapter a brief summary of antenna diversity techniques for mobile radio systems is provided based on [BBS97, Bla98]. Further, the different antenna types, which are of special interest to this thesis, i.e., the antenna types used for realizing spatial macro diversity and spatial micro diversity, are described according to [BBS97]. As already mentioned in Section 1.3, antenna diversity techniques, including adaptive antennas, are treated in a unified manner with respect to the application of JD in TD–CDMA. The benefits of using antenna diversity with respect to JD in TD–CDMA are investigated in depth in Chapter 4.

3.2 Antenna diversity

As already mentioned in Section 2.2.2, the use of the multiple access method CDMA creates MAI at the receiver. Moreover, both time variance and frequency selectivity of the mobile radio channel, see Section 2.2.1, are undesired in mobile radio communications, because they increase the sensitivity of the receiver to MAI [Hess93, BBS97]. Therefore, if a certain quality of service [HV99] has to be guaranteed, the increased sensitivity to MAI has to be compensated by reducing MAI [BBS97]. Such a reduction can be achieved by decreasing the number of users per cell and/or increasing the cluster size, both of which directly lower capacity [BBS97]. It is well known that the detrimental effects of time variance and frequency selectivity can be combatted by diversity, i.e., by transmitting the desired signal not only over one, but over several channels, and by properly combining the channel output signals at the receiver [KSS95, BBS97, BSPJ97, Bla98]. The more uncorrelated these channels are, the more pronounced the benefits of diversity become [BBS97]. As another positive aspect of diversity, the differences of MAI powers and time variance on the different channels lead to interferer diversity, which can be exploited to improve the resulting MAI statistics [Ste96]. In the case of single port antennas at the transmitter and receiver, two of the possible ways to translate the diversity principles into action are time diversity, realized, e.g., by interleaving in combination with FEC (Forward Error Correction) coding [Vit95], and frequency diversity, realized, e.g., by frequency hopping or spreading (CDMA) [BBS97]. In both cases, in fact different channels are not actually used, but one and the same channel is accessed at different instants of time or at different carrier frequencies [BBS97].

A basically different diversity approach is antenna diversity, which is characterized by employing for each BS and/or MS instead of only one single port antenna a number of such antennas which are separately accessible. If these antennas are closely spaced, an antenna array is produced [Haa97a]. According to (2.5) the propagation environment

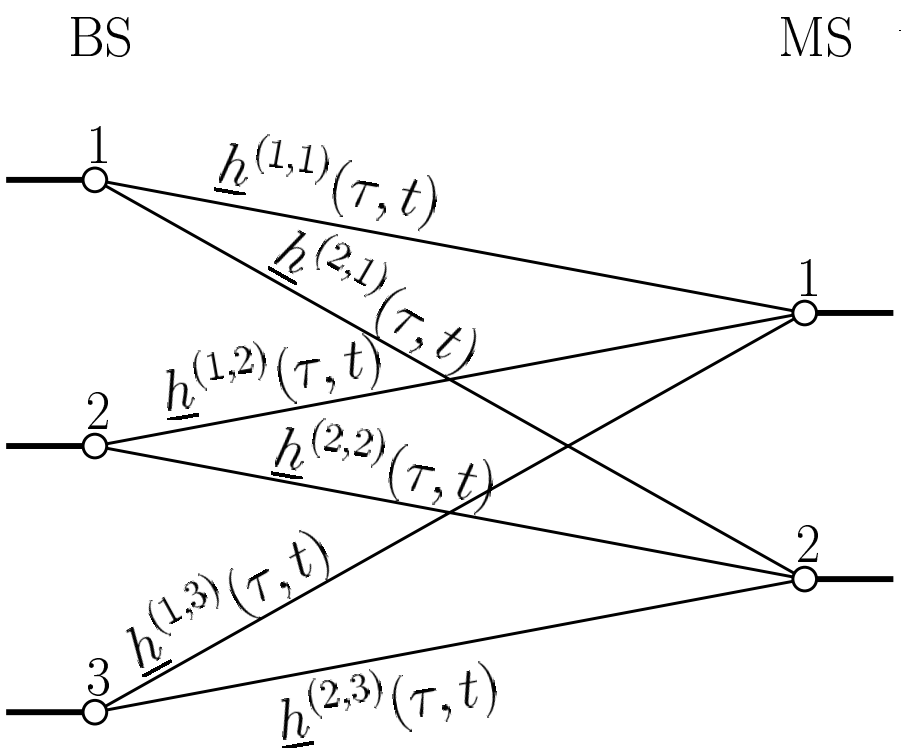

Figure 3.1. Multiport network (taken from [BBS97])

offers the potential to obtain, depending on the chosen antennas, a variety of more or less independent channel impulse responses between each pair of transmitter and receiver locations. Antenna diversity can be applied as the only diversity approach or in addition to, e.g., time diversity and frequency diversity [BBS97]. However, it should be mentioned that there is a limit to the total diversity benefit achievable [BBS97, Bla98].

With the antenna numbers $K_{\mathrm{a}}^{(\mathrm{BS})}$ and $K_{\mathrm{a}}^{(\mathrm{MS})}$ at the BS and the MS, respectively, the antenna system can be considered as a multiport network [BBS97]. Fig. 3.1 shows such a network for the case $K_{\mathrm{a}}^{(\mathrm{BS})}$ equal to three and $K_{\mathrm{a}}^{(\mathrm{MS})}$ equal to two. The multiport network is characterized by $K_{\mathrm{a}}^{(\mathrm{BS})} \cdot K_{\mathrm{a}}^{(\mathrm{MS})}$ channel impulse responses $\underline{h}^{(\mu,\nu)}(\tau,t)$, $\mu \in \{1 \ldots K_{\mathrm{a}}^{(\mathrm{BS})}\}$, $\nu \in \{1 \ldots K_{\mathrm{a}}^{(\mathrm{MS})}\}$, see Fig. 3.1. Each of these impulse responses originates by a weighted superposition of the impulse responses of a selection of paths, the weighting and selection being determined by the characteristics of the employed antennas, see also Section 2.2.1. In contrast to time diversity or frequency diversity with single port antennas at both stations, novel channels are generated by antenna diversity, and a new dimension of diversity is opened by the following basic effects [BBS97]:

- Introduction of additional paths: Sets of paths not used for the transmission of the signal when employing single port antennas can be made usable.
- Path separation: Portions of the same signal transmitted over different sets of paths can be separately received and processed.

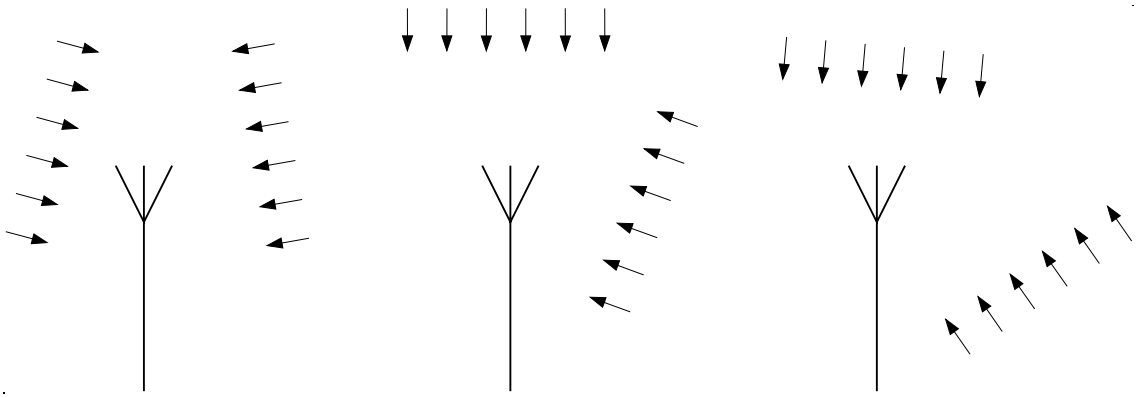

Figure 3.2. Macro structure: Different wavefronts impinge at each of the antenna locations (taken from [BBS97])

- Reuse of paths: Portions of a signal having traveled over a set of paths can be used several times with different complex weightings.

On account of space limitations at the MSs, multi–antenna configurations can be much easier implemented at the BSs. Therefore, only multi–antenna configurations at the BSs are considered in this thesis, with the number of BS antennas termed K_{a}, see also Chapter 2. However, it is known that antenna diversity techniques can be also utilized at the MSs [FBB95].

According to [BBS97], multi–antenna arrangements are classified into macro structures and micro structures. The difference between these two antenna types will be explained next in this chapter by considering the receiver side of multi–antenna systems.

3.3 Antenna types

3.3.1 Macro structures

In the case of macro structures, the K_{a} antennas are so far apart, e.g., tens of wavelengths, that different wavefronts impinge at each of the K_{a} antenna locations, see Fig. 3.2. Macro structures enable spatial macro diversity [SBS66, BSPJ97, Bla98, BBS97] and can be implemented in the form of BS diversity and of remote antennas. By spatial macro diversity additional paths are introduced [BBS97], see the analysis presented in Section 3.2.

In the following, it is shown how the channel impulse responses $\underline{h}^{(k_{\mathrm{a}})}(\tau, t)$, $k_{\mathrm{a}} = 1 \ldots K_{\mathrm{a}}$, result from the differential directional channel impulse responses introduced in Section 2.1, see (2.4), when macro structures are used at the BS. Here, for each of the K_{a} antenna locations a different set of directional channel impulse responses contained in the matrix

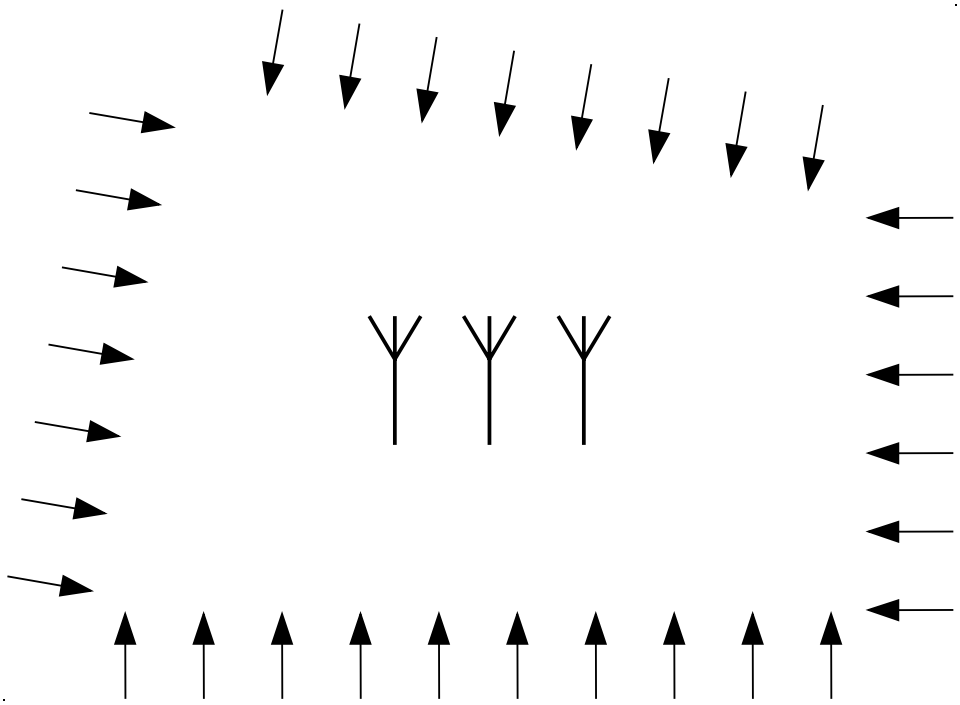

Figure 3.3. Micro structure: Each antenna is hit by the same impinging wavefronts (taken from [BBS97])

$\underline{\mathbf{G}}_{\mathrm{c}}^{(k_a)}(\vartheta, \varphi, \Theta, \Phi, \tau, t)$, $k_{\mathrm{a}} = 1 \ldots K_{\mathrm{a}}$, is valid. If it is assumed that all K_{a} antennas are equal and equally oriented, i.e., the characteristics of each antenna are described by the vector $\underline{\mathbf{f}}_{\mathrm{r}}(\Theta, \Phi)$, see (2.3), then the K_{a} channel impulse responses are expressed as [BBS97]

$$\underline{h}^{(k_{\mathrm{a}})}(\tau, t) = \int\int_{\substack{\vartheta, \Theta = 0 \ldots \pi \\ \varphi, \Phi = 0 \ldots 2\pi}} \int\int \underline{\mathbf{f}}_{\mathrm{r}}^{\mathrm{T}}(\Theta, \Phi) \cdot \underline{\mathbf{G}}_{\mathrm{c}}^{(k_{\mathrm{a}})}(\vartheta, \varphi, \Theta, \Phi, \tau, t) \cdot \underline{\mathbf{f}}_{\mathrm{t}}(\vartheta, \varphi) \cdot \sin\vartheta \cdot d\,\vartheta \cdot \sin\Theta \cdot d\,\Theta \cdot d\,\varphi \cdot \cdot d\,\Phi, \quad k_{\mathrm{a}} = 1 \ldots K_{\mathrm{a}}, \tag{3.1}$$

where $\underline{\mathbf{f}}_{\mathrm{t}}(\vartheta, \varphi)$ is defined in (2.2). As seen from (3.1), the use of macro structures has the effect that K_{a} channel impulse responses exist between the BS and each MS, which experience more or less independent fading processes. Owing to space diversity, the effective fading depths can be reduced by appropriately combining the received signals, e.g., by maximal ratio combining (MRC) [BSPJ97, Bla98, BBS97]. However, depending on the directional properties of the received signals, it is necessary to separate the receiver antennas by rather large distances in order to guarantee for independent fading processes. Concerning the TD–CDMA air interface, which is considered in this thesis, the use of the space diversity concept implemented by the class of macro structures is analyzed in Chapter 9 when comparing the uplink with the downlink performance. In the next section, the class of micro structures is considered. Micro structures are of special interest in this thesis, since they are used for implementing adaptive antennas in the TD–CDMA air interface.

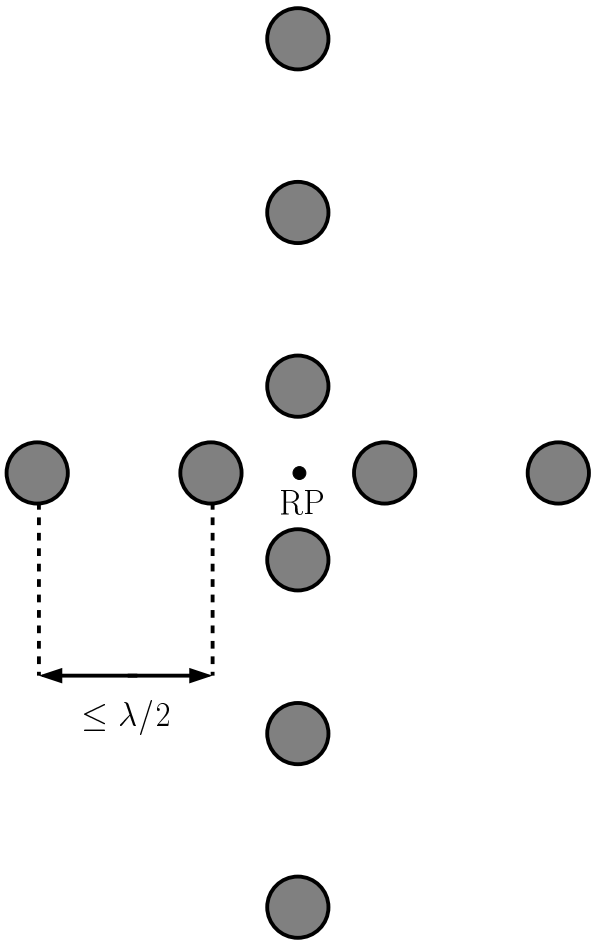

Figure 3.4. Cross configuration with $K_a = 10$ antennas

3.3.2 Micro structures

In the case of micro structures, the K_a antennas are so closely spaced that each of the antennas is hit by the same impinging wavefronts, although with different delays, see Fig. 3.3. Practical concepts which apply micro structures are the following [BBS97]:

- Polarization diversity realized by a set of K_a co–located antennas with different orientations of polarization [ETO93], which results in path separation and in the introduction of additional paths.
- Field component diversity realized by a set of K_a antennas, with different antennas having different characteristics for the electric and magnetic field compo-

nents [Lee82, Lee89]. This leads to path separation and to the introduction of additional paths.

- Directional diversity realized by a set of K_a co–located directional antennas covering different solid angles [BJSB96], which leads to path separation.
- Spatial micro diversity realized by antenna arrays of K_a generally equal and equally oriented antennas at closely spaced locations [FHNP95], which has the effect of path reuse and path separation.

The last of the above mentioned concepts applying micro structures, i.e., spatial micro diversity, is of special interest in this thesis. Practical antenna configurations which belong to the class of micro structures and realize spatial micro diversity are the centro–symmetric array configurations, e.g., uniform linear arrays (ULAs), uniform rectangular arrays (URAs), and cross array configurations. In Fig. 3.4 a cross array configuration is shown with K_a equal to ten antenna elements. The centro–symmetric array configurations are the most important antenna types in this thesis, because they can be used for applying adaptive antenna concepts in TD–CDMA mobile radio systems. Throughout this thesis it is assumed that the used centro–symmetric array configurations are free from errors and perturbations. As mentioned in Section 1.3, in real systems these ideal conditions are practically not met and the system performance is influenced by the amount the real conditions deviate from the ideal ones [God97a]. Therefore, array calibration techniques should always support the operation of adaptive antennas. However, the consideration of array calibration techniques is beyond the scope of this thesis. For a detailed consideration of array calibration the reader is referred to [PN97, PN98, Pen99].

4 Data detection

4.1 General

One of the first problems encountered when dealing with a communications system is the data detection problem [Pro89]. This chapter deals with the problem of data detection in the TD–CDMA uplink. The data detection problem for the downlink case is analyzed separately and compared to the uplink in Chapter 9. It is noted that the analysis of this chapter is done under the assumption that the channel impulse responses are perfectly known at the BS receiver. The problem of channel estimation in TD–CDMA is treated separately in Chapter 5.

4.2 System model

In this section the discrete time system model of a TD–CDMA air interface is described in the equivalent lowpass domain. This system model considers only data block α of a transmitted burst, see Fig. 1.2, since the analysis is similar for data block β [Kle96, Bla98]. It is assumed that TD–CDMA operates synchronously [Kle96, Naß95], and that burst synchronization is achieved by using particular access and synchronization bursts, as it is, e.g., the case in GSM [ETSI88]. First, the system model is derived for the use of a single antenna at the BS. Then, the system model is considered, when multi–antenna configurations are used at the BS receiver. The separate treatment of the single and multi–antenna case will be useful for providing a novel view on the benefits offered by the use of multi–antenna configurations in TD–CDMA, compared to single antennas. In the following, the dimension of vectors as well as the dimensions of matrices are always given in chips, see also Section 1.2 and Fig. 1.2.

When a single antenna is used at the BS receiver, the mobile radio channel can be characterized by K channel impulse responses $\underline{\mathbf{h}}^{(k)}$ of dimension W [SK93], each valid for an individual user k, $k = 1 \ldots K$, see Fig. 4.1 and [Naß95, Ste95, Kle96, Bla98]. With the user specific CDMA codes contained in the vector $\underline{\mathbf{c}}^{(k)}$ [Naß95, Kle96], $k = 1 \ldots K$, of dimension Q, the $KNQ \times KN$ block diagonal CDMA code matrix [PHFB97, PFBP99]

$$\underline{\mathbf{C}}_{\mathrm{u}} = \mathrm{blockdiag}\left[\underline{\mathbf{C}}^{(1)} \ldots \underline{\mathbf{C}}^{(K)}\right], \tag{4.1}$$

$$\underline{\mathbf{C}}^{(k)} = \mathbf{I}^{(N)} \otimes \underline{\mathbf{c}}^{(k)}, \quad k = 1 \ldots K, \tag{4.2}$$

can be formed. In (4.2) $\otimes$ denotes the Kronecker product [Gra81] and $\mathbf{I}^{(N)}$ is the $N \times N$ identity matrix, where N is the number of symbols contained in each data section of the

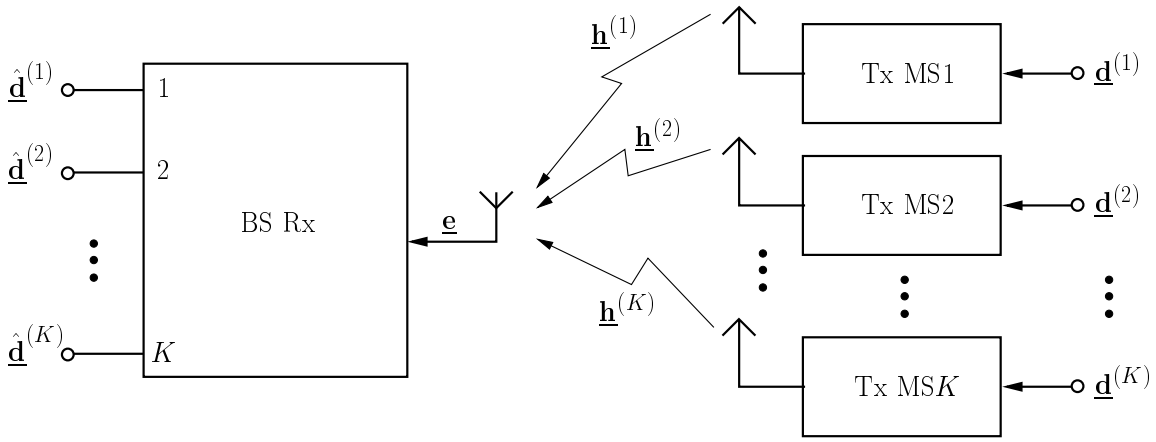

Figure 4.1. Uplink system model for TD–CDMA, when a single antenna is used at the BS

burst transmitted by each user, see Section 1.2 and Fig. 1.2. With the channel impulse responses $\underline{\mathbf{h}}^{(k)}$ the $(NQ+W-1) \times KNQ$ channel impulse response matrix

$$\underline{\mathbf{H}}_{\mathrm{u,s}} = \left[\underline{\mathbf{H}}_{\mathrm{u,s}}^{(1)} \ldots \underline{\mathbf{H}}_{\mathrm{u,s}}^{(K)}\right], \tag{4.3}$$

$$\left[\underline{\mathbf{H}}_{\mathrm{u,s}}^{(k)}\right]_{n+w-1,n} = \begin{cases} \underline{h}_w^{(k)} & , w = 1 \ldots W, \\ & \quad n = 1 \ldots NQ \\ 0 & , \text{otherwise} \end{cases}$$

can be obtained. According to (4.1) and (4.3), the system matrix [Kle96]

$$\underline{\mathbf{A}}_{\mathrm{u,s}} = \underline{\mathbf{H}}_{\mathrm{u,s}}\, \underline{\mathbf{C}}_{\mathrm{u}} \tag{4.4}$$

can be established, when a single antenna is used at the BS receiver. If the data vectors $\underline{\mathbf{d}}^{(k)}$, $k = 1 \ldots K$, of all K users are combined to the total data vector [KB92b, Kle96]

$$\underline{\mathbf{d}} = \left[\underline{\mathbf{d}}^{(1)\mathrm{T}} \ldots \underline{\mathbf{d}}^{(K)\mathrm{T}}\right]^{\mathrm{T}} \tag{4.5}$$

of dimension KN, the received total signal originating from the K simultaneously transmitted data vectors $\underline{\mathbf{d}}^{(k)}$, $k = 1 \ldots K$, is represented by the vector [KB92b, Kle96, Naß95]

$$\underline{\mathbf{e}}_{\mathrm{u,s}} = \underline{\mathbf{A}}_{\mathrm{u,s}}\, \underline{\mathbf{d}} + \underline{\mathbf{n}} \tag{4.6}$$

of dimension $NQ+W-1$, which contains, in addition to the desired signals, an additive vector $\underline{\mathbf{n}}$, which represents the received intercell MAI [KB92b, Kle96].

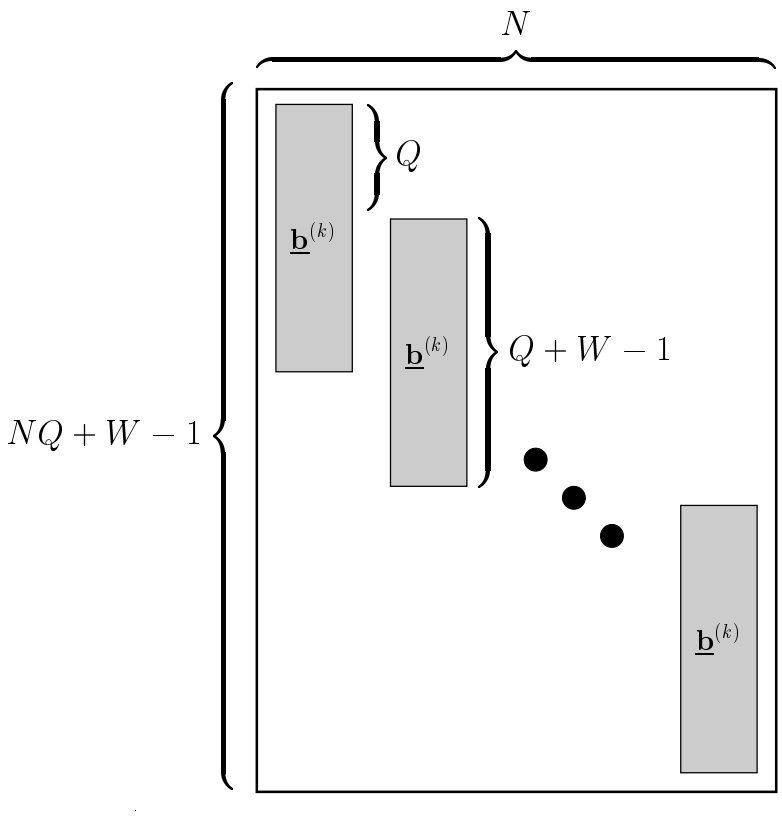

Figure 4.2. Structure of a block $\underline{\mathbf{A}}_{\mathrm{u,s}}^{(k)}$, see (4.9), of the system matrix $\underline{\mathbf{A}}_{\mathrm{u,s}}$, see (4.8)

An equivalent representation of the system model can be obtained by considering the composite channel impulse response $\underline{\mathbf{b}}^{(k)}$, $k = 1 \ldots K$, which is the convolution of the channel impulse response $\underline{\mathbf{h}}^{(k)}$ and the user specific CDMA code $\underline{\mathbf{c}}^{(k)}$ [KB92b, Kle96, Naß95]:

$$\underline{\mathbf{b}}^{(k)} = \underline{\mathbf{c}}^{(k)} * \underline{\mathbf{h}}^{(k)}, \quad k = 1 \ldots K, \tag{4.7}$$

where $*$ denotes the operation of discrete convolution. $\underline{\mathbf{b}}^{(k)}$, $k = 1 \ldots K$, has the dimension $(Q + W - 1)$ [KB92b]. With $\underline{\mathbf{b}}^{(k)}$, $k = 1 \ldots K$, given by (4.7), the system matrix is determined as follows [Kle96]:

$$\underline{\mathbf{A}}_{\mathrm{u,s}} = \left[\underline{\mathbf{A}}_{\mathrm{u,s}}^{(1)} \ldots \underline{\mathbf{A}}_{\mathrm{u,s}}^{(K)} \right] \tag{4.8}$$

$$\left[\underline{\mathbf{A}}_{\mathrm{u,s}}^{(k)} \right]_{(n-1)Q+l,n} = \begin{cases} \underline{b}_l^{(k)}, & n = 1 \ldots N, \\ & l = 1 \ldots Q + W - 1, \\ 0, & \text{otherwise.} \end{cases} \tag{4.9}$$

Note that (4.8) is an expression equivalent to (4.4). In Fig. 4.2 the structure of a block $\underline{\mathbf{A}}_{\mathrm{u,s}}^{(k)}$, $k = 1 \ldots K$, is shown with the respective dimensions, see also [Kle96, Naß95].

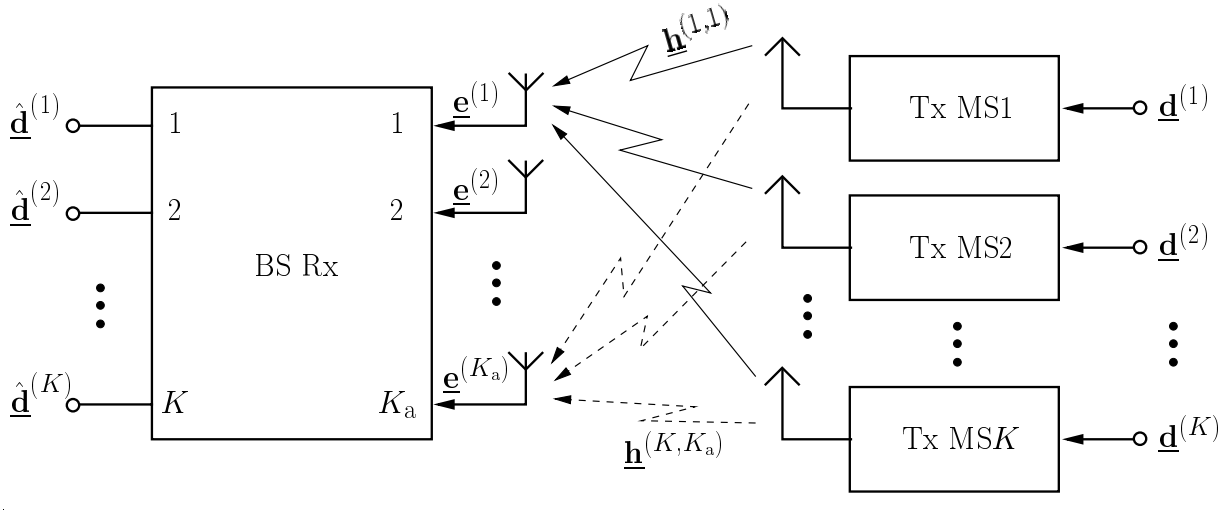

Figure 4.3. Uplink system model for TD–CDMA, when multi–antenna configurations are used at the BS

When multi–antenna configurations of K_a antennas are used at the BS receiver, see for instance Fig. 3.2 and Fig. 3.3, the mobile radio channel can be characterized by KK_a channel impulse responses $\underline{\mathbf{h}}^{(k,k_\mathrm{a})}$ [BBP97, Bla98], $k_\mathrm{a} = 1 \ldots K_\mathrm{a}$, $k = 1 \ldots K$, see Fig. 4.3. This characterization of the mobile radio channel includes the use of any multi–antenna configuration at the BS receiver. With the channel impulse responses $\underline{\mathbf{h}}^{(k,k_\mathrm{a})}$ the $K_\mathrm{a}(NQ + W - 1) \times KNQ$ channel impulse response matrix

$$\underline{\mathbf{H}}_{\mathrm{u,m}} = \left[\underline{\mathbf{H}}_{\mathrm{u,m}}^{(1)\mathrm{T}} \ldots \underline{\mathbf{H}}_{\mathrm{u,m}}^{(K_\mathrm{a})\mathrm{T}}\right]^{\mathrm{T}} \tag{4.10}$$

$$\underline{\mathbf{H}}_{\mathrm{u,m}}^{(k_\mathrm{a})} = \left[\underline{\mathbf{H}}_{\mathrm{u,m}}^{(1,k_\mathrm{a})} \ldots \underline{\mathbf{H}}_{\mathrm{u,m}}^{(K,k_\mathrm{a})}\right]$$

$$\left[\underline{\mathbf{H}}_{\mathrm{u,m}}^{(k,k_\mathrm{a})}\right]_{n+w-1,n} = \begin{cases} \underline{h}_w^{(k,k_\mathrm{a})} & , w = 1 \ldots W, \\ & \quad n = 1 \ldots NQ \\ 0 & , \text{otherwise} \end{cases}$$

can be obtained. Then, according to (4.10) and (4.1), the system matrix

$$\underline{\mathbf{A}}_{\mathrm{u,m}} = \underline{\mathbf{H}}_{\mathrm{u,m}}\, \underline{\mathbf{C}}_{\mathrm{u}} \tag{4.11}$$

can be established when multi–antenna configurations are used at the BS receiver. $\underline{\mathbf{C}}_{\mathrm{u}}$ of (4.1) is valid for both the single antenna and the multi–antenna case, compare (4.4) and (4.11). However, this is not the case for the channel impulse response matrix $\underline{\mathbf{H}}_{\mathrm{u,m}}$, compare (4.3) and (4.10). However, in analogy to the single antenna system, see (4.6), the received total signal from all K_a antennas and all K users is expressed by [BBNS94, BHP97, Bla98]

$$\underline{\mathbf{e}}_{\mathrm{u,m}} = \underline{\mathbf{A}}_{\mathrm{u,m}}\, \underline{\mathbf{d}} + \underline{\mathbf{n}}. \tag{4.12}$$

$\underline{\mathbf{e}}_{\mathrm{u,m}}$ and $\underline{\mathbf{n}}$ of (4.12) have dimension $K_{\mathrm{a}}(NQ+W-1)$. (4.12) includes the use of any multi–antenna configuration at the BS. This explains the fact that data detection in TD–CDMA is treated in a unified manner when antenna diversity is considered, including the use of adaptive antennas, see also Section 1.3.

An equivalent representation of the system model with multi–antenna configurations at the BS receiver can be obtained by the composite channel impulse responses [Naß95]

$$\underline{\mathbf{b}}^{(k,k_{\mathrm{a}})} = \underline{\mathbf{c}}^{(k)} * \underline{\mathbf{h}}^{(k,k_{\mathrm{a}})}, \quad k = 1 \ldots K, \quad k_{\mathrm{a}} = 1 \ldots K_{\mathrm{a}}. \tag{4.13}$$

As in the single antenna system, $\underline{\mathbf{b}}^{(k,k_{\mathrm{a}})}$, $k = 1 \ldots K$, $k_{\mathrm{a}} = 1 \ldots K_{\mathrm{a}}$, has the dimension $(Q+W-1)$. With $\underline{\mathbf{b}}^{(k,k_{\mathrm{a}})}$, $k = 1 \ldots K$, $k_{\mathrm{a}} = 1 \ldots K_{\mathrm{a}}$, given by (4.13) the system matrix of (4.11) is equivalently defined as [Bla98]

$$\underline{\mathbf{A}}_{\mathrm{u,m}} = \begin{bmatrix} \underline{\mathbf{A}}_{\mathrm{u,m}}^{(1,1)} & \cdots & \underline{\mathbf{A}}_{\mathrm{u,m}}^{(K,1)} \\ \vdots & & \vdots \\ \underline{\mathbf{A}}_{\mathrm{u,m}}^{(1,K_{\mathrm{a}})} & \cdots & \underline{\mathbf{A}}_{\mathrm{u,m}}^{(K,K_{\mathrm{a}})} \end{bmatrix} \tag{4.14}$$

$$\left[\underline{\mathbf{A}}_{\mathrm{u,m}}^{(k,k_{\mathrm{a}})}\right]_{(n-1)Q+l,n} = \begin{cases} \underline{b}_l^{(kk_{\mathrm{a}})}, & n = 1 \ldots N, \\ & l = 1 \ldots Q+W-1, \\ 0, & \text{otherwise.} \end{cases} \tag{4.15}$$

The structure of each block $\underline{\mathbf{A}}_{\mathrm{u,m}}^{(k,k_{\mathrm{a}})}$, $k = 1 \ldots K$, $k_{\mathrm{a}} = 1 \ldots K_{\mathrm{a}}$, is the same as the structure of $\underline{\mathbf{A}}_{\mathrm{u,s}}^{(k)}$ shown in Fig. 4.2.

In the following, a novel approach concerning data detection in TD–CDMA is presented. This approach aims at illustrating the main difference between single and multi–antenna systems by comparing the received total signal $\underline{\mathbf{e}}_{\mathrm{u,s}}$ of (4.6) with the received signal $\underline{\mathbf{e}}_{\mathrm{u,m}}$ of (4.12). (4.6) and (4.12) represent linear systems of equations [BPW99], where the number of unknowns, i.e., the KN data symbols of the K simultaneously active users contained in the total data vector $\underline{\mathbf{d}}$, see (4.5), remains unchanged, when more than one antenna is used at the BS receiver. However, the number of components of the received total signal $\underline{\mathbf{e}}_{\mathrm{u,m}}$ in (4.12) is K_{a} times larger than the number of components of the received total signal $\underline{\mathbf{e}}_{\mathrm{u,s}}$ in (4.6). Equivalently stated, although the number of components of the total data vector $\underline{\mathbf{d}}$ remains unchanged when more than one antenna is used at the BS receiver, the number of equations becomes K_{a} times larger. This increase of the number of equations while the number of unknowns remains unchanged is known as the problem of appending additional rows to a linear system of equations in estimation theory and computational analysis [Gol69, LH74], and leads to an improvement of the estimation or the computation of the vector containing the unknown parameters. Concerning (4.6) and (4.12), the previous statement means that an improved estimation quality of the total data vector $\underline{\mathbf{d}}$ is expected when (4.12) is applied, compared to the case where (4.6) is used. The improvement of the estimation quality of $\underline{\mathbf{d}}$ when multi–antenna configurations

are used is valid for both macro and micro structures, see Section 3.3 and Section 3.4, respectively [BPW99]. However, the amount of the improvement achieved by each configuration depends on the mobile radio channel type in which the system operates [BPW99]. In Sections 4.3 and 4.4 it is shown that the increase of the number of equations while keeping the number of unknowns unchanged can be directly translated into a more favourable structure of the matrix $\underline{\mathbf{A}}_{\mathrm{u,m}}^{*\mathrm{T}}\underline{\mathbf{A}}_{\mathrm{u,m}}$, see (4.11), valid for multi–antenna systems, compared to the matrix $\underline{\mathbf{A}}_{\mathrm{u,s}}^{*\mathrm{T}}\underline{\mathbf{A}}_{\mathrm{u,s}}$, see (4.4), valid for single antenna systems. This more favourable structure directly depends on the channel type where the multi–antenna configuration is used. Before proceeding with the investigation of the influence of the channel type on the structure of $\underline{\mathbf{A}}_{\mathrm{u,m}}$, though, the data detection algorithms for TD–CDMA are considered in the following section, where the importance of the above mentioned matrices $\underline{\mathbf{A}}_{\mathrm{u,s}}^{*\mathrm{T}}\underline{\mathbf{A}}_{\mathrm{u,s}}$ and $\underline{\mathbf{A}}_{\mathrm{u,m}}^{*\mathrm{T}}\underline{\mathbf{A}}_{\mathrm{u,m}}$ for single and multi–antenna systems, respectively, is illustrated.

4.3 Detection algorithms

4.3.1 Preliminaries

In this section the main types of equalizer algorithms developed for TD–CDMA are described. For a detailed analysis of the different equalizers applicable to TD–CDMA the reader is referred to [Kle96]. The task of the equalization or data detection algorithms is to determine an estimate $\hat{\underline{\mathbf{d}}}$ of the total data vector $\underline{\mathbf{d}}$, see (4.5), based on the received total signal $\underline{\mathbf{e}}_{\mathrm{u,s}}$ of (4.6) or $\underline{\mathbf{e}}_{\mathrm{u,m}}$ of (4.12). In TD–CDMA mobile radio systems the data detection algorithms require a priori information about [Kle96]

- the CDMA codes $\underline{\mathbf{c}}^{(k)}$, $k = 1 \ldots K$, of all users, see (4.2),
- the channel impulse responses $\underline{\mathbf{h}}^{(k)}$, $k = 1 \ldots K$, for the single antenna case, see (4.3), or $\underline{\mathbf{h}}^{(k,k_{\mathrm{a}})}$, $k = 1 \ldots K$, $k_{\mathrm{a}} = 1 \ldots K_{\mathrm{a}}$, for the multi–antenna case, see (4.10),
- the data symbol alphabet $\underline{V}_{\mathrm{d}}$ of size $\mid V_{\mathrm{d}} \mid$ equal to M,
- in some cases the covariance matrix

$$\underline{\mathbf{R}}_{\mathrm{d}} = \mathrm{E}\left\{\underline{\mathbf{d}}\ \underline{\mathbf{d}}^{*\mathrm{T}}\right\} \tag{4.16}$$

  of the total data vector $\underline{\mathbf{d}}$, see (4.5), and
- in some cases the covariance matrix

$$\underline{\mathbf{R}}_{\mathrm{n}} = \mathrm{E}\left\{\underline{\mathbf{n}}\ \underline{\mathbf{n}}^{*\mathrm{T}}\right\} \tag{4.17}$$

  of the additive intercell MAI vector $\underline{\mathbf{n}}$, see (4.6) and (4.12).

The data detection algorithms for TD–CDMA can be divided into three general categories:

- Maximum likelihood algorithms,
- linear algorithms, and
- algorithms with decision feedback.

As already mentioned in Section 1.2, one of the most important characteristics of TD–CDMA is the use of JD. Therefore, in the following we concentrate on JD techniques [KB92b, Kle96], and the most important data detection algorithms derived for TD–CDMA are described.

4.3.2 Maximum likelihood algorithms

In this section two optimum algorithms performing JD are briefly described. According to the approach of [Kay93], these algorithms belong to the classical estimation algorithms, since the total data vector $\underline{\mathbf{d}}$ of (4.5) to be estimated is unknown, but deterministic. It is noted that these algorithms are an extension of the algorithms presented in [KIH82a, KIH83, Ver86] for the single path channel. For a more detailed analysis the reader is referred to [Kle96].

The first optimum equalizer described in this section is the maximum likelihood sequence estimator (MLSE). The MLSE minimizes the sequence error probability, which is equivalent to maximizing the conditional probability $\mathrm{Prob}\{\underline{\mathbf{d}} \mid \underline{\mathbf{e}}\}$ with respect to the total data vector $\underline{\mathbf{d}}$ when the received total vector $\underline{\mathbf{e}}$ is given at the receiver [Kle96]. $\underline{\mathbf{e}}$ stands for one of the received signals of (4.6) or (4.12) for the single antenna or the multi–antenna case, respectively. The estimate determined by the MLSE is given by [For72, Ett76, Ver86, Kle96]

$$\hat{\underline{\mathbf{d}}}_{\mathrm{MLSE}} = \arg \max_{\underline{\mathbf{d}} \in \underline{V}_{\mathrm{d}}^{KN}} \mathrm{Prob}\{\underline{\mathbf{d}} \mid \underline{\mathbf{e}}\} = \arg \min_{\underline{\mathbf{d}} \in \underline{V}_{\mathrm{d}}^{KN}} \mid \underline{\mathbf{e}} - \underline{\mathbf{A}}\,\underline{\mathbf{d}} \mid^2, \tag{4.18}$$

where arg denotes the argument of the function, and $\underline{\mathbf{A}}$ expresses one of the system matrices $\underline{\mathbf{A}}_{\mathrm{u,s}}$, see (4.4), or $\underline{\mathbf{A}}_{\mathrm{u,m}}$, see (4.11), for the single antenna or the multi–antenna case, respectively. The MLSE minimizes the squared Euclidean distance between the received vector $\underline{\mathbf{e}}$ and the noise–free received vector $\underline{\mathbf{A}}\,\underline{\mathbf{d}}$. The estimated vector $\hat{\underline{\mathbf{d}}}_{\mathrm{MLSE}}$ is the total data vector, which has most likely been transmitted among all possible transmitted data vectors [Kle96]. The MLSE defined by (4.18) can be realized by using an extended version of the Viterbi algorithm [Ett76, Ver86], the number of states of which is determined by [Kle96]

1. the maximum number of data symbols which contribute to a single sample $\underline{e}_i$, $i = 1 \ldots NQ + W - 1$ for the single antenna and $i = 1 \ldots K_{\mathrm{a}}(NQ + W - 1)$ for the multi–antenna case, of the received vector $\underline{\mathbf{e}}$, which form the ISI, and

2. the number of simultaneously active users K, which form the MAI in CDMA systems, see also Section 2.2.2 and Section 3.2.

For K equal to eight users, for the size of the symbol alphabet M equal to four, and K_{a} equal to one, the number of states of the Viterbi algorithm takes on extremely high values (in the order of 10^{13}). This implies that the unrealistically high computational cost of the MLSE makes its implementation with today's hardware impossible [Kle96]. Therefore, suboptimum linear equalizer algorithms have been developed for TD–CDMA, which are feasible in realtime, see Section 4.3.3.

The second optimum equalizer performing JD for TD–CDMA mobile radio systems is the maximum likelihood symbol–by–symbol estimator (MLSSE). The MLSSE minimizes the symbol error probability, which is equivalent to maximizing the conditional probability Prob $\left\{\underline{d}_j \mid \underline{\mathbf{e}}\right\}$ for each data symbol $\underline{d}_j$ when the received total vector $\underline{\mathbf{e}}$ is provided at the receiver [Kle96]. The estimate determined by the MLSSE is given by [HR90, Kle96]

$$\underline{\hat{d}}_{\mathrm{MLSSE},j} = \arg \max_{\underline{d}_j \in \underline{V}_{\mathrm{d}}} \mathrm{Prob}\left\{\underline{d}_j \mid \underline{\mathbf{e}}\right\}, \quad j = 1 \ldots KN. \tag{4.19}$$

$\underline{\hat{d}}_{\mathrm{MLSSE},j}$, $j = 1 \ldots KN$, see (4.19), is the data symbol which has most likely been transmitted among all possible transmitted data symbols [Kle96]. The MLSSE performs slightly better than the MLSE, but is even more complex than the MLSE [Kle96]. Therefore, as in the case of the MLSE, the unrealistically high computational cost of the MLSSE excludes its realtime implementation.

4.3.3 Linear and decision feedback algorithms

4.3.3.1 General

The unrealistically high computational cost for implementing the optimum MLSE and MLSSE, see Section 4.3.2, has led to the development of suboptimum estimators for TD–CDMA [Kle96]. In contrast to the optimum estimators of Section 4.3.2, the estimators presented in [Kle96] are suboptimum in the sense that they deliver estimates of the total data vector $\underline{\mathbf{d}}$ of (4.5) without using the constraint that $\underline{\mathbf{d}}$ is taken from a specific data symbol alphabet $\underline{V}_{\mathrm{d}}$ during the estimation process [Kle96, Kay93]. However, they can be implemented with today's hardware and their performance meets the specifications for the realtime operation of TD–CDMA [MSW97b, BEM98a, BEM98b].

The suboptimum data detection algorithms developed for TD–CDMA can be classified into two main categories [Kle96]:

- Linear algorithms and

- algorithms with decision feedback.

A thorough investigation of the algorithms with decision feedback applicable to TD–CDMA can be found in [Kle96]. The linear algorithms are [Kle96]

- the decorrelating matched filter (DMF),
- the zero forcing block linear equalizer (ZF–BLE), and
- the minimum mean square error block linear equalizer (MMSE–BLE).

From the above mentioned linear algorithms without feedback which perform JD, the ZF–BLE is the state of the art algorithm for TD–CDMA with single antennas [MSW97b], which makes JD one of the main features of the TD–CDMA mobile radio air interface, see also Section 1.2. The ZF–BLE outperforms the DMF and performs equally well with the MMSE–BLE [Kle96], whereas the computational cost of the ZF–BLE is smaller than the one of the MMSE–BLE. Therefore, the ZF–BLE is exclusively considered in this thesis. Based on the ZF–BLE, a novel view on the JD process in TD–CDMA is presented in the following section.

4.3.3.2 ZF–BLE

The received total signal in TD–CDMA is determined by one of the equations (4.6) or (4.12), see Section 4.2. Here, in order to deal generally with the ZF–BLE, we express the received signal as

$$\underline{\mathbf{e}} = \underline{\mathbf{A}}\ \underline{\mathbf{d}} + \underline{\mathbf{n}}, \tag{4.20}$$

where $\underline{\mathbf{e}}$ stands for one of the received total signals of (4.6) or (4.12), and the system matrix $\underline{\mathbf{A}}$ expresses one of the system matrices $\underline{\mathbf{A}}_{\mathrm{u,s}}$ of (4.6) or $\underline{\mathbf{A}}_{\mathrm{u,m}}$ of (4.12), respectively, see also Section 4.3.2. In (4.20), $\underline{\mathbf{e}}$ is known at the receiver. This is also approximately true for the system matrix $\underline{\mathbf{A}}$ with the accuracy of $\underline{\mathbf{A}}$ depending on the accuracy of the channel impulse response estimates [BPW99]. As already mentioned in Section 4.1, throughout this chapter the channel impulse responses are assumed to be perfectly known at the receiver. Consequently, $\underline{\mathbf{A}}$ is also assumed to be perfectly known. Further, the vectors $\underline{\mathbf{d}}$ and $\underline{\mathbf{n}}$ in (4.20) are unknown. However, the covariance matrix $\underline{\mathbf{R}}_{\mathrm{n}}$ of $\underline{\mathbf{n}}$, see (4.17), shall be assumed to be known. The task of data detection consists in determining $\underline{\mathbf{d}}$, see (4.5), from (4.20). This equation can be considered as a linear system of equations for the KN unknown data symbols contained in $\underline{\mathbf{d}}$, see also the analysis of Section 4.2. Then, by applying the ZF–BLE to perform JD, a linear estimate [Kle96, Naß95, Bla98]

$$\hat{\underline{\mathbf{d}}} = \left(\underline{\mathbf{A}}^{*\mathrm{T}}\underline{\mathbf{R}}_{\mathrm{n}}^{-1}\underline{\mathbf{A}}\right)^{-1}\underline{\mathbf{A}}^{*\mathrm{T}}\underline{\mathbf{R}}_{\mathrm{n}}^{-1}\underline{\mathbf{e}} = \underline{\mathbf{M}}\ \underline{\mathbf{e}} \tag{4.21}$$

for $\underline{\mathbf{d}}$ can be obtained from (4.20), where [POB99]

$$\underline{\mathbf{M}} = \left(\underline{\mathbf{A}}^{*\mathrm{T}} \underline{\mathbf{R}}_{\mathrm{n}}^{-1} \underline{\mathbf{A}}\right)^{-1} \underline{\mathbf{A}}^{*\mathrm{T}} \underline{\mathbf{R}}_{\mathrm{n}}^{-1}. \tag{4.22}$$

If the expression for $\underline{\mathbf{e}}$ in (4.20) is substituted into (4.21), the equation

$$\hat{\underline{\mathbf{d}}} = \underline{\mathbf{d}} + \underline{\mathbf{M}}\ \underline{\mathbf{n}} = \underline{\mathbf{d}} + \underline{\mathbf{n}}_{\mathrm{out}} \tag{4.23}$$

is valid, where

$$\underline{\mathbf{n}}_{\mathrm{out}} = \underline{\mathbf{M}}\ \underline{\mathbf{n}}. \tag{4.24}$$

(4.23) and (4.24) offer a novel view on the JD process in TD–CDMA, when the channel impulse responses $\underline{\mathbf{h}}^{(k)}$, $k = 1 \ldots K$, see (4.3), or $\underline{\mathbf{h}}^{(k,k_{\mathrm{a}})}$, $k = 1 \ldots K$, $k_{\mathrm{a}} = 1 \ldots K_{\mathrm{a}}$, see (4.10), for the single antenna or the multi–antenna case, respectively, are known at the receiver [BPW99, POB99]. The JD process according to (4.23) is transparent for the data transmitted by the users assigned to the considered BS [BPW99, POB99]. The only effect of the JD process is a transformation of the input intercell MAI vector $\underline{\mathbf{n}}$, see (4.20), into an output MAI vector $\underline{\mathbf{n}}_{\mathrm{out}}$ according to (4.24) [BPW99, POB99]. This transformation depends on the information contained in the matrix $\underline{\mathbf{M}}$, i.e., the channel type, the CDMA codes $\underline{\mathbf{c}}^{(k)}$, $k = 1 \ldots K$, and the used antenna configuration at the BS receiver, and not on the way the user data are coded, interleaved, and modulated [BPW99, POB99]. Since (4.23) and (4.24) are also valid for the case where adaptive antennas are used [Bla98], one should not explicitly think of DOAs and beamforming techniques performed at the BS receiver, when $\underline{\mathbf{M}}$, see (4.22), is applied to the received signal of (4.20). If the channel impulse responses for the links between each user and each antenna are known at the BS receiver, see Fig. 4.1 and Fig. 4.3, the ZF–BLE performs optimally among all linear detectors which perform JD. It is noted, though, that the equivalent receiver representation of [BHP97, PWBB98], which explicitly includes the beamformers for the DOAs of each user, is valid. However, since the representation of [BHP97, PWBB98] departs considerably from the straightforward explanation of the effect of JD in TD–CDMA offered by (4.23) and (4.24), that representation is not followed in this thesis. Moreover, the straightforward explanation of the effect of JD of according to (4.23) and (4.24) constitutes the basic step for the formulation of a novel simulation concept for TD–CDMA, including the use of adaptive antennas, which offers a reduced computational cost compared to the original simulation concept developed for TD–CDMA [Naß95, Bla98]. This novel simulation concept is presented in detail in Chapter 6, where the effect of channel estimation on the JD process is also included.

Additionally to the novel view on the JD process in TD–CDMA given by (4.23) and (4.24), a relatively straightforward method for evaluating the system performance is presented in what follows. To this end, the covariance matrix $\underline{\mathbf{R}}_{\mathrm{n,out}}$ of the vector $\underline{\mathbf{n}}_{\mathrm{out}}$ of (4.24) is used, which is defined as [Kle96, Bla98]

$$\underline{\mathbf{R}}_{\mathrm{n,out}} = \mathrm{E}\left\{\underline{\mathbf{n}}_{\mathrm{out}}\ \underline{\mathbf{n}}_{\mathrm{out}}^{*\mathrm{T}}\right\} = \left(\underline{\mathbf{A}}^{*\mathrm{T}} \underline{\mathbf{R}}_{\mathrm{n}}^{-1} \underline{\mathbf{A}}\right)^{-1}. \tag{4.25}$$

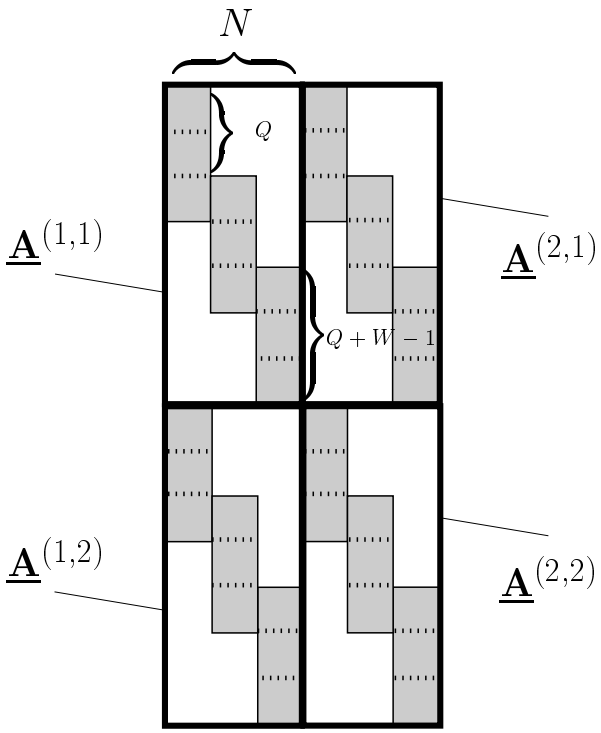

Figure 4.4. Structure of the matrix $\underline{\mathbf{A}}$; $K_\mathrm{a} = 2$, $K = 2$, $N = 3$, $Q = 2$, $W = 2$

In what follows in this chapter it is assumed that the additive intercell MAI noise vector $\underline{\mathbf{n}}$ is white and Gaussian distributed, i.e., $\underline{\mathbf{R}}_\mathrm{n}$ of (4.17) is expressed as [Ste95, Naß95, Kle96]

$$\underline{\mathbf{R}}_\mathrm{n} = \sigma^2 \mathbf{I}^{(K_\mathrm{a}(NQ+W-1))}, \tag{4.26}$$

where σ^2 denotes the noise power, which is assumed to be equal for all components of $\underline{\mathbf{n}}$. The influence of the intercell MAI covariance matrix $\underline{\mathbf{R}}_\mathrm{n}$ on the performance of TD–CDMA is analyzed in detail in Section 7.4. For the scope of this chapter, if (4.26) is valid, $\underline{\mathbf{R}}_\mathrm{n,out}$ takes the form

$$\underline{\mathbf{R}}_\mathrm{n,out} = \sigma^2 \, \underline{\mathbf{Z}}^{-1}, \tag{4.27}$$

with

$$\underline{\mathbf{Z}} = \underline{\mathbf{A}}^{*\mathrm{T}} \, \underline{\mathbf{A}}. \tag{4.28}$$

As it is shown in detail in Chapter 6, $\underline{\mathbf{R}}_\mathrm{n,out}$ of (4.27), and consequently the matrix $\underline{\mathbf{Z}}$ of (4.28), plays an important role for the signal–to–noise ratio (SNR) degradation in TD–CDMA, which is the key quantity to characterize the system performance [BPW99] according to the following rule: If the diagonal elements of $\underline{\mathbf{Z}}^{-1}$ are small, a favourable system performance is obtained, whereas large values of the diagonal elements of $\underline{\mathbf{Z}}^{-1}$ lead directly to degradations of the system performance, see Chapter 6 for a detailed analysis. Therefore, because of the importance of $\underline{\mathbf{Z}}$, see (4.28), for TD–CDMA, in the rest of this section it is explained how the structure of $\underline{\mathbf{Z}}$ influences the behaviour of TD–CDMA.

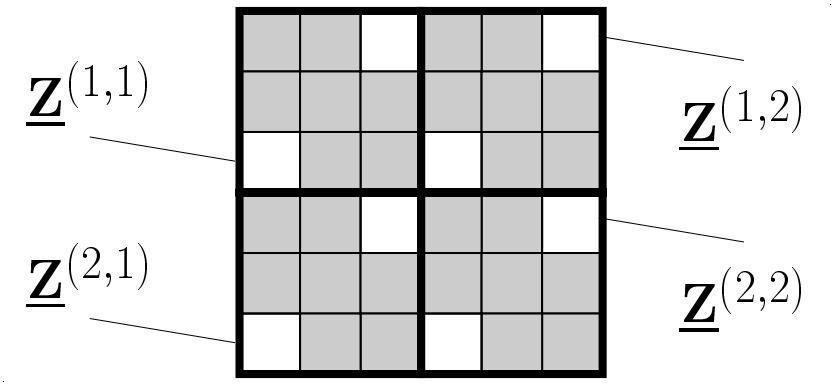

Figure 4.5. Structure of the matrix $\underline{\mathbf{Z}}$; $K_{\mathrm{a}} = 2$, $K = 2$, $N = 3$, $Q = 2$, $W = 2$

Setting out from the structure of the system matrix $\underline{\mathbf{A}}$, see (4.4), (4.11) and Fig. 4.2, the matrix $\underline{\mathbf{Z}}$ of (4.28) is Hermitian and consists of K^2 blocks $\underline{\mathbf{Z}}^{(k_1,k_2)}$, $k_1 = 1 \ldots K$, $k_2 = 1 \ldots K$, of dimensions $N \times N$ each. The diagonal blocks $\underline{\mathbf{Z}}^{(k,k)}$, $k = 1 \ldots K$, are Toeplitz and Hermitian matrices, whereas the off–diagonal blocks $\underline{\mathbf{Z}}^{(k_1,k_2)}$, $k_1 \neq k_2$, are only Toeplitz. Figs. 4.4 and 4.5 illustrate the structure of the system matrix $\underline{\mathbf{A}}$ and the matrix $\underline{\mathbf{Z}}$, respectively, for

$$K_{\mathrm{a}} = 2, \quad K = 2, \quad N = 3, \quad Q = 2, \quad W = 2, \tag{4.29}$$

where the shaded regions in Figs. 4.5 and 4.5 indicate that the respective matrix element is different from zero. However, since

$$NQ + W - 1 >> Q + W - 1 \tag{4.30}$$

is valid in TD–CDMA [Naß95, Kle96, Bla98], the blocks $\underline{\mathbf{Z}}^{(k_1,k_2)}$, $k_1 = 1 \ldots K$, $k_2 = 1 \ldots K$, of $\underline{\mathbf{Z}}$, see (4.28), are rather sparse matrices and, in the general case where multi–antenna configurations are employed at the BS receiver, they can be expressed in the following fashion:

$$\underline{\mathbf{Z}}^{(k_1,k_2)} = \sum_{k_{\mathrm{a}}=1}^{K_{\mathrm{a}}} \underline{\mathbf{A}}^{(k_1,k_{\mathrm{a}})*\mathrm{T}} \underline{\mathbf{A}}^{(k_2,k_{\mathrm{a}})}, \quad k_1 = 1 \ldots K, \; k_2 = 1 \ldots K. \tag{4.31}$$

Then, the following Theorem holds, the proof of which is given in Appendix B.1:

Theorem: If the diagonal elements of the matrix $\underline{\mathbf{Z}}$, see (4.28), are multiplied by a constant factor l greater than one, with the resulting matrix denoted as $\underline{\mathbf{Z}}_{\mathrm{l}}$, the diagonal elements of $\underline{\mathbf{Z}}_{\mathrm{l}}^{-1}$ take lower values compared to the values of the diagonal elements of $\underline{\mathbf{Z}}^{-1}$.

According to this Theorem, if the elements of the off–diagonal blocks $\underline{\mathbf{Z}}^{(k_1,k_2)}$, $k_1 \neq k_2$, see for instance the blocks $\underline{\mathbf{Z}}^{(1,2)}$ and $\underline{\mathbf{Z}}^{(2,1)}$ of Fig. 4.5, take small values compared to the values of the elements of the diagonal blocks $\underline{\mathbf{Z}}^{(k,k)}$, $k = 1 \ldots K$, see the blocks $\underline{\mathbf{Z}}^{(1,1)}$ and

$\underline{\mathbf{Z}}^{(2,2)}$ of Fig. 4.5, i.e., if $\underline{\mathbf{Z}}$ has a structure close to the block diagonal structure [Gant91], it is expected that the diagonal elements of the inverse matrix $\underline{\mathbf{Z}}^{-1}$, which determine the SNR degradation and consequently the system performance [BPW99], take also small values and the system performance is favourable. In this case, the matrix $\underline{\mathbf{Z}}$ is said to have favourable structural properties. In contrast to this situation, if the elements of the off–diagonal blocks $\underline{\mathbf{Z}}^{(k_1,k_2)}$, $k_1 \neq k_2$, take large values compared to the values of the elements of the diagonal blocks $\underline{\mathbf{Z}}^{(k,k)}$, $k = 1 \ldots K$, i.e., if the structure of $\underline{\mathbf{Z}}$ differs considerably from the block diagonal structure [Gant91], it is expected that the diagonal elements of $\underline{\mathbf{Z}}^{-1}$ take also large values and the system performance is degraded. In this case, the matrix $\underline{\mathbf{Z}}$ is said to have unfavourable structural properties. The unfavourable structure of $\underline{\mathbf{Z}}$, see (4.28) and Fig. 4.5, is closely related to the code–channel mismatch problem, which is treated in detail in Section 7.2. In Section 4.4 the conditions under which the matrix $\underline{\mathbf{Z}}$ has favourable structural properties, or, equivalently, offers a favourable system behaviour, are investigated. Goal of the investigations is the illustration of the benefits of adaptive antennas compared to single antennas.

4.4 Benefits of adaptive antennas

4.4.1 Introduction

In Section 3.4 centro–symmetric array configurations are described. Centro–symmetric array configurations belong to the class of micro structures, and they are used for applying adaptive antennas in mobile radio, see also Section 3.4. In this section, the benefits offered by adaptive antennas are investigated both theoretically and by simulations for the two channel types introduced in Section 2.4, i.e., the large cell and the small cell channel type. In the simulations the modified COST 207 channel models, see Section 2.3.2, are used, which, in contrast to the more sophisticated UKL 2 directional channel models, see Section 2.3.3, enable the investigation of adaptive antennas in a tutorial manner, see also the analysis of Section 1.3.

4.4.2 Large cell channel type

When centro–symmetric array configurations are used in the large cell channel type, see Section 2.4.2, there is a rather easy procedure for evaluating the benefits of adaptive antennas in TD–CDMA. Without loss of generality we assume that the number of DOAs ${K_\mathrm{d}}^{(k)}$ from user k, $k = 1 \ldots K$, equals one, see Section 2.4.2 and Fig. 2.6. In this case, the channel impulse response matrix $\underline{\mathbf{H}}^{(k,k_\mathrm{a})}$, see (4.10), can be written in the following fashion [PFBP99]

$$\underline{\mathbf{H}}^{(k,k_\mathrm{a})} = \underline{a}_{\mathrm{s},k_\mathrm{a}}^{(k)} \cdot \underline{\mathbf{H}}_\mathrm{d}^{(k)}, \tag{4.32}$$

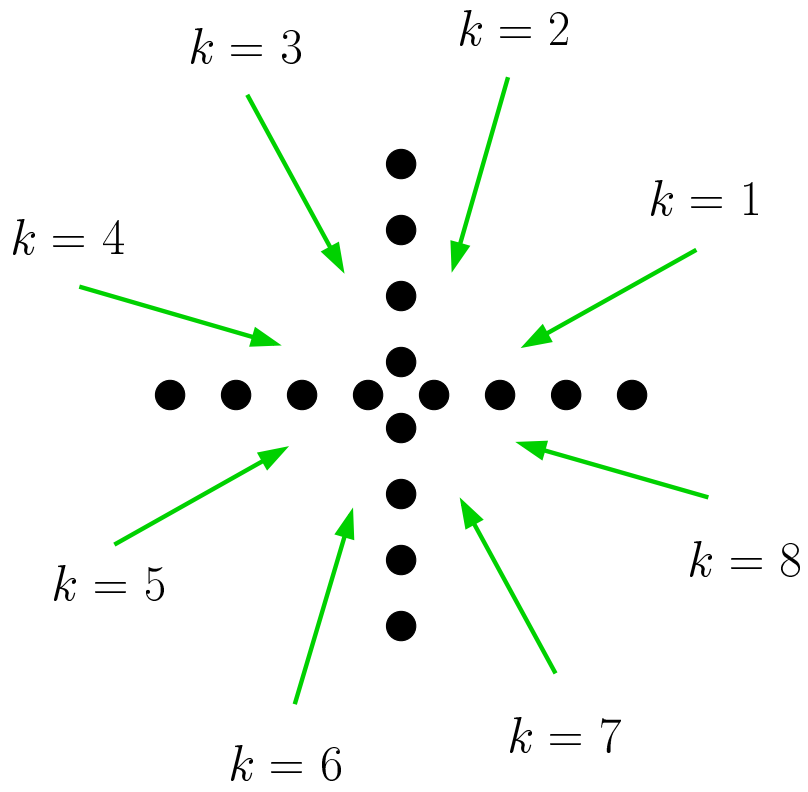

Figure 4.6. Considered spatial scenario for the large cell channel type; modified COST 207 RA channel model; $K = 8$ users

where $\underline{a}_{\mathrm{s},k_\mathrm{a}}^{(k)}$ denotes the k_a–th component of the user specific steering vector $\underline{\mathbf{a}}_\mathrm{s}^{(k)}$ [Haa97a, BHP97], and $\underline{\mathbf{H}}_\mathrm{d}^{(k)}$ is the user specific channel impulse response matrix which contains the directional channel impulse response, see Section 2.4.2, which pertains to user k, $k = 1 \ldots K$, and is measured by a single omnidirectional antenna positioned at the RP of the centro–symmetric array configuration used at the BS [BPW99, Bla98]. Then, the (k, k_a)–th block $\underline{\mathbf{A}}^{(k,k_\mathrm{a})}$, see (4.14) and Fig. 4.4, of the system matrix $\underline{\mathbf{A}}$ is written as

$$\underline{\mathbf{A}}^{(k,k_\mathrm{a})} = \underline{a}_{\mathrm{s},k_\mathrm{a}}^{(k)} \cdot \underline{\mathbf{A}}_\mathrm{d}^{(k)}, \tag{4.33}$$

where

$$\underline{\mathbf{A}}_\mathrm{d}^{(k)} = \underline{\mathbf{H}}_\mathrm{d}^{(k)} \, \underline{\mathbf{C}}^{(k)}, \tag{4.34}$$

see (4.32) and (4.2). According to (4.33), (4.31) takes the simple form

$$\underline{\mathbf{Z}}^{(k_1,k_2)} = \underline{\mathbf{a}}_\mathrm{s}^{(k_1)*\mathrm{T}} \underline{\mathbf{a}}_\mathrm{s}^{(k_2)} \underline{\mathbf{A}}_\mathrm{d}^{(k_1)*\mathrm{T}} \underline{\mathbf{A}}_\mathrm{d}^{(k_2)}, \quad k_1,\ k_2 = 1 \ldots K. \tag{4.35}$$

In the worst case, where all user signals impinge from the same DOA,

$$\underline{\mathbf{a}}_\mathrm{s}^{(k_1)*\mathrm{T}} \underline{\mathbf{a}}_\mathrm{s}^{(k_2)} = K_\mathrm{a}, \quad k_1,\ k_2 = 1 \ldots K, \tag{4.36}$$

holds. Therefore, according to (4.35), a centro–symmetric array configuration offers a gain factor equal to K_a compared to single antenna systems, since in this case the elements of the matrix $\underline{\mathbf{Z}}$ valid for the centro–symmetric array configuration are K_a times larger than the corresponding elements of the matrix $\underline{\mathbf{Z}}$ valid for a single antenna. However, in any other case of the spatial distribution of the user signals in the large cell channel type, an additional gain factor is observed, since the values of the elements of the off–diagonal blocks of $\underline{\mathbf{Z}}$, see (4.28), take smaller values compared to the elements of the diagonal blocks, see also the Theorem of Section 4.3.3.2. This is due to the fact that (4.36) holds only in the case where the signals from users k_1 and k_2 impinge on the BS receiver from the same DOA. In any other case, $\underline{\mathbf{a}}_s^{(k_1)*T}\underline{\mathbf{a}}_s^{(k_2)}$, $k_1 \neq k_2$, delivers a smaller value than K_a, cf. (4.36). As a final remark, it is noted that a simple channel assignment strategy, which explicitly takes into account the DOAs of the impinging signals, would lead to a more favourable behaviour of TD–CDMA in the large cell channel type, compared to the case where the information about the DOAs is not explicitly taken into account, see Section 7.3 for a detailed analysis.

In order to illustrate the benefits of adaptive antennas in TD–CDMA for the large cell channel type, the scenario depicted in Fig. 4.6 is considered. There are K equal to eight users active in the same frequency band and time slot and, moreover, they are spatially ideally separated, see Fig. 4.6. The chip duration T_c equals 0.5 μs. Further, the modified COST207 RA channel model introduced in Section 2.3.2, which belongs to the large cell channel type, is used. A cross array configuration with K_a equal to 16 antennas, see Fig. 4.6, is assumed to be used at the BS receiver. Each user transmits N equal to ten data symbols and the channel impulse responses are assumed to be perfectly known at the BS. In the following, a single time slot is considered. For the considered scenario, the signal from user $k = 8$ is received with the highest energy, whereas the signal from user $k = 3$ is received with the lowest energy. In order to enable a direct comparison of the single antenna with the adaptive antenna case, the normalized matrix $\underline{\tilde{\mathbf{Z}}}$ is introduced, the elements of which are defined according to

$$\left[\underline{\tilde{\mathbf{Z}}}\right]_{i,j} = \frac{1}{\max\limits_{i,j} \mid [\underline{\mathbf{Z}}]_{i,j} \mid} [\underline{\mathbf{Z}}]_{i,j}\,, \quad i,j = 1 \ldots KN. \tag{4.37}$$

In Figs. 4.7 and 4.8 the absolute values of the elements of the blocks $\underline{\tilde{\mathbf{Z}}}^{(3,3)}$ and $\underline{\tilde{\mathbf{Z}}}^{(3,8)}$, respectively, are shown, when a single antenna is used at the BS receiver. In Figs. 4.9 and 4.10 the respective values are shown, when a cross array configuration with K_a equal to 16 antennas, see Fig. 4.6, is used at the BS receiver. From Figs. 4.7 and 4.8 the unfavourable structure of the matrix $\underline{\tilde{\mathbf{Z}}}$, see (4.37), and consequently of the matrix $\underline{\mathbf{Z}}$ of (4.28), is obvious, when a single antenna is used at the receiver, since the elements of the off–diagonal block $\underline{\tilde{\mathbf{Z}}}^{(3,8)}$ have large values compared to the elements of the diagonal block $\underline{\tilde{\mathbf{Z}}}^{(3,3)}$. In contrast to this situation, the structure of the matrix $\underline{\tilde{\mathbf{Z}}}$ of (4.37) is more favourable, when adaptive antennas are used at the BS receiver, see Figs. 4.9 and 4.10. This favourable matrix structure depends on the favourable spatial separation between the users, see the spatial scenario of Fig. 4.6 and (4.35). Finally, in order to illustrate

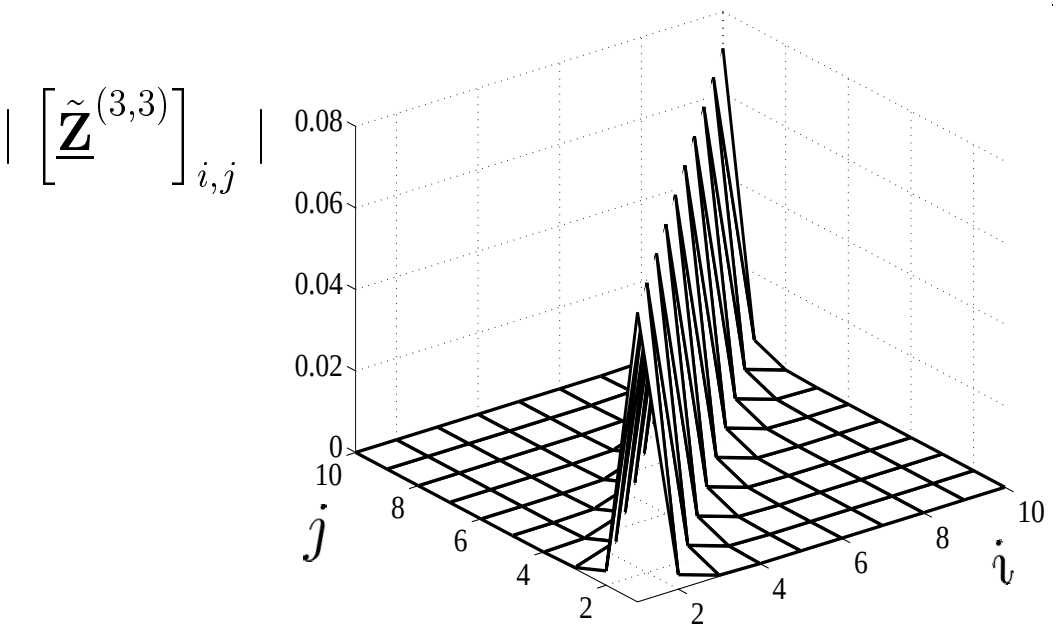

Figure 4.7. Absolute value of the elements of the block $\underline{\tilde{\mathbf{Z}}}^{(3,3)}$ for the scenario of Fig. 4.6, when a single antenna is used

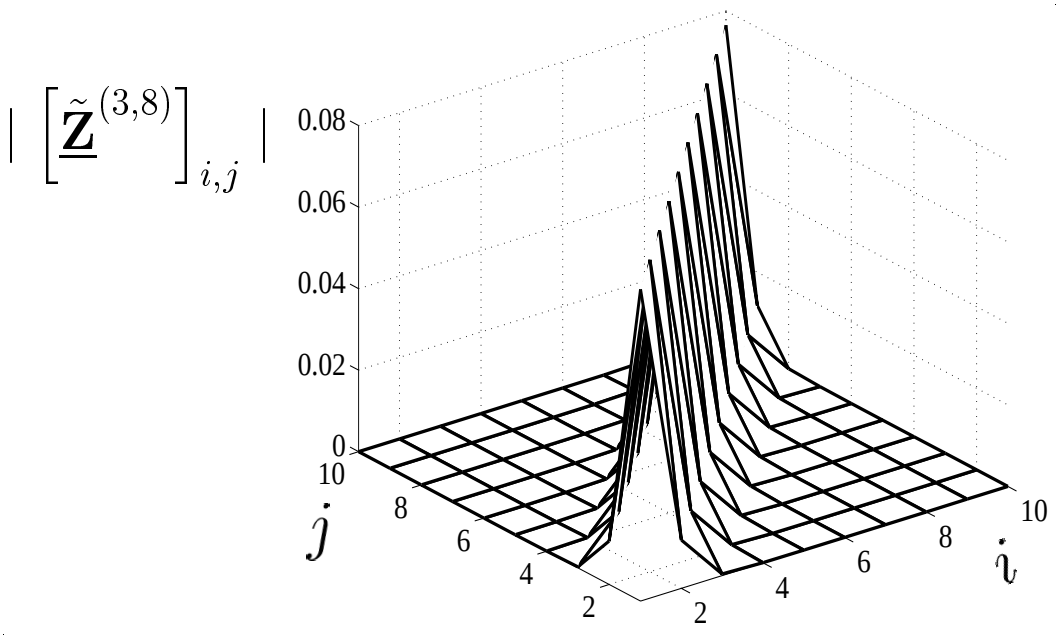

Figure 4.8. Absolute value of the elements of the block $\underline{\tilde{\mathbf{Z}}}^{(3,8)}$ for the scenario of Fig. 4.6, when a single antenna is used

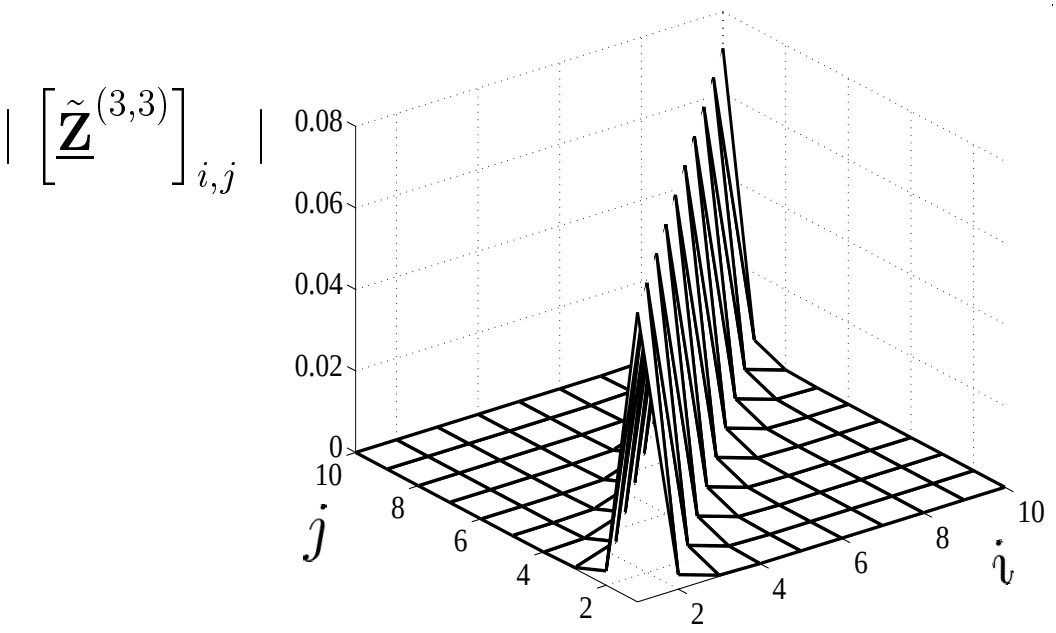

Figure 4.9. Absolute value of the elements of the block $\underline{\tilde{\mathbf{Z}}}^{(3,3)}$ for the scenario of Fig. 4.6, when adaptive antennas are used

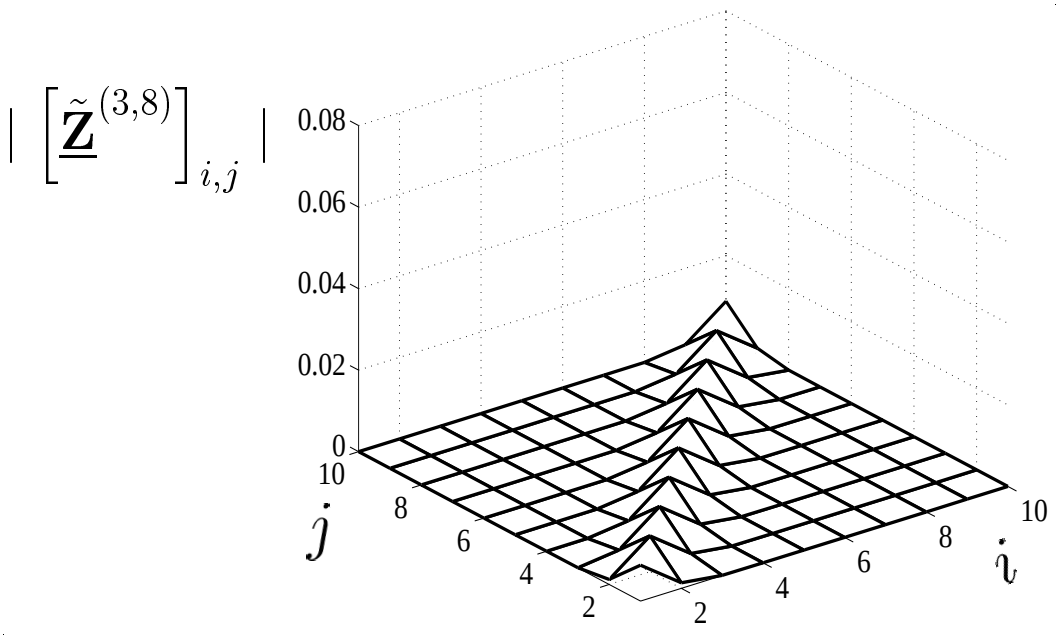

Figure 4.10. Absolute value of the elements of the block $\underline{\tilde{\mathbf{Z}}}^{(3,8)}$ for the scenario of Fig. 4.6, when adaptive antennas are used

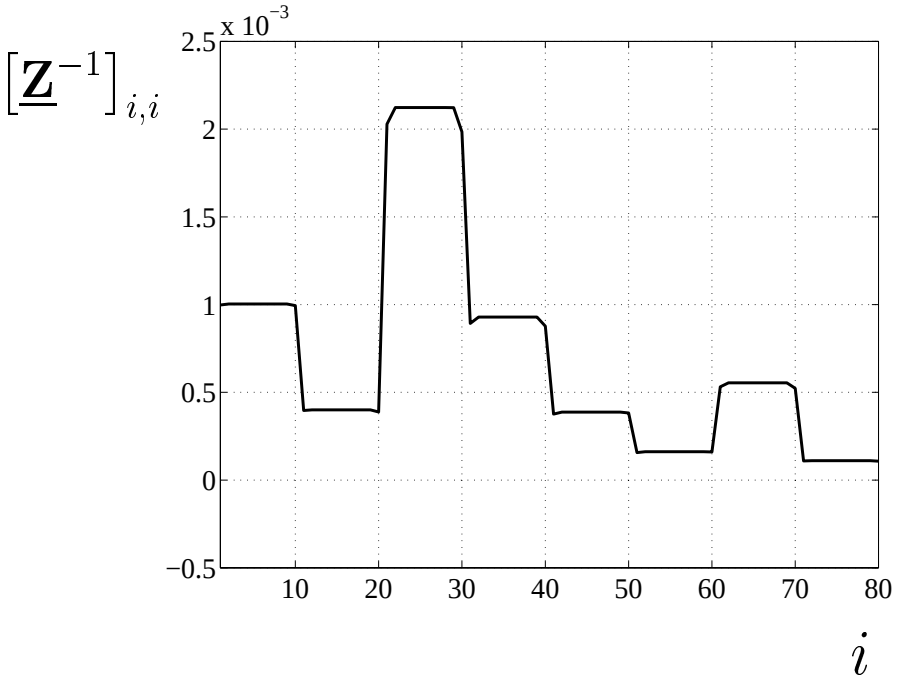

Figure 4.11. Value of the diagonal elements of $\underline{\mathbf{Z}}^{-1}$ for the scenario of Fig. 4.6, when a single antenna is used

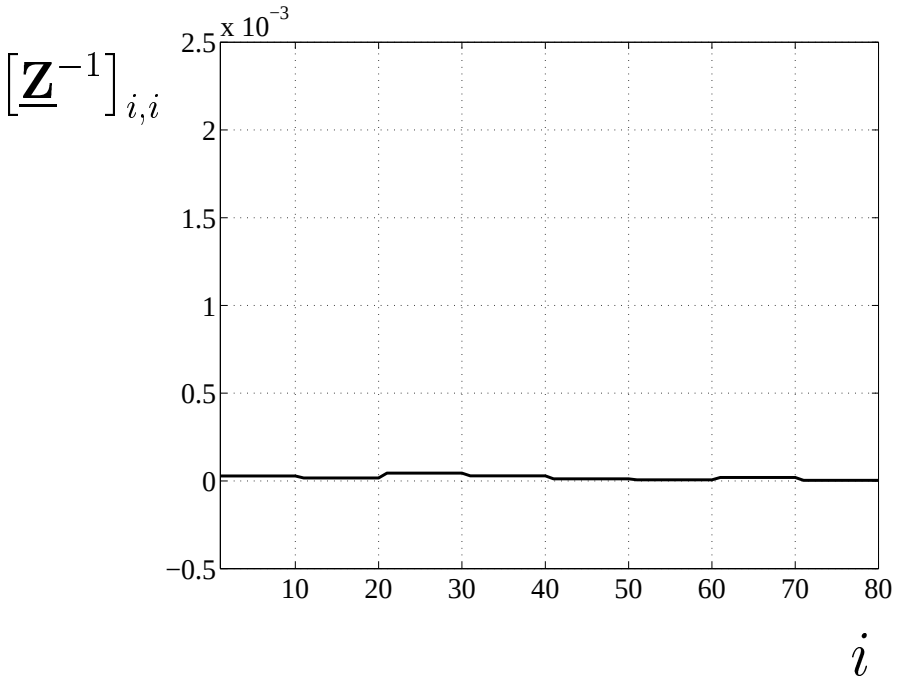

Figure 4.12. Value of the diagonal elements of $\underline{\mathbf{Z}}^{-1}$ for the scenario of Fig. 4.6, when adaptive antennas are used

the influence of the structure of the matrix $\underline{\mathbf{Z}}$, see (4.28), on the system performance, the values of the diagonal elements of the matrix $\underline{\mathbf{Z}}^{-1}$ are shown in Figs. 4.11 and 4.12 for the single antenna and the adaptive antenna case, respectively. As mentioned in Section 4.3.3.2, small values of the diagonal elements of the matrix $\underline{\mathbf{Z}}^{-1}$ lead directly to small values of the SNR degradation, which is the key quantity when evaluating the performance of TD–CDMA [BPW99]. Therefore, comparing Fig. 4.11 with Fig. 4.12, the more favourable performance of TD–CDMA is obvious, when adaptive antennas are used at the BS receiver, compared to single antenna systems.

4.4.3 Small cell channel type

If centro–symmetric array configurations are used in the small cell channel type, see Section 2.4.3 and Fig. 2.7, the diagonal elements of the block $\underline{\mathbf{Z}}^{(k_1,k_2)}$, $k_1 \neq k_2$, can be written in the following fashion:

$$\left[\underline{\mathbf{Z}}^{(k_1,k_2)}\right]_{i,i} = \underline{\mathbf{h}}_{\mathrm{d}}^{(k_1)*\mathrm{T}} \underline{\mathbf{Z}}_{\mathrm{d}}^{(k_1,k_2)} \underline{\mathbf{h}}_{\mathrm{d}}^{(k_2)}, \quad i = 1 \ldots N. \tag{4.38}$$

In (4.38) $\underline{\mathbf{h}}_{\mathrm{d}}^{(k)}$ denotes the vector of dimension W with the arguments and amplitudes of each directional component of the channel impulse response of user k, $k = 1 \ldots K$, observed by a single omnidirectional antenna positioned at the RP of the centro–symmetric array configuration. $\underline{\mathbf{Z}}_{\mathrm{d}}^{(k_1,k_2)}$ is a $W \times W$ matrix with elements

$$\left[\underline{\mathbf{Z}}_{\mathrm{d}}^{(k_1,k_2)}\right]_{w_1,w_2} = \underline{\mathbf{a}}_{\mathrm{s}}^{(k_1,w1)*\mathrm{T}} \underline{\mathbf{a}}_{\mathrm{s}}^{(k_2,w_2)} \underline{\mathrm{R}}_{\mathrm{c},w_1,w_2}^{(k_1,k_2)}, \quad w_1, w_2 = 1 \ldots W, \tag{4.39}$$

where $\underline{\mathrm{R}}_{\mathrm{c},w_1,w_2}^{(k_1,k_2)}$ denotes the (w_1, w_2)–th element of the crosscorrelation function between the CDMA codes $\underline{\mathbf{c}}^{(k_1)}$ and $\underline{\mathbf{c}}^{(k_2)}$ of users k_1 and k_2, respectively, and $\underline{\mathbf{a}}_{\mathrm{s}}^{(k,w)}$ is the steering vector, which pertains to the DOA of the w–th component of the channel impulse response of user k, $k = 1 \ldots K$ [BPW99]. (4.38) and (4.39) demonstrate that the resulting values of the elements of the off–diagonal blocks $\underline{\mathbf{Z}}^{(k_1,k_2)}$, $k_1 \neq k_2$, are normally kept small, since it is not probable for all W DOAs between two users in the small cell channel type to be closely spatially situated. Moreover, good crosscorrelation properties of the CDMA codes lead to small values of the elements of the off-diagonal blocks even in the case, when the DOAs between two users are closely spatially situated, see (4.39).

In order to illustrate the benefits of adaptive antennas in the small cell channel type, the spatial scenario depicted in Fig. 4.13 is considered. Here, the modified COST207 BU channel model introduced in Section 2.3.2, which belongs to the small cell channel type, is used. The remaining parameters are the same as the ones used for the simulation results presented in Figs. 4.7 to 4.12. In the considered scenario, the signal from user $k = 8$ is received with the highest energy, whereas the signal from user $k = 3$ is received with the lowest energy. In Figs. 4.14 and 4.15 the absolute value of the elements of the blocks $\tilde{\underline{\mathbf{Z}}}^{(3,3)}$ and $\tilde{\underline{\mathbf{Z}}}^{(3,8)}$, respectively, see (4.37), are shown when a single antenna is used at the BS

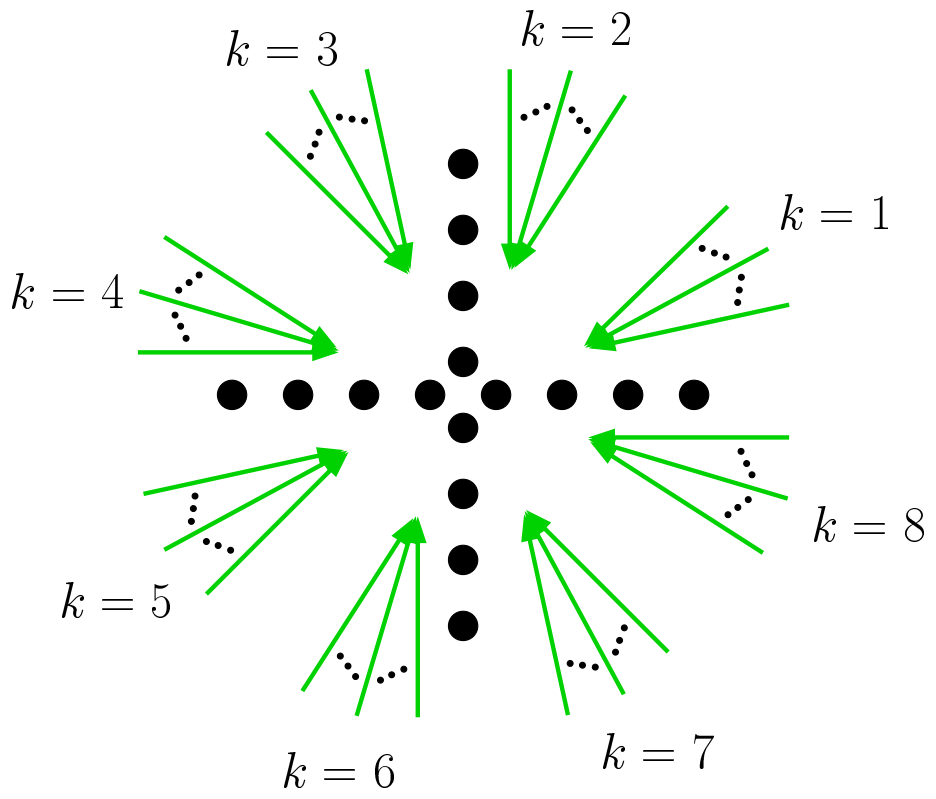

Figure 4.13. Considered spatial scenario for the small cell channel type; modified COST 207 BU channel model; $K = 8$ users

receiver. In Figs. 4.16 and 4.17 the respective values are shown when a cross array configuration of K_a equal to 16 antennas, see Fig. 4.7, is used at the BS receiver. From Figs. 4.14 and 4.15 the unfavourable structure of the matrix $\underline{\tilde{\mathbf{Z}}}$, see (4.37), and consequently of the matrix $\underline{\mathbf{Z}}$ of (4.28), is obvious when a single antenna is employed at the receiver. This unfavourable structure of the matrix $\underline{\mathbf{Z}}$, see (4.28), has been also observed in the large cell channel type, see Figs. 4.7 and 4.8. In contrast to this situation, a favourable structure of the matrix $\underline{\tilde{\mathbf{Z}}}$ of (4.37) occurs when adaptive antennas are used, see Figs. 4.16 and 4.17. Finally, in order to illustrate the influence of the structure of the matrix $\underline{\mathbf{Z}}$, see (4.28), on the system performance, the values of the diagonal elements of the matrix $\underline{\mathbf{Z}}^{-1}$ are shown in Figs. 4.18 and 4.19 for the single antenna and the adaptive antenna case, respectively. As in the large cell channel type, see Figs. 4.11 and 4.12, the comparison of Fig. 4.18 with Fig. 4.19 shows the more favourable system behaviour when adaptive antennas are used in the small cell channel type. As it is demonstrated in Chapter 6 concerning the BER performance of TD–CDMA, the improvement illustrated by Figs. 4.11 and 4.12 for the large cell channel type and by Figs. 4.18 and 4.19 for the small cell channel type leads directly to improvements of the BER performance of TD–CDMA when adaptive antennas are used, compared to the single antenna case. However, before proceeding with the investigation of the BER performance of TD–CDMA, the channel estimation problem is tackled in the following chapter.

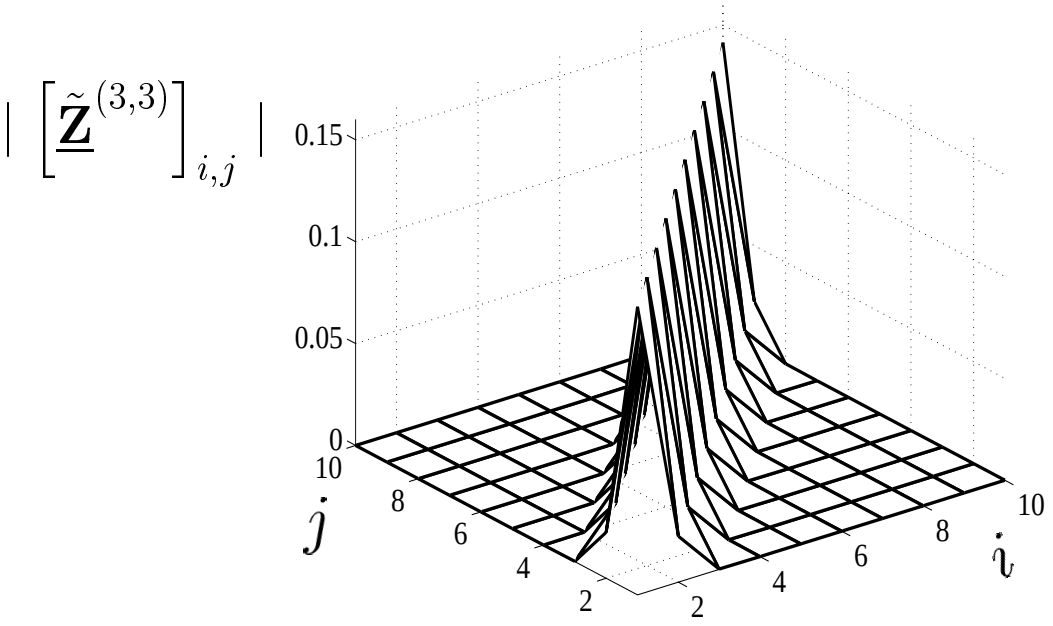

Figure 4.14. Absolute value of the elements of the block $\underline{\tilde{\mathbf{Z}}}^{(3,3)}$ for the scenario of Fig. 4.13, when a single antenna is used

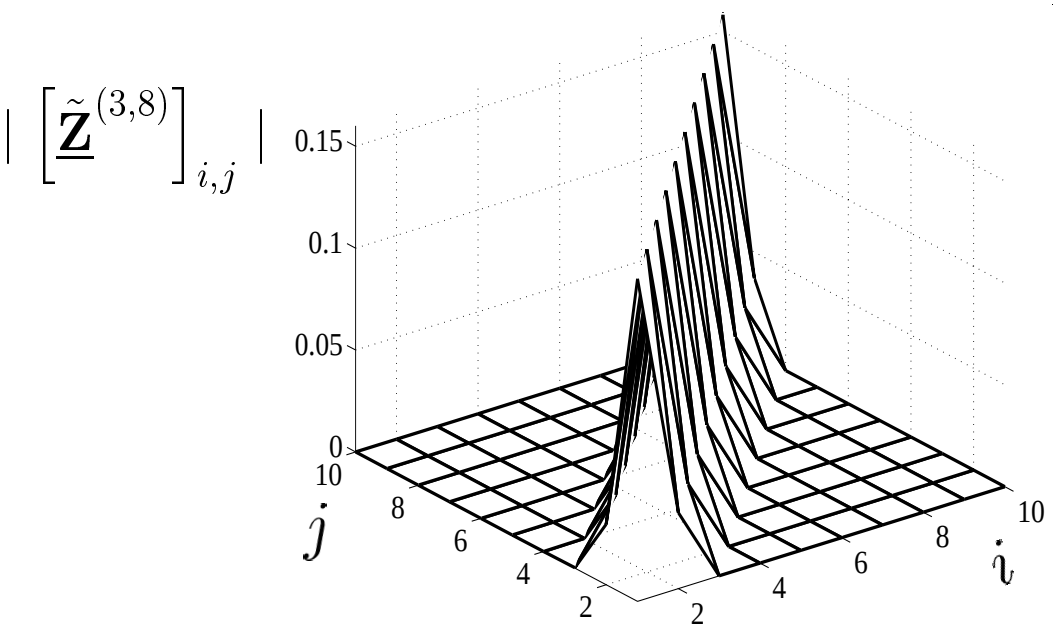

Figure 4.15. Absolute value of the elements of the block $\underline{\tilde{\mathbf{Z}}}^{(3,8)}$ for the scenario of Fig. 4.13, when a single antenna is used

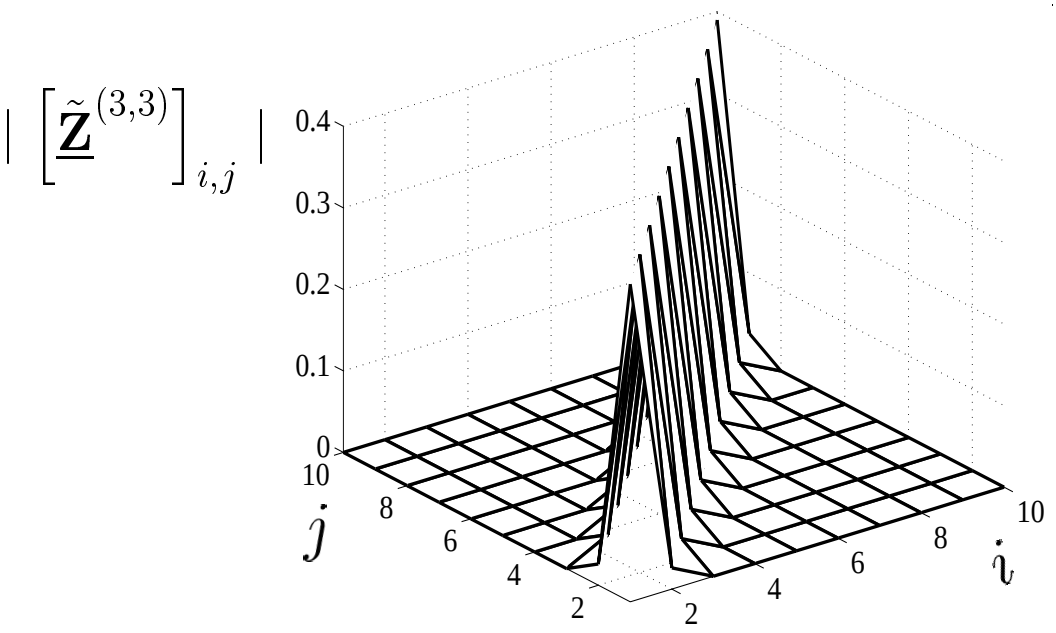

Figure 4.16. Absolute value of the elements of the block $\underline{\tilde{\mathbf{Z}}}^{(3,3)}$ for the scenario of Fig. 4.13, when adaptive antennas are used

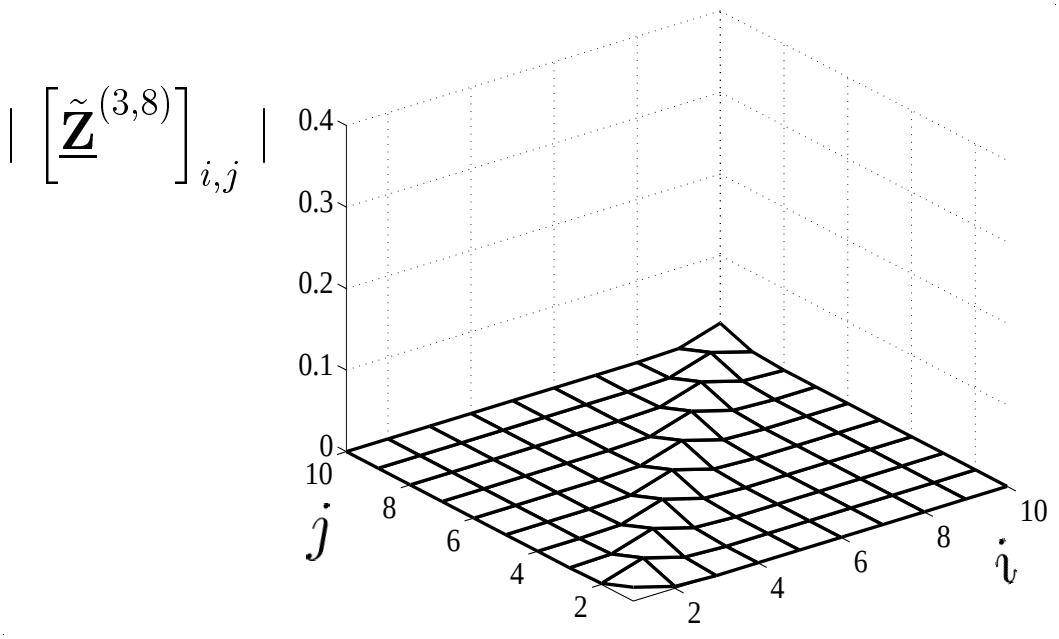

Figure 4.17. Absolute value of the elements of the block $\underline{\tilde{\mathbf{Z}}}^{(3,8)}$ for the scenario of Fig. 4.13, when adaptive antennas are used

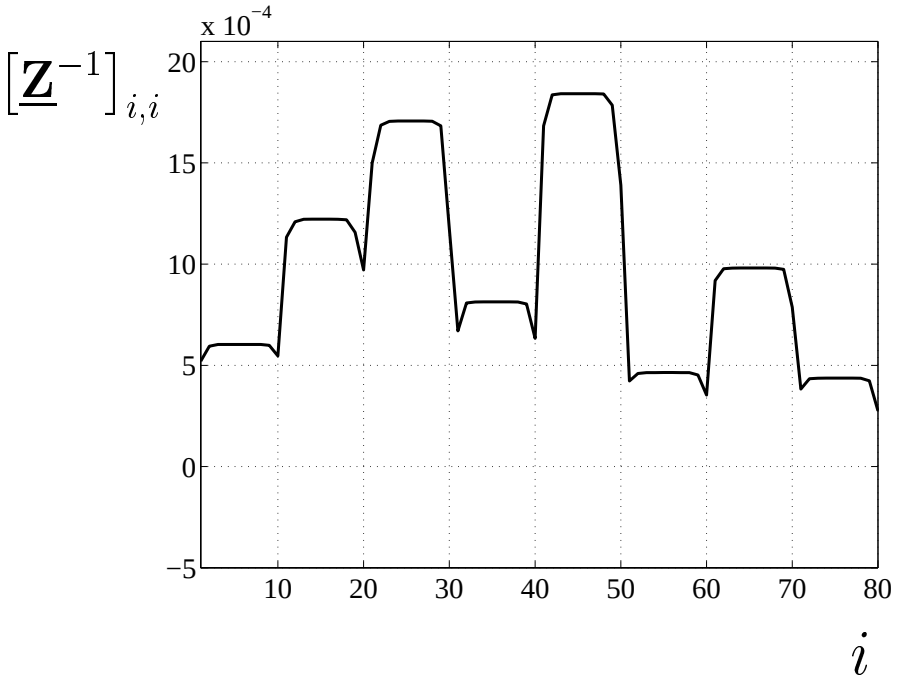

Figure 4.18. Value of the diagonal elements of $\underline{\mathbf{Z}}^{-1}$ for the scenario of Fig. 4.13, when a single antenna is used

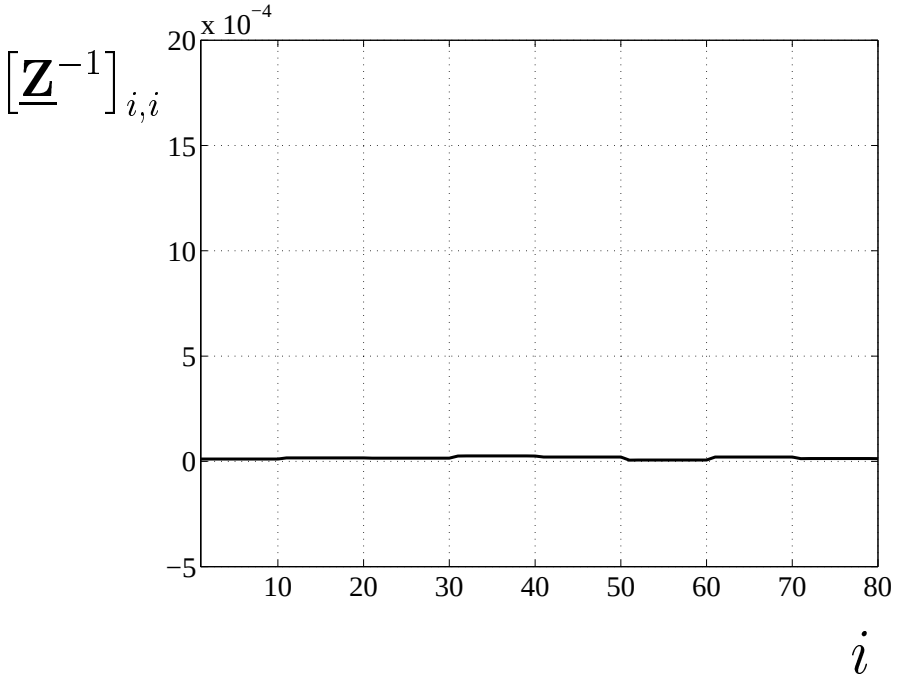

Figure 4.19. Value of the diagonal elements of $\underline{\mathbf{Z}}^{-1}$ for the scenario of Fig. 4.13, when adaptive antennas are used

5 Channel estimation

5.1 Introduction

In Chapter 4 the benefits of adaptive antennas in TD–CDMA are investigated under the assumption that the channel impulse responses are perfectly known at the BS receiver. Therefore, the results presented in Chapter 4 should be considered as an illustration of the increased potential of adaptive antennas for transmission quality and capacity enhancement in TD–CDMA. In practice, though, the time variance and frequency selectivity of the mobile radio channel, see Section 2.2, makes the knowledge about the channel state in each transmitted burst mandatory. As a consequence, channel estimation techniques should be applied for obtaining the information about the channel impulse responses. In this chapter, it is shown how the accuracy of the channel impulse response estimates, which are necessary for the JD of the user data [KB92b, Kle96], see also Section 4.3.3.2, can be increased in TD–CDMA, when adaptive antennas are used at the BS receiver. The analysis presented in this chapter is based on the large cell and the small cell channel types introduced in Section 2.4, which enables a unified approach for channel estimation in TD–CDMA. However, before jumping into the advanced channel estimation techniques developed for systems with adaptive antennas, the Steiner estimator [SK93, Ste95], which is the state of the art channel estimation technique for TD–CDMA, is addressed in the following section. The generalization of the Steiner estimator for multi–antenna configurations constitutes the first step of all advanced channel estimation techniques developed for systems with adaptive antennas in this chapter. Finally, throughout this chapter, if not otherwise stated, it is assumed that a vector of dimension A belongs to the subspace $\mathbb{C}^A$ of the vector space $\mathbb{C}$ over the field of complex numbers, while a matrix of dimensions $B_1 \times B_2$ belongs to the subspace $\mathbb{C}^{B_1 \times B_2}$ of $\mathbb{C}$.

5.2 Steiner estimator

The state of the art channel estimation technique for TD–CDMA has been proposed by Steiner in [SK93, Ste95], and has been verified by extensive simulation results [Ste95, Naß95] and field tests performed with a TD–CDMA hardware demonstrator [MSW97b, BEM98a, BEM98b]. Steiner developed a technique for jointly estimating the channel impulse responses $\underline{\mathbf{h}}^{(k)}$, $k = 1 \ldots K$, see Fig. 4.1, between each active user in the considered cell and a single antenna at the receiver. By taking advantage of the midamble section inserted between the two data sections of the burst transmitted by each user, see Section 1.2 and Fig. 1.2, the novelty of the Steiner estimator is associated with the design of the midamble training sequences. If the midamble training sequences of all users are derived from a single periodic basic code, the channel estimator can be implemented as a low cost cyclic correlator [Ste95]. In general, channel estimation in TD–CDMA, when a single antenna is used at the BS receiver, can be described mathematically as follows. The

received signal $\underline{\mathbf{e}}_{\mathrm{m}}$ at the BS, which exclusively depends on the midamble section and not on the data sections of the transmitted burst of each user, has dimension [SK93, Ste95]

$$L = L_{\mathrm{m}} - W + 1, \tag{5.1}$$

where L_{m} is the total dimension of the midamble in chips, see Fig. 1.2, and W is the dimension of each channel impulse response $\underline{\mathbf{h}}^{(k)}$, $k = 1 \ldots K$, see (4.3). The channel impulse responses from all K users are combined to the total channel impulse response vector

$$\underline{\mathbf{h}} = \left[\underline{\mathbf{h}}^{(1)\mathrm{T}} \ldots \underline{\mathbf{h}}^{(K)\mathrm{T}}\right]^{\mathrm{T}}. \tag{5.2}$$

of dimension KW according to [SK93, Ste95]. Let now $\underline{\mathbf{m}}^{(k)}$, $k = 1 \ldots K$, be the L_{m}–long midamble training sequence of user k, $k = 1 \ldots K$, which is periodic with period L [Ste95]. Then, the $L \times W$ Toeplitz matrix of the midamble training sequence for the k–th user takes the form [Ste95]

$$\underline{\mathbf{G}}^{(k)} = \begin{bmatrix} \underline{m}_W^{(k)} & \underline{m}_{W-1}^{(k)} & \cdots & \underline{m}_1^{(k)} \\ \underline{m}_{W+1}^{(k)} & \underline{m}_W^{(k)} & \cdots & \underline{m}_2^{(k)} \\ \cdot & \cdot & & \cdot \\ \cdot & \cdot & & \cdot \\ \cdot & \cdot & & \cdot \\ \underline{m}_{L-1}^{(k)} & \underline{m}_{L-2}^{(k)} & \cdots & \underline{m}_{L-W}^{(k)} \\ \underline{m}_L^{(k)} & \underline{m}_{L-1}^{(k)} & \cdots & \underline{m}_{L-W+1}^{(k)} \\ \cdot & \cdot & & \cdot \\ \cdot & \cdot & & \cdot \\ \cdot & \cdot & & \cdot \\ \underline{m}_{W-1}^{(k)} & \underline{m}_{W-2}^{(k)} & \cdots & \underline{m}_L^{(k)} \end{bmatrix}, \tag{5.3}$$

which means that the matrix $\underline{\mathbf{G}}^{\mathrm{T}}$ can be defined by any of its column vectors, i.e., it is right–circulant [Mar87]. The matrix $\underline{\mathbf{G}}$ of all K user specific midamble training sequences, known at the receiver, which is used for channel estimation, is given by [Ste95]

$$\underline{\mathbf{G}} = \left[\underline{\mathbf{G}}^{(1)} \ldots \underline{\mathbf{G}}^{(K)}\right] \quad \in \{-1, 1, -\mathrm{jj}\}^{L \times KW}, \tag{5.4}$$

where $\underline{\mathbf{G}}^{(k)}$, $k = 1 \ldots K$, is defined in (5.3). If we further admit an additive intercell MAI noise vector $\underline{\mathbf{n}}_{\mathrm{m}}$ of dimension L disturbing channel estimation, the received signal becomes [SK93, Ste95]

$$\underline{\mathbf{e}}_{\mathrm{m}} = \underline{\mathbf{G}}\ \underline{\mathbf{h}} + \underline{\mathbf{n}}_{\mathrm{m}}. \tag{5.5}$$

Generally L is chosen to be slightly larger than KW, which means that the system of equations in (5.5) is slightly overdetermined. From (5.5), according to the maximum–likelihood principle [Wha71, Kay93], the estimate of $\underline{\mathbf{h}}$, see (5.2), is given by [SK93, Ste95]

$$\hat{\underline{\mathbf{h}}} = \left(\underline{\mathbf{G}}^{*\mathrm{T}} \underline{\mathbf{R}}_{\mathrm{m,t}}^{-1} \underline{\mathbf{G}}\right)^{-1} \underline{\mathbf{G}}^{*\mathrm{T}} \underline{\mathbf{R}}_{\mathrm{m,t}}^{-1} \underline{\mathbf{e}}_{\mathrm{m}}, \tag{5.6}$$

where the $L \times L$ matrix $\underline{\mathbf{R}}_{\mathrm{m,t}}$ denotes the temporal covariance matrix of the intercell MAI vector $\underline{\mathbf{n}}_{\mathrm{m}}$ [PHFB97, Bla98]. In [BHP97, Bla98] it is shown that the Steiner estimator can be generalized to take into account the use of multi–antenna configurations at the BS receiver. If

$$\underline{\mathbf{h}} = \left[\underline{\mathbf{h}}^{(1)\mathrm{T}} \ldots \underline{\mathbf{h}}^{(K_{\mathrm{a}})\mathrm{T}}\right]^{\mathrm{T}} \tag{5.7}$$

now represents the total channel impulse response vector of dimension $K_{\mathrm{a}}KW$ valid for all links between each user k, $k = 1 \ldots K$, and each antenna k_{a}, $k_{\mathrm{a}} = 1 \ldots K_{\mathrm{a}}$, see Fig. 4.3, with

$$\underline{\mathbf{h}}^{(k_{\mathrm{a}})} = \left[\underline{\mathbf{h}}^{(1,k_{\mathrm{a}})\mathrm{T}} \ldots \underline{\mathbf{h}}^{(K,k_{\mathrm{a}})\mathrm{T}}\right]^{\mathrm{T}}, \quad k_{\mathrm{a}} = 1 \ldots K_{\mathrm{a}}, \tag{5.8}$$

then the received signal $\underline{\mathbf{e}}_{\mathrm{m}}$ of dimension $K_{\mathrm{a}}L$ from all K_{a} antennas can be written as [PHFB97, Bla98]

$$\underline{\mathbf{e}}_{\mathrm{m}} = \left(\mathbf{I}^{(K_{\mathrm{a}})} \otimes \underline{\mathbf{G}}\right) \underline{\mathbf{h}} + \underline{\mathbf{n}}_{\mathrm{m}}. \tag{5.9}$$

In (5.9) $\underline{\mathbf{n}}_{\mathrm{m}}$ represents the received intercell MAI vector from all K_{a} antennas of dimension $K_{\mathrm{a}}L$. The $K_{\mathrm{a}}L \times K_{\mathrm{a}}L$ covariance matrix of $\underline{\mathbf{n}}_{\mathrm{m}}$, denoted as the total intercell MAI covariance matrix [WPS99], can be expressed as [Bla98, PFBP99]

$$\underline{\mathbf{R}}_{\mathrm{m}} = \underline{\mathbf{R}}_{\mathrm{s}} \otimes \underline{\mathbf{R}}_{\mathrm{m,t}}, \tag{5.10}$$

where $\underline{\mathbf{R}}_{\mathrm{s}}$ denotes the $K_{\mathrm{a}} \times K_{\mathrm{a}}$ spatial intercell MAI covariance matrix, and $\underline{\mathbf{R}}_{\mathrm{m,t}}$ expresses the $L \times L$ temporal intercell MAI covariance matrix valid for channel estimation [Bla98, PFBP99], see also (5.6). In Section 7.4, the detailed derivation of (5.10) and the conditions, under which (5.10) is valid, are given. For the purpose of this chapter, the expression for $\underline{\mathbf{R}}_{\mathrm{m}}$ by the tensorial product of (5.10) is sufficient. Then, from (5.9), the estimate

$$\hat{\underline{\mathbf{h}}} = \left[\mathbf{I}^{(K_{\mathrm{a}})} \otimes \left(\underline{\mathbf{G}}^{*\mathrm{T}} \underline{\mathbf{R}}_{\mathrm{m,t}}^{-1} \underline{\mathbf{G}}\right)^{-1} \underline{\mathbf{G}}^{*\mathrm{T}} \underline{\mathbf{R}}_{\mathrm{m,t}}^{-1}\right] \underline{\mathbf{e}}_{\mathrm{m}}, \tag{5.11}$$

of the channel impulse response vector $\underline{\mathbf{h}}$, see (5.7), is obtained [BHP97, Bla98, PFBP99]. (5.11) expresses the generalization of the Steiner estimator, see (5.6), when multi–antenna configurations are used at the BS receiver. Note that, as in the single antenna case, see (5.6), the spatial intercell MAI covariance matrix $\underline{\mathbf{R}}_{\mathrm{s}}$, see (5.10), is not used in (5.11).

At this point, a novel view on channel estimation in TD–CDMA is presented, when the Steiner estimator is applied. The main idea of this view is similar to the one presented in Section 4.2 for data detection in TD–CDMA. However, in contrast to the case of data detection, see Section 4.2, by comparing (5.5) and (5.9), we note that, as the number of antennas increase from one to K_{a}, the number of unknown components contained in the vector $\underline{\mathbf{h}}$ increases proportionally from KW to $K_{\mathrm{a}}KW$. Equivalently stated, by increasing the number of equations in (5.9) compared to (5.5), the number of unknowns in (5.9) increases proportionally compared to (5.5). This observation implies that the

advantage offered by multi–antenna configurations for data detection, where the number of unknowns remains unchanged as the number of antennas increase, see Section 4.2, is not valid for channel estimation, if the generalized Steiner estimator is applied. Therefore, the estimation quality of $\hat{\underline{\mathbf{h}}}$ from (5.11) is expected to be in the order of the quality of $\hat{\underline{\mathbf{h}}}$ from (5.6). This statement can be also explained by observing that (5.11) describes K_a individual channel estimation processes as the one described by (5.6), each valid for the respective antenna of the used multi–antenna configuration:

$$\hat{\underline{\mathbf{h}}}^{(k_\mathrm{a})} = \left(\underline{\mathbf{G}}^{*\mathrm{T}}\underline{\mathbf{R}}_{\mathrm{m,t}}^{-1}\underline{\mathbf{G}}\right)^{-1}\underline{\mathbf{G}}^{*\mathrm{T}}\underline{\mathbf{R}}_{\mathrm{m,t}}^{-1}\underline{\mathbf{e}}_\mathrm{m}^{(k_\mathrm{a})}, \qquad k_\mathrm{a} = 1\ldots K_\mathrm{a}. \tag{5.12}$$

Therefore, the generalized Steiner estimator does not offer additional advantages, when multi–antenna configurations are used in TD–CDMA, compared to single antenna systems. In the following sections of this chapter, it is shown how novel channel estimation techniques developed for adaptive antennas in TD–CDMA overcome this drawback of the Steiner estimator, i.e., the proportional increase of the number of unknowns as the number of equations increase. As a final remark, the receiver using the generalized Steiner estimator will be addressed in the following as the conventional channel estimation scheme in order to distinguish it from the novel channel estimation techniques presented in Section 5.3 and Section 5.4, which will be addressed as the novel channel estimation schemes.

5.3 Adaptive antennas for the large cell channel type

5.3.1 Preliminary remark

The channel estimation technique for the large cell channel type considered in this section is presented in [BHP97, Bla98]. Here, the system model valid for the large cell channel type is extended to include the use of 2D array configurations at the BS receiver. Moreover, a novel view on the benefits offered by adaptive antennas in the large cell channel type is presented, compared to the use of the Steiner estimator, see Section 5.2. However, for the purpose of this section, the reader is explicitely referred to [BHP97, Bla98], which serves as the basis for the following considerations.

5.3.2 System model

In this section the system model valid for channel estimation in the large cell channel type, see Section 2.4.2, is considered when 2D centro–symmetric array configurations [XRK94, Haa97a], see also Section 3.4, are used at the BS receiver. In Fig. 5.1 the definition of parameters associated with the use of 2D array configurations is illustrated. In this section, only the parameters valid for the information carrying signals, i.e., the signals which produce the intracell MAI in a TD–CDMA mobile radio system, see Section 2.2, are considered. The parameters valid for the intercell MAI are explained

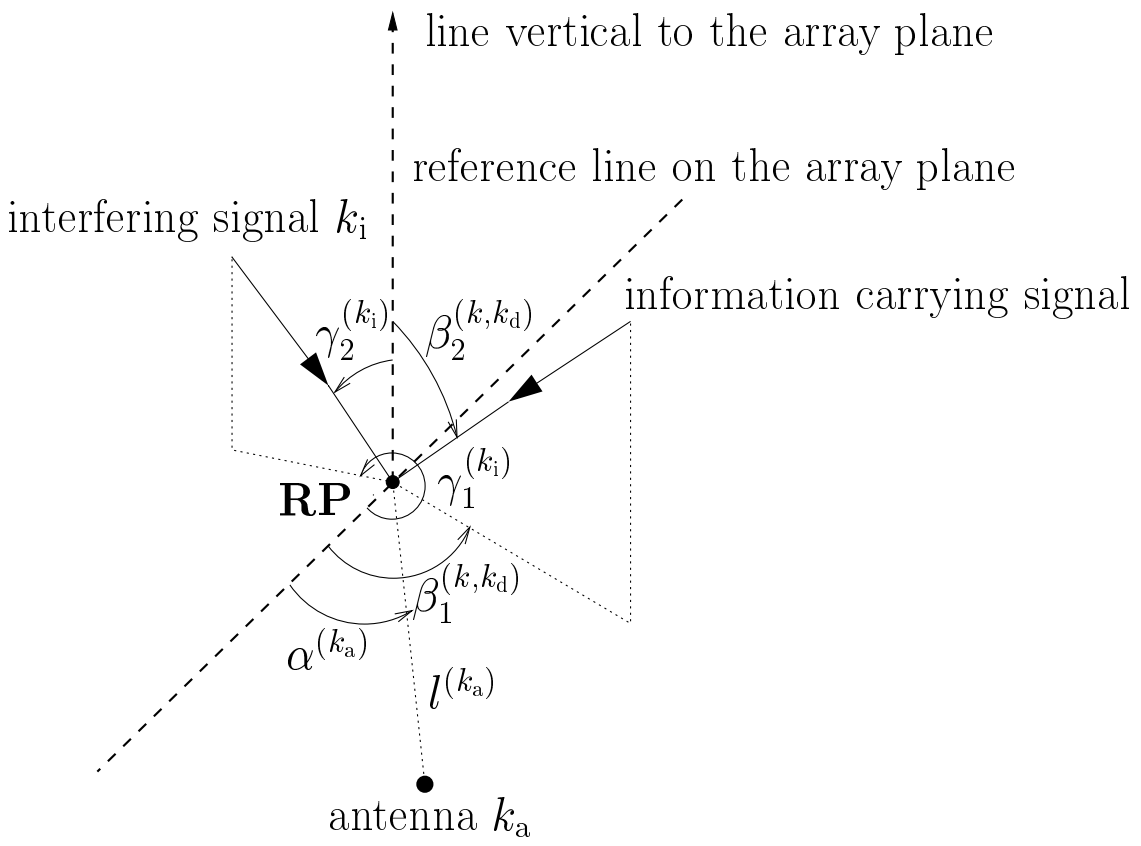

Figure 5.1. For the definition of 2D centro–symmetric array configuration parameters

in Section 7.4, where the total intercell MAI covariance matrix $\underline{\mathbf{R}}_\mathrm{m}$, see (5.10), is derived for a TD–CDMA mobile radio system with adaptive antennas.

According to Fig. 5.1, the k_a–th array element has a distance of $l^{(k_\mathrm{a})}$ to an assumed RP and the angle spanned by the reference line and the line on the array plane connecting the referred array element with the RP is termed $\alpha^{(k_\mathrm{a})}$, $k_\mathrm{a} = 1 \ldots K_\mathrm{a}$. The k_d–th DOA of a signal coming from transmitter k, $k = 1 \ldots K$, is split into the azimuth angle $\beta_1^{(k,k_\mathrm{d})}$ and the elevation angle $\beta_2^{(k,k_\mathrm{d})}$, $k_\mathrm{d} = 1 \ldots K_\mathrm{d}^{(k)}$, $k = 1 \ldots K$. As already mentioned in Section 2.4.2 for the large cell channel type, for each DOA of a desired signal one channel impulse response can be defined, which could be observed by an omnidirectional antenna located at the RP of the used array configuration [BHP97, PHFB97]. The channel impulse response vector for the k_d–th DOA of the k–th user is denoted by $\underline{\mathbf{h}}_\mathrm{d}^{(k,k_\mathrm{d})}$, $k_\mathrm{d} = 1 \ldots K_\mathrm{d}^{(k)}$, $k = 1 \ldots K$, and has dimension W [PFBP99]. $\underline{\mathbf{h}}_\mathrm{d}^{(k,k_\mathrm{d})}$ represents the directional channel impulse response valid for the k_d–th DOA of user k, see also Sections 2.2.1 and 2.3. With the user specific $W \times K_\mathrm{d}^{(k)}$ matrices [PHFB97, Bla98]

$$\underline{\mathbf{H}}_\mathrm{d}^{(k)} = \left[\underline{\mathbf{h}}_\mathrm{d}^{(k,1)} \ldots \underline{\mathbf{h}}_\mathrm{d}^{(k,K_\mathrm{d}^{(k)})}\right], \; k = 1 \ldots K, \tag{5.13}$$

the directional channel impulse response vectors from all users can be combined to the $W \times K_\mathrm{d}$ matrix

$$\underline{\mathbf{H}}_\mathrm{d} = \left[\underline{\mathbf{H}}_\mathrm{d}^{(1)} \ldots \underline{\mathbf{H}}_\mathrm{d}^{(K)}\right], \tag{5.14}$$

where

$$K_\mathrm{d} = \sum_{k=1}^{K} K_\mathrm{d}^{(k)}. \tag{5.15}$$

Accordingly, the channel impulse response vectors corresponding to the links between the k–th user and each array element k_a, $k_\mathrm{a} = 1 \ldots K_\mathrm{a}$, are combined to the $W \times K_\mathrm{a}$ matrix

$$\underline{\mathbf{H}}^{(k)} = \left[\underline{\mathbf{h}}^{(k,1)} \ldots \underline{\mathbf{h}}^{(k,K_\mathrm{a})}\right], \tag{5.16}$$

see also (5.8), and the channel impulse responses from all users are then arranged to the $KW \times K_\mathrm{a}$ matrix

$$\underline{\mathbf{H}} = \left[\underline{\mathbf{H}}^{(1)\mathrm{T}} \ldots \underline{\mathbf{H}}^{(K)\mathrm{T}}\right]^\mathrm{T}, \tag{5.17}$$

see also (5.7). As mentioned in Section 2.3.2, the signals are assumed to be narrowband, i.e., their amplitudes and phases vary slowly with respect to the propagation time across the array. Then, the propagation delay can be modeled by multiplying the complex signal envelope by a complex exponential [RK89], the phase factor $\mathrm{e}^{\mathrm{j}\psi(k,k_\mathrm{a},k_\mathrm{d})}$, where

$$\psi(k, k_\mathrm{a}, k_\mathrm{d}) = 2\pi \frac{l^{(k_\mathrm{a})}}{\lambda} \cos(\beta_1^{(k,k_\mathrm{d})} - \alpha^{(k_\mathrm{a})}) \sin(\beta_2^{(k,k_\mathrm{d})}), \tag{5.18}$$

$k = 1 \ldots K$, $k_\mathrm{a} = 1 \ldots K_\mathrm{a}$, $k_\mathrm{d} = 1 \ldots K_\mathrm{d}$, are the spatial frequencies with respect to the RP [Haa97a], see also Fig. 5.1, and λ denotes the carrier wavelength. If it is further assumed that the array element outputs are stacked columnwise, progressing downwards the reference line on the array plane, see Fig. 5.1, the steering vector

$$\underline{\mathbf{a}}^{(k,k_\mathrm{d})} = \left[\mathrm{e}^{\mathrm{j}\psi(k,1,k_\mathrm{d})} \ \ldots \mathrm{e}^{\mathrm{j}\psi(k,K_\mathrm{a},k_\mathrm{d})}\right]^\mathrm{T} \tag{5.19}$$

can be defined, which contains the K_a phase factors for the k–th user and its k_d–th DOA. In this case, the channel impulse response vector $\underline{\mathbf{h}}^{(k,k_\mathrm{a})}$, see (5.8), is related to the directional channel impulse responses $\underline{\mathbf{h}}_\mathrm{d}^{(k,k_\mathrm{d})}$, $k_\mathrm{d} = 1 \ldots K_\mathrm{d}$, see (5.13), corresponding to the different DOAs of the k–th user, by [PHFB97]

$$\underline{\mathbf{h}}^{(k,k_\mathrm{a})} = \sum_{k_\mathrm{d}=1}^{K_\mathrm{d}^{(k)}} \mathrm{e}^{\mathrm{j}\psi(k,k_\mathrm{a},k_\mathrm{d})} \ \underline{\mathbf{h}}_\mathrm{d}^{(k,k_\mathrm{d})}. \tag{5.20}$$

With

$$\underline{\mathbf{A}}_\mathrm{s}^{(k)} = \left[\underline{\mathbf{a}}^{(k,1)} \ldots \underline{\mathbf{a}}^{(k,K_\mathrm{d}^{(k)})}\right], \quad k = 1 \ldots K, \tag{5.21}$$

the $K_\mathrm{a} \times K_\mathrm{d}^{(k)}$ user specific steering matrix [RK89, HN95, Haa97a], the relation between the channel impulse responses for the k-th user contained in the matrix $\underline{\mathbf{H}}^{(k)}$, see (5.16), and the directional channel impulse responses for the k-th user contained in the matrix $\underline{\mathbf{H}}_\mathrm{d}^{(k)}$, see (5.13), is expressed by [PHFB97]

$$\underline{\mathbf{H}}^{(k)} = \sum_{k_\mathrm{d}=1}^{K_\mathrm{d}^{(k)}} \underline{\mathbf{h}}_\mathrm{d}^{(k,k_\mathrm{d})} \underline{\mathbf{a}}^{(k,k_\mathrm{d})\mathrm{T}} = \underline{\mathbf{H}}_\mathrm{d}^{(k)} \underline{\mathbf{A}}_\mathrm{s}^{(k)\mathrm{T}}. \tag{5.22}$$

The part of the received signal for each array element which depends exclusively on the midamble training sequences is denoted by $\underline{\mathbf{e}}_\mathrm{m}^{(k_\mathrm{a})}$, $k_\mathrm{a} = 1 \ldots K_\mathrm{a}$, see also Section 5.2, and these K_a vectors are arranged columnwise in the $L \times K_\mathrm{a}$ matrix $\underline{\mathbf{E}}_\mathrm{m}$. If we further admit an intercell MAI vector $\underline{\mathbf{n}}_\mathrm{m}^{(k_\mathrm{a})}$, $k_\mathrm{a} = 1 \ldots K_\mathrm{a}$, at each array element and arrange these K_a noise vectors columnwise in the $L \times K_\mathrm{a}$ matrix $\underline{\mathbf{N}}_\mathrm{m}$, then the expression

$$\underline{\mathbf{E}}_\mathrm{m} = \underline{\mathbf{G}}\ \underline{\mathbf{H}} + \underline{\mathbf{N}}_\mathrm{m} \tag{5.23}$$

relates the received signals at the K_a array elements, which depend exclusively on the midamble training sequences, to the channel impulse responses from all K users, where the matrix $\underline{\mathbf{G}}$ is defined in (5.4). Note that (5.23) is equivalent to (5.9), since

$$\underline{\mathbf{e}}_\mathrm{m} = \mathrm{vec}\left\{\underline{\mathbf{E}}_\mathrm{m}\right\}, \tag{5.24}$$

$$\underline{\mathbf{h}} = \mathrm{vec}\left\{\underline{\mathbf{H}}\right\}, \tag{5.25}$$

$$\underline{\mathbf{n}}_\mathrm{m} = \mathrm{vec}\left\{\underline{\mathbf{N}}_\mathrm{m}\right\}, \tag{5.26}$$

where the vec$\{\cdot\}$–operator denotes a vector–valued function that maps an $m \times n$ matrix into an mn–dimensional column vector by stacking the columns of the matrix [Gra81], and [PFBP99]

$$\mathrm{vec}\left\{\underline{\mathbf{G}}\ \underline{\mathbf{H}}\right\} = \left(\mathbf{I}^{(K_\mathrm{a})} \otimes \underline{\mathbf{G}}\right)\ \underline{\mathbf{h}} \tag{5.27}$$

holds. Then, inserting (5.4), (5.17), and (5.22) into (5.23) yields

$$\begin{aligned} \underline{\mathbf{E}}_\mathrm{m} &= \left[\underline{\mathbf{G}}^{(1)} \ldots \underline{\mathbf{G}}^{(K)}\right] \cdot \left[\underline{\mathbf{A}}_\mathrm{s}^{(1)} \underline{\mathbf{H}}_\mathrm{d}^{(1)\mathrm{T}} \ldots \underline{\mathbf{A}}_\mathrm{s}^{(K)} \underline{\mathbf{H}}_\mathrm{d}^{(K)\mathrm{T}}\right]^\mathrm{T} + \underline{\mathbf{N}}_\mathrm{m} \\ &= \sum_{k=1}^{K} \underline{\mathbf{G}}^{(k)} \underline{\mathbf{H}}_\mathrm{d}^{(k)} \underline{\mathbf{A}}_\mathrm{s}^{(k)\mathrm{T}} + \underline{\mathbf{N}}_\mathrm{m}. \end{aligned} \tag{5.28}$$

If we further define

$$\underline{\mathbf{h}}_\mathrm{d} = \mathrm{vec}\left\{\underline{\mathbf{H}}_\mathrm{d}\right\}, \tag{5.29}$$

where $\underline{\mathbf{H}}_\mathrm{d}$ is given by (5.14), and use the relation [Gra81]

$$\mathrm{vec}\left\{\underline{\mathbf{G}}^{(k)} \underline{\mathbf{H}}_\mathrm{d}^{(k)} \underline{\mathbf{A}}_\mathrm{s}^{(k)\mathrm{T}}\right\} = \left(\underline{\mathbf{A}}_\mathrm{s}^{(k)} \otimes \underline{\mathbf{G}}^{(k)}\right)\ \underline{\mathbf{h}}_\mathrm{d}^{(k)}, \tag{5.30}$$

where

$$\underline{\mathbf{h}}_{\mathrm{d}}^{(k)} = \mathrm{vec}\left\{\underline{\mathbf{H}}_{\mathrm{d}}^{(k)}\right\}, \tag{5.31}$$

see (5.13), (5.28) can be written as

$$\underline{\mathbf{e}}_{\mathrm{m}} = \underline{\mathbf{G}}_{\mathrm{d}}\ \underline{\mathbf{h}}_{\mathrm{d}} + \underline{\mathbf{n}}_{\mathrm{m}}, \tag{5.32}$$

with

$$\underline{\mathbf{G}}_{\mathrm{d}} = \left[\underline{\mathbf{A}}_{\mathrm{s}}^{(1)} \otimes \underline{\mathbf{G}}^{(1)} \ldots \underline{\mathbf{A}}_{\mathrm{s}}^{(K)} \otimes \underline{\mathbf{G}}^{(K)}\right], \tag{5.33}$$

see also (5.4) and (5.21). The representations (5.9) and (5.32) of the received signal from all K_{a} array elements, which depends exclusively on the midamble training sequences, will be used for the channel estimation technique for the large cell channel type described in the next section. However, before proceeding with this channel estimation technique, a novel view on the main difference between the generalized Steiner estimator, which is based on (5.9), and the channel estimation technique for the large cell channel type, which is based on (5.32), is presented. Note that the basis of this view is similar to the one presented in Section 4.2 for data detection in TD–CDMA and in Section 5.2 for the Steiner estimator.

We set out from (5.9) and (5.32). (5.9) describes the received signal when the generalized Steiner estimator is applied, whereas (5.32) describes the received signal when the novel channel estimation technique of this section is used. Comparing (5.9) and (5.32), we observe that the number of equations, i.e., the number of components of the received signal $\underline{\mathbf{e}}_{\mathrm{m}}$, is the same in both expressions. However, if the number of antennas of the centro–symmetric array configuration is chosen to fulfill the inequality

$$K_{\mathrm{a}} > {K_{\mathrm{d}}}^{(k)}, \quad k = 1 \ldots K, \tag{5.34}$$

the number of unknown parameters in (5.32), i.e., the $K_{\mathrm{d}}W$ components of the directional channel impulse response vector $\underline{\mathbf{h}}_{\mathrm{d}}$, is reduced, compared to the $K_{\mathrm{a}}KW$ unknown components of the channel impulse response vector $\underline{\mathbf{h}}$. E.g., when considering the rural propagation environment, see Sections 2.3.2 and 2.3.3, ${K_{\mathrm{d}}}^{(k)}$, $k = 1 \ldots K$, is assumed to be equal to one. Then, if K_{a} is chosen to be, e.g., equal to eight, a considerable reduction of the number of unknowns in (5.32) is achieved, compared to the $K_{\mathrm{a}}KW$ unknown components in (5.9). This reduction of the number of unknown parameters is known as the problem of reducing or deleting variables from a linear system of equations in estimation theory and computational analysis [Gol69, LH74], and leads to an improvement of the estimation or the computation of the vector containing the reduced number of unknown parameters, compared to the original vector of the unknowns. Concerning (5.9) and (5.32), the previous statement means that an improved estimation quality of the vector $\underline{\mathbf{h}}_{\mathrm{d}}$ from (5.32) is expected, compared to the estimation quality of $\underline{\mathbf{h}}$ from (5.32). The reduction of the number of the unknowns in $\underline{\mathbf{h}}_{\mathrm{d}}$ compared to the number of the unknowns in $\underline{\mathbf{h}}$ is considered to be the most important benefit offered by adaptive antennas in the large cell

channel type, see also [Bla98, BPW99, PSWB99]. As a final observation, refering to the problem of appending additional rows to a linear system of equations, which is used in Section 4.2 for explaining the main difference between single and multi–antenna systems with respect to joint data detection, the problem of reducing or deleting variables, which is valid for channel estimation in TD–CDMA with adaptive antennas, may be viewed as its inverse problem. Therefore, according to the opinion of the author of this thesis, a novel unified theoretical approach is achieved for explaining the benefits of adaptive antennas in a straightforward manner for both data detection and channel estimation in TD–CDMA mobile radio systems.

5.3.3 Novel channel estimation

5.3.3.1 Introduction

In this section, the channel estimation technique for the large cell channel type is described according to [BHP97, Bla98], when adaptive antennas are used at the BS receiver. This approach can be divided into three steps [BHP97, Bla98, PFBP99]:

- In a first step, the channel impulse responses $\underline{\mathbf{h}}^{(k,k_\mathrm{a})}$, $k_\mathrm{a} = 1 \ldots K_\mathrm{a}$, $k = 1 \ldots K$, see (5.20), for the links between each user and each antenna are estimated according to the generalized Steiner estimator, see Section 5.2, leading to the separation of the channel impulse responses which belong to the different users.
- Then, the user specific channel impulse responses are used for a user specific DOA estimation.
- In a third step, the information about the DOAs and the channel impulse responses of each user is exploited for an enhanced joint channel estimation, which leads to improved channel impulse response estimates compared to the channel impulse response estimates delivered by the generalized Steiner estimator, see the theoretical analysis of Section 5.3.2.

In the large cell channel type, see Section 2.4.2, (5.34) is valid, i.e., the number of directional channel impulse responses is small compared to the number of the elements of the used array configuration. This is due to the fact that in rural or typical urban channel models the impinging signals are confined within relative small spatial ranges [KM96, Egg94, Egg95, Fuh97, Bla98], see also Section 2.3.2 and Section 2.3.3. In such models, one dominant DOA from each spatial range is used for the third step of the channel estimation technique developed for the large cell channel type, see also Fig. 2.6. In Section 5.5 simulation results illustrate the improvement achieved by the channel estimation technique described in this section with respect to the channel impulse response estimates, compared to the generalized Steiner estimator. The BER performance of the considered TD–CDMA

mobile radio system using this technique is evaluated in Chapter 6 for different scenarios in rural and typical urban channel models, i.e., in the large cell channel type.

5.3.3.2 DOA estimation

As shown in detail in Section 5.2, the result of the application of the generalized Steiner estimator is to produce separate estimates for the elements of the channel impulse response vectors $\underline{\mathbf{h}}^{(k_\mathrm{a})}$, $k_\mathrm{a} = 1 \ldots K_\mathrm{a}$, see (5.11) and (5.12), and consequently for the combined channel impulse response vector $\underline{\mathbf{h}}$, see (5.6). The parts of $\hat{\underline{\mathbf{h}}}$ which belong to the same user can be used for the purpose of a user specific DOA estimation as described in what follows.

Let $\hat{\underline{\mathbf{H}}}$ denote the matrix which contains the estimates of the channel impulse responses, arranged as in (5.17). Then, the estimate of the channel impulse response vector $\underline{\mathbf{h}}$ can be expressed as

$$\hat{\underline{\mathbf{h}}} = \mathrm{vec}\left\{\hat{\underline{\mathbf{H}}}\right\}, \tag{5.35}$$

see also (5.25). By using (5.23) and (5.25), (5.11) can be written as

$$\hat{\underline{\mathbf{H}}} = \underline{\mathbf{H}} + \underline{\mathbf{M}}_\mathrm{m}\underline{\mathbf{N}}_\mathrm{m} \tag{5.36}$$

where

$$\underline{\mathbf{M}}_\mathrm{m} = \left(\underline{\mathbf{G}}^{*\mathrm{T}}\underline{\mathbf{R}}_{\mathrm{m,t}}^{-1}\underline{\mathbf{G}}\right)^{-1}\underline{\mathbf{G}}^{*\mathrm{T}}\underline{\mathbf{R}}_{\mathrm{m,t}}^{-1}. \tag{5.37}$$

Then, based on (5.36), the matrix $\hat{\underline{\mathbf{H}}}$ can be written in its transposed form as

$$\hat{\underline{\mathbf{H}}}^{\mathrm{T}} = \underline{\mathbf{H}}^{\mathrm{T}} + \underline{\mathbf{N}}_\mathrm{m}^{\mathrm{T}}\underline{\mathbf{M}}_\mathrm{m}^{\mathrm{T}}, \tag{5.38}$$

According to (5.17), we can use the blocks of $\underline{\mathbf{H}}$ which depend only on one user in order to perform a user specific DOA estimation for each user k, $k = 1 \ldots K$. The extraction of the blocks $\underline{\mathbf{H}}^{(k)\mathrm{T}}$, $k = 1 \ldots K$, can be described as

$$\underline{\mathbf{H}}^{(k)\mathrm{T}} = \underline{\mathbf{H}}^{\mathrm{T}}(\mathbf{u}^{(k)} \otimes \mathbf{I}^{(W)}), \tag{5.39}$$

where $\mathbf{u}^{(k)}$ is the $K \times 1$ identity column vector for the k–th user, with its elements defined as

$$u_l^{(k)} = \begin{cases} 1 & , \quad l = k, \\ 0 & , \text{ otherwise}, \end{cases} \tag{5.40}$$

and $\mathbf{I}^{(W)}$ is the $W \times W$ identity matrix. According to (5.39), the relation

$$\underline{\hat{\mathbf{H}}}^{(k)\mathrm{T}} = \underline{\mathbf{A}}_{\mathrm{s}}^{(k)} \underline{\mathbf{H}}_{\mathrm{d}}^{(k)\mathrm{T}} + \underline{\mathbf{N}}_{\mathrm{m}}^{\mathrm{T}} \underline{\mathbf{M}}_{\mathrm{m}}^{\mathrm{T}} (\mathbf{u}^{(k)} \otimes \mathbf{I}^{(W)}), \quad k = 1 \ldots K, \tag{5.41}$$

can be obtained from (5.38) and (5.22). If we define

$$\underline{\mathbf{X}}^{(k)} = \underline{\hat{\mathbf{H}}}^{(k)\mathrm{T}}, \tag{5.42}$$

$$\underline{\mathbf{S}}^{(k)} = \underline{\mathbf{H}}_{\mathrm{d}}^{(k)\mathrm{T}}, \tag{5.43}$$

$$\underline{\mathbf{N}}^{(k)} = \underline{\mathbf{N}}_{\mathrm{m}}^{\mathrm{T}} \underline{\mathbf{M}}_{\mathrm{m}}^{\mathrm{T}} (\mathbf{u}^{(k)} \otimes \mathbf{I}^{(W)}), \tag{5.44}$$

(5.41) can be written as

$$\underline{\mathbf{X}}^{(k)} = \underline{\mathbf{A}}_{\mathrm{s}}^{(k)} \underline{\mathbf{S}}^{(k)} + \underline{\mathbf{N}}^{(k)}, \quad k = 1 \ldots K. \tag{5.45}$$

According to the notation used in DOA estimation theory, see for instance [RK89, HN95, Haa97a], $\underline{\mathbf{X}}^{(k)}$ denotes the noise–corrupted measurement matrix [Haa97a] of the k–th user composed by W snapshots. $\underline{\mathbf{S}}^{(k)}$ and $\underline{\mathbf{N}}^{(k)}$ are the signal and noise matrices [Haa97a] of the k–th user, respectively, and $\underline{\mathbf{A}}_{\mathrm{s}}^{(k)}$ is the array steering matrix, which depends on the DOAs of the user k, see (5.21). According to (5.45), K independent DOA estimation processes can be performed. An algorithm producing an increased estimation accuracy with a reduced computational burden is Unitary ESPRIT [HN95]. Unitary ESPRIT can be applied to centro–symmetric array configurations [Haa97a], which are used for implementing adaptive antennas in TD–CDMA, see Section 3.4. This algorithm is used in the simulations for the estimation of the DOAs for each user. In Appendix C.1, a summary of the 2D Unitary ESPRIT algorithm is given for the general case that 2D centro–symmetric array configurations are used at the BS receiver. It is finally noted that the performance of 2D Unitary ESPRIT can be considerably enhanced, when the information about the covariance matrix of $\underline{\mathbf{N}}^{(k)}$ of (5.45) is used in the estimation process. In Appendix C.2, the covariance matrix of $\underline{\mathbf{N}}^{(k)}$, $k = 1 \ldots K$, see (5.45), is derived for the large cell channel type. Note that this additional information is used in Chapter 8 for system performance enhancement, when the spectrum efficiency and capacity of TD–CDMA with adaptive antennas are determined for the large cell channel type.

5.3.3.3 Enhanced joint channel estimation

Since the process of DOA estimation produces DOA estimates for each user k, and, consequently, for the user specific array steering matrices $\underline{\mathbf{A}}_{\mathrm{s}}^{(k)}$, $k = 1 \ldots K$, see (5.21), the maximum–likelihood estimate of the combined directional channel impulse response vector $\underline{\mathbf{h}}_{\mathrm{d}}$, see (5.29), can be expressed from (5.32) as [BHP97, Bla98, PSWB99, PFBP99]

$$\underline{\hat{\mathbf{h}}}_{\mathrm{d}} = (\underline{\mathbf{G}}_{\mathrm{d}}^{*\mathrm{T}} \underline{\mathbf{R}}_{\mathrm{m}}^{-1} \underline{\mathbf{G}}_{\mathrm{d}})^{-1} \underline{\mathbf{G}}_{\mathrm{d}}^{*\mathrm{T}} \underline{\mathbf{R}}_{\mathrm{m}}^{-1} \underline{\mathbf{e}}_{\mathrm{m}}, \tag{5.46}$$

where the matrix $\underline{\mathbf{R}}_{\mathrm{m}}$ denotes the total intercell MAI covariance matrix valid for the channel estimation, see (5.10). According to (5.46), the additional advantage of taking into account the total intercell MAI covariance matrix $\underline{\mathbf{R}}_{\mathrm{m}}$ is illustrated when adaptive antennas

are used, compared to the generalized Steiner estimator where only the temporal intercell MAI covariance matrix $\underline{\mathbf{R}}_{\mathrm{m,t}}$ can be incorporated in the estimation process, see (5.11). This property of the enhanced joint channel estimation, see (5.46), is due to the joint temporal and spatial processing of the outputs $\underline{\mathbf{e}}_{\mathrm{m}}^{(k_{\mathrm{a}})}$, $k_{\mathrm{a}} = 1 \ldots K_{\mathrm{a}}$, of the antennas, see (5.46). As already mentioned in Section 5.2, the generalized Steiner estimator processes the outputs of the K_{a} antennas separately, i.e., only a temporal processing is performed, see (5.11). The joint spatial and temporal signal processing performed by the enhanced joint channel estimation expressed by (5.46) can be also illustrated by the equivalent representation of the enhanced channel estimator derived in [BHP97, PWBB98], which explicitely includes the beamformers for the DOAs of each user. However, as for data detection, see the rationale of Section 4.3.3.2, since the representation of [BHP97, PWBB98] departs considerably from the straightforward explanation presented in Section 5.3.2 for the benefits of adaptive antennas in TD–CDMA, it is not followed in this thesis.

5.4 Adaptive antennas for the small cell channel type

5.4.1 System model

In the present section the system model for channel estimation is presented for the small cell channel type, when adaptive antennas are used at the BS. As already mentioned in Section 2.4.3, each of the W elements of a directional channel impulse response is associated with more or less a single direction of incidence. In the following, the general case is considered, where $K_{\mathrm{d}}^{(k,w)}$, $k = 1 \ldots K$, $w = 1 \ldots W$, DOAs are present in the w–th tap of the channel impulse response of the user k. Further, it is assumed that

$$K_{\mathrm{d}}^{(k,w)} < K_{\mathrm{a}}, \quad k = 1 \ldots K, \quad w = 1 \ldots W, \tag{5.47}$$

which is a reasonable assumption in the small cell channel type, e.g., in a dense urban propagation environment [BPW99, PSWB99]. Then, let $\underline{h}_{\mathrm{d},k_{\mathrm{d}}}^{(k,w)}$ describe the channel impulse response corresponding to the k_{d}–th DOA of the w–th tap of the k–th user, which can be observed by an omnidirectional antenna located at the RP of the centro–symmetric array configuration used at the BS receiver, see Fig. 5.1. If $\underline{\mathbf{a}}^{(k,w,k_{\mathrm{d}})}$ represents the associated steering vector, the w–th tap of the channel impulse response vector corresponding to the link between the k–th user and array element k_{a} is given by

$$\underline{h}_{w}^{(k,k_{\mathrm{a}})} = \sum_{k_{\mathrm{d}}=1}^{K_{\mathrm{d}}^{(k,w)}} \underline{a}_{k_{\mathrm{a}}}^{(k,w,k_{\mathrm{d}})} \, \underline{h}_{\mathrm{d},k_{\mathrm{d}}}^{(k,w)}, \; k_{\mathrm{a}} = 1 \ldots K_{\mathrm{a}}, \; w = 1 \ldots W, \; k = 1 \ldots K. \tag{5.48}$$

If we define

$$\underline{\mathbf{A}}_{\mathrm{s}}^{(k,w)} = \left[\underline{\mathbf{a}}^{(k,w,1)} \; \underline{\mathbf{a}}^{(k,w,2)} \ldots \underline{\mathbf{a}}^{(k,w,K_{\mathrm{d}}^{(k,w)})} \right] \tag{5.49}$$

and

$$\underline{\mathbf{h}}_{\mathrm{d}}^{(k,w)} = \left[\underline{h}_{\mathrm{d},1}^{(k,w)}\ \underline{h}_{\mathrm{d},2}^{(k,w)} \ldots \underline{h}_{\mathrm{d},K_{\mathrm{d}}^{(k,w)}}^{(k,w)}\right]^{\mathrm{T}}, \tag{5.50}$$

(5.48) is expressed in matrix–vector form as

$$\underline{\mathbf{h}}_{w}^{(k)} = \underline{\mathbf{A}}_{\mathrm{s}}^{(k,w)}\ \underline{\mathbf{h}}_{\mathrm{d}}^{(k,w)}, \quad k = 1 \ldots K, \quad w = 1 \ldots W. \tag{5.51}$$

Furthermore, if

$$\underline{\mathbf{h}}_{\mathrm{d}}^{(k)} = \left[\underline{\mathbf{h}}_{\mathrm{d}}^{(k,1)\mathrm{T}} \ldots \underline{\mathbf{h}}_{\mathrm{d}}^{(k,W)\mathrm{T}}\right]^{\mathrm{T}}, \ k = 1 \ldots K, \tag{5.52}$$

expresses the directional channel impulse response of user k, where $\underline{\mathbf{h}}_{\mathrm{d}}^{(k,w)}$ is defined in (5.50), the directional channel impulse response vector of all K users is written as

$$\underline{\mathbf{h}}_{\mathrm{d}} = \left[\underline{\mathbf{h}}_{\mathrm{d}}^{(1)\mathrm{T}} \ldots \underline{\mathbf{h}}_{\mathrm{d}}^{(K)\mathrm{T}}\right]^{\mathrm{T}}, \tag{5.53}$$

and its dimension

$$K_{\mathrm{d}} = \sum_{k=1}^{K} \sum_{w=1}^{W} K_{\mathrm{d}}^{(k,w)}. \tag{5.54}$$

Then, if

$$\begin{aligned} \underline{\mathbf{A}}_{\mathrm{d}} \ = \ & \Big[\underline{\mathbf{A}}_{\mathrm{s}}^{(1,1)} \otimes \mathbf{u}^{(1,1)} \ldots \underline{\mathbf{A}}_{\mathrm{s}}^{(1,W)} \otimes \mathbf{u}^{(1,W)} \cdots \\ & \underline{\mathbf{A}}_{\mathrm{s}}^{(K,1)} \otimes \mathbf{u}^{(K,1)} \ldots \underline{\mathbf{A}}_{\mathrm{s}}^{(K,W)} \otimes \mathbf{u}^{(K,W)}\Big], \end{aligned} \tag{5.55}$$

with $\underline{\mathbf{A}}_{\mathrm{s}}^{(k,w)}$, $k = 1 \ldots K$, $w = 1 \ldots W$, defined in (5.49), and $\mathbf{u}^{(k,w)}$, $k = 1 \ldots K$, $w = 1 \ldots W$, being a column vector with elements

$$u_{l}^{(k,w)} = \begin{cases} 1 & , \quad l = (k-1)K + w, \\ & \\ 0 & , \text{ otherwise}, \end{cases} \tag{5.56}$$

the following expression relates $\underline{\mathbf{h}}$ of (5.7) and $\underline{\mathbf{h}}_{\mathrm{d}}$ of (5.53):

$$\underline{\mathbf{h}} = \underline{\mathbf{A}}_{\mathrm{d}}\ \underline{\mathbf{h}}_{\mathrm{d}}. \tag{5.57}$$

According to (5.57), (5.9) can be written in the fashion

$$\underline{\mathbf{e}}_{\mathrm{m}} = (\mathbf{I}^{(K_{\mathrm{a}})} \otimes \underline{\mathbf{G}})\ \underline{\mathbf{A}}_{\mathrm{d}}\ \underline{\mathbf{h}}_{\mathrm{d}} + \underline{\mathbf{n}}_{\mathrm{m}} \tag{5.58}$$

for the small cell channel type. If the expression for $\underline{\mathbf{A}}_{\mathrm{d}}$, see (5.55), is further used, (5.58) can be brought in the equivalent form

$$\underline{\mathbf{e}}_{\mathrm{m}} = \underline{\mathbf{G}}_{\mathrm{d,s}}\ \underline{\mathbf{h}}_{\mathrm{d}} + \underline{\mathbf{n}}_{\mathrm{m}}, \tag{5.59}$$

where

$$\underline{\mathbf{G}}_{\mathrm{d,s}} = \left[\underline{\mathbf{A}}_{\mathrm{s}}^{(1,1)} \otimes \underline{\mathbf{g}}^{(1,1)} \ldots \underline{\mathbf{A}}_{\mathrm{s}}^{(1,W)} \otimes \underline{\mathbf{g}}^{(1,W)} \ldots \right.$$
$$\left. \underline{\mathbf{A}}_{\mathrm{s}}^{(K,1)} \otimes \underline{\mathbf{g}}^{(K,1)} \ldots \underline{\mathbf{A}}_{\mathrm{s}}^{(K,W)} \otimes \underline{\mathbf{g}}^{(K,W)} \right], \tag{5.60}$$

with $\underline{\mathbf{g}}^{(k,w)}$, $k = 1 \ldots K$, $w = 1 \ldots W$, being the w–th column of the matrix $\underline{\mathbf{G}}^{(k)}$, see (5.4). The representations (5.9) and (5.59) of the signal received by all K_{a} array elements, which depends exclusively on the midamble training sequences, will be used for the novel channel estimation technique for the small cell channel type presented in the next section. Before proceeding with the technique, though, it is noted that the comparison between (5.9) and (5.59) leads to the same conclusions as the ones of Section 5.3.2. As in the large cell channel type, see Section 5.3.2, we observe by comparing (5.9) and (5.59) that the number of equations is the same in both expressions. However, the number of unknown parameters in (5.59), i.e., the KW components of the directional channel impulse response vector $\underline{\mathbf{h}}_{\mathrm{d}}$, see (5.53), is reduced compared to the $K_{\mathrm{a}}KW$ unknown components of the channel impulse response vector $\underline{\mathbf{h}}$, see (5.7). This is always valid in the small cell channel type, since

$$KW < K_{\mathrm{a}}KW \tag{5.61}$$

for K_{a} greater than one. Therefore, as in the large cell channel type, an improved estimation quality of the vector $\underline{\mathbf{h}}_{\mathrm{d}}$ from (5.59) is expected, compared to the estimation quality of $\underline{\mathbf{h}}$ from (5.9).

As a final remark, (5.61), as a mathematical expression, is always valid independently of the used channel type. However, (5.61) explicitly refers to the number of DOAs in the small cell channel type and, certainly, it is not valid for the large cell channel type, for which (5.34) holds. Furthermore, by comparing Section 5.3.2 and Section 5.4.1, the real difference between the large cell and the cell small cell channel type is related to the number of DOAs for one user k, $k = 1 \ldots K$, and one channel impulse response tap w, $w = 1 \ldots W$. In the large cell channel type only a single DOA for one user k and one channel impulse response tap w can be observed. In contrast to this situation, in the small cell channel type there can be more than one DOAs for one user k and one channel impulse response tap w. However, the analysis presented next in Section 5.4.2 only holds if K_{d} defined in (5.54) is smaller than $K_{\mathrm{a}}KW$, which is an equivalent assumption to (5.61).

5.4.2 Novel channel estimation

5.4.2.1 Introduction

In this section a novel channel estimation technique for the small cell channel type is presented. As for the large cell channel type, this technique can be divided into the

three steps mentioned in Section 5.3.3.1. The only difference when considering the small cell channel type concerns the second step of Section 5.3.3.1. In the small cell channel type, DOA estimation takes place for each tap of each user. However, the effect of the novel channel estimation technique for the small cell channel type is the same as the one described in Section 5.3.3. As in Section 5.3.3, the improvement achieved by the novel channel estimation technique presented in this section depends on the reduced number of unknown complex elements of the directional channel impulse responses valid in the small cell channel type, see (5.53), compared to the unknown complex elements of the channel impulse responses for the links between each user and each array element valid when the generalized Steiner estimator is used, see (5.7). In Section 5.5, simulation results will demonstrate the improvement achieved by the novel channel estimation technique presented in this section concerning the channel impulse response estimates, compared to the generalized Steiner estimator, see Section 5.2. The link level performance of the considered TD–CDMA mobile radio system using this technique is evaluated in Chapter 6 for different scenarios in dense urban environments.

5.4.2.2 DOA estimation

Since the result of the application of the generalized Steiner estimator, see (5.11), is to produce separate estimates for the $K_{\mathrm{a}}KW$ components of the channel impulse response vector $\underline{\mathbf{h}}$, see (5.7), the parts of $\hat{\underline{\mathbf{h}}}$ from (5.11) which belong to the same user and the same tap can be used for the purpose of a DOA estimation, as described in the following.

Setting out from (5.39), $\underline{\mathbf{h}}_w^{(k)}$, $w = 1 \ldots W$, $k = 1 \ldots K$, of (5.51) is expressed as

$$\underline{\mathbf{h}}_w^{(k)} = \underline{\mathbf{H}}^{\mathrm{T}} \left(\mathbf{u}^{(k)} \otimes \mathbf{I}^{(W)} \right) \mathbf{u}^{(w)}, \tag{5.62}$$

where $\mathbf{u}^{(w)}$, $w = 1 \ldots W$, is the $W \times 1$ identity column vector, with its elements defined as in (5.40). Then, according to (5.38) and (5.62), the estimate $\hat{\underline{\mathbf{h}}}_w^{(k)}$ of $\underline{\mathbf{h}}_w^{(k)}$, see (5.51), is written as

$$\hat{\underline{\mathbf{h}}}_w^{(k)} = \underline{\mathbf{A}}_{\mathrm{s}}^{(k,w)} \underline{\mathbf{h}}_{\mathrm{d}}^{(k,w)} + \underline{\mathbf{n}}_w^{(k)}, \;\; w = 1 \ldots W, \;\; k = 1 \ldots K, \tag{5.63}$$

with

$$\underline{\mathbf{n}}_w^{(k)} = \underline{\mathbf{N}}_{\mathrm{m}}^{\mathrm{T}} \, \underline{\mathbf{M}}_{\mathrm{m}}^{\mathrm{T}} \left(\mathbf{u}^{(k)} \otimes \mathbf{I}^{(W)} \right) \mathbf{u}^{(w)}, \tag{5.64}$$

see also (5.62). According to (5.63), KW independent DOA estimation processes can be performed by using the 2D Unitary ESPRIT algorithm, since 2D centro–symmetric array configurations are assumed to be used at the BS, see Fig. 5.1. Then, estimates for the matrices $\underline{\mathbf{A}}_{\mathrm{s}}^{(k,w)}$, $w = 1 \ldots W$, $k = 1 \ldots K$, see (5.49), can be obtained. Finally, it is noted that the performance of 2D Unitary ESPRIT can be considerably enhanced, when the information about the covariance matrix of $\underline{\mathbf{n}}_w^{(k)}$, see (5.64), is used in the estimation process. In Appendix C.3 the covariance matrix of $\underline{\mathbf{n}}_w^{(k)}$ is derived for the small cell channel type. Note that this additional information is used in Chapter 8 for system performance

enhancement, when the spectrum efficiency and capacity of TD–CDMA with adaptive antennas are determined for the small cell channel type.

5.4.2.3 Enhanced joint channel estimation

Since the DOA estimation processes of Section 5.4.2.2 produce DOA estimates for the DOAs for each tap w, $w = 1 \ldots W$, of each user k, $k = 1 \ldots K$, and consequently for the matrix $\underline{\mathbf{A}}_{\mathrm{d}}$, see (5.55), the maximum–likelihood estimate of the channel impulse response vector $\underline{\mathbf{h}}_{\mathrm{d}}$, see (5.53), can be expressed as [Wha71]

$$\hat{\underline{\mathbf{h}}}_{\mathrm{d}} = (\underline{\mathbf{G}}_{\mathrm{d,s}}^{*\mathrm{T}} \underline{\mathbf{R}}_{\mathrm{m}}^{-1} \underline{\mathbf{G}}_{\mathrm{d,s}})^{-1} \underline{\mathbf{G}}_{\mathrm{d,s}}^{*\mathrm{T}} \underline{\mathbf{R}}_{\mathrm{m}}^{-1} \underline{\mathbf{e}}_{\mathrm{m}}, \tag{5.65}$$

see (5.59). As for the large cell channel type, see (5.46), (5.65) illustrates the additional advantage of using the total intercell MAI covariance matrix $\underline{\mathbf{R}}_{\mathrm{m}}$, see (5.10), when adaptive antennas are used in the small cell channel type, compared to the generalized Steiner estimator, see (5.11).

5.5 Performance of channel estimation

5.5.1 Novel measure for assessing the channel estimation performance

In mobile radio the distribution of the energy of the channel impulse response $\underline{h}(\tau, t)$, see (2.5), along the delay τ depends on the propagation environment. In rural environments small delay spreads are present, whereas in urban environments large delay spreads normally prevail [Par92, BKM96, BBS97]. The effect of small or large delay spreads is observed in the lowpass discrete time channel impulse response $\underline{\mathbf{h}}^{(k,k_{\mathrm{a}})}$, $k = 1 \ldots K$, $k_{\mathrm{a}} = 1 \ldots K_{\mathrm{a}}$, see (5.20) for the large cell channel type and (5.48) for the small cell channel type, by the distribution of the channel impulse response energy along the components $\underline{h}_w^{(k,k_{\mathrm{a}})}$, $w = 1 \ldots W$, of $\underline{\mathbf{h}}^{(k,k_{\mathrm{a}})}$.

In rural environments the delay spread normally does not exceed 1 μs [Naß95, Bla98]. Based on the parameters of the considered TD–CDMA mobile radio system [Bla98], the chip duration T_{c}, which expresses the time delay between two successive components $\underline{h}_w^{(k,k_{\mathrm{a}})}$, $w = 1 \ldots W$, of $\underline{\mathbf{h}}^{(k,k_{\mathrm{a}})}$, is 0.5 μs, see Table 5.1. Therefore, only the first one or two components of $\underline{\mathbf{h}}^{(k,k_{\mathrm{a}})}$, $k = 1 \ldots K$, $k_{\mathrm{a}} = 1 \ldots K_{\mathrm{a}}$, have considerable energy, and the contribution of the remaining $W - 1$ or $W - 2$ components may be neglected. On the other hand, in urban environments the delay spread takes values between 5 μs and 10 μs [Naß95, Bla98], which means that the energy of $\underline{\mathbf{h}}^{(k,k_{\mathrm{a}})}$, $k = 1 \ldots K$, $k_{\mathrm{a}} = 1 \ldots K_{\mathrm{a}}$, is distributed over a larger number of components.

Therefore, when evaluating the quality of the channel impulse response estimates, a measure has to be used which explicitly takes into account the energy of each component of

Table 5.1. System parameters for the TD–CDMA mobile radio system considered in the simulations, see also [Bla98].

multiple access scheme:	
width of a partial frequency band	$B = 1.6$ MHz
duration of a TDMA frame	$T_{\mathrm{fr}} = 6$ ms
duration of a time slot	$T_{\mathrm{bu}} = 0.5$ ms
number of time slots per frame	$N_{\mathrm{t}} = 12$
maximum allowable number of simultaneously active users in a time slot	$K_{\max} = 8$
burst structure:	
duration of a data block	$T_{\mathrm{d}} = 168$ μs
duration of the midamble	$T_{\mathrm{m}} = 134$ μs
duration of the guard interval	$T_{\mathrm{g}} = 30$ μs
duration of a data symbol	$T_{\mathrm{s}} = 7$ μs
duration of a chip	$T_{\mathrm{c}} = 0.5$ μs
size of the data symbol alphabet	$M = 4$
number of data symbols per data block	$N = 24$
number of chips of a CDMA code	$Q = 14$
number of chips of a midamble training sequence	$L_{\mathrm{m}} = 268$
convolutional coder:	
constraint length	$K_{\mathrm{c}} = 5$
code rate	$R_{\mathrm{c}} = 1/2$
generator polynome (octal)	23, 35
block interleaver:	
interleaving depth	$I_{\mathrm{d}} = 4$ bursts
interleaving matrix	4×96
filters:	
chip impulse filter	linear filtering with the GMSK–basic impulse $C_0(\tau)$ of time–bandwidth product 0.3
digital receive filter	approximately ideal lowpass, 1 MHz cutoff frequency
netto data rate of a single user	8 kbit/s $\leq R \leq$ 768 kbit/s

the channel impulse responses to be evaluated, thus achieving a fair comparison between the used channel estimation techniques. Moreover, the quality of the channel impulse response estimates should be independent of the total energy of the channel impulse responses. In order to fulfill the above mentioned requirements, a suitable measure for assessing the quality of channel estimation is proposed in the following.

Since the complex channel impulse responses in the equivalent lowpass domain are considered, the real part and the imaginary part of their components are treated separately. To this end, let $h_{\mathrm{r},w}^{(k,k_{\mathrm{a}})}$ and $h_{\mathrm{i},w}^{(k,k_{\mathrm{a}})}$ denote the real and the imaginary part of $h_w^{(k,k_{\mathrm{a}})}$, $w = 1 \ldots W$,

$k = 1 \ldots K$, $k_\mathrm{a} = 1 \ldots K_\mathrm{a}$, see (5.20) and (5.48). Further, let $\Delta h_{\mathrm{r},w}^{(k,k_\mathrm{a})}$ denote the difference between $h_{\mathrm{r},w}^{(k,k_\mathrm{a})}$ and its estimate $\hat{h}_{\mathrm{r},w}^{(k,k_\mathrm{a})}$, and $\Delta h_{\mathrm{i},w}^{(k,k_\mathrm{a})}$ denote the difference between $h_{\mathrm{i},w}^{(k,k_\mathrm{a})}$ and its estimate $\hat{h}_{\mathrm{i},w}^{(k,k_\mathrm{a})}$, i.e.,

$$\Delta h_{\mathrm{r},w}^{(k,k_\mathrm{a})} = \hat{h}_{\mathrm{r},w}^{(k,k_\mathrm{a})} - h_{\mathrm{r},w}^{(k,k_\mathrm{a})}, \quad w = 1 \ldots W,\ k = 1 \ldots K,\ k_\mathrm{a} = 1 \ldots K_\mathrm{a}, \tag{5.66}$$

$$\Delta h_{\mathrm{i},w}^{(k,k_\mathrm{a})} = \hat{h}_{\mathrm{i},w}^{(k,k_\mathrm{a})} - h_{\mathrm{i},w}^{(k,k_\mathrm{a})}, \quad w = 1 \ldots W,\ k = 1 \ldots K,\ k_\mathrm{a} = 1 \ldots K_\mathrm{a}. \tag{5.67}$$

Then, the desired measures for assessing the quality of the channel impulse response estimates are given by

$$\epsilon_\mathrm{r}^{(k,k_\mathrm{a})} = \mathrm{E}\left\{ \frac{\sum_{w=1}^{W} \mid \Delta h_{\mathrm{r},w}^{(k,k_\mathrm{a})} h_{\mathrm{r},w}^{(k,k_\mathrm{a})} \mid^2}{\sum_{w=1}^{W} \left(h_{\mathrm{r},w}^{(k,k_\mathrm{a})} \right)^2} \right\},\ k = 1 \ldots K, k_\mathrm{a} = 1 \ldots K_\mathrm{a}, \tag{5.68}$$

$$\epsilon_\mathrm{i}^{(k,k_\mathrm{a})} = \mathrm{E}\left\{ \frac{\sum_{w=1}^{W} \mid \Delta h_{\mathrm{i},w}^{(k,k_\mathrm{a})} h_{\mathrm{i},w}^{(k,k_\mathrm{a})} \mid^2}{\sum_{w=1}^{W} \left(h_{\mathrm{i},w}^{(k,k_\mathrm{a})} \right)^2} \right\},\ k = 1 \ldots K, k_\mathrm{a} = 1 \ldots K_\mathrm{a}, \tag{5.69}$$

for the real part and the imaginary part, respectively, where $\mathrm{E}\{\cdot\}$ denotes the expectation operator. In practice the expectations in (5.66) and (5.67) have to be obtained by a finite but large number of experiments, e.g., 10^3. It is obvious from (5.66) and (5.67) that the proposed measure of the channel estimation error

- first, is the weighted sum of the errors corresponding to each component of the channel impulse response, the weights depending on the received energy of each component, and
- second, is independent of the total channel impulse response energy.

Therefore, the measure fulfills the requirements stated above in this section for assessing the channel estimation performance. Finally, in order to have a global measure for assessing the channel estimation performance in TD–CDMA, i.e., a measure which jointly considers all KK_a channel impulse responses, the mean estimation error

$$\epsilon_\mathrm{r} = \frac{1}{KK_\mathrm{a}} \sum_{k=1}^{K} \sum_{k_\mathrm{a}=1}^{K_\mathrm{a}} \epsilon_\mathrm{r}^{(k,k_\mathrm{a})} \tag{5.70}$$

$$\epsilon_\mathrm{i} = \frac{1}{KK_\mathrm{a}} \sum_{k=1}^{K} \sum_{k_\mathrm{a}=1}^{K_\mathrm{a}} \epsilon_\mathrm{i}^{(k,k_\mathrm{a})} \tag{5.71}$$

of the real part and the imaginary part, respectively, can be introduced. In the following, ϵ_r, see (5.68), and ϵ_i, see (5.71), are determined for the large cell and the small cell channel type, respectively, by simulations.

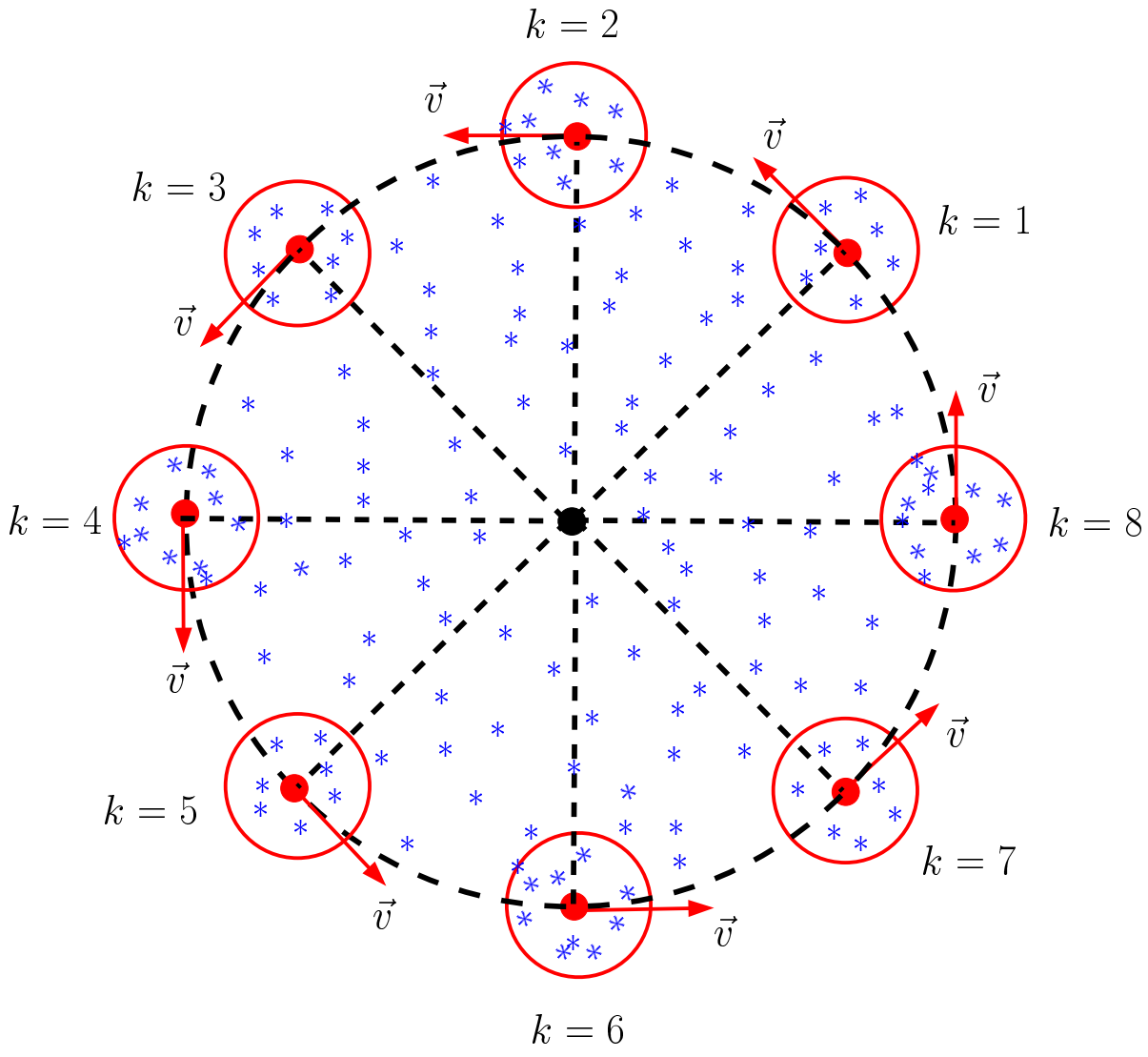

Figure 5.2. Considered spatial scenario for the large cell channel type; UKL 2 rural channel model; $K = 8$ users; $v = 3$ km/h

5.5.2 Simulation results

5.5.2.1 Preliminary remarks

In this section, the quality of the channel impulse response estimates achieved by the techniques of Sections 5.2 to 5.4 is investigated by simulation results in the uplink of TD–CDMA, with 2D centro–symmetric array configurations being used at the BS receiver, see Fig. 3.4 and Fig. 5.1. Concerning the channel models chosen for the simulations, it is noted that when the modified COST 207 channel models, see Section 2.3.2, are

used, since the directional inhomogeneity of the mobile radio channel is modeled by single DOAs, these DOAs can be assumed to be perfectly known at the BS receiver [PFBP99]. This assumption, however, is not valid when the UKL 2 directional channel models, see Section 2.3.3, are used. This is due to the fact that the definition of scattering areas by the UKL 2 directional channel models gives rise to the existence of a great number of single DOAs, valid for the link between each MS and the considered BS, see also [Bla98]. Therefore, the influence of DOA estimation on the channel estimation performance should be explicitly investigated only for the modified COST 207 channel models, because only the use of these models provides the possibility of perfect DOA knowledge. However, since the channel estimation performance has been already extensively assessed for the modified COST 207 channel models, see [PW99], in this section only the UKL 2 directional channel models are considered. First, the generalized Steiner estimator, see Section 5.2, is compared with the channel estimation technique for the large cell channel type, see Section 5.3.2. Then, the generalized Steiner estimator is compared with the novel channel estimation technique for the small cell channel type, see Section 5.4.2. Simulation results for the BER performance including channel estimation are presented in Chapter 6.

5.5.2.2 Large cell channel type

In this section the performance of channel estimation is assessed for the large cell channel type, see Section 2.4.2. In the simulations the UKL 2 rural channel model, see Section 2.3.3, is used, which belongs to the large cell channel type. The spatial scenario is illustrated in Fig. 5.2. There are K equal to eight users active in the same frequency band and time slot, and all users move within the scenario on a fictitious circular path with velocity vector $\vec{v}$ as shown in Fig. 5.2. For each user, v is assumed to be equal to 3 km/h. Further, a cross array configuration of K_a equal to eight antennas is used at the BS, see also Fig. 3.4. The parameters of TD–CDMA valid for channel estimation can be taken from Table 5.1, see also Fig. 1.2. Finally, the intercell MAI is assumed to be white and Gaussian distributed, i.e., $\underline{\mathbf{R}}_\mathrm{m}$ of (5.10) equals the $K_\mathrm{a}L \times K_\mathrm{a}L$ identity matrix.

In Figs. 5.3 and 5.4 the estimation errors ϵ_r and ϵ_i, see (5.68) and (5.69), respectively, are depicted versus the mean input SNR $\bar{\gamma}_\mathrm{in}$, which is defined in (6.23) of Section 6.3.2. The results are averaged over 10^3 transmitted bursts. It is noted that after the implementation of (5.46), (5.22) is applied, thus enabling the comparison of the generalized Steiner estimator with the channel estimation technique of Section 5.3. The number of impinging DOAs are estimated according to the modified MDL criterion for centro–symmetric array configurations [XRK94], see also Section 1.3, and the DOAs themselves are estimated by the 2D Unitary ESPRIT algorithm [HN95, Haa97a], see Appendix C.1. The considerable improvement offered by the channel estimation technique for the large cell channel type, compared to the generalized Steiner estimator, is obvious from Figs. 5.3 and 5.4, especially at low values of the mean input SNR $\bar{\gamma}_\mathrm{in}$. As shown in Chapter 6, where the BER performance of TD–CDMA with adaptive antennas is investigated, the critical values of $\bar{\gamma}_\mathrm{in}$ which lead to small values of the BER lie in that region, where the improvement of the channel estimation technique of Section 5.3.2 is large compared to

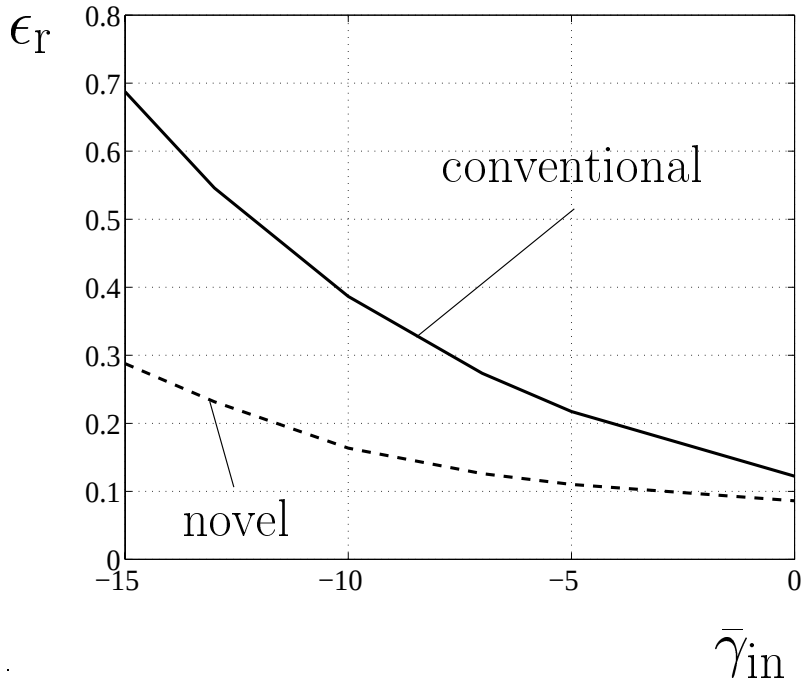

Figure 5.3. Estimation error ϵ_{r} of (5.68) versus the mean input SNR $\bar{\gamma}_{\mathrm{in}}$ of (6.23); UKL 2 rural channel model; spatial scenario as in Fig. 5.2; $K = 8$ users; $K_{\mathrm{a}} = 8$ antennas; $v = 3$ km/h

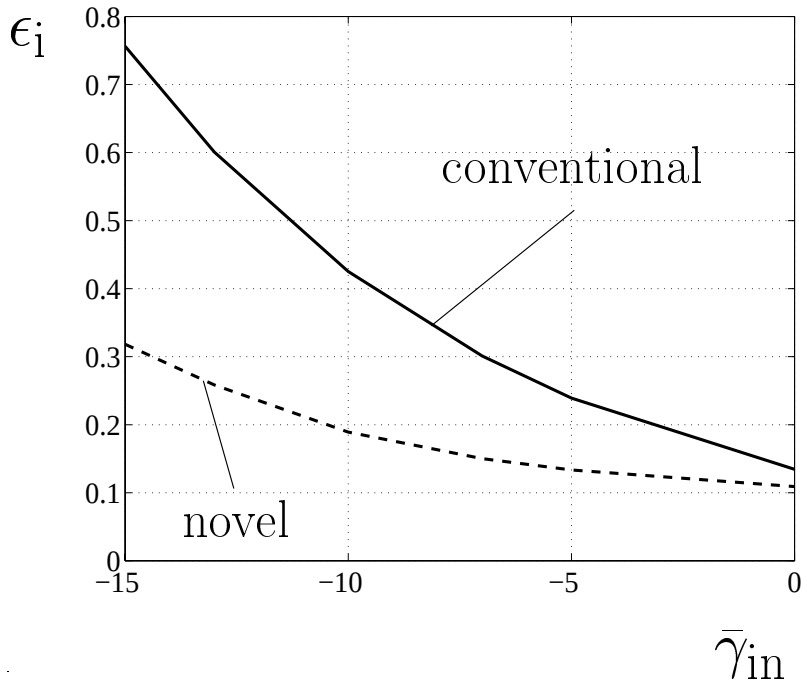

Figure 5.4. Estimation error ϵ_{i} of (5.69) versus the mean input SNR $\bar{\gamma}_{\mathrm{in}}$ of (6.23); UKL 2 rural channel model; spatial scenario as in Fig. 5.2; $K = 8$ users; $K_{\mathrm{a}} = 8$ antennas; $v = 3$ km/h

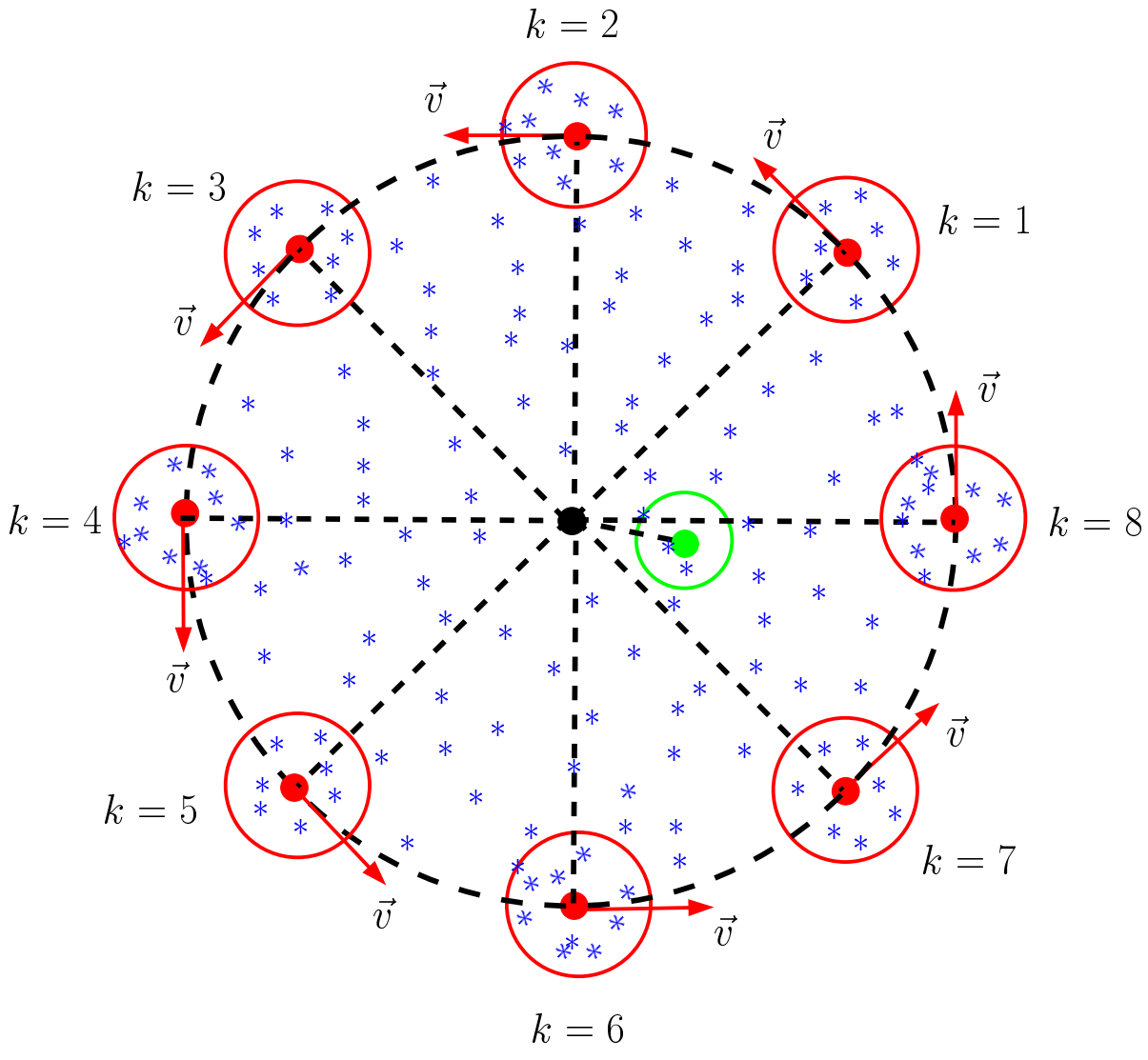

Figure 5.5. Considered spatial scenario for the small cell channel type; UKL 2 dense urban channel model; $K = 8$ users; $v = 3$ km/h; the circle in gray represents the additional scattering area defined by the used channel type, see Section 2.3.3 and Table 2.1

the generalized Steiner estimator, i.e., between -10 dB and -5 dB, see Figs. 5.3 and 5.4. Finally, it is noted that the performance improvement achieved by the channel estimation technique of Section 5.3.2 compared to the generalized Steiner estimator becomes larger as the number of antennas increase.

5.5.2.3 Small cell channel type

In this section the performance of channel estimation is assessed for the small cell channel

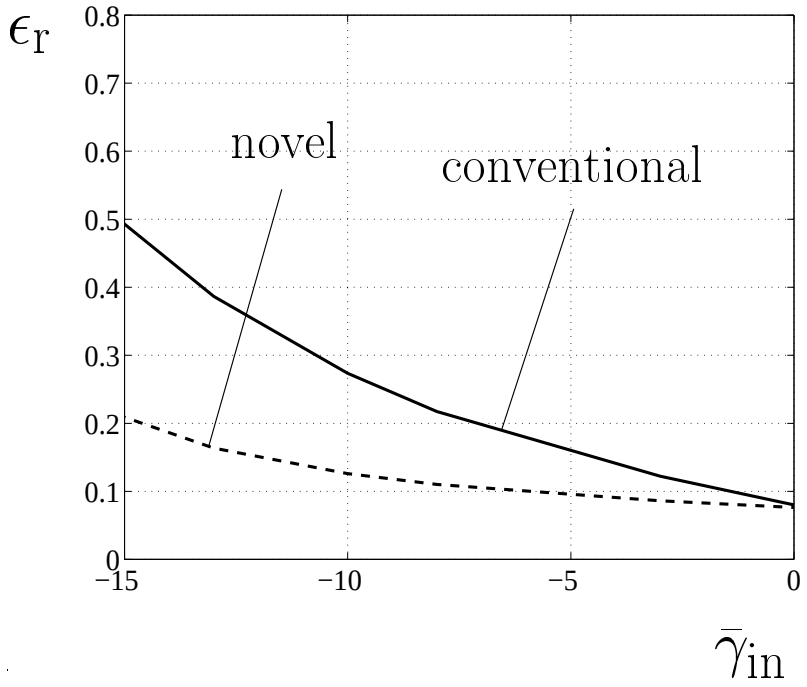

Figure 5.6. Estimation error ϵ_r of (5.68) versus the mean input SNR $\bar{\gamma}_{in}$ of (6.23); UKL 2 dense urban channel model; spatial scenario as in Fig. 5.5; $K = 8$ users; $K_a = 8$ antennas; $v = 3$ km/h

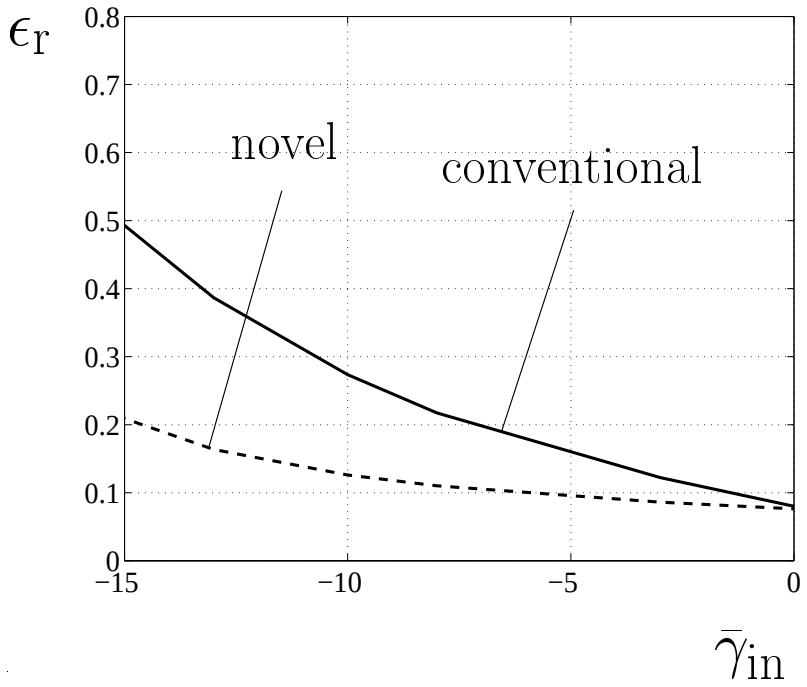

Figure 5.7. Estimation error ϵ_i of (5.69) versus the mean input SNR $\bar{\gamma}_{in}$ of (6.23); UKL 2 dense urban channel model; spatial scenario as in Fig. 5.5; $K = 8$ users; $K_a = 8$ antennas; $v = 3$ km/h

type, see Section 2.4.3. In the simulations the UKL 2 dense urban channel model, see Section 2.3.3, is used, which belongs to the small cell channel type. The considered spatial scenario is shown in Fig. 5.5. The other parameters are the same as those used in the simulations performed for the large cell channel type, see Section 5.5.2.2. In Figs. 5.6 and 5.7 the estimation errors ϵ_{r} and ϵ_{i}, see (5.68) and (5.69), respectively, are shown versus the mean input SNR $\bar{\gamma}_{\mathrm{in}}$ for the UKL 2 dense urban channel model, where the results are obtained by averaging over 10^3 transmitted bursts. The generalized Steiner estimator and the novel channel estimation technique presented in Section 5.4.2 are compared with respect to the quality of the channel impulse response estimates. As in the large cell channel type, after the implementation of (5.65), (5.57) is applied, thus enabling the comparison of the generalized Steiner estimator with the novel channel estimation technique for the small cell channel type. In the simulations, only a single DOA per tap is considered, see Section 2.4.3. Moreover, the DOAs are estimated by the 2D Unitary ESPRIT algorithm [HN95, Haa97a], see Appendix C.1. The considerable improvement offered by the novel channel estimation technique for the small cell channel type compared to the generalized Steiner estimator is obvious from Figs. 5.6 and 5.7, especially at low values of the mean input SNR $\bar{\gamma}_{\mathrm{in}}$. As it is shown in Chapter 6, where the BER performance of TD–CDMA with adaptive antennas is investigated, the critical values of $\bar{\gamma}_{\mathrm{in}}$, which lead to small values of the BER, lie in that region where the improvement of the novel channel estimation technique of Section 5.4.2 is large compared to the generalized Steiner estimator, i.e., between -12 dB and -6 dB. Finally, the comparison of the curves of Figs. 5.6 and 5.7 with those of Figs. 5.3 and 5.4 leads to the conclusion that the improvement achieved by the novel channel estimation technique for the small cell channel type is smaller than the one for the large cell channel type, compared to the generalized Steiner estimator. This is due to the increased diversity of the UKL 2 dense urban channel model compared to the UKL 2 rural channel model, see also [Bla98]. In any case, though, the channel estimation improvement achieved by adaptive antenna concepts in TD–CDMA is considerable, compared to the Steiner estimator, which is the state of the art channel estimation technique for TD–CDMA [BPW99]. This improvement leads directly to a more favourable BER performance of TD–CDMA, which is illustrated in Chapter 6.

6 Performance assessment methods for TD–CDMA with adaptive antennas

6.1 Introduction

In Chapter 4 the problem of data detection in a TD–CDMA mobile radio system is treated in detail. There, the benefits of adaptive antennas are demonstrated in the case of known channel impulse responses. The problem of channel estimation in TD–CDMA is considered separately in Chapter 5, where the benefits of adaptive antennas are illustrated both by a theoretical analysis and simulation results. In this chapter, two performance assessment methods for TD–CDMA, including the use of adaptive antennas, are presented. The first method is a novel simulation concept for TD–CDMA which offers a reduced simulation time and complexity compared to the existing simulation concepts for TD–CDMA [Naß95, Bla98]. The second method is based on the SNR degradation valid for TD–CDMA receivers [Kle96], which is the key quantity when evaluating the performance of TD–CDMA. Both methods are used alternatively in this thesis for assessing the performance of TD–CDMA with adaptive antennas.

6.2 Novel simulation concept for TD–CDMA

6.2.1 General

The design of communications systems can be considerably eased by computer–aided engineering methods [Edr94, Naß95]. One of the most important engineering methods is the simulation of complex communications systems, such as the TD–CDMA mobile radio systems [BSS84, JBS92]. Although sophisticated simulation concepts offer the advantage of rather cost efficient investigations compared to measurements with realtime experimental hardware setups, simulations are still connected with an enormous expense of time [POB99]. This is mainly due to the fact that the existing simulation concepts model the entire system behaviour without taking advantage of the system structure [POB99]. In this section, a novel simulation concept of reduced computational complexity is presented for a TD–CDMA mobile radio system, including the use adaptive antennas. The novel simulation concept and the simulation concept applied up to now [Naß95, Bla98], which is addressed as the original simulation concept for TD–CDMA, are compared with regard to computational complexity and accuracy through simulation results in Section 6.4.

6.2.2 Simulation methods for communications systems

A communications system can be mathematically analyzed in closed form either in an approximative manner or not at all [Edr94, Naß95]. There is, though, the possibility

to analyze and optimize a communications system by the use of experimental methods or by modeling and simulating the system on the digital computer. The experimental production of results is not only time consuming, but it also requires a large number on experienced personnel [Naß95]. Further, the possibility of changing the system parameters or the basic system components is excluded most of the time [Edr94, Naß95]. Therefore, in order to save time and complexity, the analysis and optimization especially of complex communications systems is performed by modeling and simulation on the digital computer [BSS84, JBS92].

The simulation model used on the digital computer should include the statistical and dynamical properties of the communications system to be investigated. When stochastic quantities are used in the simulation model, then the simulation method is termed Monte Carlo [BSS84, JBS92, Edr94, Naß95]. Monte Carlo simulations have been used worldwide for the standardization and optimization of 3G mobile radio systems [ASS98, Naß95, Ste95, Kle96]. The produced results by Monte Carlo simulations depend generally on the number of conducted experiments. As the number of experiments increase, the precision of the results increases [BSS84, JBS92]. Certainly, there is always a trade–off between simulation precision and simulation time. Therefore, a confidence interval and a confidence probability is defined for the produced results from a Monte Carlo simulation [Naß95]. The confidence probability of a result describes the probability that a produced result by the Monte Carlo method lies within a fixed interval. This interval is called confidence interval for the considered Monte Carlo simulation result [Naß95]. Relying on the analysis of [Naß95], if $10^{-\mu}$ denotes the BER $\bar{P}_\mathrm{b}$ to be estimated by simulations, all simulation results producing an estimate of $\bar{P}_\mathrm{b}$ which lies, with a confidence probability greater than 95%, within the confidence interval $[0.9 \cdot 10^{-\mu}, 1.1 \cdot 10^{-\mu}]$ are considered as reliable.

The task and goal of modeling and simulating a communications system is to represent the real world as closely as possible, whereas simultaneously the simulation complexity and time should be held as low as possible [Edr94, Naß95]. At this point, a compromise between the close representation of the real world and the simulation complexity and time has to be found. The simulation complexity and, consequently, the simulation time can be considerably reduced, if only the basic components of the complex communications system to be investigated are modeled, whereas the components which do not play a decisive role in the system evaluation may be neglected [Edr94, Naß95]. Further, a very important issue concerning the modeling and simulation of a communications system is the choice of the simulation tool. The precision of the results, the necessary hardware and software, as well as the total financial cost depend very much on this choice [BSS84, JBS92, Edr94, Naß95]. Certainly, the experience of the persons who make this choice can ease the final decision considerably [BSS84, JBS92, Edr94, Naß95].

Concerning the TD–CDMA mobile radio system, a simulation concept already exists, which models and analyzes the system behaviour for different given operation situations [Naß95, Bla98]. The main characteristic of this simulation concept for TD–CDMA is the modeling of the entire system behaviour, i.e., the original simulation concept for TD–

CDMA does not take advantage of the specific structure of TD–CDMA receivers [POB99].

As the original simulation concept, the novel simulation concept for TD–CDMA presented in this section belongs to the class of signal flow driven simulators, which, in contrast to time driven simulators, offer the advantages of [Naß95]

- blockwise signal transfer between modules, i.e., transfer of signal vectors,
- the choice of any sampling frequency, which is an important parameter related to the efficient usage of the total system bandwidth,
- fewer calls of subroutines, and
- smaller complexity and simulation time

at the cost of a more complex programming, especially of the interfaces between modules, since signal vectors are always transferred. Further, the novel simulation concept is capable of taking into account

- adaptive antenna concepts applied at the BS transceiver, and
- channel estimation errors,

like the original simulation concept for TD–CDMA [Naß95, Bla98]. However, in contrast to the original simulation concept, the novel simulation concept explicitly exploits the main characteristic of TD–CDMA receivers, which is the JD of the user data [Kle96], see also Section 1.2 and Section 4.3.3.2. The novel simulation concept for TD–CDMA is presented in detail in the following.

6.2.3 Detailed analysis of the novel simulation concept for TD–CDMA

6.2.3.1 Preliminaries

In Section 4.2 a detailed description of the system model of a TD–CDMA mobile radio system including adaptive antennas is given. Here, we assume that the received signal in TD–CDMA is determined in general by

$$\underline{\mathbf{e}} = \underline{\mathbf{A}}\ \underline{\mathbf{d}} + \underline{\mathbf{n}}, \tag{6.1}$$

see also (4.20). In (6.1) $\underline{\mathbf{A}}$ represents the system matrix, which includes the use of adaptive antenna concepts at the BS, see (4.11). $\underline{\mathbf{d}}$, see (4.5), is the combined data vector of

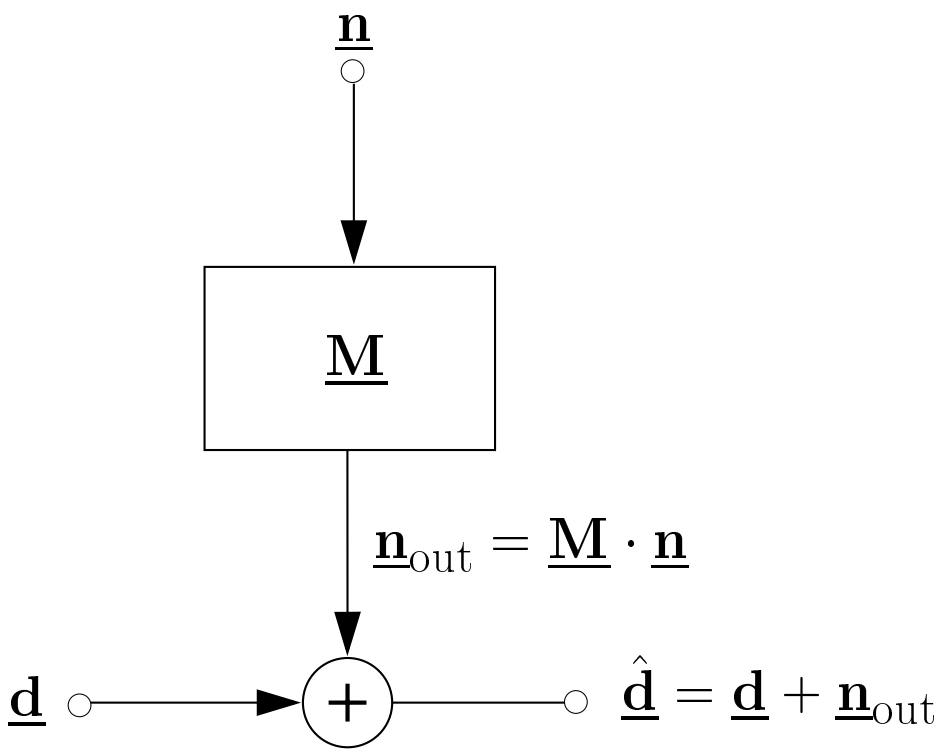

Figure 6.1. Schematic representation of the novel view on the JD process according to (6.2) and (6.5), see also [POB99]

all K users active in the same frequency band and time slot, and $\underline{\mathbf{n}}$ represents the additive noise vector, which is made up by intercell MAI in the interference–limited case, see also Section 4.3.3.2. In this chapter we deal with the uplink of TD–CDMA. The analysis of the novel simulation concept presented in this section can be transferred unaltered to the downlink of TD–CDMA [POB99].

6.2.3.2 Known channels

First, it is assumed that the channel impulse responses valid for the links between each user and each antenna of the array configuration used at the BS, see Fig. 4.3, are perfectly known at the receiver. In this case, by applying the ZF–BLE, see Section 4.3.2.2, a linear estimate

$$\underline{\hat{\mathbf{d}}} = \left(\underline{\mathbf{A}}^{*\mathrm{T}}\underline{\mathbf{R}}_{\mathrm{n}}^{-1}\underline{\mathbf{A}}\right)^{-1}\underline{\mathbf{A}}^{*\mathrm{T}}\underline{\mathbf{R}}_{\mathrm{n}}^{-1}\underline{\mathbf{e}} = \underline{\mathbf{M}}\ \underline{\mathbf{e}}, \tag{6.2}$$

of the combined data vector $\underline{\mathbf{d}}$, see (4.5), can be obtained, where $\underline{\mathbf{R}}_{\mathrm{n}}$ denotes the covariance matrix of the intercell MAI, see also (4.21). The matrix

$$\underline{\mathbf{M}} = \left(\underline{\mathbf{A}}^{*\mathrm{T}}\underline{\mathbf{R}}_{\mathrm{n}}^{-1}\underline{\mathbf{A}}\right)^{-1}\underline{\mathbf{A}}^{*\mathrm{T}}\underline{\mathbf{R}}_{\mathrm{n}}^{-1}, \tag{6.3}$$

see also the analysis presented in Section 4.3.3.2, plays a fundamental role for the development of the novel simulation, and is addressed as the channel matrix in what follows [POB99]. (6.2) can be also written in the form

$$\hat{\underline{\mathbf{d}}} = \underline{\mathbf{d}} + \underline{\mathbf{M}}\ \underline{\mathbf{n}} = \underline{\mathbf{d}} + \underline{\mathbf{n}}_{\text{out}} \tag{6.4}$$

with

$$\underline{\mathbf{n}}_{\text{out}} = \underline{\mathbf{M}}\ \underline{\mathbf{n}}. \tag{6.5}$$

As also mentioned in Section 4.3.3.2, (6.4) and (6.5) offer a novel view on the JD process. If the channel impulse responses, and consequently the system matrix $\underline{\mathbf{A}}$, see (6.1), are perfectly known at the receiver, the JD process according to (6.4) is transparent for the data transmitted by the users assigned to the considered BS. The only effect of the JD process is a transformation of the input intercell MAI vector $\underline{\mathbf{n}}$, see (6.1), into an output intercell MAI vector $\underline{\mathbf{n}}_{\text{out}}$ according to (6.5), see also Section 4.3.3.2. This transformation depends on the specifics contained in the matrix $\underline{\mathbf{M}}$, see (6.3), i.e., the channel model, the CDMA codes, and the used antenna configuration at the BS receiver, and not on the way the user data are modulated, interleaved, and coded. This characteristic of the JD process is schematically illustrated in Fig. 6.1.

In the following, the implementation of the novel simulation concept for TD–CDMA is analyzed in detail. In TD–CDMA the total available system bandwidth B_{sys} is divided into N_{par} partial frequency bands each of size B [Bla98], see Fig. 1.1. A single partial frequency band of size B is considered in the following. As already mentioned in Section 1.2, the TDMA component of TD–CDMA offers the possibility of partitioning the time in TDMA bursts, each of length T_{bu}, see Fig. 1.1. In each burst a number of K users is simultaneously active, and a specific number of TDMA bursts constitutes a TDMA frame of length T_{fr}, see Fig. 1.1. It is assumed that in each TDMA burst a different user group l, $l = 0 \ldots T_{\text{fr}}/T_{\text{bu}} - 1$, is active. This scheme allows the repetitive transmission of data pertaining to a specific user within a user group. Then, a general burst number i is assigned to each transmitted TDMA burst [POB99]. This number depends on the ratio $T_{\text{fr}}/T_{\text{bu}}$ and on the considered user group l. The general burst number i is defined as [POB99]

$$i = i^{(l)} = l + \mu \frac{T_{\text{fr}}}{T_{\text{bu}}}, \quad \mu = 0, 1, 2, \ldots \tag{6.6}$$

If, e.g., the user group $l = 0$ is considered, a series of general burst numbers valid for this user group can be defined according to (6.6)

$$i = i^{(0)} = \mu \frac{T_{\text{fr}}}{T_{\text{bu}}}, \quad \mu = 0, 1, 2, \ldots \tag{6.7}$$

The general burst numbers of a TDMA frame are depicted in Fig. 6.2, when

$$\frac{T_{\text{fr}}}{T_{\text{bu}}} = 8. \tag{6.8}$$

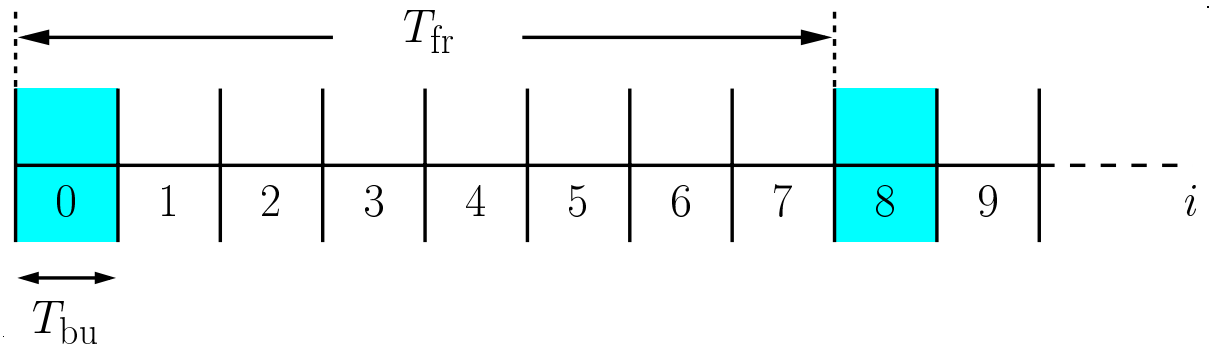

Figure 6.2. General burst numbers i in a TDMA frame, when $T_{\mathrm{fr}}/T_{\mathrm{bu}}$ equals eight

The shaded regions in Fig. 6.2 represent the bursts utilized by the user group $l = 0$. In the example of Fig. 6.2, the user group $l = 0$ utilizes the general burst numbers $0, 8, 16, 32 \ldots$, see (6.7).

Exactly as a general burst number i is assigned to each transmitted TDMA burst, a channel matrix $\underline{\mathbf{M}}_\nu$, $\nu = 0, 1, 2, \ldots$, see (6.3), is valid for each transmitted TDMA burst. It is assumed that the channel matrix $\underline{\mathbf{M}}_\nu$, $\nu = 0, 1, 2, \ldots$, see (6.3), remains unaltered for the duration of a TDMA burst [POB99]. It is further assumed that the users within a user group move with a constant velocity v, and the smallest possible non–zero velocity of a user group is denoted by v_0. The transition from the channel matrix $\underline{\mathbf{M}}_\nu$ to the channel matrix $\underline{\mathbf{M}}_{\nu+1}$ takes place, when the users of the considered user group l, $l = 0 \ldots T_{\mathrm{fr}}/T_{\mathrm{bu}} - 1$, [POB99]

- move with the smallest non–zero velocity v_0, and
- utilize a successive burst.

In the special case that the users of a user group do not move at all, i.e., v is equal to zero, the channel matrix $\underline{\mathbf{M}}_\nu$ remains the same, when successive bursts are utilized. In general, the index ν of the channel matrix $\underline{\mathbf{M}}_\nu$ depends on

1. the considered user group l, $l = 0 \ldots T_{\mathrm{fr}}/T_{\mathrm{bu}} - 1$,
2. the general burst number i, see (6.6), and
3. the velocity v of the users of the considered user group.

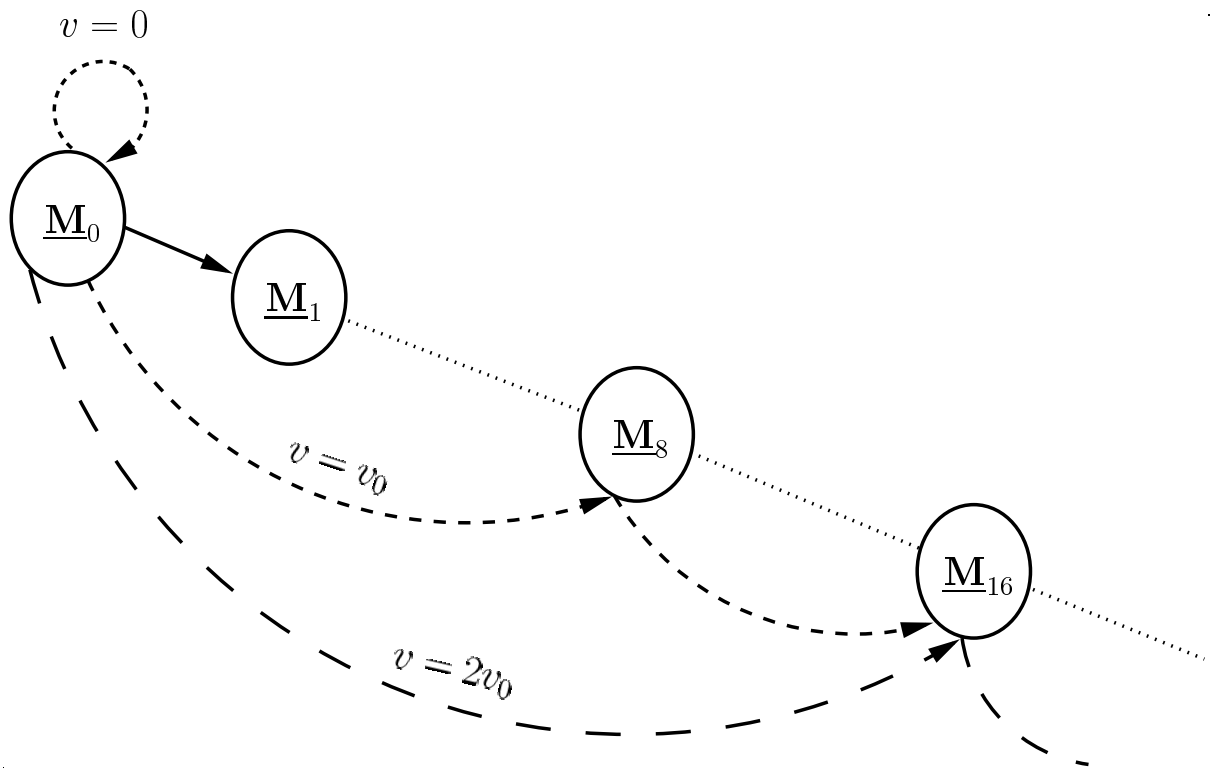

Figure 6.3. Series of channel matrices for the user group $l = 0$; $T_{\mathrm{fr}}/T_{\mathrm{bu}} = 8$

Then, as in the case of the general burst numbers, see (6.6), a series $\underline{\mathbf{M}}_\nu$ of channel matrices valid for user group l can be defined [POB99]. The index ν of the channel matrices $\underline{\mathbf{M}}_\nu$ valid for the considered user group l, $l = 0 \ldots T_{\mathrm{fr}}/T_{\mathrm{bu}} - 1$, is given by [POB99]

$$\nu = \left(l + i^{(0)}\right) \cdot \frac{v}{v_0} = \left(l + \mu \frac{T_{\mathrm{fr}}}{T_{\mathrm{bu}}}\right) \cdot \frac{v}{v_0}, \quad \mu = 0, 1, 2, \ldots , \tag{6.9}$$

where $i^{(l)}$ is defined in (6.6). In Fig. 6.3 the series of channel matrices valid for user group $l = 0$ is illustrated for the cases $v = 0$, $v = v_0$, and $v = 2v_0$, respectively. Here, it is assumed that (6.8) is valid. E.g., if the users within user group $l = 0$ move with a velocity v equal to v_0 and $T_{\mathrm{fr}}/T_{\mathrm{bu}}$ equals 8, the index ν of the channel matrices valid for this group takes the values $0, 8, 16, 24, 32, \ldots$, whereas, if v equals $2v_0$, the index ν takes the values $0, 16, 32, \ldots$.

After having shown the usage of the channel matrices $\underline{\mathbf{M}}_\nu$, see (6.5) and (6.9), in the novel simulation concept according to (6.5) an intercell MAI noise vector $\underline{\mathbf{n}}$ for each transmitted burst is required in order to obtain the output MAI vector $\underline{\mathbf{n}}_{\mathrm{out}}$. It is assumed that for each general burst number i, see (6.6), an independent intercell MAI vector $\underline{\mathbf{n}}$ of dimension $K_{\mathrm{a}}(NQ + W - 1)$ is produced, which has a given covariance matrix $\underline{\mathbf{R}}_{\mathrm{n}}$, see (4.17). If the

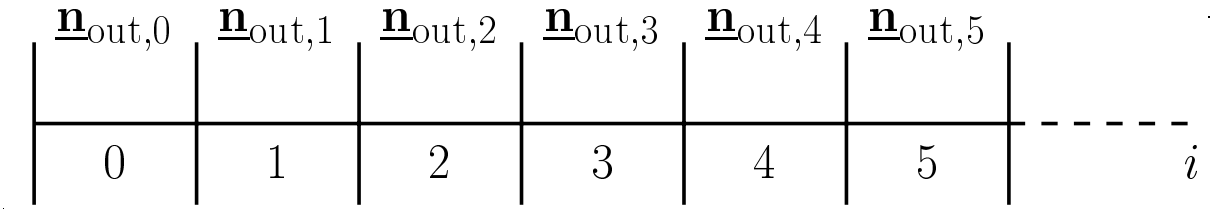

Figure 6.4. Series of output intercell MAI vectors $\underline{\mathbf{n}}_{\text{out},i}$, $i = 0, 1, 2, \ldots$

link level system performance of TD–CDMA is investigated, the intercell MAI covariance matrix is given by (4.26). Then, by first generating a vector $\underline{\mathbf{n}}_{\text{w}}$ with covariance matrix

$$\underline{\mathbf{R}}_{\text{n,w}} = \text{E}\left\{\underline{\mathbf{n}}_{\text{w}}\underline{\mathbf{n}}_{\text{w}}^{*\text{T}}\right\} = \mathbf{I}^{(K_{\text{a}}(NQ+W-1))}, \tag{6.10}$$

i.e., the components of $\underline{\mathbf{n}}_{\text{w}}$ are samples of independent complex Gaussian random variables with zero mean and variance equal to one [Pap65], the desired input intercell MAI vector $\underline{\mathbf{n}}$ is created according to

$$\underline{\mathbf{n}} = \sqrt{\sigma^2}\ \underline{\mathbf{n}}_{\text{w}}, \tag{6.11}$$

where σ^2 denotes the noise power, which is assumed to be equal for all components of $\underline{\mathbf{n}}$. If the system level performance of TD–CDMA is investigated, the intercell MAI covariance matrix $\underline{\mathbf{R}}_{\text{n}}$, see (5.10), can be factorized by Cholesky decomposition according to [Mar87]

$$\underline{\mathbf{R}}_{\text{n}} = \underline{\mathbf{L}}_{\text{n}}^{*\text{T}}\underline{\mathbf{L}}_{\text{n}}. \tag{6.12}$$

In (6.12) $\underline{\mathbf{L}}_{\text{n}}$ is an upper triangular matrix with nonzero real diagonal elements [Mar87]. Then, by first generating a vector $\underline{\mathbf{n}}_{\text{w}}$ with a covariance matrix as in (6.10), the desired input intercell MAI vector $\underline{\mathbf{n}}$ is created according to

$$\underline{\mathbf{n}} = \underline{\mathbf{L}}_{\text{n}}^{*\text{T}}\underline{\mathbf{n}}_{\text{w}}. \tag{6.13}$$

If the input intercell MAI vector $\underline{\mathbf{n}}$ is available, see (6.11) or (6.13), according to (6.5) it is possible to produce an output intercell MAI vector $\underline{\mathbf{n}}_{\text{out},i}$ for each general burst number i, $i = 0, 1, \ldots$ In Fig. 6.4 the series of output MAI vectors $\underline{\mathbf{n}}_{\text{out},i}$ are shown schematically versus the general burst numbers i, see also Fig. 6.2.

It has been already shown that the only effect of the JD process is a transformation of the received intercell MAI vector $\underline{\mathbf{n}}$, see (6.1), into an output intercell MAI vector $\underline{\mathbf{n}}_{\text{out}}$, see (6.5) and Fig. 6.1. Since this transformation is independent of the way the data symbols are processed prior to transmission, it is possible to investigate any linear scheme of data modulation, interleaving, and channel coding by

	1	2		384
$\underline{\mathbf{n}}_{\text{out},0}$	0.0318 - j0.0488	-0.0059 - j0.0438	•••	-0.0080 - j0.0079
$\underline{\mathbf{n}}_{\text{out},1}$	0.0194 + j0.0588	0.0052 + j0.0502	•••	0.0004 + j0.0122
$\underline{\mathbf{n}}_{\text{out},2}$	-0.0220 - j0.0219	-0.0159 - j0.0184	•••	0.0012 + j0.0094
⋮	⋮	⋮		⋮
$\underline{\mathbf{n}}_{\text{out},100}$	0.0151 - j0.0263	-0.0054 - j0.0348	•••	-0.0115 + j0.0051
⋮	⋮	⋮		⋮

Figure 6.5. Example of a database with the output intercell MAI vectors $\underline{\mathbf{n}}_{\text{out},i}$, $i = 0, 1, 2, \ldots$; $K = 8$ users; $N = 24$ data symbols per user; $K_{\text{a}} = 1$; channel model: COST 207 RA; $\sigma^2 = 1$

- first, storing a number of output intercell MAI vectors $\underline{\mathbf{n}}_{\text{out},i}$, $i = 0, 1, 2 \ldots$, see (6.5) and Fig. 6.4, which are valid for a certain simulation scenario, in a two dimensional database, and
- then, adding the vectors from the database to the transparently transmitted user data contained in the vector $\underline{\mathbf{d}}$, see (4.5), according to (6.4).

If the output intercell MAI vectors $\underline{\mathbf{n}}_{\text{out},i}$, $i = 0, 1, 2 \ldots$, see (6.5), are generated under the condition that the users move with the smallest non–zero velocity v_0, see (6.9), then the influence of any user velocity v which is an integer multiple of v_0 can be investigated, without having to repeat the simulation for generating the database. This is due to the fact that if the users of a user group l, $l = 0 \ldots T_{\text{fr}}/T_{\text{bu}} - 1$, move with a velocity v which is a multiple of v_0, only the relevant vectors $\underline{\mathbf{n}}_{\nu}$ from the database may be used for investigating the BER performance, where ν is defined in (6.9). This issue constitutes another advantage of the novel simulation concept for TD–CDMA with respect to simulation time, compared to the original simulation concept for TD–CDMA [Naß95, Bla98]. Finally, if the link level performance is investigated, where (4.26) is valid, the noise power σ^2, see (4.26) and (6.11), of each output intercell MAI vector $\underline{\mathbf{n}}_{\text{out},i}$ from the

database can be scaled according to [POB99]

$$\underline{\mathbf{n}}'_{\mathrm{out},i} = \underline{\mathbf{n}}_{\mathrm{out},i} \cdot \frac{\bar{\gamma}_{\mathrm{in}}}{\bar{\gamma}'_{\mathrm{in}}}, \tag{6.14}$$

where $\bar{\gamma}_{\mathrm{in}}$ denotes the mean input SNR used for creating the respective database, and $\bar{\gamma}'_{\mathrm{in}}$ denotes the mean input SNR to be investigated. Then, the BER performance can be investigated additionally for different values of the input SNR, without the need for repeating the simulations for producing the database, each time the influence of a new value of the input SNR $\bar{\gamma}'_{\mathrm{in}}$ has to be examined [POB99]. Summarizing, in contrast to the original simulation concept for TD–CDMA [Naß95, Bla98], when the novel simulation concept for TD–CDMA is used, there is no need for repeating the simulations for generating a database, when the effects of

- a new data modulation, interleaving, and channel coding scheme,
- a new user velocity v, which is an integer multiple of v_0, or
- a new input SNR $\bar{\gamma}'_{\mathrm{in}}$,

have to be investigated, because the same output intercell MAI vectors $\underline{\mathbf{n}}_{\mathrm{out},i}$ for the considered scenario, i.e., the used channel model, CDMA codes, and antenna configuration, can be used from the database. In Fig. 6.5 an example of a database is illustrated for the following simulation scenario in a TD–CDMA mobile radio system:

$$K = 8, \quad N = 24, \quad K_{\mathrm{a}} = 1, \quad \text{channel model : COST 207 RA}, \quad \sigma^2 = 1.$$

6.2.3.3 Estimated channels

In Section 6.2.3.2 the novel simulation concept for TD–CDMA is presented under the assumption of perfectly known channel impulse responses at the receiver. Certainly, this assumption is unrealistic for the realtime operation of a TD–CDMA mobile radio system. Since the results of a simulation concept should be as close to the real world as possible, see Section 6.2.2, the influence of channel estimation on the system performance should be included. Therefore, the novel simulation concept is extended in this section to include the impact of channel estimation errors on the JD process and, consequently, on the overall system performance. If

$$\hat{\underline{\mathbf{A}}} = \underline{\mathbf{A}} + \Delta\underline{\mathbf{A}} \tag{6.15}$$

represents the estimated system matrix, with $\Delta\underline{\mathbf{A}}$ depending on the channel estimation errors [POB99], and

$$\hat{\underline{\mathbf{M}}} = \left(\hat{\underline{\mathbf{A}}}^{*\mathrm{T}} \mathbf{R}_{\mathrm{n}}^{-1} \hat{\underline{\mathbf{A}}}\right)^{-1} \hat{\underline{\mathbf{A}}}^{*\mathrm{T}} \mathbf{R}_{\mathrm{n}}^{-1} \tag{6.16}$$

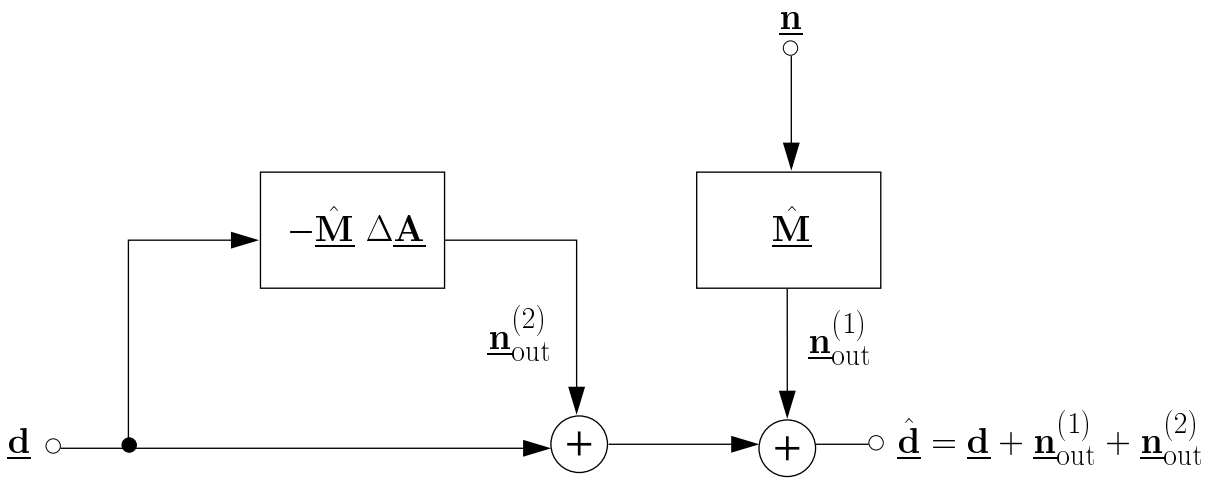

Figure 6.6. Schematic representation of the novel view on the JD precess including channel estimation

is the estimated channel matrix with $\hat{\underline{\mathbf{A}}}$ defined in (6.15), see also (6.3), then the estimated data vector $\hat{\underline{\mathbf{d}}}$ from all K users can be written in the form

$$\hat{\underline{\mathbf{d}}} = \underline{\mathbf{d}} + \underline{\mathbf{n}}_{\text{out}}^{(1)} + \underline{\mathbf{n}}_{\text{out}}^{(2)}, \tag{6.17}$$

where

$$\underline{\mathbf{n}}_{\text{out}}^{(1)} = \hat{\underline{\mathbf{M}}}\,\underline{\mathbf{n}}, \tag{6.18}$$

$$\underline{\mathbf{n}}_{\text{out}}^{(2)} = -\hat{\underline{\mathbf{M}}}\,\Delta\underline{\mathbf{A}}\,\underline{\mathbf{d}}. \tag{6.19}$$

Note that the intercell interference covariance matrix $\underline{\mathbf{R}}_{\text{n}}$, see (4.17) and (6.12), is assumed to be perfectly known at the BS receiver. From (6.17) and (6.18) we observe that the output intercell MAI vector $\underline{\mathbf{n}}_{\text{out}}^{(1)}$ additionally depends on the input SNR $\bar{\gamma}_{\text{in}}$. This is due to the fact that the quality of the channel impulse response estimates contained in $\hat{\underline{\mathbf{A}}}$, see (6.15), and consequently the estimated channel matrix $\hat{\underline{\mathbf{M}}}$, see (6.16), depend on the mean input SNR $\bar{\gamma}_{\text{in}}$, see the simulation results presented in Section 5.5. Further, from (6.17) and (6.19), it is observed that the vector $\underline{\mathbf{n}}_{\text{out}}^{(2)}$ depends, in addition to its dependence on the mean input SNR $\bar{\gamma}_{\text{in}}$, on the way the data are modulated, interleaved and coded, since $\underline{\mathbf{d}}$ is contained explicitly in (6.19). This novel view on the JD process which includes channel estimation is illustrated in Fig. 6.6.

According to (6.17), we can deduce that, in contrast to the case where the channel impulse responses are perfectly known at the receiver, see Section 6.2.3.2, it is now necessary to create for each mean input SNR $\bar{\gamma}_{\text{in}}$ and simulation scenario, determined by the channel model, the CDMA codes $\underline{\mathbf{c}}^{(k)}$, $k = 1 \ldots K$, see (4.2), and the antenna configuration,

two databases, which contain the vectors $\underline{\mathbf{n}}_{\text{out}}^{(1)}$, see (6.18), and $\underline{\mathbf{n}}_{\text{out}}^{(2)}$, see (6.19), respectively. The advantages of the novel simulation concept presented in Section 6.2.3.2, which are valid for the investigation of any data modulation, interleaving, and channel coding scheme, as well as with any user velocity v which is an integer multiple of v_0, hold only for the first database containing the vectors $\underline{\mathbf{n}}_{\text{out}}^{(1)}$, see (6.18). Concerning the second database containing the vectors $\underline{\mathbf{n}}_{\text{out}}^{(2)}$, see (6.19), only the advantage valid for the investigation of any user velocity v, which is an integer multiple of v_0, holds. Nevertheless, the computational cost of the novel simulation concept including channel estimation is reduced compared to the original simulation concept for TD–CDMA [POB99]. The gain concerning this computational cost is calculated and compared to the one valid for the original simulation concept for TD–CDMA in Section 6.4.

6.3 SNR degradation of TD–CDMA receivers

6.3.1 General

As already shown in Section 4.3.3.2, the intracell MAI is eliminated by JD in TD–CDMA. The price to be paid for this benefit is an SNR degradation valid for TD–CDMA receivers [SK93, Kle96], which means that, to a certain degree, the impact of intercell MAI is enhanced, compared to receivers which do not utilize JD. In this section a new definition of the SNR degradation of TD–CDMA receivers is presented. This SNR degradation is considered as the basis of the second performance assessment method for TD–CDMA used in this thesis, the first being the novel simulation concept for TD–CDMA presented in Section 6.2. Note that, in addition to the benefits of using the SNR degradation as a performance assessment method for TD–CDMA, the SNR degradation constitutes the basis for obtaining a simplified version of the novel simulation concept presented in Section 6.2.3.2.

6.3.2 Definition of the SNR degradation

As in Section 6.2, it is assumed that the received signal in TD–CDMA is determined in general by (6.1). Further, the channel impulse responses are assumed to be perfectly known at the receiver. Moreover, it is accepted that each transmitted symbol $\underline{d}_i$, $i = 1 \ldots KN$, has the magnitude

$$| \underline{d}_i | = 1, \quad i = 1 \ldots KN. \tag{6.20}$$

In order to enable a unified treatment of single and adaptive antennas, it is assumed that in the case of adaptive antennas the received energy E_i associated with each transmitted symbol $\underline{d}_i$, $i = 1 \ldots KN$, see (4.5), is the energy measured by a fictitious single antenna placed at the RP of the antenna configuration used at the BS, see Fig. 5.1. Then, independently of the use of single or adaptive antennas, the received energy E_i valid for a data

symbol $\underline{d}_i$, $i = 1 \ldots KN$, of transmitter k, $k = 1 \ldots K$, is exclusively determined by the composite channel impulse response $\underline{\mathbf{b}}^{(k)}$, see (4.7), valid for transmitter k, $k = 1 \ldots K$, according to

$$E_i = \frac{|\,\underline{\mathbf{b}}^{(k)}\,|^2}{2}, \tag{6.21}$$

where (6.20) has been used. $|\,\underline{\mathbf{b}}^{(k)}\,|$ in (6.21) depends on the distance between transmitter and receiver as well as on the presence of slow fading and fast fading, see Section 2.2.1 for a detailed analysis. In the following, it is assumed that the dependence on said distance is eliminated by power control [GVGZ92, Zan92a, Zan92b] and that the slow and fast fading processes are stationary [Pap65]. Then, the mean received energy

$$E = \frac{\mathrm{E}\{|\,\underline{\mathbf{b}}^{(k)}\,|^2\}}{2} \tag{6.22}$$

per symbol and the mean input SNR

$$\bar{\gamma}_{\mathrm{in}} = \frac{\mathrm{E}\{|\,\underline{\mathbf{b}}^{(k)}\,|^2\}}{2\,\sigma^2\,Q} \tag{6.23}$$

are defined, where Q is the spreading factor, and σ^2 is the variance of each component of the intercell MAI vector $\underline{\mathbf{n}}$, see also Section 6.2.3.2. The expectation operator $\mathrm{E}\{\cdot\}$ in (6.22) and (6.23) is applied to the composite channel impulse responses $\underline{\mathbf{b}}^{(k)}$ from all K users.

In what follows, it is assumed that (4.26) is valid. Then, based on the received signal $\underline{\mathbf{e}}$, see (6.1), the ZF–BLE [KB92b, Kle96] gives the linear estimate

$$\underline{\hat{\mathbf{d}}} = \left(\underline{\mathbf{A}}^{*\mathrm{T}}\underline{\mathbf{A}}\right)^{-1}\underline{\mathbf{A}}^{*\mathrm{T}}\underline{\mathbf{e}} = \underline{\mathbf{d}} + \left(\underline{\mathbf{A}}^{*\mathrm{T}}\underline{\mathbf{A}}\right)^{-1}\underline{\mathbf{A}}^{*\mathrm{T}}\underline{\mathbf{n}} \tag{6.24}$$

of the combined data vector $\underline{\mathbf{d}}$ defined in (4.5), see also (6.2). According to (6.24) and (6.20) and by some manipulation, it can be shown that the symbol SNR at the output of the ZF–BLE becomes [Kle96]

$$\gamma_{\mathrm{ZF},i} = \frac{1}{2\sigma^2\left[\left(\underline{\mathbf{A}}^{*\mathrm{T}}\underline{\mathbf{A}}\right)^{-1}\right]_{i,i}}, \quad i = 1 \ldots KN, \tag{6.25}$$

where $[\cdot]_{i,i}$ denotes the i–th diagonal element of the matrix in brackets.

In [Kle96] an SNR degradation is defined, which relates $\gamma_{\mathrm{ZF},i}$, $i = 1 \ldots KN$, see (6.25), to the SNR per transmitted symbol at the output of the DMF, see Section 4.3.3.1, which is inherent in the ZF–BLE [Kle96]. However, a more adequate definition of the SNR degradation of TD–CDMA receivers should relate $\gamma_{\mathrm{ZF},i}$, $i = 1 \ldots KN$, see (6.25), directly to the mean input SNR $\bar{\gamma}_{\mathrm{in}}$, see (6.23), in order to achieve the consideration of the overall receiver structure. With (6.23) and (6.25), this SNR degradation is defined as

$$\delta_i = \frac{\bar{\gamma}_{\mathrm{in}}}{\gamma_{\mathrm{ZF},i}} = \frac{\mathrm{E}\{|\,\underline{\mathbf{b}}^{(k)}\,|^2\}}{Q}\,\left[\left(\underline{\mathbf{A}}^{*\mathrm{T}}\underline{\mathbf{A}}\right)^{-1}\right]_{i,i}, \quad i = 1 \ldots KN, \tag{6.26}$$

see also (6.22). In the following section, the properties of the SNR degradation δ_i, $i = 1 \ldots KN$, of TD–CDMA receivers are presented.

6.3.3 Properties of the SNR degradation

6.3.3.1 Introduction

In Section 6.3.2 the definition of the SNR degradation of TD–CDMA receivers is presented, see (6.26). The factor $\mathrm{E}\{|\,\underline{\mathbf{b}}^{(k)}\,|^2\}/Q$ in (6.26) can be considered as a constant weighting factor for the SNR degradation δ_i, $i = 1 \ldots KN$, which exclusively depends on the mean energy of the composite channel impulse responses, see (6.22), and the spreading factor Q. Therefore, it can be incorporated in the system matrix $\underline{\mathbf{A}}$ by defining the normalized matrix

$$\underline{\tilde{\mathbf{A}}} = \sqrt{\frac{Q}{\mathrm{E}\{|\,\underline{\mathbf{b}}^{(k)}\,|^2\}}}\;\;\underline{\mathbf{A}}. \tag{6.27}$$

Then, the SNR degradation of (6.26) can be written as

$$\delta_i = \left[\left(\underline{\tilde{\mathbf{A}}}^{*\mathrm{T}}\,\underline{\tilde{\mathbf{A}}}\right)^{-1}\right]_{i,i}, \quad i = 1 \ldots KN. \tag{6.28}$$

In the following, we discuss the properties of this SNR degradation of TD–CDMA receivers.

6.3.3.2 Structure of the SNR degradation

In this section the structure of the SNR degradation δ_i, $i = 1 \ldots KN$, see (6.28), is investigated. It is assumed that a single antenna is used at the BS receiver. The generalization to multi–antenna configurations, including adaptive antennas, is straightforward.

The SNR degradation δ_i, $i = 1 \ldots KN$, see (6.28), is the i–th diagonal element of the inverse of the matrix

$$\underline{\tilde{\mathbf{Z}}} = \underline{\tilde{\mathbf{A}}}^{*\mathrm{T}}\,\underline{\tilde{\mathbf{A}}}. \tag{6.29}$$

If $\underline{\tilde{\mathbf{Z}}}_{i,i}$ denotes the matrix $\underline{\tilde{\mathbf{Z}}}$ of (6.29) without its i–th row and i–th column, (6.28) takes the form [Gant91]

$$\delta_i = \frac{\det\left(\underline{\tilde{\mathbf{Z}}}_{i,i}\right)}{\det\left(\underline{\tilde{\mathbf{Z}}}\right)}, \quad i = 1 \ldots KN, \tag{6.30}$$

where the operator $\det(\cdot)$ stands for the determinant of the matrix in parentheses. The energies $|\,\underline{\mathbf{b}}^{(k)}\,|^2$ of the composite channel impulse responses $\underline{\mathbf{b}}^{(k)}$, $k = 1 \ldots K$, see (4.7),

valid for a transmitted burst, cannot be equalized for all K users. Therefore, if we define the $KN \times KN$ block diagonal matrix

$$\underline{\mathbf{F}} = \text{blockdiag}\left[\underline{\mathbf{F}}^{(1)} \ldots \underline{\mathbf{F}}^{(K)}\right], \tag{6.31}$$

with

$$\underline{\mathbf{F}}^{(k)} = \sqrt{\frac{\mathrm{E}\{\mid \underline{\mathbf{b}}^{(k)} \mid^2\}}{Q}} \; \frac{1}{\mid \underline{\mathbf{b}}^{(k)} \mid} \mathbf{I}^{(N)}, \quad k = 1 \ldots K, \tag{6.32}$$

the normalized matrix

$$\underline{\tilde{\tilde{\mathbf{Z}}}} = \underline{\mathbf{F}}\, \underline{\tilde{\mathbf{Z}}}\, \underline{\mathbf{F}} \tag{6.33}$$

is independent of $\mid \underline{\mathbf{b}}^{(k)} \mid^2$, $k = 1 \ldots K$, and the factor $\mathrm{E}\{\mid \underline{\mathbf{b}}^{(k)} \mid^2\}/Q$, see (6.26), i.e., all KN diagonal elements of $\underline{\tilde{\tilde{\mathbf{Z}}}}$ are equal to one. $\underline{\tilde{\tilde{\mathbf{Z}}}}$ consists of K^2 blocks

$$\underline{\tilde{\tilde{\mathbf{Z}}}}^{(l,m)} = \underline{\tilde{\tilde{\mathbf{Z}}}}^{(m,l)*\mathrm{T}} = \frac{1}{b^{(l,m)}} \underline{\tilde{\mathbf{Z}}}^{(l,m)}, \quad l, m = 1 \ldots K, \tag{6.34}$$

of dimensions $N \times N$, where

$$b^{(l,m)} = \frac{Q}{\mathrm{E}\{\mid \underline{\mathbf{b}}^{(k)} \mid^2\}} \; \mid \underline{\mathbf{b}}^{(l)} \mid \mid \underline{\mathbf{b}}^{(m)} \mid, \quad l, m = 1 \ldots K. \tag{6.35}$$

According to (6.33), a normalized SNR degradation per transmitted symbol can be defined, which exclusively depends on the structure of the composite channel impulse responses $\underline{\mathbf{b}}^{(k)}$, $k = 1 \ldots K$, see (4.7), and not on the received energies of $\underline{\mathbf{b}}^{(k)}$, $k = 1 \ldots K$, and the mean input SNR $\bar{\gamma}_{\mathrm{in}}$, see (6.23):

$$\delta_{\mathrm{n},i} = \frac{\det\left(\underline{\tilde{\tilde{\mathbf{Z}}}}_{i,i}\right)}{\det\left(\underline{\tilde{\tilde{\mathbf{Z}}}}\right)}, \quad i = 1 \ldots KN. \tag{6.36}$$

If (6.36) is available, the determination of δ_i, see (6.30) and (6.26), is accomplished by multiplying $\delta_{\mathrm{n},i}$, $i = 1 \ldots KN$, with the value $1/\mid \underline{\mathbf{b}}^{(k)} \mid^2$, which pertains to the considered user k, $k = 1 \ldots K$, and the factor $\mathrm{E}\{\mid \underline{\mathbf{b}}^{(k)} \mid^2\}/Q$. Therefore, independently of the received energy per composite channel impulse response $\underline{\mathbf{b}}^{(k)}$, $k = 1 \ldots K$, and the mean input SNR $\bar{\gamma}_{\mathrm{in}}$, the SNR degradation δ_i, $i = 1 \ldots KN$, see (6.26), can be kept low if the channel impulse response $\underline{\mathbf{h}}^{(k)}$ and the CDMA code $\underline{\mathbf{c}}^{(k)}$ of a specific user k, $k = 1 \ldots K$, and among the K simultaneously active users are well matched. This statement means that the values of the off–diagonal elements of $\underline{\tilde{\tilde{\mathbf{Z}}}}$, see (6.33), should be small compared to values of the diagonal elements, which are all equal to one, see also Section 4.3.2.2 for an equivalent observation concerning data detection in TD–CDMA mobile radio systems. In Section 7.2 this observation is used to produce composite channel impulse responses $\underline{\mathbf{b}}^{(k)}$, $k = 1 \ldots K$, see (4.7), which are well matched. This novel technique leads to considerable performance improvements, which are illustrated in Section 7.2 by using the SNR degradation of TD–CDMA receivers as the basis for a performance assessment method.

6.3.3.3 Dependence on the number of transmitted symbols

In this section the influence of the number of transmitted symbols on the SNR degradation is investigated. In order to get an insight into this problem, the easy to survey cases

$$K_{\mathrm{a}} = 1, \quad K = 2, \quad Q = 2, \quad W = 1, \tag{6.37}$$

with N equal to one and N equal to two are considered, respectively. In the case of N equal to one, the system matrix $\underline{\mathbf{A}}$, see (4.8), is written as

$$\underline{\mathbf{A}} = \left[\begin{array}{cc} \underline{\mathbf{b}}^{(1)} & \underline{\mathbf{b}}^{(2)} \end{array} \right], \tag{6.38}$$

and the matrix $\underline{\tilde{\mathbf{Z}}}$, see (6.29), takes the form

$$\underline{\tilde{\mathbf{Z}}} = \left[\begin{array}{cc} \underline{\tilde{z}}_{1,1} & \underline{\tilde{z}}_{1,2} \\ \underline{\tilde{z}}^{*}_{1,2} & \underline{\tilde{z}}_{2,2} \end{array} \right], \tag{6.39}$$

where

$$\underline{\tilde{z}}_{1,1} = \sqrt{\frac{Q}{\mathrm{E}\{ \mid \underline{\mathbf{b}}^{(k)} \mid^2 \}}}\, \underline{\mathbf{b}}^{(1)*\mathrm{T}} \underline{\mathbf{b}}^{(1)}, \tag{6.40}$$

$$\underline{\tilde{z}}_{2,2} = \sqrt{\frac{Q}{\mathrm{E}\{ \mid \underline{\mathbf{b}}^{(k)} \mid^2 \}}}\, \underline{\mathbf{b}}^{(2)*\mathrm{T}} \underline{\mathbf{b}}^{(2)}, \tag{6.41}$$

$$\underline{\tilde{z}}_{1,2} = \sqrt{\frac{Q}{\mathrm{E}\{ \mid \underline{\mathbf{b}}^{(k)} \mid^2 \}}}\, \underline{\mathbf{b}}^{(1)*\mathrm{T}} \underline{\mathbf{b}}^{(2)}, \tag{6.42}$$

According to (6.30), the SNR degradation of the transmitted symbol of the first user is

$$\delta_1 \mid_{N=1} = \frac{\underline{\tilde{z}}_{2,2}}{\underline{\tilde{z}}_{1,1}\underline{\tilde{z}}_{2,2} - \mid \underline{\tilde{z}}_{1,2} \mid^2} \tag{6.43}$$

and of the second user is

$$\delta_2 \mid_{N=1} = \frac{\underline{\tilde{z}}_{1,1}}{\underline{\tilde{z}}_{1,1}\underline{\tilde{z}}_{2,2} - \mid \underline{\tilde{z}}_{1,2} \mid^2}. \tag{6.44}$$

If N equal to two symbols are transmitted by each user, the system matrix takes the form

$$\underline{\mathbf{A}} = \left[\begin{array}{cccc} \underline{\mathbf{b}}^{(1)} & \mathbf{0} & \underline{\mathbf{b}}^{(2)} & \mathbf{0} \\ \mathbf{0} & \underline{\mathbf{b}}^{(1)} & \mathbf{0} & \underline{\mathbf{b}}^{(2)} \end{array} \right], \tag{6.45}$$

where $\mathbf{0}$ is the zero vector of dimension 2, and the matrix $\underline{\tilde{\mathbf{Z}}}$, see (6.29), is expressed as

$$\underline{\tilde{\mathbf{Z}}} = \left[\begin{array}{cccc} \underline{\tilde{z}}_{1,1} & 0 & \underline{\tilde{z}}_{1,2} & 0 \\ 0 & \underline{\tilde{z}}_{1,1} & 0 & \underline{\tilde{z}}_{1,2} \\ \underline{\tilde{z}}^{*}_{1,2} & 0 & \underline{\tilde{z}}_{2,2} & 0 \\ 0 & \underline{\tilde{z}}^{*}_{1,2} & 0 & \underline{\tilde{z}}_{2,2} \end{array} \right] \tag{6.46}$$

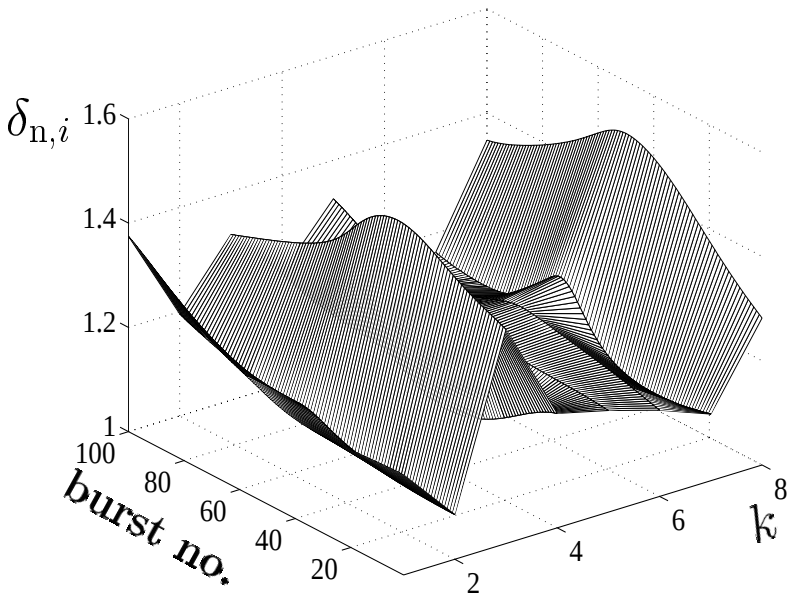

Figure 6.7. Normalized SNR degradation $\delta_{\mathrm{n},i}$; $K_{\mathrm{a}} = 1$; $K = 8$; COST 207 RA; $N = 24$; $Q = 14$, $W = 23$, v=3 km/h; 100 transmitted bursts

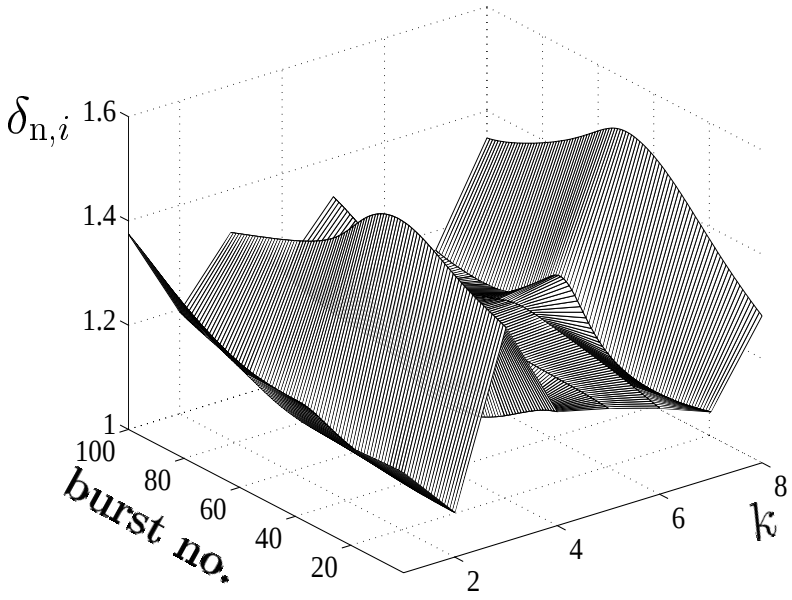

Figure 6.8. Normalized SNR degradation $\delta_{\mathrm{n},i}$; $K_{\mathrm{a}} = 1$; $K = 8$; COST 207 RA; $N = 4$; $Q = 14$, $W = 23$, v=3 km/h; 100 transmitted bursts

with its elements defined in (6.40) to (6.42). In this case and after some manipulation, the SNR degradation of the transmitted symbols of the first user is

$$\delta_1 \mid_{N=2} = \delta_2 \mid_{N=2} = \frac{\tilde{\underline{z}}_{2,2}(\tilde{\underline{z}}_{1,1}\tilde{\underline{z}}_{2,2} - \mid \tilde{\underline{z}}_{1,2} \mid^2)}{(\tilde{\underline{z}}_{1,1}\tilde{\underline{z}}_{2,2} - \mid \tilde{\underline{z}}_{1,2} \mid^2)^2} \tag{6.47}$$

and of the second user is

$$\delta_3 \mid_{N=2} = \delta_4 \mid_{N=2} = \frac{\tilde{\underline{z}}_{1,1}(\tilde{\underline{z}}_{1,1}\tilde{\underline{z}}_{2,2} - \mid \tilde{\underline{z}}_{1,2} \mid^2)}{(\tilde{\underline{z}}_{1,1}\tilde{\underline{z}}_{2,2} - \mid \tilde{\underline{z}}_{1,2} \mid^2)^2}. \tag{6.48}$$

From (6.43), (6.47) and (6.44), (6.48), respectively, we observe that the produced values of the SNR degradation for both users are identical.

In the previous example only MAI is considered, since K is equal to two, but no ISI is present, since W is chosen to be equal to one. Unfortunately, when we want to deal with realistic parameters of TD–CDMA, see Table 5.1, there is no closed form expression for the SNR degradation δ_i, $i = 1 \ldots KN$, see (6.26), which explicitly depends on the elements of the matrix $\underline{\tilde{\mathbf{Z}}}$, see (6.29). In this case, the SNR degradation δ_i has to be determined by simulations. In Fig. 6.7 the normalized SNR degradation $\delta_{\mathrm{n},i}$, see (6.36), of the symbols in the middle of each transmitted burst from each user k, $k = 1 \ldots K$, are shown for 10^2 bursts. The chosen parameters are

$$K_\mathrm{a} = 1, \quad K = 8, \quad N = 24, \quad Q = 14, \quad W = 23, \tag{6.49}$$

and the COST 207 RA channel model is used [COS89], see also Section 2.3.2. The velocity v of the simultaneously active users is chosen to be 3 km/h. In Fig. 6.8 the respective values are shown for the same parameters except for the number N of the transmitted symbols, which is chosen to be equal to four. The comparison of the representations in Fig. 6.7 and Fig. 6.8 shows that the values of the normalized SNR degradation are practically the same. This result demonstrates that only a certain number N of transmitted symbols is necessary for determining the normalized SNR degradation $\delta_{\mathrm{n},i}$, $i = 1 \ldots KN$, see (6.36), and, consequently the SNR degradation δ_i, $i = 1 \ldots KN$, see (6.26). The number N of transmitted symbols for determining δ_i, $i = 1 \ldots KN$, see (6.26), should be chosen to be at least equal to the number of symbols N which contribute to ISI. Concerning the parameters valid for Fig. 6.7, the number of symbols N which contribute to ISI is equal to three, see also Table 5.1. Therefore, N has been chosen to be equal to four for the simulation results presented in Fig. 6.8. This reduction of the required number of transmitted symbols for determining δ_i, $i = 1 \ldots KN$, see (6.26), on the one hand, makes the SNR degradation the basis of a powerful performance assessment method of low computational cost, and, on the other hand, constitutes the basic step for developing a simplified version of the novel simulation concept for TD–CDMA presented in Section 6.2. As a final remark, the SNR degradation of TD–CDMA receivers can be used for CDMA code optimization, which is considered as an additional advantage of the utilization of the SNR degradation. In Appendix B.2 upper and lower bounds of the SNR degradation are presented, which can serve as guidelines for CDMA code optimization in TD–CDMA mobile radio systems.

6.3.4 Simplified version of the novel simulation concept

In this section a simplified version of the novel simulation concept for TD–CDMA, see Section 6.2, is presented. The basis of this simplified version is the SNR degradation δ_i, $i = 1 \ldots KN$, see (6.26), which allows the determination of the noise values which corrupt the transparently transmitted data symbols $\underline{d}_i$, $i = 1 \ldots KN$, see (4.5), from all K users. These noise values are determined in the following.

The value of the mean input SNR $\bar{\gamma}_{\text{in}}$, see (6.23), depends on the noise variance σ^2 at the input of the receiver. Therefore, it is possible to set the mean input SNR $\bar{\gamma}_{\text{in}}$, see (6.23), to a desired value by controlling the value of σ^2. According to (6.23), σ^2 can be written as

$$\sigma^2 = \frac{\mathrm{E}\{|\ \underline{\mathbf{b}}^{(k)}\ |^2\}}{2\bar{\gamma}_{\text{in}}\ Q}, \tag{6.50}$$

see also (6.22). From (6.25) and (6.50), the variance of the noise component $\underline{n}_{\text{out},i}$, $i = 1 \ldots KN$, which corrupts the data symbol $\underline{d}_i$, $i = 1 \ldots KN$, at the output of the ZF–BLE is given by

$$\mathrm{var}\{\underline{n}_{\text{out},i}\} = \frac{\mathrm{E}\{|\ \underline{\mathbf{b}}^{(k)}\ |^2\}}{2\ \bar{\gamma}_{\text{in}}\ Q} \left[\left(\underline{\mathbf{A}}^{*\mathrm{T}}\underline{\mathbf{A}}\right)^{-1}\right]_{i,i}, \quad i = 1 \ldots KN. \tag{6.51}$$

Then, (6.51) takes the form

$$\mathrm{var}\{\underline{n}_{\text{out},i}\} = \frac{1}{2\bar{\gamma}_{\text{in}}}\ \delta_i, \quad i = 1 \ldots KN, \tag{6.52}$$

where δ_i, $i = 1 \ldots KN$, is the SNR degradation defined in (6.26), and $\bar{\gamma}_{\text{in}}$ is the mean input SNR defined in (6.23).

The SNR degradation δ_i, $i = 1 \ldots KN$, see (6.26), can be stored in databases by following the method described in Section 6.2.3.2 for the novel simulation concept for TD–CDMA. However, by taking advantage of the result presented in Section 6.3.3.3, only N equal to four data symbols are sufficient for determining the SNR degradation of TD–CDMA for the considered simulation scenario, which considerably reduces the simulation time necessary for producing the respective database. Further, only the SNR degradation valid for the symbol positioned in the middle of each burst transmitted by user k, $k = 1 \ldots K$, needs to be stored in the database. Then, the SNR degradation δ_i can be assumed to be equal for all data symbols transmitted by a certain user k, $k = 1 \ldots K$. Note that this assumption is somewhat pessimistic, since it is known from [SK93, Kle96] that the SNR degradation valid for the symbols at the head and the tail of each transmitted burst take lower values, compared to the SNR degradation of the symbols transmitted in the middle of each burst. However, simulations performed by the author of this thesis have shown that the overall system performance is affected marginally by this choice, while the required memory for storing the databases is considerably reduced.

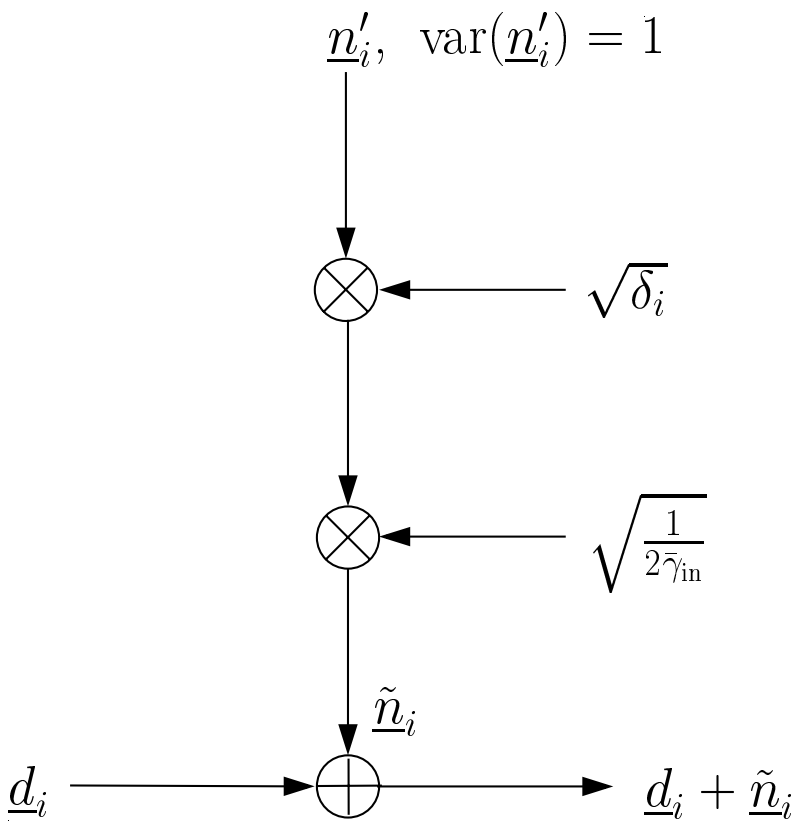

Figure 6.9. Schematic representation of the simplified version of the novel simulation concept

If the SNR degradations δ_i, $i = 1 \ldots KN$, see (6.26), are available in the form of databases, the simplified version of the novel simulation concept for TD–CDMA, see Section 6.2.3.2, consists of three steps:

- First, a vector $\underline{\mathbf{n}}'$ of dimension KN is created with each component $\underline{n}'_i$, $i = 1 \ldots KN$, having unit variance.
- Second, each $\underline{n}'_i$, $i = 1 \ldots KN$, is multiplied by the square root of the SNR degradation δ_i valid for the considered user, and the square root of the inverse of the factor $2\ \bar{\gamma}_{\mathrm{in}}$, according to (6.52).
- Third, the resulting value $\underline{\tilde{n}}_i$, $i = 1 \ldots KN$, from the second step is added to the transparently transmitted data symbol $\underline{d}_i$, $i = 1 \ldots KN$, see also Section 6.2.3.2 and Fig. 6.1. Thus, estimates for the transmitted data of each of the K users – after channel coding, interleaving, and modulation – can be obtained. Then, the data estimates produced by the simplified novel simulation concept must be demodulated, deinterleaved and decoded, and the BER can be calculated, exactly as for the novel simulation concept presented Section 6.2.3.2.

Figure 6.9 schematically shows the simplified version of the novel simulation concept for TD–CDMA. By comparing $\underline{n}_{\mathrm{out},i}$, $i = 1 \ldots KN$, see Fig. 6.1 and (6.5), determined by the novel simulation concept for TD–CDMA, with $\underline{\tilde{n}}_i$, $i = 1 \ldots KN$, see Fig. 6.9, determined by its simplified version, it is observed that, although both have the same variance given by (6.52), $\underline{n}_{\mathrm{out},i}$, $i = 1 \ldots KN$, explicitly contains the correlations of the components $\underline{n}_i$, $i = 1 \ldots KN$, of the input intercell MAI vector $\underline{\mathbf{n}}$ produced by multiplying the channel matrix $\underline{\mathbf{M}}$ with the $\underline{\mathbf{n}}$, see (6.5), whereas $\underline{\tilde{n}}_i$, $i = 1 \ldots KN$, is not directly related to the input intercell MAI vector $\underline{\mathbf{n}}$, see Fig. 6.9. Therefore, although the simplified version reduces the simulation time, it is expected that its accuracy is degraded, compared to the accuracy of the novel simulation concept for TD–CDMA presented in Section 6.2.3.2. The accuracy and the required simulation time for the simplified version of the novel simulation concept for TD–CDMA are investigated in the following Section 6.4.

6.4 Comparison of novel and original simulation concepts for TD–CDMA

In this section the novel simulation concept presented in Section 6.2 and its simplified version presented in Section 6.3.4 are compared with the original simulation concept for TD–CDMA [BBNS94, Naß95, Bla98]. The average coded BER $\bar{P}_{\mathrm{b}}$ is investigated versus the mean input SNR $\bar{\gamma}_{\mathrm{in}}$, see (6.23), by simulations using the COST 207 RA channel model [COS89], see also Section 2.3.2. A single antenna is used at the BS receiver, and K equal to eight users are active within the same frequency band and time slot. The user group 0 is considered, see Section 6.2.3.2 and Fig. 6.2, whereas for intercell MAI (4.26) is valid, i.e., the link level performance is investigated. Moreover, variations of the received power due to path loss and shadowing are assumed to be perfectly eliminated by power control, see also Section 2.2.1. However, the variations of the received power due to Rayleigh fading are present in the received signals, see Section 2.3.2. The parameters of TD–CDMA used in the simulations can be taken from Table 5.1. It is noted that the user bandwidth B of 1.6 MHz is smaller than the inverse of the chip duration T_{c}. This results from the choice of a digital chip impulse filter having an impulse response equal to the GMSK basic impulse $C_0(\tau)$ of time bandwidth product 0.3, leading to a compact spectrum, see [BKNS94b, Naß95] for a detailed analysis. Furthermore, the digital chip impulse filter and the user specific CDMA codes have been designed in such a way that the magnitude of the complex envelopes of the transmitted signals are approximately constant [BKNS94b, Kle96, Naß95].

In Fig. 6.10 the coded BER performance is presented for

- the original simulation concept for TD–CDMA [BBNS94, Naß95, Bla98],
- the novel simulation concept, see Section 6.2.3.2, and

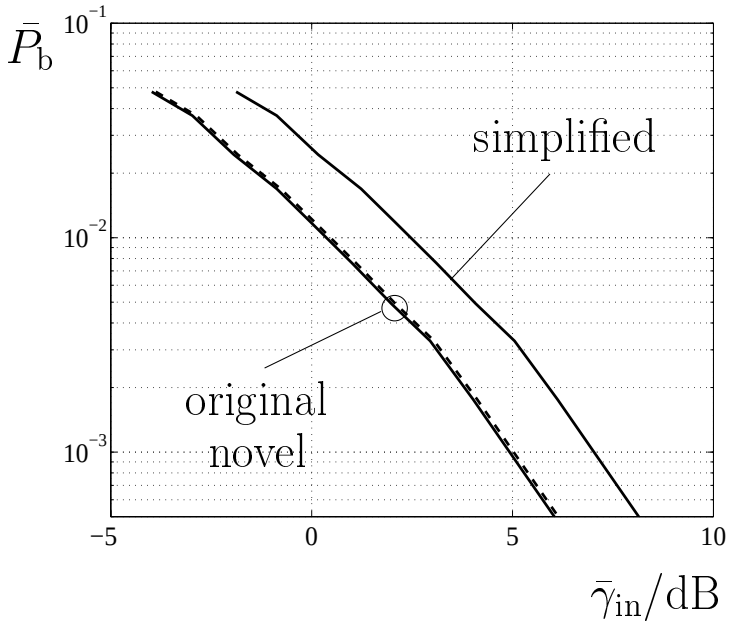

Figure 6.10. Coded BER $\bar{P}_\mathrm{b}$ versus the mean input SNR $\bar{\gamma}_\mathrm{in}$ of (6.23); COST 207 RA channel model; $K_\mathrm{a} = 1$ antenna; $K = 8$ users; $v = 3$ km/h; perfectly known channel impulse responses

- the simplified version of the novel simulation concept, see Section 6.3.4,

under the assumption that the channel impulse responses are perfectly known at the BS receiver. From the curves in Fig. 6.10 it is observed that the original and the novel simulation concept for TD–CDMA are virtually equivalent, whereas the simulation time required by the novel simulation concept is reduced by approximately 70% compared to the original one. This fact shows that the novel simulation concept retains the accuracy of the original simulation concept and, simultaneously, considerably reduces the simulation time. In Fig. 6.10 the simulation results for the simplified version of the novel simulation concept are also illustrated. Unfortunately, although the simplified version of the novel simulation concept, presented in Section 6.3.4, reduces the simulation time by additionally 20%, it does not retain the accuracy of the original concept. This is due to the fact that, when using the simplified version of the novel simulation concept for TD–CDMA, the correlations among the components of input intercell MAI vector $\underline{\mathbf{n}}$, see (6.5), are not considered when generating the vector $\tilde{\underline{\mathbf{n}}}$, see Fig. 6.9 and the analysis presented in Section 6.3.4. Therefore, in the subsequent sections of this chapter only the novel simulation concept presented in Section 6.2 is used for assessing the BER performance of TD–CDMA. However, the SNR degradation δ_i, $i = 1 \ldots KN$, see (6.26), which is the basis of the simplified version of the novel simulation concept for TD–CDMA, is used for assessing the performance of TD–CDMA in Chapter 7 and Chapter 9 in different operation situations. Finally, it is noted that results similar to those of Fig. 6.10 have been observed when adaptive antennas are used at the BS. Therefore, the conclusions drawn

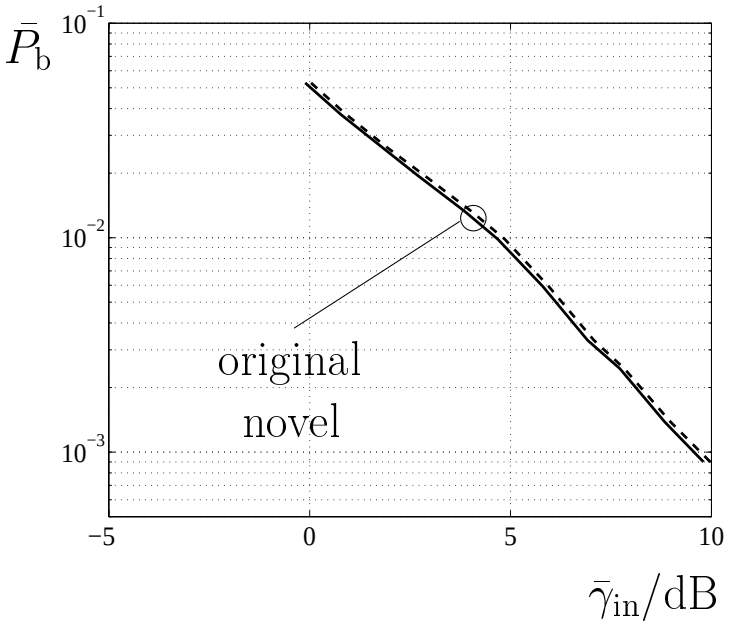

Figure 6.11. Coded BER $\bar{P}_\mathrm{b}$ versus the mean input SNR $\bar{\gamma}_\mathrm{in}$ of (6.23); COST 207 RA channel model; $K_\mathrm{a} = 1$ antenna; $K = 8$ users; $v = 3$ km/h; estimated channel impulse responses

from the simulation results presented in Fig. 6.10 are also valid for the use of adaptive antennas in TD–CDMA mobile radio systems.

In Fig. 6.11 simulation results comparing the original and the novel simulation concept, see Section 6.2.3.3, are shown when the channel impulse responses are estimated at the BS receiver. As in the case of known channel impulse responses, see Fig. 6.10, it is observed that the curves for both concepts are virtually equivalent, whereas the simulation time of the novel concept is reduced by approximately 40% compared to the original one. Similar results have been observed by the author of this thesis for the comparison between the original and the novel simulation concept, when adaptive antennas are used in TD–CDMA. Therefore, the novel simulation concept for TD–CDMA presented in Section 6.2 is exclusively used in the rest of this chapter for assessing the BER performance of TD–CDMA including the use of adaptive antennas. Simulation results concerning the spectrum efficiency and capacity of TD–CDMA are presented separately in Chapter 8.

6.5 Simulation results for the case of known channel impulse responses

6.5.1 Preliminaries

In this section the novel simulation concept presented in Section 6.2.3.2 is used for assessing the uplink link level performance of TD–CDMA with adaptive antennas in the

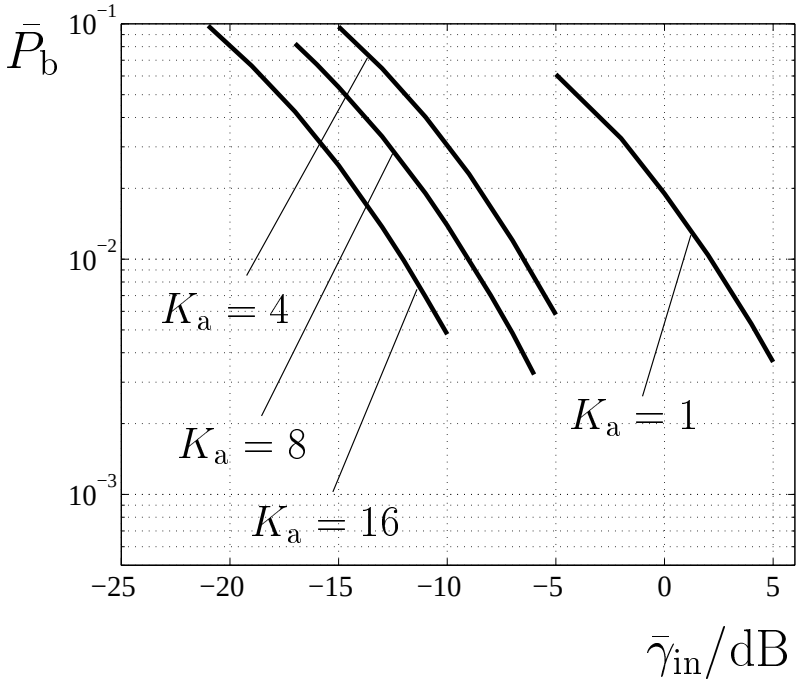

Figure 6.12. Uncoded BER $\bar{P}_\mathrm{b}$ versus the mean input SNR $\bar{\gamma}_\mathrm{in}$ of (6.23); modified Rural Area COST 207 channel model; $K = 8$ users; $v = 3$ km/h

case of known channel impulse responses at the BS receiver. Since the channel impulse responses are known, the simulation results presented in this section should be viewed as a demonstration of the potential of adaptive antennas in TD–CDMA for system performance enhancement, compared to single antenna systems. The influence of channel estimation on the link level performance of TD–CDMA is investigated in Section 6.6.

In the simulations always user group 0 is considered, see Section 6.2.3.2, and the number K of users of user group 0 is equal to eight. Further, the modified COST 207 channel models, see Section 2.3.2, and the UKL 2 directional channel models, see Section 2.3.3, are alternatively used. Note that, without loss of generality, the directional information of the used channel models is confined to the azimuth, i.e., the elevation angle of DOAs of signals impinging on the BS is assumed to be equal to 90°, see Fig. 5.1. The remaining parameters of the TD–CDMA mobile radio system can be taken from Table 5.1, see also [PFBP99, PWBB98, Bla98].

6.5.2 Influence of the number of antennas

First, the influence of the number K_a of antennas on the average uncoded and coded BER $\bar{P}_\mathrm{b}$ is investigated. In the simulations, a cross array configuration, see Fig. 3.4, is used, when adaptive antennas are employed at the BS receiver. Further, the modified

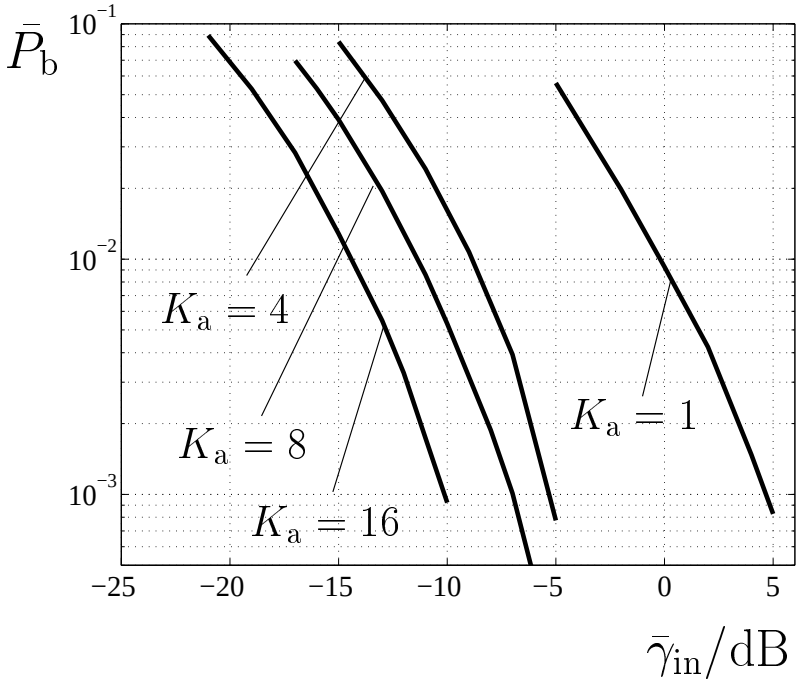

Figure 6.13. Coded BER $\bar{P}_\mathrm{b}$ versus the mean input SNR $\bar{\gamma}_\mathrm{in}$ of (6.23); modified Rural Area COST 207 channel model; $K = 8$ users; $v = 3$ km/h

COST 207 RA channel model, see Section 2.3.2, is used, whereas the spatial scenario is illustrated in Fig. 4.6. In Figs. 6.12 and 6.13 the simulation results for the average uncoded and coded BER $\bar{P}_\mathrm{b}$, respectively, are presented. The influence of the number K_a of antennas can be translated into a gain of approximately 8 dB at an average uncoded BER $\bar{P}_\mathrm{b} = 10^{-2}$ as the number of antennas K_a increase from one to four, see Fig. 6.12. Further, a gain of approximately 3 dB at an average uncoded BER $\bar{P}_\mathrm{b} = 10^{-2}$ is achieved each time the number of antennas K_a is doubled, see Fig. 6.12. Note that the observation of the respective curves of the average coded BER $\bar{P}_\mathrm{b}$, see Fig. 6.13, leads to the same conclusions concerning the gain achieved by adaptive antennas compared to the use of single antennas. The increased gain achieved when K_a equal to four, compared to K_a equal to one, is due to the ideal spatial separation of the K equal to eight simultaneously active users, see Fig. 4.6. When the spatial scenario of Fig. 4.6 is investigated, the gain achieved by adaptive antennas is considerably reduced, when the number of antennas K_a increases from four to eight or from eight to 16. However, the ideal spatial scenario of Fig. 4.6 is not normally observed in real world applications [PWBB98]. The influence of the user spatial separation on the system performance is a critical issue for adaptive antennas [PWBB98], which is investigated in detail in Section 7.3. Nevertheless, the results presented in Figs. 6.12 and 6.13 illustrate the increased potential of adaptive antennas for improving the performance of TD–CDMA mobile radio systems compared to single antennas, when the channel impulse responses are known at the BS receiver. As a final remark, it can be observed that the curve corresponding to K_a equal to one in

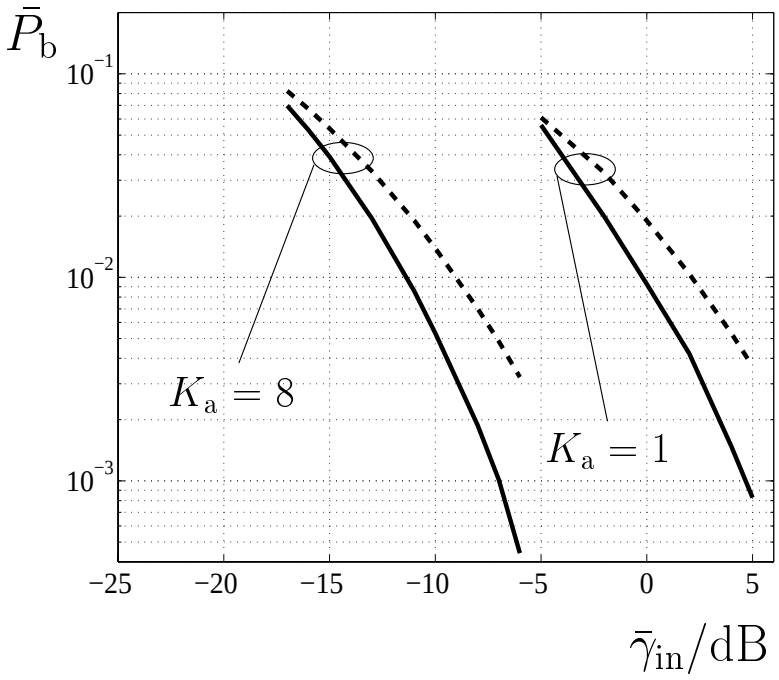

Figure 6.14. Coded and uncoded BER $\bar{P}_\mathrm{b}$ versus the mean input SNR $\bar{\gamma}_\mathrm{in}$ of (6.23); modified COST 207 RA channel model; $K = 8$ users; $v = 3$ km/h

Fig. 6.13 does not perfectly match the corresponding one in Fig. 6.10. This is due to the fact that the number of experiments for obtaining the results in Fig. 6.10 is smaller than the one simulated for Fig. 6.13. In Fig. 6.10 the goal of the simulations is the illustration of the fact that there is no real difference between the original and the novel simulation concept. In Fig. 6.13 more simulations are run in order to achieve accurate results for the BER performance of TD–CDMA using the modified COST 207 channel model.

6.5.3 Influence of the channel model

In this section the influence of the channel model on the link level performance of TD–CDMA is investigated. First, the modified COST 207 channel models, see Section 2.3.2, are considered. Then, the UKL 2 directional channel models, see Section 2.3.3, are used. Further, a cross array configuration with K_a equal to eight antennas is assumed to be used, when adaptive antennas are investigated.

In Figs. 6.14 to 6.16 the influence of the channel model on the system performance is investigated, when the modified COST 207 channel models are used, see Section 2.3.2 and Fig. 2.2. In the case of Fig. 6.14 the modified COST 207 RA channel model is used, and the adopted spatial scenario is shown in Fig. 4.6. In the case of Fig. 6.15 the modified COST 207 TU channel model is used. It is reminded that, because of the directional characteristics of the channel impulse responses, the modified COST 207 RA and

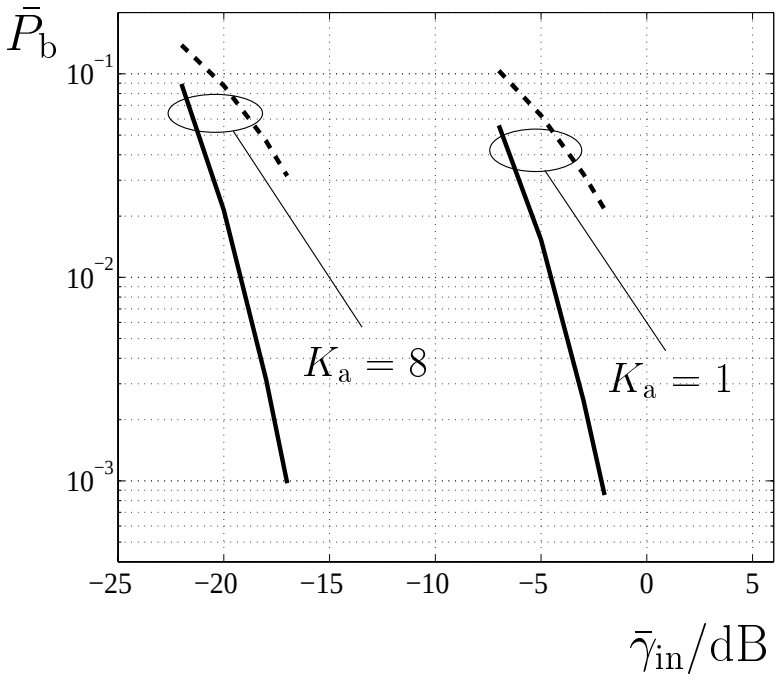

Figure 6.15. Coded and uncoded BER $\bar{P}_\mathrm{b}$ versus the mean input SNR $\bar{\gamma}_\mathrm{in}$ of (6.23); modified COST 207 TU channel model; $K = 8$ users; $v = 3$ km/h

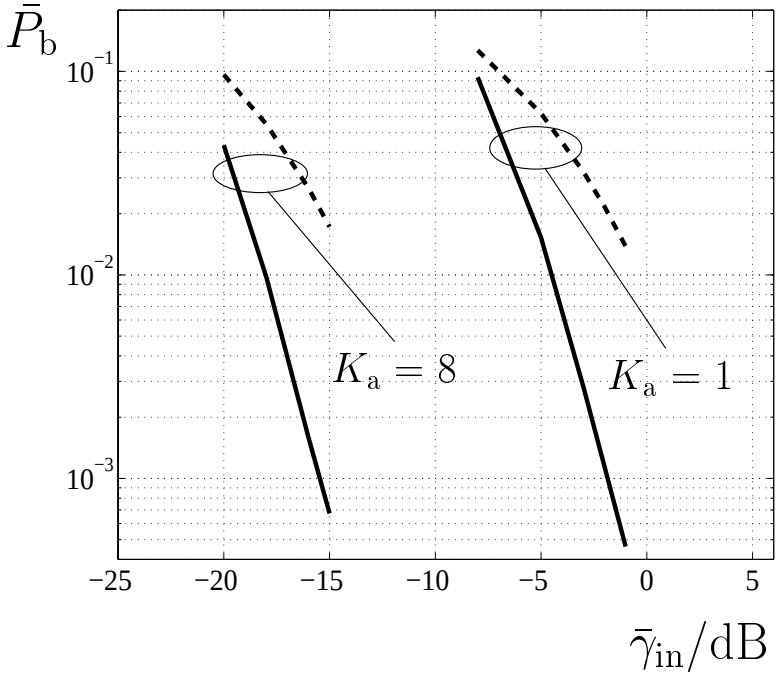

Figure 6.16. Coded and uncoded BER $\bar{P}_\mathrm{b}$ versus the mean input SNR $\bar{\gamma}_\mathrm{in}$ of (6.23); modified COST 207 BU channel model; $K = 8$ users; $v = 3$ km/h

TU channel models can be classified into the large cell channel type, see Section 2.4.2. Further, the modified COST 207 BU channel model is used for the simulation results shown in Fig. 6.16. The adopted spatial scenario is illustrated in Fig. 4.13. The modified COST 207 BU channel model is classified into the small cell channel type, since each tap of the channel impulse response of each user is associated with a single DOA, see also Section 2.3.2. Concerning the average uncoded BER $\bar{P}_\mathrm{b}$, see the dashed curves in Figs. 6.14 to 6.16, the gain achieved by adaptive antennas compared to single antennas, ranges from approximately 11 dB at an average uncoded BER $\bar{P}_\mathrm{b}$ equal to 10^{-2} for the modified COST 207 RA channel model, to approximately 13 dB at an average uncoded BER $\bar{P}_\mathrm{b}$ equal to $2 \cdot 10^{-2}$ for the modified COST 207 TU and BU channel models. Moreover, it is noted from the dashed curves of Figs. 6.14 to 6.16 that the uncoded BER decreases more rapidly as the input SNR $\bar{\gamma}_\mathrm{in}$ increases, when the modified COST 207 TU and BU channel models are used, see Figs. 6.15 and 6.16, compared to the modified COST 207 RA channel model, see Fig. 6.14. This is due to the fact that the modified COST 207 TU and BU channel models have an increased diversity compared to the modified COST 207 RA channel model, see also [Naß95] for a similar result. This increased diversity of the modified COST 207 TU and BU channel models compared to the modified COST 207 RA channel model has two effects on the average coded BER:

- First, as for the average uncoded BER, there is a more rapid decrease of the average coded BER as the mean input SNR $\bar{\gamma}_\mathrm{in}$ increases, when the modified COST 207 TU and BU channel models are used, compared to the modified COST 207 RA channel model.

- Second, there is a greater coded gain compared to the uncoded gain, when the modified COST 207 TU and BU channel models are used, compared to the modified COST 207 RA channel model. This gain is approximately 11 dB at an average coded BER $\bar{P}_\mathrm{b}$ equal to 10^{-3} for the modified COST 207 RA channel model, see the solid lines of Fig. 6.14, almost as for the results for the uncoded BER, whereas the coded gain for the modified COST 207 BU and TU channel models exceeds 15 dB at an average coded BER $\bar{P}_\mathrm{b}$ equal to 10^{-3}, see the solid lines of Figs. 6.15 and 6.16, respectively. An additional gain of more than 2 dB for the coded BER compared to the uncoded BER is observed when the modified COST 207 TU and BU channel models are used, compared to the modified COST 207 RA channel model. This result shows that adaptive antennas work more favourably in propagation environments with increased diversity potential, like the modified COST 207 TU and BU channel models, compared to propagation environments with limited diversity potential, like the modified COST 207 RA channel model.

Next in this section the influence of the channel model on the link level performance of TD–CDMA is investigated, when the UKL 2 directional channel models are used, see Section 2.3.3. As discussed in Section 2.3.3, these channel models incorporate the directional inhomogeneity of the mobile radio channel in a more realistic manner, compared to the

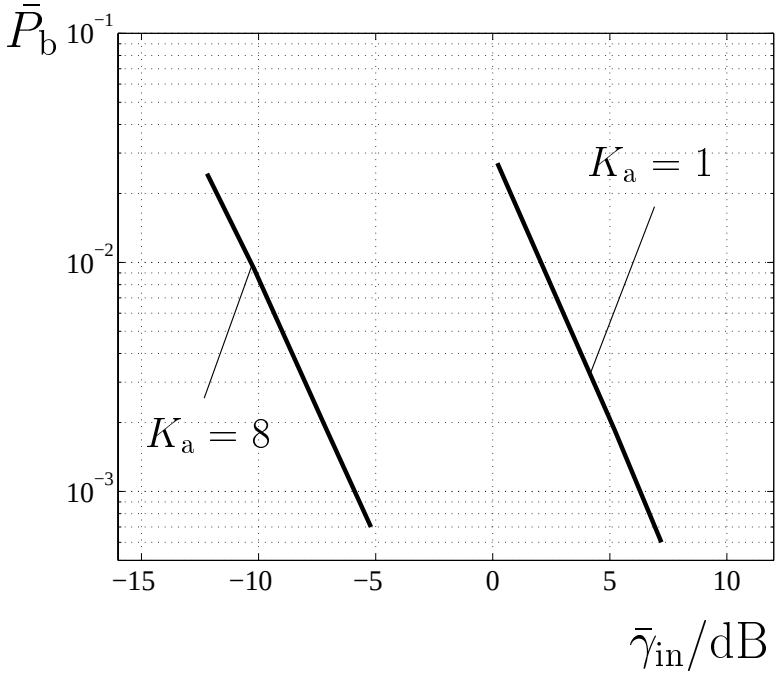

Figure 6.17. Coded BER $\bar{P}_\mathrm{b}$ versus the mean input SNR $\bar{\gamma}_\mathrm{in}$ of (6.23); UKL 2 rural channel model; $K = 8$ users; $v = 3$ km/h

modified COST 207 channel models presented in Section 2.3.2. First, the UKL 2 rural channel model is considered, see Fig. 2.5a. The spatial scenario is illustrated in Fig. 5.2. Next, the UKL 2 urban channel model is used, see Fig. 2.5b. Finally, the UKL 2 dense urban channel model is employed, see Fig. 2.5c. The spatial scenarios for the UKL 2 urban and dense urban channel models are illustrated in Fig. 5.5.

In Figs. 6.17 to 6.19 the influence of the propagation environment on the average coded BER $\bar{P}_\mathrm{b}$ performance is illustrated when the UKL 2 directional channel models are used. The results for the average uncoded BER performance are not shown in Figs. 6.17 to 6.19, since they lead to similar conclusions like the ones presented for the modified COST 207 channel models, see Figs. 6.14 to 6.16, concerning the difference between coded and uncoded BER performance. In Fig. 6.17 the average coded BER $\bar{P}_\mathrm{b}$ is shown versus the mean input SNR $\bar{\gamma}_\mathrm{in}$, when the UKL 2 rural channel model is used. In Figs. 6.18 and 6.19 the corresponding curves are shown, when the UKL 2 urban and the UKL 2 dense urban channel models are used, respectively. As shown in Fig. 6.17 for the UKL 2 rural channel model, the achieved gain is approximately 12 dB at an average coded BER $\bar{P}_\mathrm{b}$ equal to 10^{-3} when K_a equal to eight antennas are used, compared to the single antenna case. The results of Fig. 6.18 for the UKL 2 urban channel model show that an increased gain of approximately 14 dB is achieved compared to the UKL 2 rural channel model, see Fig. 6.17. This increased gain of the coded BER is due to the fact that the UKL 2 urban channel model has an increased diversity compared to the UKL 2 rural channel model, see also the analysis presented in this section for the modified COST 207 channel models.

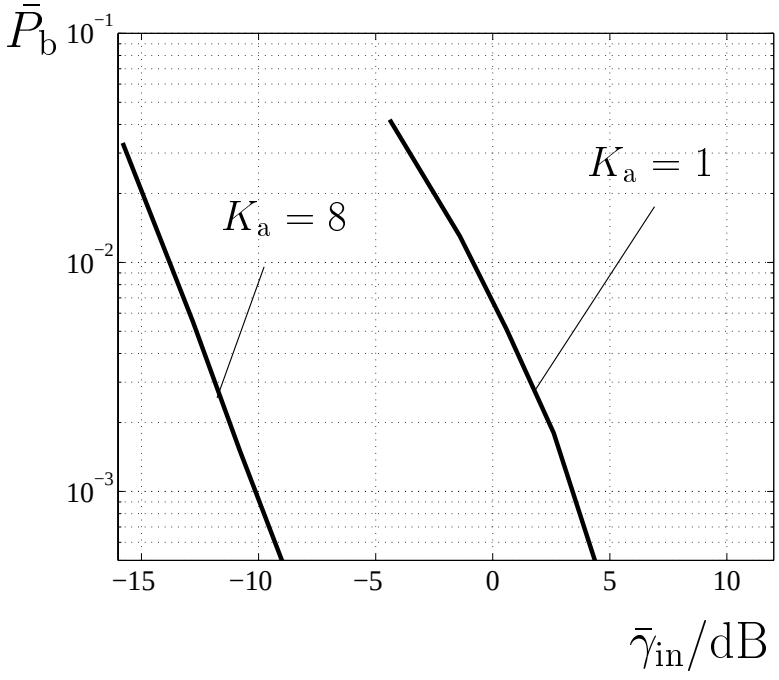

Figure 6.18. Coded BER $\bar{P}_\mathrm{b}$ versus the mean input SNR $\bar{\gamma}_\mathrm{in}$ of (6.23); UKL 2 urban channel model; $K = 8$ users; $v = 3$ km/h

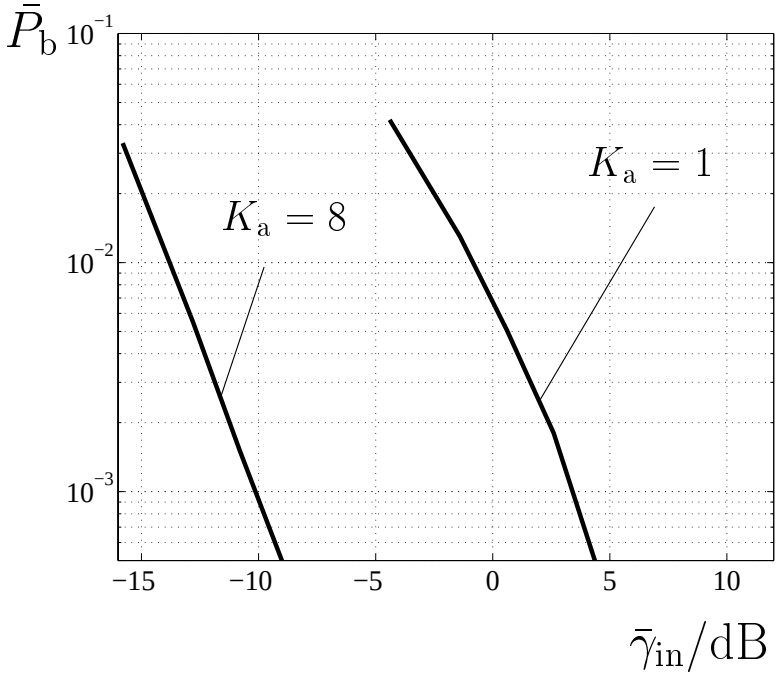

Figure 6.19. Coded BER $\bar{P}_\mathrm{b}$ versus the mean input SNR $\bar{\gamma}_\mathrm{in}$ of (6.23); UKL 2 dense urban channel model; $K = 8$ users; $v = 3$ km/h

The results of Fig. 6.19, where the UKL 2 dense urban channel model is used, are similar to the ones of Fig. 6.18 for the UKL 2 urban channel model. This observation implies that only the presence of the additional scattering area has practically a significant influence on the link level performance of TD–CDMA, and not its distance to the considered BS, compare Figs. 2.6b and 2.6c. However, when channel estimation is considered, see Chapter 5, the treatment of the UKL 2 urban channel model is different compared to the one of the UKL 2 dense urban channel model. Simulation results for the UKL 2 directional channel models including channel estimation are presented in Section 6.6.2.

As a final issue in this section, the modified COST 207 channel models are compared to the UKL 2 directional channel models, with respect to the required mean input SNR $\bar{\gamma}_{\text{in}}$, see (6.23), for achieving an average coded BER $\bar{P}_{\text{b}}$ equal to 10^{-3}. Since the modified COST 207 channel models model the directional inhomogeneity of the mobile radio channel by assuming single DOAs for the impinging signals on the BS array, see Section 2.3.2, the required mean input SNR $\bar{\gamma}_{\text{in}}$ for achieving an average coded BER $\bar{P}_{\text{b}}$ equal to 10^{-3} is in all cases lower than the required mean input SNR $\bar{\gamma}_{\text{in}}$ for the UKL 2 directional channel models, compare Figs. 6.14 to 6.16 with Figs. 6.17 to 6.19. This result implies that, when using the modified COST 207 channel models, upper bounds for the performance of adaptive antennas can be obtained. However, when using directional channel models which come closer to the real world like the UKL 2 directional channel models, a performance degradation is observed compared to the use of the modified COST 207 channel models. This performance degradation amounts to approximately 2 dB for the UKL 2 rural channel model, compared to the modified COST 207 RA channel model. For both UKL 2 urban and dense urban channel models, the performance degradation is approximately 6 dB, compared to the modified COST 207 TU and BU channel models, respectively.

6.5.4 Influence of the user velocity

In this section the influence of the user velocity v on the link level performance of TD–CDMA is investigated by simulations. The goal of this investigation is the illustration of the advantages offered by the novel simulation concept presented in Section 6.2.3.2 compared to the original simulation concept for TD–CDMA, when the influence of different user velocities on the system performance has to be examined. As already shown in Section 6.2.3.2, the database with the output intercell MAI vectors $\underline{\mathbf{n}}_{\text{out},i}$, $i = 0, 1, 2, \ldots$, see Fig. 6.5, pertaining to a certain simulation scenario is produced for the smallest non–zero velocity v_0 of the K users. If the influence of a different user velocity v on the system performance has to be investigated, there is no need for repeating the procedure of producing the respective database, see Section 6.2.3.2. The same database can be directly used, by selecting the output intercell MAI vectors $\underline{\mathbf{n}}_{\text{out},i}$ from the database, which are valid for the considered velocity v. E.g., if the desired user velocity v is equal to v_0, the

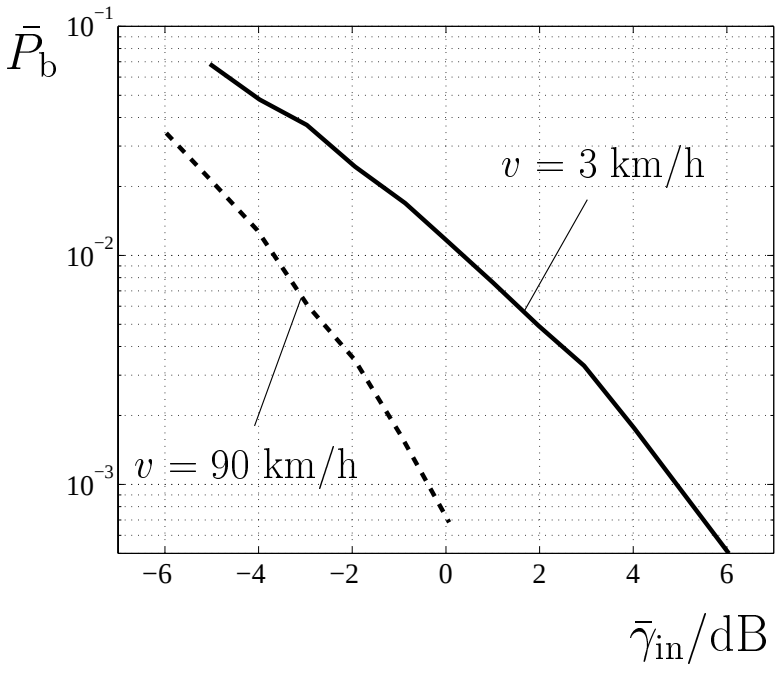

Figure 6.20. Coded BER $\bar{P}_\mathrm{b}$ versus the mean input SNR $\bar{\gamma}_\mathrm{in}$ of (6.23); COST 207 RA channel model; $K_\mathrm{a} = 1$; $K = 8$ users

output intercell MAI vectors $\underline{\mathbf{n}}_{\mathrm{out},i}$, $i = 0, 1, 2, \ldots$, have to be used. On the other hand, if

$$v = m \cdot v_0, \tag{6.53}$$

where m is an integer different from zero, the output intercell MAI vectors $\underline{\mathbf{n}}_{\mathrm{out},i}$, $i = m\mu$, $\mu = 0, 1, 2, \ldots$, have to be selected. Therefore, the simulation time can be significantly reduced compared to the simulation time of the original simulation concept for TD–CDMA, where all simulation steps have to be repeated for each user velocity v, see also Section 6.2.3.2.

In the simulations the COST 207 RA and BU channel models have been used, and a single antenna is employed at the BS receiver. In Fig. 6.20 the simulation results for the COST 207 RA channel model are shown. The smallest non–zero velocity v_0 for producing the databases is chosen to be equal to 3 km/h. Then, the user velocities v equal to 3 km/h and v equal to 90 km/h are investigated, respectively. The increased diversity offered by the velocity of v equal to 90 km/h has the following effects on the system performance:

- First, the required mean input SNR $\bar{\gamma}_\mathrm{in}$ for achieving an average coded BER $\bar{P}_\mathrm{b}$ equal to 10^{-3} is approximately 5 dB smaller for v equal to 90 km/h, compared to the case where the user velocity v equals 3 km/h.

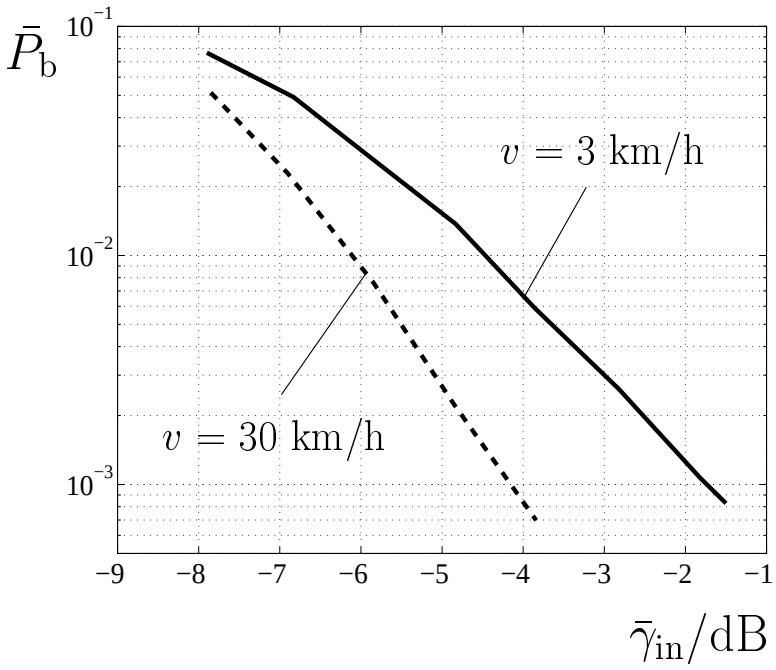

Figure 6.21. Coded BER $\bar{P}_\mathrm{b}$ versus the mean input SNR $\bar{\gamma}_\mathrm{in}$ of (6.23); COST 207 BU channel model; $K_\mathrm{a} = 1$; $K = 8$ users

- Second, for the same amount of increase of the mean input SNR $\bar{\gamma}_\mathrm{in}$, there is a more rapid development of the curve valid for v equal to 90 km/h towards smaller values of the average coded BER $\bar{P}_\mathrm{b}$, compared to the case where v equals 3 km/h.

Note that similar results obtained by using the original simulation concept for TD–CDMA are presented in [Naß95]. Compared to the results of [Naß95], the novel simulation concept presented in Section 6.2 offers a reduction of approximately 70% of the simulation time, while the accuracy of the simulation results is retained. In Fig. 6.21 the respective curves are shown for the COST 207 BU channel model. Here, the user velocity v equals 3 km/h and 30 km/h, respectively. It is observed that the achieved gain at the higher user velocity v equal to 30 km/h is approximately 2 dB at an average coded BER $\bar{P}_\mathrm{b}$ equal to 10^{-3}, compared to the case where v equals 3 km/h. This gain is considerably smaller compared to the COST 207 RA channel model, see Fig. 6.20, since the COST 207 BU channel model used in the simulations has already an increased diversity potential even in smaller user velocities compared to the COST 207 RA channel model. As for Fig. 6.20, the novel simulation concept presented in Section 6.2 offers a reduction of approximately 70% of the simulation time compared to the original simulation concept, see [Naß95]. Finally, it is noted that similar improvements of the BER performance have been observed, when adaptive antennas are used at the BS receiver for both the modified COST RA and BU channel models. These results are not explicitly shown here, but they can be taken from [PFBP99, BPH00].

6.6 Simulation results for the case of estimated channel impulse responses

6.6.1 Preliminaries

In Section 6.5 the link level performance of TD–CDMA with adaptive antennas is investigated, when the channel impulse responses are perfectly known at the BS receiver. As already mentioned in Section 6.5.1, the results presented in Section 6.5 should be viewed as a demonstration of the potential offered by adaptive antennas for performance enhancement in TD–CDMA. In practice, though, the BER performance should be investigated by additionally taking into account channel estimation. In this section the link level performance of TD–CDMA is investigated by using the novel simulation concept presented in Section 6.2.3.3, which includes the influence of channel estimation errors. The present section is structured as follows: First, the influence of channel estimation errors is investigated for the UKL 2 directional channel models, see Section 2.3.3. Then, the influence of DOA estimation errors on the system performance is investigated for the modified COST 207 RA and BU channel models, see Section 2.3.2. Finally, the link level performance is evaluated, when different centro–symmetric array configurations are used at the BS receiver.

6.6.2 Influence of channel estimation errors

In the simulations the UKL 2 directional channel models are used, see Section 2.3.3. Further, user group 0 is considered, see Section 6.2.3.2, and the number K of users of user group 0 is equal to eight. In Figs. 6.22 to 6.24 the simulation results for the coded BER $\bar{P}_{\mathrm{b}}$ versus the mean input SNR $\bar{\gamma}_{\mathrm{in}}$, see (6.23), are shown for

- a single antenna at the BS receiver (solid line),
- a cross array configuration of K_{a} equal to eight elements, when the generalized Steiner estimator, see Section 5.2, is used (dashed line), and
- a cross array configuration of K_{a} equal to eight elements, when the novel channel estimation techniques for the large cell channel type, see Section 5.3, and the small cell channel type, see Section 5.4, are used (dash–dotted line), respectively.

It is reminded that the UKL 2 rural and urban channel models belong to the large cell channel type, see Section 2.4.2, whereas the UKL 2 dense urban channel model belongs to the small cell channel type, see Section 2.4.3. Further, the number of impinging DOAs per user are estimated according to the modified MDL criterion for centro–symmetric array configurations [XRK94], see also Section 1.2, and the DOAs themselves are estimated by

the 2D Unitary ESPRIT algorithm [HN95, Haa97a], see Appendix C.1. Finally, note that the conclusions drawn in this section for the UKL 2 directional channel models are also valid for the modified COST 207 channel models, see Section 2.3.2. Therefore, the results for the modified COST 207 channel models are not explicitly shown here.

In Fig. 6.22 the simulation results for the UKL 2 rural channel model are presented. The spatial scenario is illustrated in Fig. 5.2. Compared to the single antenna case, see the solid line in Fig. 6.22, the receiver using the generalized Steiner estimator, see the dashed line in Fig. 6.22, offers an SNR gain of approximately 10 dB at an average coded BER $\bar{P}_\mathrm{b}$ equal to 10^{-3}. In Figs. 5.5 and 5.6 the improvement of the channel impulse response estimates is illustrated, when the channel estimation technique for the large cell channel type, see Section 5.3, is used, compared to the generalized Steiner estimator. This improvement of the channel estimation technique for the large cell channel type is translated into an SNR gain of about 3 dB at an average coded BER $\bar{P}_\mathrm{b}$ equal to 10^{-3}, when the BER performance is evaluated, compared to the receiver using the generalized Steiner estimator. Compared to the results of Fig. 6.17 for perfectly known channel impulse responses, the following observations can be made from Fig. 6.22:

- For the single antenna case, there is a performance degradation of about 3.5 dB at an average coded BER $\bar{P}_\mathrm{b} = 10^{-3}$ when channel estimation is included, compared to the case of known channel impulse responses, see Fig. 6.17.
- For the multi–antenna case, the use of the generalized Steiner estimator leads to an SNR degradation of about 6 dB compared to the case where the channel impulse responses are perfectly known at the BS receiver, see Fig. 6.17. In contrast to this situation, the use of adaptive antennas, see the dash–dotted line of Fig. 6.22, entails a performance degradation of only 3 dB compared to the case, where the channel impulse responses are perfectly known at the BS receiver. Note that this performance degradation is comparable to the one valid for the single antenna case.

In Fig. 6.23 the simulation results for the UKL 2 urban channel model are presented. The spatial scenario is similar to the one of Fig. 5.5. Compared to the single antenna case, see the solid line of Fig. 6.23, the receiver using the generalized Steiner estimator, see the dashed line of Fig. 6.23, offers an SNR gain of approximately 10 dB at an average coded BER $\bar{P}_\mathrm{b}$ equal to 10^{-3}. Further, the channel estimation technique for the large cell channel type, see Section 5.3, offers an additional SNR gain of 3 dB at an average coded BER $\bar{P}_\mathrm{b}$ equal to 10^{-3}. Finally, note that the comparison of Fig. 6.23 with Fig. 6.18, where the channel impulse responses are perfectly known at the receiver, leads to the same conclusions as for the UKL 2 rural channel model, i.e., adaptive antennas are connected with an SNR performance degradation comparable to the single antenna case, whereas the receiver using the generalized Steiner estimator achieves an average coded BER $\bar{P}_\mathrm{b}$ equal to 10^{-3} at an SNR which lies 3 dB higher, compared to the adaptive antenna case, see Fig. 6.23.

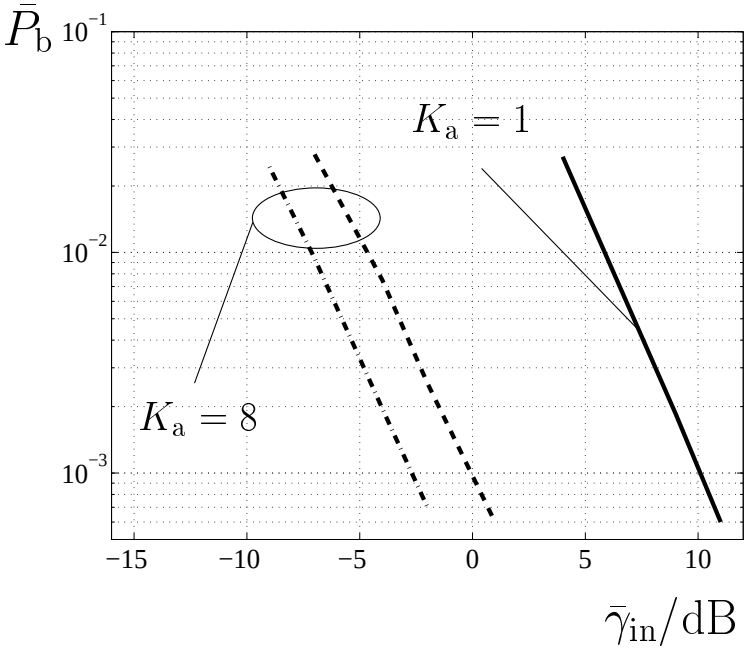

Figure 6.22. Coded BER $\bar{P}_\mathrm{b}$ versus the mean input SNR $\bar{\gamma}_\mathrm{in}$ of (6.23); UKL 2 rural channel model; $K = 8$ users; $v = 3$ km/h; the curves can be compared with the ones in Fig. 6.17

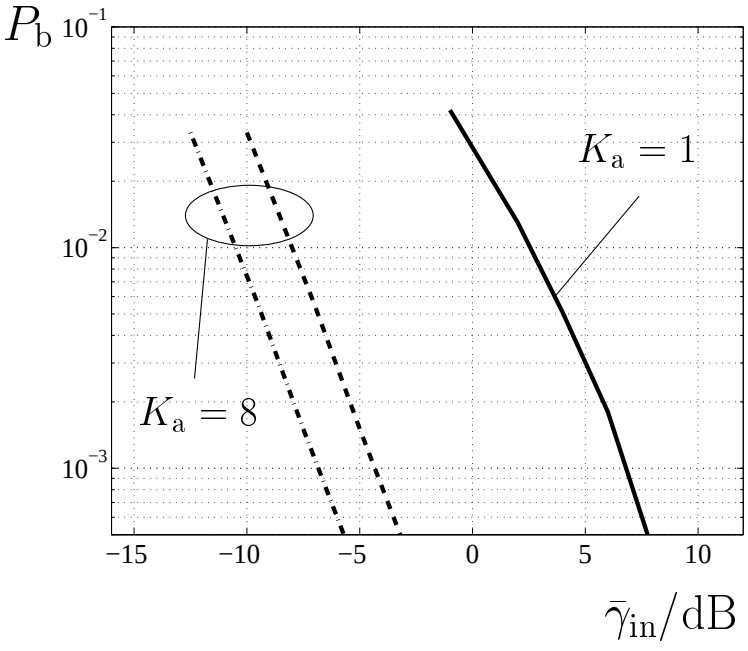

Figure 6.23. Coded BER $\bar{P}_\mathrm{b}$ versus the mean input SNR $\bar{\gamma}_\mathrm{in}$ of (6.23); UKL 2 urban channel model; $K = 8$ users; $v = 3$ km/h; the curves can be compared with the ones in Fig. 6.18

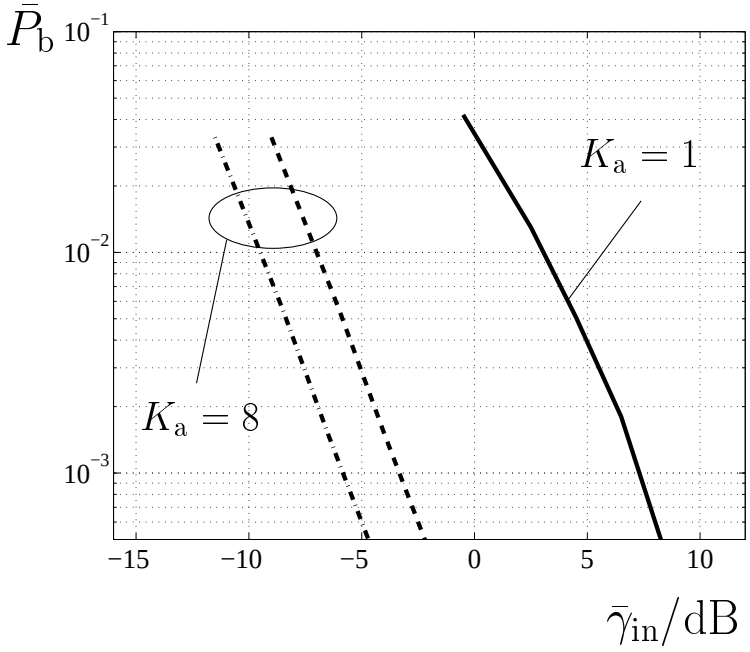

Figure 6.24. Coded BER $\bar{P}_\mathrm{b}$ versus the mean input SNR $\bar{\gamma}_\mathrm{in}$ of (6.23); UKL 2 dense urban channel model; $K = 8$ users; $v = 3$ km/h; the curves can be compared with the ones in Fig. 6.19

In Fig. 6.24 the simulation results for the UKL 2 dense urban channel model are presented. The spatial scenario is illustrated in Fig. 5.5. Compared to the single antenna case, see the solid line of Fig. 6.24, the receiver using the generalized Steiner estimator, see the dashed line of Fig. 6.24, offers an SNR gain of approximately 10 dB at an average coded BER $\bar{P}_\mathrm{b}$ equal to 10^{-3}. Further, the novel channel estimation technique for the small cell channel type, presented in Section 5.4, achieves an additional SNR gain of 3 dB at an average coded BER $\bar{P}_\mathrm{b}$ equal to 10^{-3}. Finally, note that the comparison of the curves in Fig. 6.24 with the curves in Fig. 6.19, where the channel impulse responses are perfectly known at the receiver, leads to the same conclusions stated above in this section for the UKL 2 rural and urban channel models.

6.6.3 Influence of DOA estimation errors

In this section the influence of DOA estimation errors on the link level performance of TD–CDMA with adaptive antennas is investigated. In the simulations the modified COST 207 RA and BU channel models are used. As already mentioned in Section 5.5.2.1, the impact of DOA estimation errors on the system performance should be investigated only for the modified COST 207 channel models, see Section 2.3.2, and not for the UKL 2 directional channel models, see Section 2.3.3. This is due to the fact that the directional inhomogeneity of the mobile radio channel is modeled by single DOAs, when using the

modified COST 207 channel models. Therefore, these DOAs can be assumed to be perfectly known at the BS receiver [PFBP99], see also Section 5.5.2.1. Further, it is reminded that the modified COST 207 RA channel model belongs to the large cell channel type, see Section 2.4.2, whereas the modified COST 207 BU channel model belongs to the small cell channel type, see Section 2.4.3. Therefore, the DOAs are estimated for the modified COST 207 RA channel model as described in Section 5.3.3.2, whereas for the modified COST 207 BU channel model, the DOAs are estimated according to the procedure presented in Section 5.4.2.2.

In Fig. 6.25 the average coded BER $\bar{P}_{\mathrm{b}}$ is shown versus the mean input SNR $\bar{\gamma}_{\mathrm{in}}$, see (6.23), for the modified COST 207 RA channel model, see Section 2.3.2. The spatial scenario is illustrated in Fig. 4.4. The remaining parameters of the TD–CDMA system can be taken from Table 5.1. Note that the array elements are spaced at 0.45 of the carrier wavelength. This choice slightly reduces the aperture of the BS array, reducing simultaneously slightly its resolution capability [PFBP99, Haa97a], but avoids the erroneous estimation associated with signals that impinge on the array from a small range around 90°, when the array elements are spaced at half of the carrier wavelength λ and 2D array configurations are used. This is actually an inherent problem of 2D ESPRIT–type algorithms and can be overcome by reducing the interelement distance [PFBP99]. The solid line in Fig. 6.25 shows the results for the average coded BER, when the DOAs of the impinging signals are perfectly known at the BS receiver. The dashed line in Fig. 6.25 shows the results for the average coded BER, when the number of DOAs and the DOAs themselves are estimated. As in the considerations made in Section 6.6.2, the number of DOAs is estimated by the MDL criterion [XRK94], and the DOAs by the 2D Unitary ESPRIT algorithm [Haa97a], see Appendix C.1. Since we refer to a channel model with single DOAs, the MDL criterion and the 2D Unitary ESPRIT algorithm provide estimates with increased accuracy for the number of DOAs and the DOAs themselves, respectively [Haa97a, PFBP99]. Therefore, from Fig. 6.25 a slight performance degradation of about 0.5 dB is observed, when DOA estimation is included, compared to the case where the DOAs are perfectly known at the BS receiver.

In Fig. 6.26 the curves corresponding to the ones shown in Fig. 6.25 are presented for the modified COST 207 BU channel model, see Section 2.3.2. The spatial scenario is illustrated in Fig. 4.13. As in the simulations for Fig. 6.25, the array elements are spaced at 0.45 of the carrier wavelength λ in order to avoid the erroneous estimation associated with signals that impinge on the array from a small range around 90°, and the array elements are spaced at half of the carrier wavelength λ. For the dashed curve in Fig. 6.26, the number of DOAs is estimated by the MDL criterion [XRK94] and the DOAs by the 2D Unitary ESPRIT algorithm [Haa97a]. As for the simulation results presented in Fig. 6.25, the MDL criterion and the 2D Unitary ESPRIT algorithm provide estimates with increased accuracy for the number of DOAs and the DOAs themselves, respectively. Therefore, from Fig. 6.26 a slight performance degradation of about 0.5 dB is observed, when DOA estimation is included, compared to the case where the DOAs are perfectly known at the BS receiver, see also Fig. 6.25 for a similar conclusion for the large cell

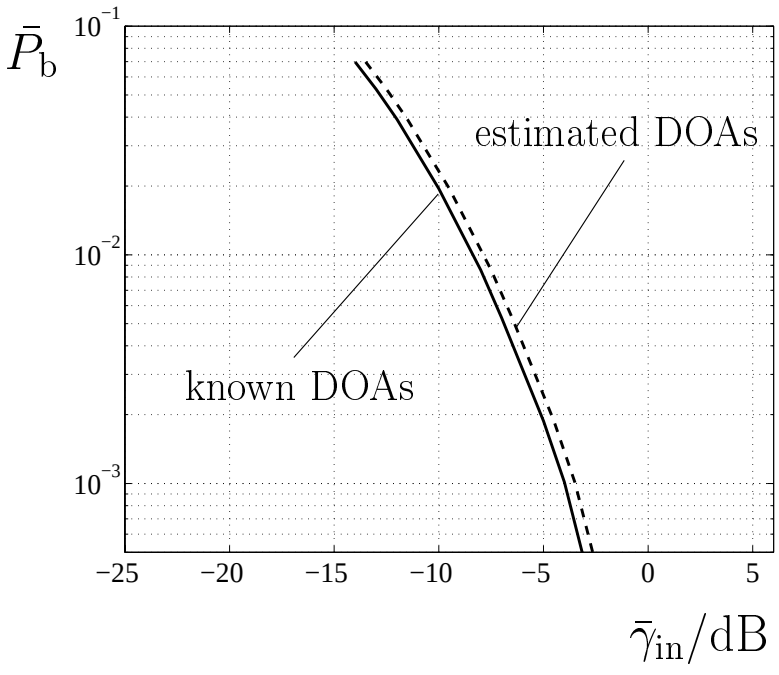

Figure 6.25. Influence of DOA estimation errors for the large cell channel type; coded BER $\bar{P}_\mathrm{b}$ versus the mean input SNR $\bar{\gamma}_\mathrm{in}$ of (6.23); modified COST 207 RA channel model; $K = 8$ users; $v = 3$ km/h

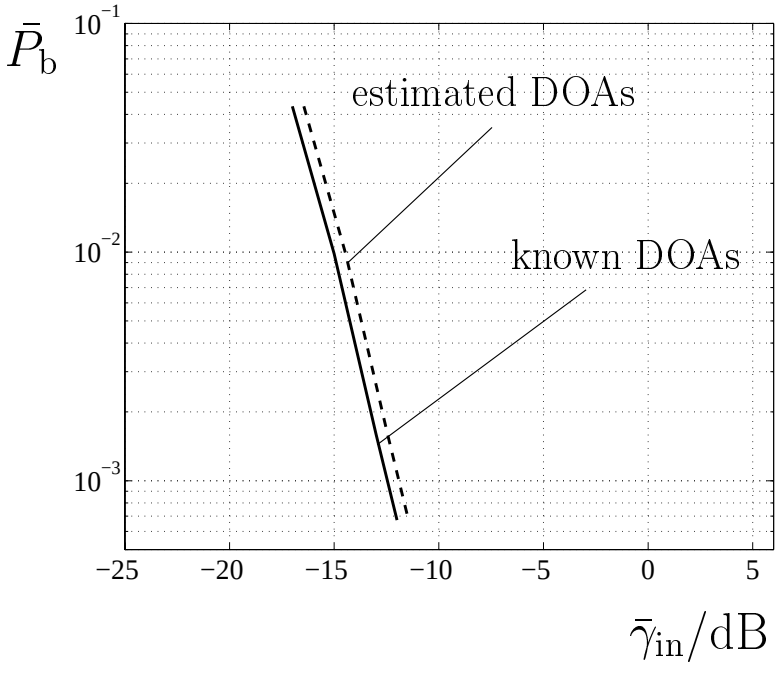

Figure 6.26. Influence of DOA estimation errors for the small cell channel type; coded BER $\bar{P}_\mathrm{b}$ versus the mean input SNR $\bar{\gamma}_\mathrm{in}$ of (6.23); modified COST 207 BU channel model; $K = 8$ users; $v = 3$ km/h

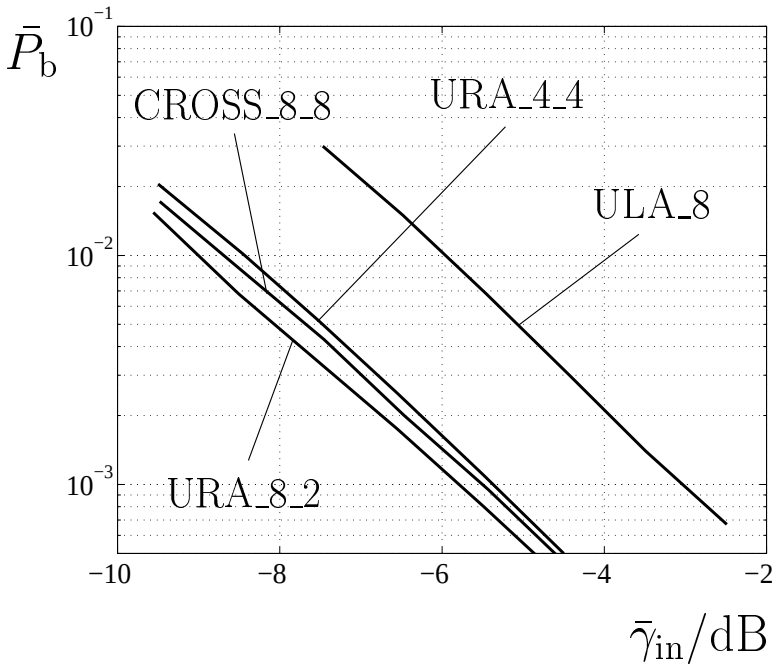

Figure 6.27. Comparison of centro–symmetric array configurations; 90° DOA sector; coded BER $\bar{P}_\mathrm{b}$ versus the mean input SNR $\bar{\gamma}_\mathrm{in}$ of (6.23); modified COST 207 RA channel model; $K = 8$ users; $v = 3$ km/h

channel type.

6.6.4 Influence of the antenna configuration

In this section the influence of the antenna configuration used at the BS receiver on the link level performance of TD–CDMA is investigated. The following centro–symmetric array configurations are compared: A URA of eight–by–two array elements, a URA of four–by–four array elements, a cross array of eight–by–eight elements and a ULA of eight omnidirectional array elements. Note that the considered 2D array configurations have the same number of antenna elements, whereas their aperture is not bigger than the one valid for the ULA. The array elements are spaced at 0.45 of the carrier wavelength. The rationale for this choice is explained in Section 6.6.3. In the simulations the modified COST 207 RA channel model is used, and there are K equal to eight users active in the same frequency band and time slot, which move with a velocity v equal to 3 km/h. The DOA of each user is randomly distributed and independent from the DOAs of the other users.

In a first step, only a sector of 90° in azimuth for the DOAs of signals assigned to the BS is considered. This sector is chosen to be towards the boresight of the ULA and the eight–by–two URA, so that an increased estimation accuracy is offered by these array

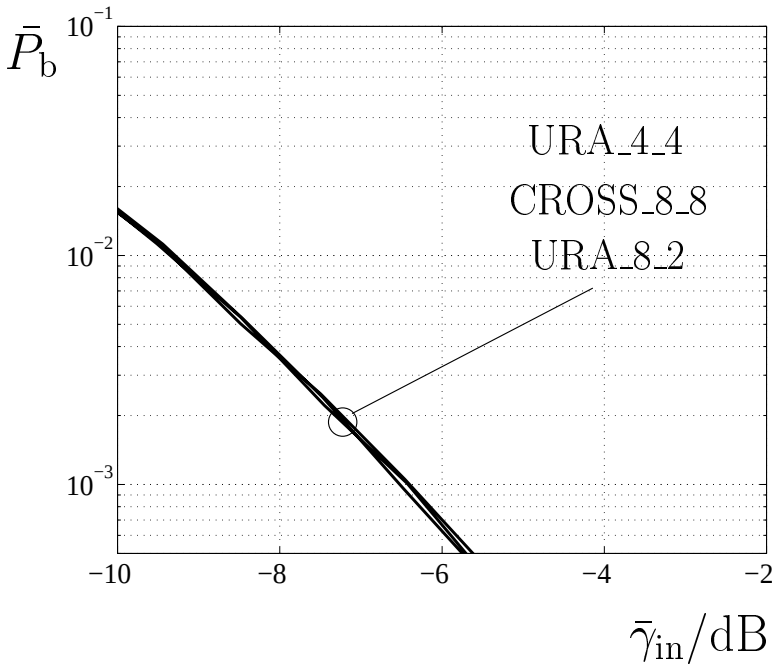

Figure 6.28. Comparison of 2D centro–symmetric array configurations; 360° DOA sector; coded BER $\bar{P}_\mathrm{b}$ versus the mean input SNR $\bar{\gamma}_\mathrm{in}$ of (6.23); modified COST 207 RA channel model; $K = 8$ users; $v = 3$ km/h

configurations [PFBP99]. Obviously, this is not the case for the four–by–four URA and the cross array, which perform independently of this choice. Since a ULA has a limited azimuthal resolution [Haa97a], the choice of a 90° DOA sector offers the possibility of a fair comparison between the ULA and the 2D array configurations, which provide a full azimuthal coverage, besides their elevation resolution capability [Haa97a, PFBP99]. In Fig. 6.27 the simulation results for the average coded BER $\bar{P}_\mathrm{b}$ versus the mean input SNR $\bar{\gamma}_\mathrm{in}$, see (6.23), compare the performance achieved by the different centro–symmetric array configurations considered in this section. Channel estimation is performed according to the channel estimation technique for the large cell channel type, see Section 5.3. The number of DOAs is estimated according to the MDL criterion [XRK94], see also Section 6.6.3, and the DOAs themselves are estimated by the 1D Unitary ESPRIT [HN95] for the ULA, and by the 2D Unitary ESPRIT [Haa97a], see Appendix C.1, for the considered 2D array configurations. The difference between the eight–by–two URA and the cross array or the four–by–four URA is an expected result because of the increased resolution offered by the eight–by–two URA at the considered DOA sector of 90°. However, this difference is less than 0.5 dB. Finally, the considerable performance improvement offered by the 2D array configurations is observed from Fig. 6.27, compared to the use of the ULA at the BS receiver. This improvement is approximately 3 dB, see Fig. 6.27.

In a second step, the whole range of 360° in azimuth for the DOAs of signals assigned to the BS is considered. In this case only the 2D array configurations considered in this

section are used in the simulations, since the ULA is no more able to provide full azimuthal coverage [Haa97a, PFBP99]. In Fig. 6.28 the simulation results for the average coded BER $\bar{P}_{\mathrm{b}}$ versus the mean input SNR $\bar{\gamma}_{\mathrm{in}}$, see (6.23), compare the performance achieved by the considered 2D array configurations. The curves for all considered 2D array configurations are virtually congruent. This means that, in average, the reduced resolution offered by the eight–by–two URA and the four–by–four URA, compared to the cross array configuration, when signals impinge from their narrowside is compensated by their increased resolution on their broadside. The most important result, though, is the performance enhancement compared to the case where only a DOA sector of 90° is considered, see Fig. 6.27. This is, of course, a feature that is offered only by 2D array configurations and not by ULAs. An improvement of approximately 1 dB at an average coded BER $\bar{P}_{\mathrm{b}} = 10^{-3}$ for each 2D array configuration can be achieved by considering the whole azimuthal range, compare Figs. 6.27 and 6.28. This is due to the fact that, in average, the users assigned to the BS are better spatially separated when the whole range of 360° is taken into account, compared to the case where only a sector of 90° is considered. Therefore, 2D array configurations should be used when adaptive antennas are applied in TD–CDMA mobile radio systems.

7 Performance improvement techniques for TD–CDMA

7.1 Introduction

In Chapters 4 and 5 data detection and channel estimation in a TD–CDMA mobile radio system with adaptive antennas are considered in detail, respectively. In Chapter 6 simulation results presented for the uplink of TD–CDMA illustrate impressively the performance improvement achieved by adaptive antennas, compared to single antennas. In this chapter three novel techniques are presented which can be used for additionally improving the performance of TD–CDMA with adaptive antennas. First, the code–channel mismatch problem is considered. The influence of code–channel mismatch is analyzed theoretically and illustrated by simulation results. Then, a novel technique is presented which leads to considerable improvements of the system performance. Second, the influence of the user spatial separation on the performance of TD–CDMA is investigated. Then, a spatial channel assignment strategy is presented, which leads to favourable user spatial separation in TD–CDMA mobile radio systems. Finally, the benefits of using the intercell MAI covariance matrix in TD–CDMA are illustrated in a straightforward manner by following a novel systematic method.

7.2 Consideration of code–channel mismatch

In Section 4.3.3.2 the application of the ZF–BLE, which performs JD of the user data in TD–CDMA, is described in detail. It is shown in Section 4.3.3.2 that the structure of the matrix $\underline{\mathbf{Z}}$, see (4.28), plays a fundamental role for the system performance in TD–CDMA. If the elements of the off–diagonal blocks of $\underline{\mathbf{Z}}$ take large values compared to the diagonal blocks of $\underline{\mathbf{Z}}$, then the system performance is degraded. $\underline{\mathbf{Z}}$ depends exclusively on the system matrix $\underline{\mathbf{A}}$, see Section 4.2. If a single antenna is used at the BS, $\underline{\mathbf{A}}$ is determined by the composite channel impulse responses $\underline{\mathbf{b}}^{(k)}$, $k = 1 \ldots K$, see (4.7). Therefore, since the off–diagonal blocks of $\underline{\mathbf{Z}}$, see (4.28), are determined by the cross–correlation properties of the composite channel impulse responses $\underline{\mathbf{b}}^{(k)}$, $k = 1 \ldots K$, see (4.7), the system performance in TD–CDMA is degraded if the composite channel impulse responses $\underline{\mathbf{b}}^{(k)}$, $k = 1 \ldots K$ exhibit unfavourable correlation properties, i.e., if there is a code–channel mismatch problem.

In order to ease the analysis of the influence of the code–channel mismatch problem, the normalized SNR degradation $\delta_{\mathrm{n},i}$, $i = 1 \ldots KN$, see (6.36) is used, which depends only on the structure of the composite channel impulse responses $\underline{\mathbf{b}}^{(k)}$, $k = 1 \ldots K$, and not on the relative received powers of the K simultaneously active users. Then, according to (6.33), the diagonal blocks of $\underline{\tilde{\tilde{\mathbf{Z}}}}$ are $N \times N$ Hermitian and Toeplitz matrices. If we

define

$$M = \mathrm{int}((W-2)/Q) + 2, \tag{7.1}$$

where W is the vector of each channel impulse response $\underline{\mathbf{h}}^{(k)}$, $k = 1 \ldots K$, Q is the vector of each CDMA code $\underline{\mathbf{c}}^{(k)}$, $k = 1 \ldots K$, and $\mathrm{int}(\cdot)$ denotes the operator which rounds the quantity in the parentheses to the closest integer towards zero, then the diagonal blocks $\underline{\tilde{\tilde{\mathbf{Z}}}}^{(k,k)}$, $k = 1 \ldots K$, of $\underline{\tilde{\tilde{\mathbf{Z}}}}$, see (6.33), are fully determined by the elements of their first row

$$\left[\underline{\tilde{\tilde{\mathbf{Z}}}}^{(k,k)}\right]_{1,j} = \begin{cases} 1 & , j = 1, \\ \frac{1}{b^{(k,k)}} \left[\underline{\mathbf{b}}^{(k)*\mathrm{T}}\right]_{(j-1)Q+1}^{Q+W-1} \left[\underline{\mathbf{b}}^{(k)}\right]_{1}^{(2-j)Q+W-1} & , j \leq M, \\ 0 & , \text{otherwise}, \end{cases} \tag{7.2}$$

where $[\underline{\mathbf{x}}]_{\mu}^{\nu}$ denotes the part of $\underline{\mathbf{x}}$ from the μ–th element to the ν–th element [Naß95], and the scalars $b^{l,m}$, $l, m = 1 \ldots K$, are defined in (6.35). The off–diagonal blocks of $\underline{\tilde{\tilde{\mathbf{Z}}}}^{(l,m)}$, $l, m = 1 \ldots K$, $l \neq m$, of $\underline{\tilde{\tilde{\mathbf{Z}}}}$ are $N \times N$ Toeplitz matrices, and they are fully determined by the elements of the first row

$$\left[\underline{\tilde{\tilde{\mathbf{Z}}}}\right]_{1,j}^{(l,m)} = \begin{cases} \frac{1}{b^{(l,m)}} \left[\underline{\mathbf{b}}^{(l)*\mathrm{T}}\right]_{(j-1)Q+1}^{Q+W-1} \left[\underline{\mathbf{b}}^{(m)}\right]_{1}^{(2-j)Q+W-1} & , j \leq M, \\ 0 & , \text{otherwise}, \end{cases} \tag{7.3}$$

and the first column

$$\left[\underline{\tilde{\tilde{\mathbf{Z}}}}\right]_{i,1}^{(l,m)} = \begin{cases} \frac{1}{b^{(l,m)}} \left[\underline{\mathbf{b}}^{(l)*\mathrm{T}}\right]_{(i-1)Q+1}^{Q+W-1} \left[\underline{\mathbf{b}}^{(m)}\right]_{1}^{(2-i)Q+W-1} & , i \leq M, \\ 0 & , \text{otherwise}, \end{cases} \tag{7.4}$$

respectively. Equivalently stated, the elements of $\underline{\tilde{\tilde{\mathbf{Z}}}}$, see (7.2)–(7.4), are the inner products of the composite channel impulse responses $\underline{\mathbf{b}}^{(k)}$, $k = 1 \ldots K$, of the same user for the diagonal blocks and among the different users for the off–diagonal blocks, as well as shifted versions of them. The inner product remains unchanged under the discrete Fourier transformation (DFT) [Mar87]. Therefore, if we define the Fourier transform of the composite channel impulse response vector $\underline{\mathbf{b}}^{(k)}$, $k = 1 \ldots K$, as

$$\left[\underline{\mathfrak{B}}^{(k)}\right]_{a}^{b} = \mathfrak{F}\left(\left[\underline{\mathbf{b}}^{(k)}\right]_{a}^{b}\right), \quad k = 1 \ldots K, \tag{7.5}$$

(7.2)–(7.4) can be written as

$$\underline{\tilde{\tilde{\mathbf{Z}}}}_{1,j}^{(k,k)} = \begin{cases} 1 & , j = 1, \\ \mathfrak{F}^{-1}\left(\frac{1}{f(j)b^{(k,k)}} \left[\underline{\mathfrak{B}}^{(k)*\mathrm{T}}\right]_{(j-1)Q+1}^{Q+W-1} \left[\underline{\mathfrak{B}}^{(k)}\right]_{1}^{(2-j)Q+W-1}\right) & , j \leq M, \\ 0 & , \text{otherwise}, \end{cases} \tag{7.6}$$

$$\underline{\tilde{\tilde{\mathbf{Z}}}}_{1,j}^{(l,m)} = \begin{cases} \frac{1}{f(j)b^{(l,m)}} \left[\underline{\mathfrak{B}}^{(l)*\mathrm{T}}\right]_{(j-1)Q+1}^{Q+W-1} \left[\underline{\mathfrak{B}}^{(m)}\right]_{1}^{(2-j)Q+W-1} & , j \leq M, \\ 0 & , \text{otherwise}, \end{cases} \tag{7.7}$$

$$\underline{\tilde{\tilde{\mathbf{Z}}}}_{i,1}^{(l,m)} = \begin{cases} \frac{1}{f(i)b^{(l,m)}} \left[\underline{\mathfrak{B}}^{(l)*\mathrm{T}}\right]_{(i-1)Q+1}^{Q+W-1} \left[\underline{\mathfrak{B}}^{(m)}\right]_{1}^{(2-i)Q+W-1} & , i \leq M, \\ 0 & , \text{otherwise}, \end{cases} \tag{7.8}$$

respectively, where

$$f(j) = (2-j)Q + W - 1, \quad j \leq M. \tag{7.9}$$

From (7.6)–(7.8) we observe that normalized SNR degradation $\delta_{\mathrm{n},i}$, $i = 1 \ldots KN$, see (6.36), of (6.36) can be kept low if the spectra of the composite channel impulse responses are well matched, i.e., their inner products produce small values for the elements of the off–diagonal blocks, see (7.7) and (7.8), compared to the elements of the diagonal blocks, see (7.6). In order to support this statement, the simulation environment described in Section 6.3.3.3, see (6.49) is adopted. Then, the normalized SNR degradation $\delta_{\mathrm{n},i}$, see (6.36), of the symbols in the middle of each transmitted burst and each user k, $k = 1 \ldots K$, are shown in Fig. 7.1 for 10^2 transmitted bursts. The variation of the normalized SNR degradation $\delta_{\mathrm{n},i}$ as the mobile move are obvious from Fig. 7.1. In order to identify the bursts for which the CDMA codes $\underline{\mathbf{c}}^{(k)}$, $k = 1 \ldots K$, and the channel impulse responses $\underline{\mathbf{h}}^{(k)}$, $k = 1 \ldots K$, are well or badly matched, the mean normalized SNR degradation $\bar{\delta}_{\mathrm{n}}$ from all K users is plotted in Fig. 7.2 for the scenario valid for Fig. 7.1. From Fig. 7.2 we can observe that the minimum mean normalized degradation appears in the 21^{st} burst, where $\bar{\delta}_{\mathrm{n}}$ is equal to 1.1598, whereas the maximum mean normalized degradation appears in the 56^{st} burst, where $\bar{\delta}_{\mathrm{n}}$ equals 1.9752. The normalized SNR degradation $\delta_{\mathrm{n},i}$ of all $K = 8$ users for the burst where the mean SNR degradation $\bar{\delta}_{\mathrm{n}}$ is minimum, i.e., for the 21^{st} burst, is plotted in Fig. 7.3, whereas the respective values for the burst where the mean SNR degradation $\bar{\delta}_{\mathrm{n}}$ is maximum, i.e., for the 56^{st} burst, are shown in Fig. 7.4. From Fig. 7.3 we observe that the normalized SNR degradation takes small values for all K users, whereas from Fig. 7.4 the normalized SNR degradation for $k = 1$ and $k = 3$ take big values. The absolute value of the Fourier transform of the combined channel impulse responses for the first user, $\underline{\mathfrak{B}}^{(1)}$, and for the third user, $\underline{\mathfrak{B}}^{(3)}$, see (7.5), are shown in Fig. 7.5 for the 21^{st} burst, where the mean normalized SNR degradation is minimum. In Fig. 7.6 the respective values for the 56^{st} burst, where the mean normalized SNR degradation is maximum, are plotted. From Fig. 7.5 we observe that in the case of the minimum mean normalized SNR degradation the spectra of the combined channel impulse responses $\underline{\mathbf{b}}^{(k)}$, $k = 1$ and $k = 3$, are well matched, i.e., the greatest part of their energy is not concentrated in the same regions. In contrast to this situation, it is observed from Fig. 7.6 that the spectra of the combined channel impulse responses $\underline{\mathbf{b}}^{(k)}$, $k = 1$ and $k = 3$, in the case of the maximum mean normalized SNR degradation $\bar{\delta}_{\mathrm{n}}$ are badly matched, see Fig. 7.6, i.e., the greatest part of their energy is concentrated in the

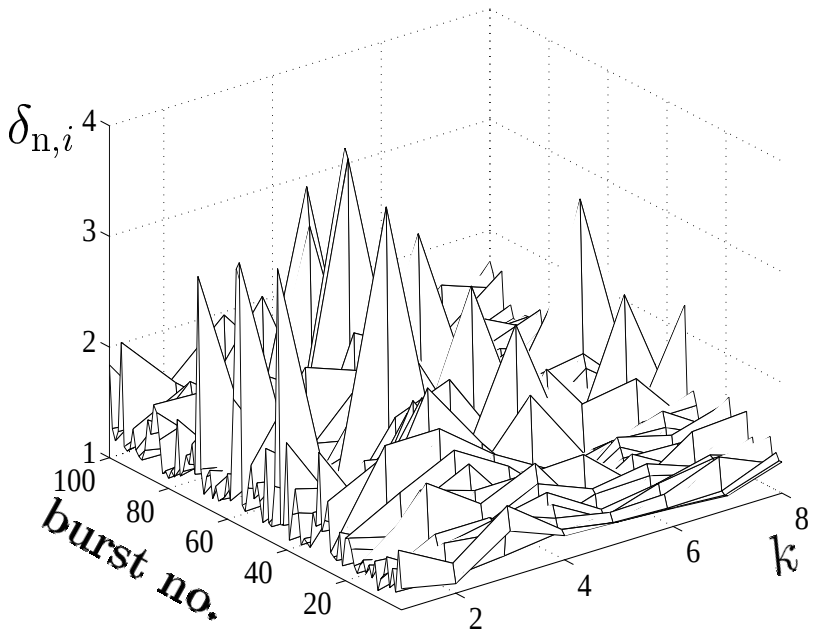

Figure 7.1. Normalized SNR degradation $\delta_{\mathrm{n},i}$; $K = 8$; COST 207 RA channel model; v=3 km/h; 100 bursts

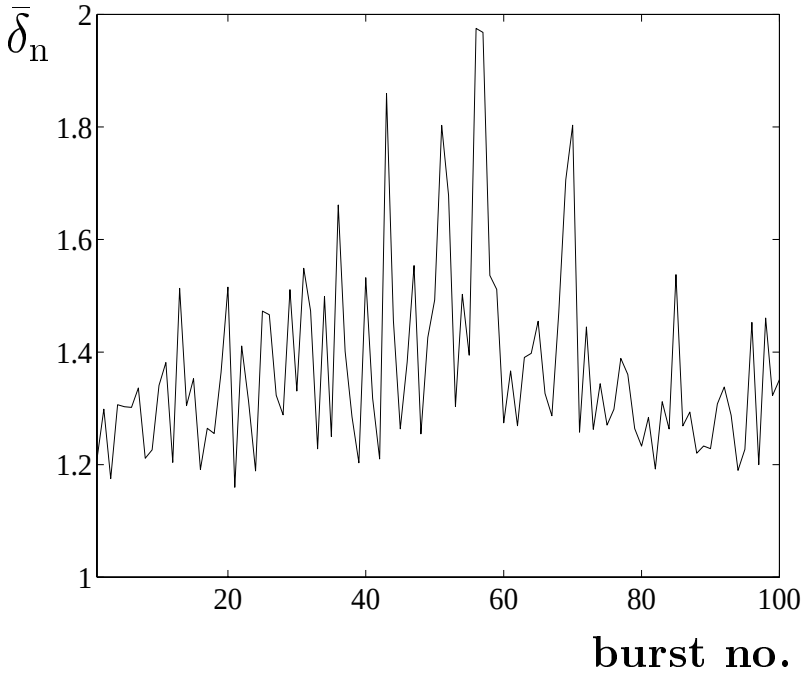

Figure 7.2. Mean normalized SNR degradation $\bar{\delta}_{\mathrm{n}}$; $K = 8$; COST 207 RA channel model; v=3 km/h; 100 bursts

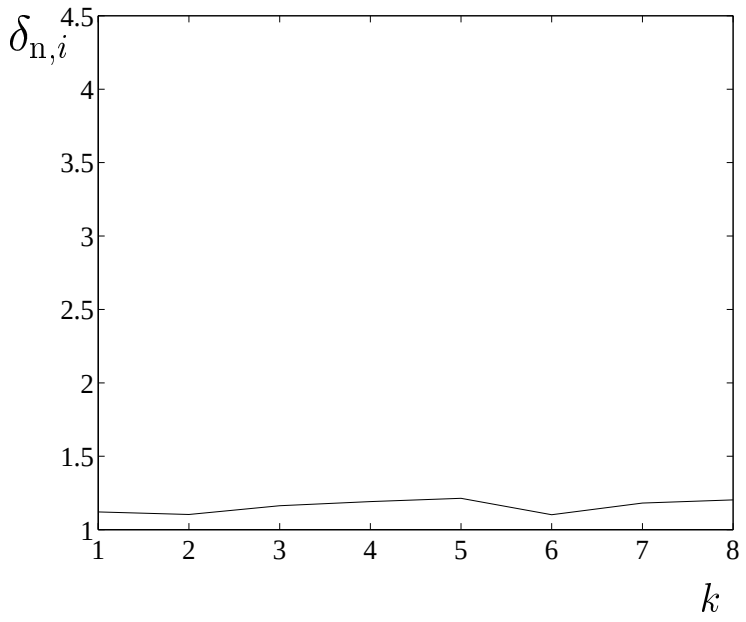

Figure 7.3. Normalized SNR degradation $\delta_{\mathrm{n},i}$ for the minimum of $\bar{\delta}_{\mathrm{n}}$; $K = 8$; COST 207 RA channel model; v=3 km/h; 21$^{\mathrm{st}}$ burst

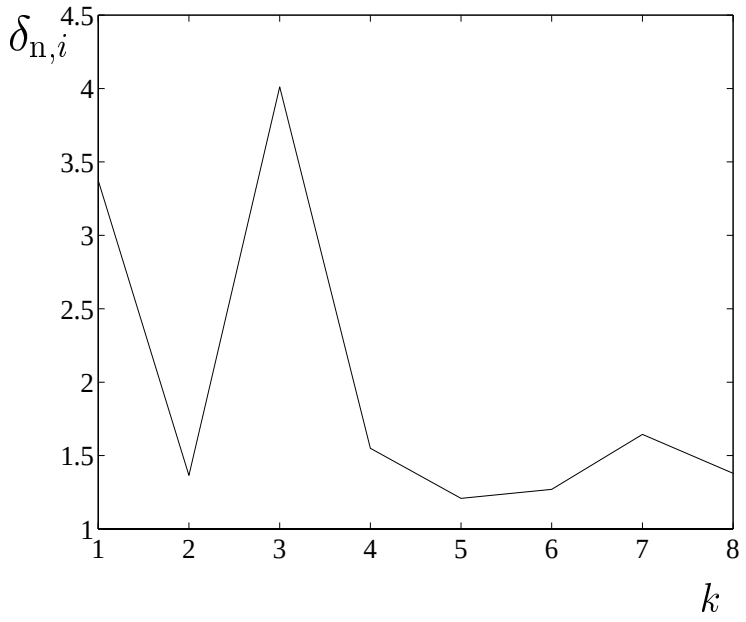

Figure 7.4. Normalized SNR degradation $\delta_{\mathrm{n},i}$ for the maximum of $\bar{\delta}_{\mathrm{n}}$; $K = 8$; COST 207 RA channel model; v=3 km/h; 56$^{\mathrm{st}}$ burst

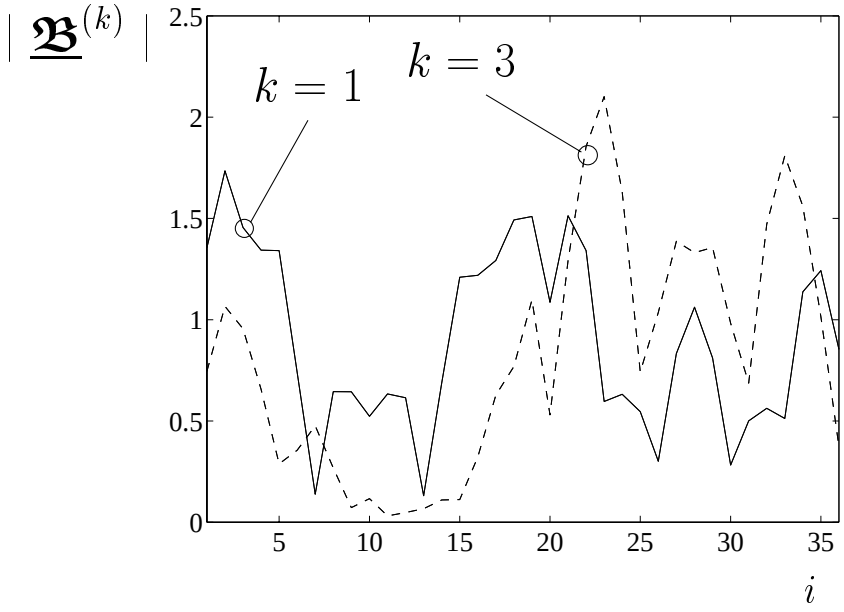

Figure 7.5. $|\ \underline{\mathfrak{B}}^{(k)}\ |$, $k = 1$ and $k = 3$, for the minimum of $\bar{\delta}_{\mathrm{n}}$; $K = 8$; COST 207 RA channel model; v=3 km/h; 21$^{\mathrm{st}}$ burst

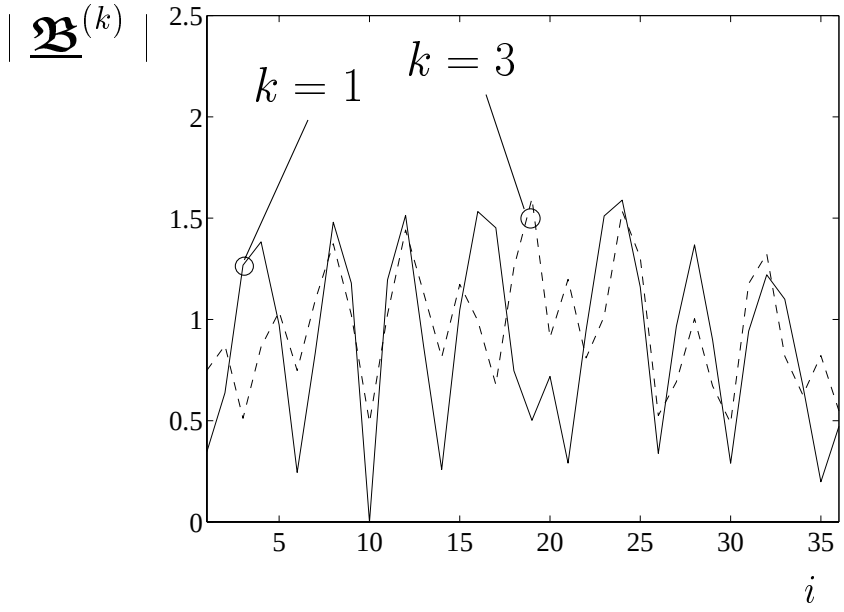

Figure 7.6. $|\ \underline{\mathfrak{B}}^{(k)}\ |$, $k = 1$ and $k = 3$, for the maximum of $\bar{\delta}_{\mathrm{n}}$; $K = 8$; COST 207 RA channel model; v=3 km/h; 56$^{\mathrm{st}}$ burst

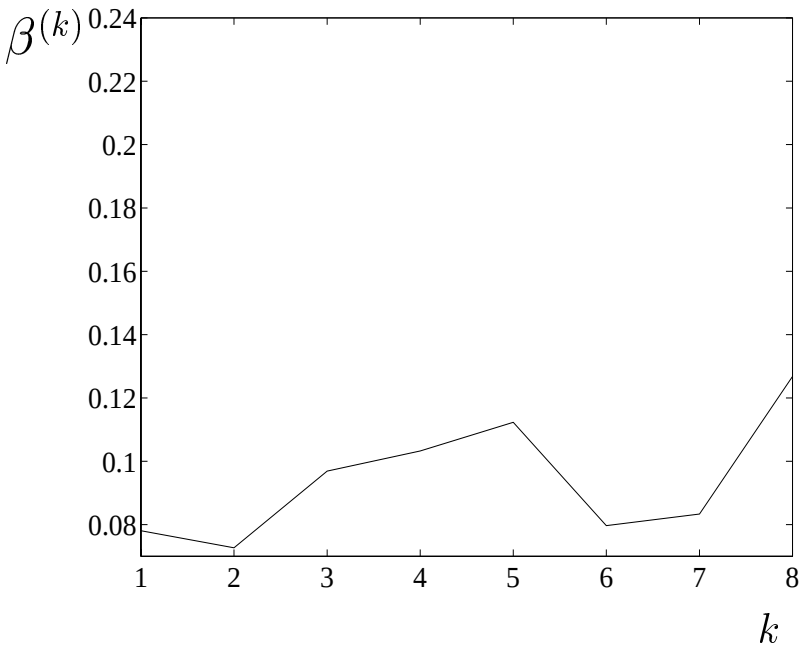

Figure 7.7. $\beta^{(k)}$, $k = 1 \ldots K$, for the minimum of $\bar{\delta}_{\mathrm{n}}$; $K = 8$; COST 207 RA channel model; v=3 km/h; 21$^{\mathrm{st}}$ burst

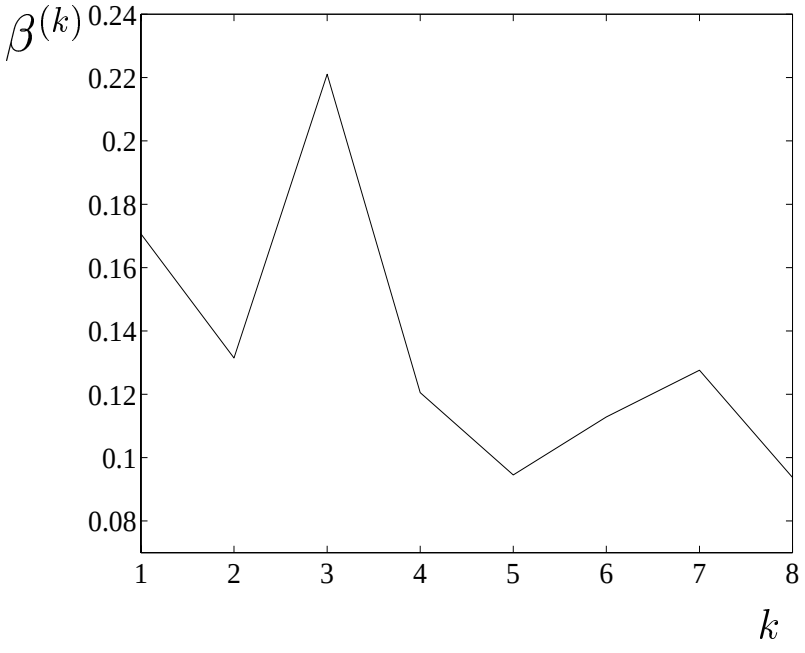

Figure 7.8. $\beta^{(k)}$, $k = 1 \ldots K$, for the maximum of $\bar{\delta}_{\mathrm{n}}$; $K = 8$; COST 207 RA channel model; v=3 km/h; 56$^{\mathrm{st}}$ burst

same regions, thus leading to big values for the normalized SNR degradation valid for the first and third user, see Fig. 7.4. It is noted that the spectra for the remaining user combinations are well–matched for both the 21^{st} and the 56^{st} burst.

Although Fig. 7.5 and Fig. 7.6 illustrate the reason for the behaviour of the normalized SNR degradation $\delta_{\text{n},i}$, $i = 1 \ldots KN$, see (6.36), a measure for a quick and efficient check of a code–channel mismatch should be available in the case of realtime implementations. If we define the $(Q + W - 1) \times K$ matrix

$$\underline{\mathbf{B}} = \left[\begin{array}{cccc} \underline{\mathbf{b}}^{(1)} & \underline{\mathbf{b}}^{(2)} & \ldots & \underline{\mathbf{b}}^{(K)} \end{array} \right], \tag{7.10}$$

the $K \times K$ matrix

$$\underline{\mathbf{R}}_{\text{b}} = \underline{\mathbf{B}}^{*\text{T}} \underline{\mathbf{B}} \tag{7.11}$$

can provide such a measure. From (7.11) we define the scalars

$$\beta^{(k)} = \frac{1}{K-1} \sum_{\substack{i=1 \\ i \neq k}}^{K} | \, [\underline{\mathbf{R}}_{\text{b}}]_{i,k} \, |, \quad k = 1 \ldots K, \tag{7.12}$$

which express the mean of the sum of the absolute values of the column elements of $\underline{\mathbf{R}}_{\text{b}}$, see (7.11). In Fig. 7.7 $\beta^{(k)}$, $k = 1 \ldots K$, is plotted for the 21^{st} burst, where the mean normalized SNR degradation is minimum, see also Fig. 7.3. In Fig. 7.8 $\beta^{(k)}$, $k = 1 \ldots K$, is plotted for the 56^{st} burst, where the mean normalized SNR degradation is maximum, see also Fig. 7.4. The comparison of Fig. 7.7 with Fig. 7.3 and Fig. 7.8 with Fig. 7.4, respectively, shows that $\beta^{(k)}$, $k = 1 \ldots K$, can be considered as a reasonable measure of code–channel mismatch. Numerous simulations performed by the author of this thesis demonstrated that a value for $\beta^{(k)}$, $k = 1 \ldots K$, greater than 0.15 leads to an increased normalized SNR degradation for user k. It is noted that the mean normalized SNR degradation $\bar{\delta}_{\text{n}}$, see Fig. 7.2, can be also used as a measure of code–channel mismatch, however having an increased computational cost, compared to the straightforward measure given by (7.12). In the following of this section, a novel technique for improving the system performance is presented, which explicitely accounts for the code–channel mismatch problem.

In scenarios where the users move relatively slow, e.g., 3 km/h, or the users do not move at all, the application of TD–CDMA in the TDD mode [NTD98], see also Section 1.1, offers the possibility for a considerable improvement of the system behaviour. The scalars $\beta^{(k)}$, $k = 1 \ldots K$, see (7.12), for each transmitted burst can be calculated at the BS receiver. Since the users are assumed not to move fast or not to move at all, it is known that the mobile radio channel state does not change considerably after the duration of one burst [Par92]. If one, or more, of the calculated $\beta^{(k)}$, $k = 1 \ldots K$, for the considered burst takes relatively large values, i.e., it lies above 0.15, then the used CDMA codes for the considered user group can be reassigned to the simultaneously active users

- either according to a prescribed assignment scheme, e.g., taking successively all possible combinations between the K CDMA codes and the K channel impulse responses,

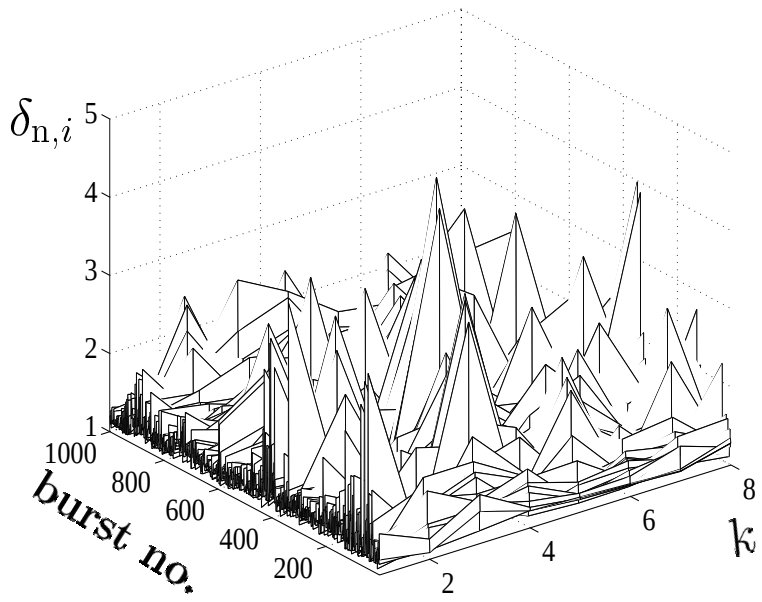

Figure 7.9. Normalized SNR degradation $\delta_{\mathrm{n},i}$; CDMA codes randomly assigned; $K = 8$ users; COST 207 RA channel model; v=3 km/h; 10^3 transmitted bursts

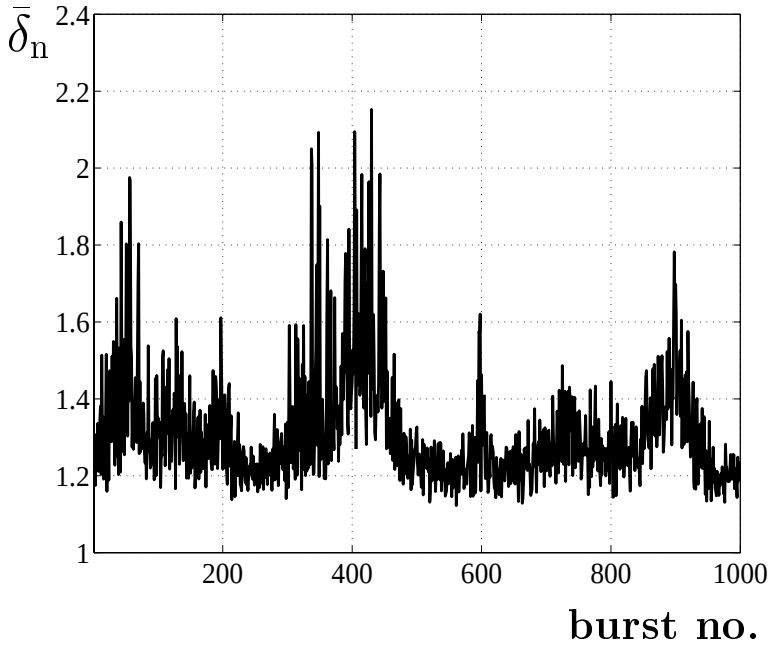

Figure 7.10. Mean normalized SNR degradation $\bar{\delta}_{\mathrm{n}}$; CDMA codes randomly assigned; $K = 8$ users; COST 207 RA channel model; v=3 km/h; 10^3 transmitted bursts

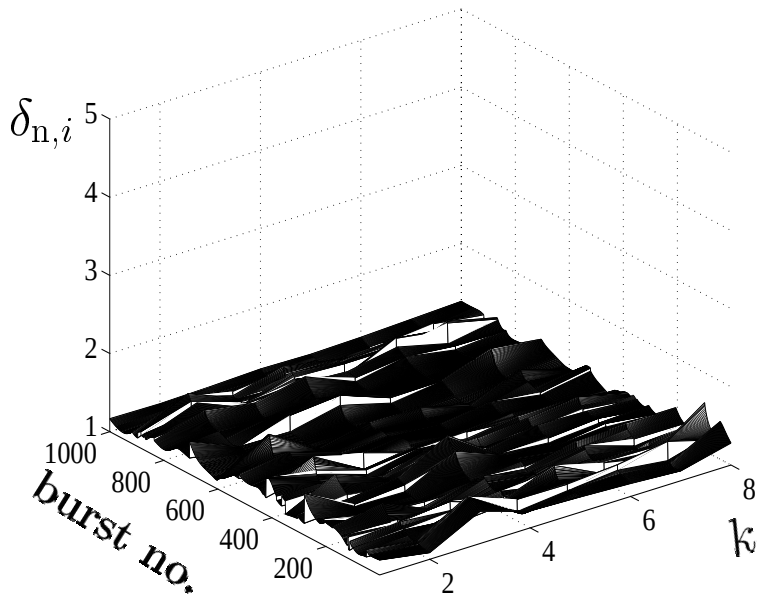

Figure 7.11. Normalized SNR degradation $\delta_{\mathrm{n},i}$; code–channel mismatch considered; $K = 8$ users; COST 207 RA channel model; v=3 km/h; 10^3 transmitted bursts

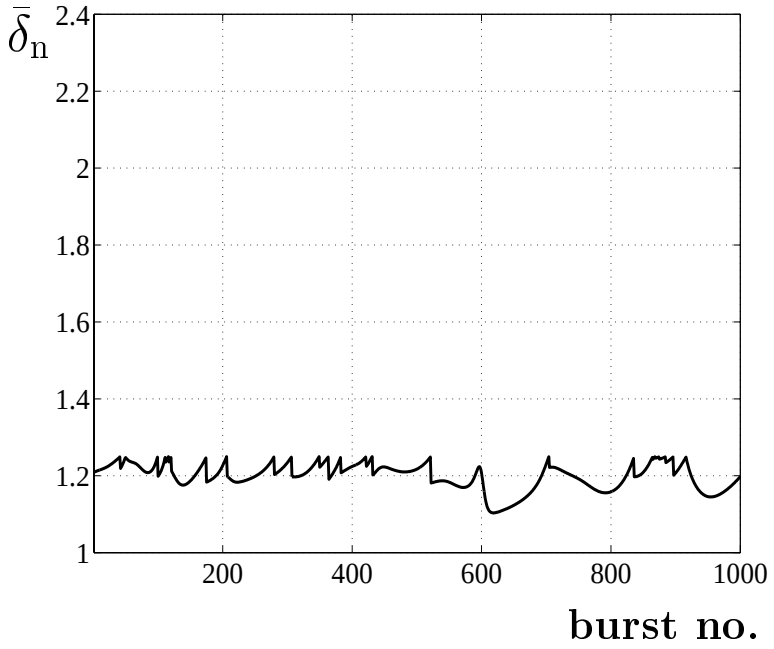

Figure 7.12. Mean normalized SNR degradation $\bar{\delta}_{\mathrm{n}}$; code–channel mismatch considered; $K = 8$ users; COST 207 RA channel model; v=3 km/h; 10^3 transmitted bursts

- or in a truly random manner,

until smaller values of $\beta^{(k)}$, $k = 1 \ldots K$, and, consequently, smaller values for the SNR degradation for all K users are achieved. Certainly, an exhaustive search of all possible combinations would deliver the best possible result according to the proposed technique. However, since the presented technique should be applied in the realtime operation of TD–CDMA, the search may be finished when all values of $\beta^{(k)}$, $k = 1 \ldots K$, lie below 0.15. Numerous simulations performed by the author of this thesis have shown that a small number of random assignments, e.g., less than ten, are in more than 90% of the cases sufficient for achieving values smaller than 0.15 for all $\beta^{(k)}$, $k = 1 \ldots K$.

According to the simulation environment valid for Figs. 7.1–7.8, the normalized SNR degradation $\delta_{\mathrm{n},i}$, see (6.36), of the symbols transmitted in the middle of each burst is shown in Fig. 7.9 for 10^3 transmitted bursts. In Fig. 7.10 the mean normalized SNR degradation $\bar{\delta}_{\mathrm{n}}$ from all $K = 8$ users is plotted versus the number of transmitted bursts. In these simulations, the CDMA codes $\underline{\mathbf{c}}^{(k)}$, $k = 1 \ldots K$, are taken from a fixed CDMA code set, according to [Schl99], and they are randomly assigned to the K simultaneously active users in each transmitted burst, i.e., the problem of code–channel mismatch is not considered. From Figs. 7.9 and 7.10, the variation of the SNR degradation and its mean is obvious, i.e., severe variations of the performance of TD–CDMA occur. In Fig. 7.11 the respective results to Fig. 7.9 are illustrated, when the problem of code–channel mismatch is considered according to the technique presented in this section. The CDMA codes $\underline{\mathbf{c}}^{(k)}$, $k = 1 \ldots K$, are reassigned in a random manner to the $K = 8$ simultaneously active users, and in each burst smaller values than 0.15 have been always achieved for $\beta^{(k)}$, $k = 1 \ldots K$, see (7.12). The considerable improvement of the system behaviour is obvious in Fig. 7.11 compared to Fig. 7.9. The SNR degradation shown in Fig. 7.11 does not exhibit the variations of the SNR degradation illustrated in Fig. 7.9, which means that the system performance is considerably improved, when the code–channel mismatch problem is taken into account. This improvement can be also viewed by comparing Fig. 7.12 with Fig. 7.10, where the mean normalized SNR degradation $\bar{\delta}_{\mathrm{n}}$ for each transmitted burst is plotted. It is noted that the novel technique presented in this section, which considers the code–channel mismatch problem, is applied in the simulations, see Figs. 7.11 and 7.12, under the assumption that the channel state is known prior to the transmission of each burst. However, even if the users move with a small velocity, the channel state does not remain unchanged from burst to burst. Therefore, the results illustrated in Figs. 7.11 and 7.12 should be viewed as a demonstration of the potential offered by the technique presented in this section for improving of the performance of TD–CDMA, when the code–channel mismatch problem is explicitely treated. This means that a system performance degradation should be expected, compared to the results presented in Figs. 7.11 and 7.12, since the state of the channel of the previous transmitted burst can be only known. Nevertheless, we can conclude that the code–mismatch problem has a remarkable influence on the system behaviour, and its consideration can lead to a considerable improvement of the system performance, as indicated by the simulation results presented in Figs. 7.9–7.12.

Finally, it is noted that the generalization of the technique presented in this section to the case of adaptive antennas is performed at the end of Section 7.3, where a joint treatment of the code–channel mismatch problem and the user spatial separation problem in TD–CDMA mobile radio systems is presented.

7.3 Spatial channel assignment strategy

In this section a novel spatial channel assignment strategy is presented, when TD–CDMA operates in the rural propagation environment. This strategy explicitely takes advantage of the DOAs of all users to be assigned to the time slots of a TDMA frame in TD–CDMA, see Fig. 1.1 and Fig. 6.2, and leads to considerable performance improvements, compared to the case where the users are assigned to the time slots of a TDMA frame without exploiting their DOAs. However, before presenting the novel spatial channel assignment strategy, the influence of the user spatial separation on the performance of TD–CDMA is investigated by simulations. The results of this investigation constitutes the motivation for developing spatial channel assignment strategies for TD–CDMA mobile radio systems [BPW99].

In the simulation scenario, a single time slot is considered, and there are K equal to eight users simultaneously active, which move with a velocity v equal to 50 km/h. A cross array configurations of K_a equal to 16 antennas is used at the BS, see Fig. 3.4, which enables a full azimuthal coverage, see also Section 6.6.4. Concerning the investigated spatial scenario, it is assumed that each user impinges on the BS array from a single DOA. For this purpose the modified COST 207 RA channel model is used in the simulations, see Section 2.3.2. Further, all DOAs are assumed to be equidistant within a total azimuthal sector s, measured in degrees (°). In the simulations s is varied from 0, i.e., all signals impinge on the array from the same DOA, which is the worst case of the user spatial separation, to 360°, i.e., two adjacent DOAs differ by 45°, which is the best case for the spatial separation for the considered $K = 8$ users. The rest of the parameters for TD–CDMA can be taken from Table 5.1.

In Fig. 7.13 the average coded BER $\bar{P}_\mathrm{b}$ is plotted versus the mean input SNR $\bar{\gamma}_\mathrm{in}$, see (6.23). Channel estimation is performed according to the channel estimation technique described in Section 5.4.2 for the large cell channel type, and the DOAs are estimated by the 2D Unitary ESPRIT algorithm [Haa97a], see Appendix C.1. The SNR improvement due to the best possible user spatial separation, i.e., when s equals 360°, is approximately 8 dB at an average coded BER $\bar{P}_\mathrm{b} = 10^{-3}$, compared to the worst user spatial separation, i.e., when s is equal to zero, see Fig. 7.13. This result shows that the performance of TD–CDMA with adaptive antennas can be severely degraded when the user signals impinge on the BS receiver from DOAs which are not well spatially separated. This observation can be explained by the fact that the elements of the off–diagonal block $\underline{\mathbf{Z}}^{(k_1,k_2)}$, $k_1, k_2 = 1 \ldots K$, see (4.31), take large values when the DOAs of the users k_1 and k_2 lie

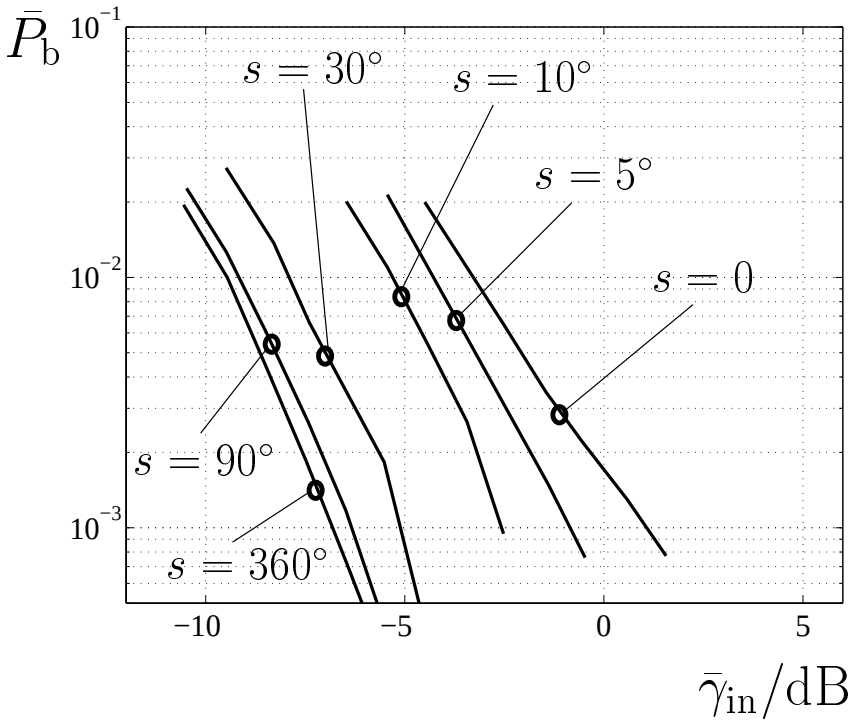

Figure 7.13. Coded BER $\bar{P}_\mathrm{b}$ versus the mean input SNR $\bar{\gamma}_\mathrm{in}$ of (6.23); modified COST 207 RA channel model; $K = 8$ users; $v = 50$ km/h

close in the spatial domain, see the analysis of Section 4.4.2 for the large cell channel type. Note, however, that already with $s = 90°$ the system performance is very close to the case where $s = 360°$, which is related to the number of antennas of the cross array configuration used at the BS, see [PBHP98]. Nevertheless, the performance of a TD–CDMA mobile radio system can be kept close to the performance of Fig. 7.13 with $s = 360°$, if channel assignment strategies are implemented, which incorporate the information about the DOAs of simultaneously active users [PW98, PBHP98]. In the following of this section, a novel spatial channel assignment strategy is presented, which leads to considerable performance improvement of TD–CDMA mobile radio systems with adaptive antennas.

A TDMA frame of a partial frequency band B is considered, see Fig. 1.1 and Fig. 6.2. As already mentioned in Section 1.2, a TDMA frame consists of N_fr time slots, and it is assumed that K_tot users have to be assigned to the N_fr time slots of a TDMA frame. If no information is available concerning the DOAs of the K_tot users to be assigned to the time slots of the TDMA frame, the users are assigned randomly to the time slots. An example of a random user assignment of K equal to 24 users in a TDMA frame consisting of N_fr equal to six time slots is shown in Fig. 7.14. From Fig. 7.14 it is obvious that if the DOA information is not available, the user spatial separation within a time slot may be unfavourable. If $\Delta\phi$ denotes the spatial distance in azimuth between two adjacent

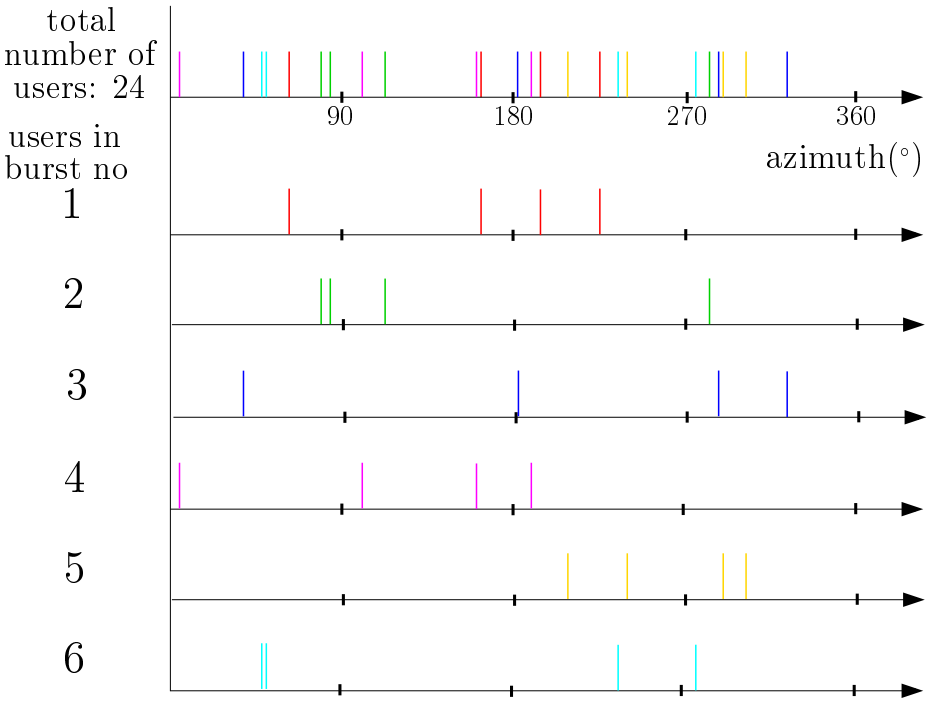

Figure 7.14. Example of a random channel assignment in the time slots of a TDMA frame; $K_{\text{tot}} = 24$ users; $N_{\text{fr}} = 6$ time slots

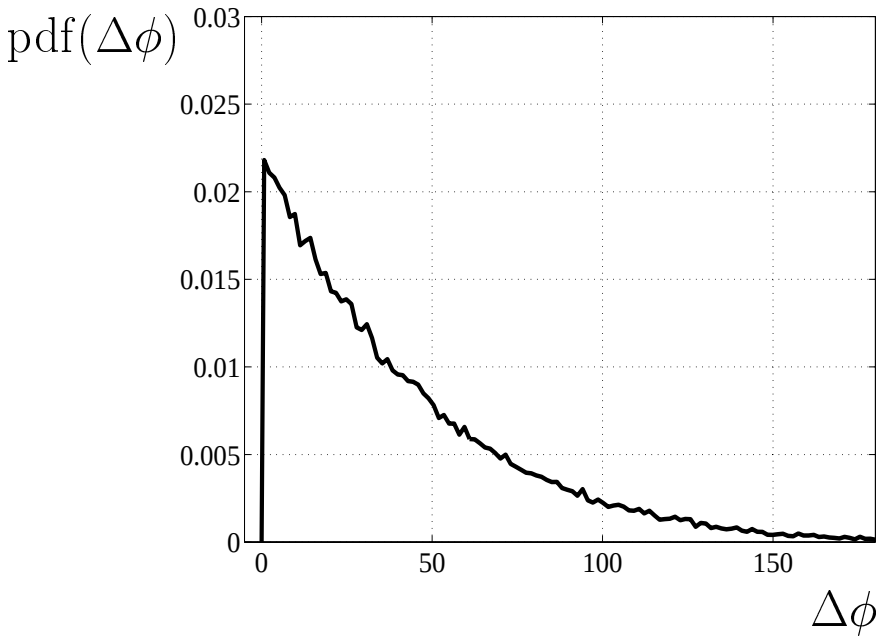

Figure 7.15. pdf of $\Delta\phi$ for a random channel assignment in the time slots of a TDMA frame; $K = 8$ users; $N_{\text{fr}} = 8$ times slots; 10^3 experiments

DOAs within a TDMA burst after the channel assignment, the pdf of $\Delta\phi$ is shown in Fig. 7.15 for a simulation scenario with $K = 64$ users and $N_{\text{fr}} = 8$ time slots. The DOAs of the K_{tot} users are uniformly distributed in the whole range of 360° in azimuth, and 10^3 independent experiments are conducted. From Fig. 7.15 it can be observed that $\Delta\phi$ takes very often small values, which is an undesired effect for the system performance, see Fig. 7.13.

However, if the information about the DOAs of all K_{tot} users to be assigned in a TDMA frame is available, a relatively straightforward channel assignment strategy can be implemented, when TD–CDMA operates in the rural propagation environment. In the rural propagation environment, the distance between the BS and the MS is large, see, e.g., the parameters of the UKL 2 rural channel model proposed in Table 2.1. Therefore, in this environment the DOA of an MS changes rather slowly as the MS moves within the cell. Let us assume that the K_{tot} users are assigned randomly in the N_{fr} time slots for the transmission of the first TDMA frame. After the transmission of the first TDMA frame, the DOAs of the users assigned to each time slot of the TDMA frame can be estimated according to the technique presented in Section 5.3.3.3 for the large cell channel type. Then, since the DOAs of the K_{tot} users valid for the next transmitted TDMA frame do not change significantly compared to the estimated DOAs, the K_{tot} users can be reassigned to the N_{fr} time slots prior to the transmission of the next TDMA frame. The goal of this reassignment is the improvement of the spatial distance between the DOAs of users which are simultaneously active in the same time slot. This improvement may be achieved by

1. first, sorting the K_{tot} user DOAs in ascending order, and
2. then, assigning the user having the n–th DOA, $n = 1 \ldots K_{\text{tot}}$, to the $\text{mod}(n - 1, N_{\text{fr}}) + 1$–th time slot, where the $\text{mod}(a, b)$ operator delivers the remainder of a divided by b, i.e., two successive users are assigned alternatively to two successive time slots, until all K_{tot} users are assigned.

Then, the described strategy can be implemented independently for each TDMA frame transmitted next.

According to the parameters valid for Fig. 7.14, the result of the implementation of the spatial channel assignment strategy presented above is shown in Fig. 7.16. The more favourable user spatial separation in each time slot is obvious from Fig. 7.16, compared to the user spatial separation of Fig. 7.14 where no spatial channel assignment is implemented. Further, for the parameters of Fig. 7.15, the pdf of $\Delta\phi$ is shown in Fig. 7.17 when the spatial channel assignment strategy presented in this section is used. Comparing Fig. 7.17 with Fig. 7.15, we can conclude that the use of a relatively simple spatial channel assignment strategy as the one presented in this section can improve considerably the user spatial separation in the time slots of a TDMA frame of TD–CDMA mobile radio systems.

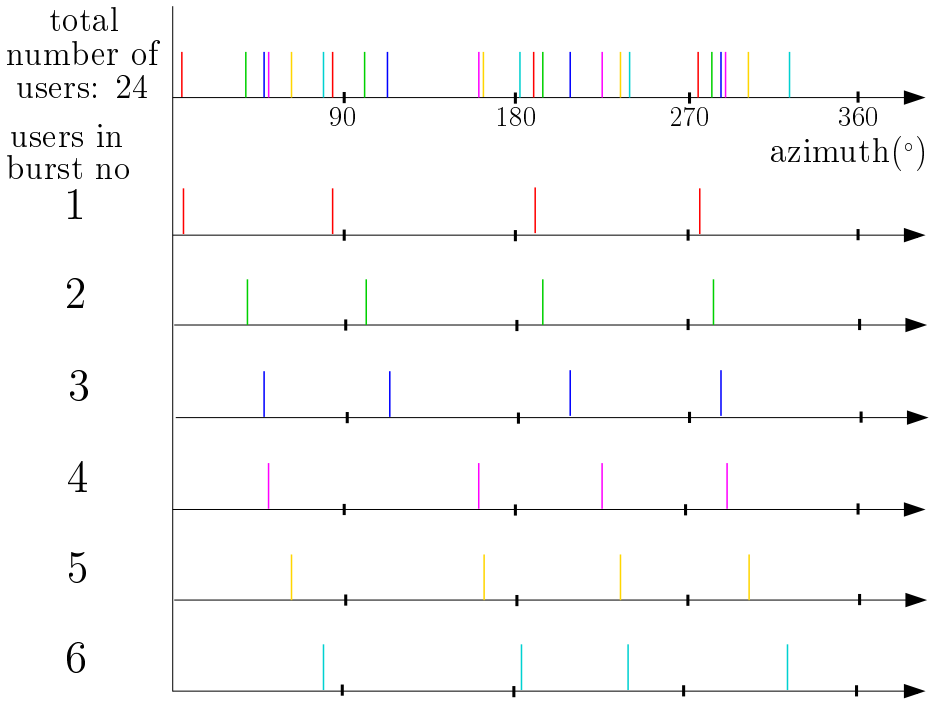

Figure 7.16. Example with spatial channel assignment in the time slots of a TDMA frame; $K_{\text{tot}} = 24$ users; $N_{\text{fr}} = 6$ time slots

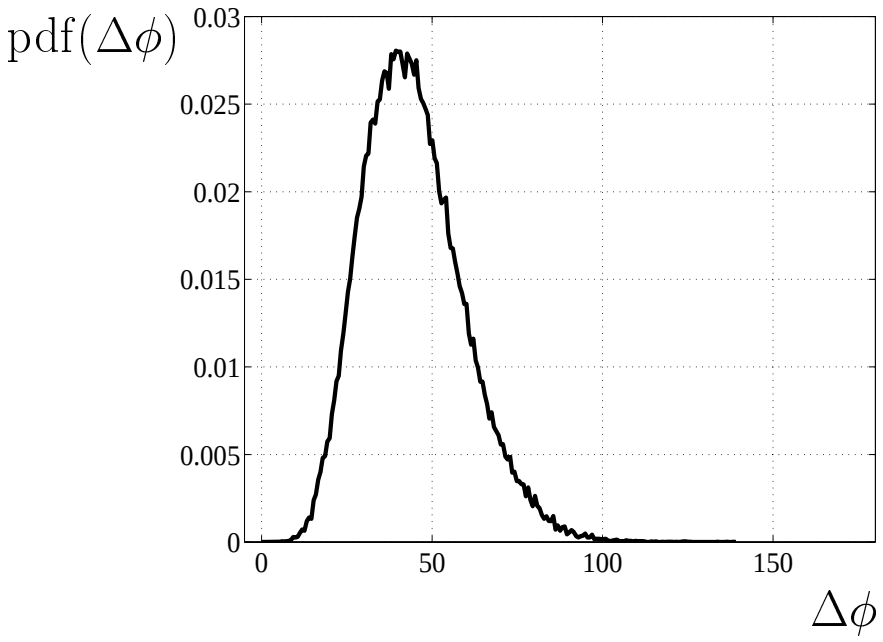

Figure 7.17. pdf of $\Delta\phi$ with spatial channel assignment in the time slots of a TDMA frame; $K = 8$ users; $N_{\text{fr}} = 8$ time slots; 10^3 experiments

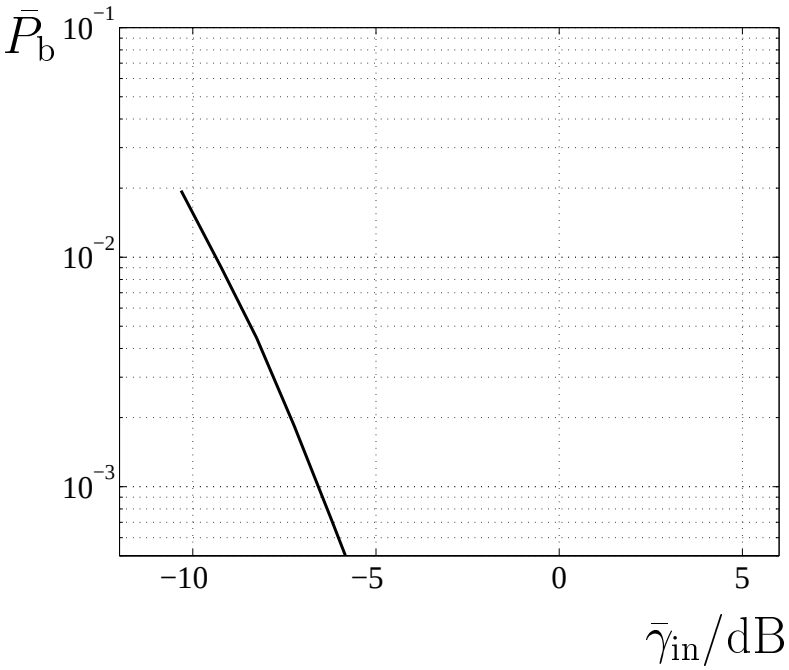

Figure 7.18. Coded BER $\bar{P}_\mathrm{b}$ versus the mean input SNR $\bar{\gamma}_\mathrm{in}$ of (6.23); spatial channel assignment strategy; propagation environment: Rural Area COST207; mobile speed: 50 km/h

The considerable improvement of the user spatial separation shown in Fig. 7.17 is translated directly to an improvement of the system performance as illustrated in Fig. 7.18. In the simulations valid for Fig. 7.18, the parameters valid for Fig. 7.13 are used with s equal to 5°, and the spatial channel assignment presented in this section is employed. Comparing Fig. 7.18 with Fig. 7.13, we can observe that the system performance is very close to the case where $s = 360°$, see Fig. 7.13, when a spatial channel assignment strategy is implemented for the users to be assigned in a TDMA frame. Further, it is noted that this strategy can be also employed when sectorized antenna configurations are used at the BS receiver, expecting a considerable system performance enhancement compared to the random channel assignment of users in a TDMA frame [BPW99].

As a final issue, it is noted that the spatial channel assignment strategy presented in this section can be combined with the technique presented in Section 7.2, i.e., a joint consideration of the code–mismatch and the user spatial separation problem can be performed. This joint consideration may be achieved by applying the technique presented in Section 7.2 to the directional channel impulse responses $\underline{\mathbf{h}}_\mathrm{d}^{(k)}$, $k = 1 \ldots K$, see (5.13), valid for the users of each time slot after the application of the spatial channel assignment strategy presented in this section. In this way, the performance of TD–CDMA in each time slot of a TDMA frame achieved by the application of the spatial channel assignment, see Fig. 7.18, can be additionally improved by taking into consideration the correlation

properties between the used CDMA codes $\underline{\mathbf{c}}^{(k)}$, $k = 1 \ldots K$, and the directional channel impulse responses $\underline{\mathbf{h}}_{\mathrm{d}}^{(k)}$, $k = 1 \ldots K$, as in the single antenna case presented in Section 7.2. However, this joint consideration of the code–mismatch and the user spatial separation problem in TD–CDMA is valid only for rural propagation environments. In the case of urban and dense urban propagation environments, novel techniques should be pursued, which achieve the benefits offered by the joint application of the techniques presented in Section 7.2 and this section for the rural propagation environment.

7.4 Consideration of the intercell MAI covariance matrix

In digital cellular mobile radio systems, the reliability and the transmission quality is determined by the MAI, see also Section 2.2.2. Therefore, digital cellular mobile radio systems are often characterized as interference limited systems [Cal88, Lee89]. The level of the MAI depends on, among other parameters, the multiple access scheme and the detection principle. In TD–CDMA mobile radio systems, the intracell interference, i.e., the interference from users assigned to the considered BS, is eliminated by using JD at the receiver, see Section 4.3.3.2. Consequently, the intercell MAI, i.e., the interference from users assigned to other BSs, plays the most important role on the transmission quality and the reliability of the system. Since we refer to a cellular system, the user signals possess the same spectral properties, which are determined by the modulation scheme, as well as the transmitter and receiver filters [Bla98, BHP97, PHFB97, PFBP99]. Furthermore, the directional inhomogeneity of the mobile radio channel introduces at the considered BS directional intercell noise components, i.e., noise signals with certain DOAs, which also have a certain impinging power. The information about the intercell MAI can be used at the receiver in order to enhance its performance [Kle96, PFBP99, WPS99]. This section is structured as follows: In a first step, the intercell MAI covariance matrix $\underline{\mathbf{R}}_{\mathrm{n}}$ is derived with respect to data detection in TD–CDMA. The analysis is also valid for channel estimation, see Section 5.3.2.4 and Section 5.4.2.3. with respect to channel estimation. Then, by following a systematic method, the influence of the intercell MAI covariance matrix $\underline{\mathbf{R}}_{\mathrm{n}}$ on the performance of TD–CDMA is investigated by simulations. For evaluating this influence, the SNR degradation of TD–CDMA receivers δ_i, see (6.26), is used, which explicitely considers the information about $\underline{\mathbf{R}}_{\mathrm{n}}$. The analysis is also valid for channel detection in TD–CDMA.

It is assumed that K_{i} interfering signals are present, each impinging on the BS array from a single DOA. Further, 2D centro–symmetric array configurations are assumed to be used at the BS receiver, see Fig. 3.4. The DOA of the k_{i}–th interfering signal, $k_{\mathrm{i}} = 1 \ldots K_{\mathrm{i}}$, is split into the azimuth angle $\gamma_1^{(k_{\mathrm{i}})}$ and the elevation angle $\gamma_2^{(k_{\mathrm{i}})}$, see Fig. 5.1. If the k_{i}–th interfering signal at the RP is expressed by the vector $\underline{\mathbf{n}}_{\mathrm{d}}^{(k_{\mathrm{i}})}$ [PFBP99, Bla98] of vector $NQ + W - 1$, see Section 4.2, the phase factor for the k_{i}–th interferer at the k_{a}–th array

element is given by [PFBP99, Haa97a, RK89]

$$\phi^{(k_\mathrm{i},k_\mathrm{a})} = 2\pi \frac{l^{(k_\mathrm{a})}}{\lambda} \cos(\gamma_1^{(k_\mathrm{i})} - \alpha^{(k_\mathrm{a})}) \sin(\gamma_2^{(k_\mathrm{i})}), \tag{7.13}$$

where $l^{(k_\mathrm{a})}$ and $\alpha^{(k_\mathrm{a})}$, $k_\mathrm{a} = 1 \ldots K_\mathrm{a}$, are defined in Fig. 5.1, see also the analysis of Section 5.3.2, and λ denotes the carrier wavelength. Note that (7.13) is the equivalent expression to (5.18), valid for an MS which contributes to the intracell MAI in TD–CDMA. Then, the intercell MAI vector at the k_a–th array element is related to the intercell MAI vectors $\underline{\mathbf{n}}_\mathrm{d}^{(k_\mathrm{i})}$, $k_\mathrm{i} = 1 \ldots K_\mathrm{i}$, via

$$\underline{\mathbf{n}}^{(k_\mathrm{a})} = \sum_{k_\mathrm{i}=1}^{K_\mathrm{i}} \mathrm{e}^{\mathrm{j}\phi(k_\mathrm{i},k_\mathrm{a})} \cdot \underline{\mathbf{n}}_\mathrm{d}^{(k_\mathrm{i})}, \tag{7.14}$$

Let now

$$\underline{\mathbf{R}}_\mathrm{n}^{(i,j)} = \mathrm{E}\left\{\underline{\mathbf{n}}^{(i)} \underline{\mathbf{n}}^{(j)*\mathrm{T}}\right\}, \qquad i,j = 1 \ldots K_\mathrm{a}, \tag{7.15}$$

denote the $NQ+W-1 \times NQ+W-1$ covariance matrix of $\underline{\mathbf{n}}_\mathrm{m}^{(i)}$, valid for the i–th array element, and $\underline{\mathbf{n}}^{(j)}$, valid for the j–th array element. Then, the covariance matrix of the combined intercell MAI vector $\underline{\mathbf{n}}$, see also (4.12), from all K_a array elements is given by

$$\underline{\mathbf{R}}_\mathrm{n} = \mathrm{E}\left\{\underline{\mathbf{n}}\ \underline{\mathbf{n}}^{*\mathrm{T}}\right\} \tag{7.16}$$

with its (i,j)–th block equal to $\underline{\mathbf{R}}_\mathrm{m}^{(i,j)}$ of (7.15), see also (4.17). $\underline{\mathbf{R}}_\mathrm{n}$, see (7.16), is denoted as the total intercell MAI covariance matrix [WPS99, WP99a, PW99].

It is assumed that the interfering signals are pairwise uncorrelated, i.e.,

$$\mathrm{E}\left\{\underline{\mathbf{n}}_\mathrm{d}^{(l)}\ \underline{\mathbf{n}}_\mathrm{d}^{(m)\ *\mathrm{T}}\right\} = 0, \quad \text{for} \quad l \neq m, \tag{7.17}$$

and they have the same spectral form, which is a valid assumption since we refer to a cellular system transmitting signals with the same spectral properties [Bla98, PHFB97, PFBP99]. If the noise power of the k_i–th interferer is defined as

$$(\sigma^{(k_\mathrm{i})})^2 = \mathrm{E}\left\{|\ \underline{n}_{\mathrm{d},l}^{(k_\mathrm{i})}\ |^2\right\}, \quad l = 1 \ldots NQ+W-1, \tag{7.18}$$

the spectral form of the interfering signals is contained in the $NQ+W-1 \times NQ+W-1$ temporal intercell MAI covariance matrix

$$\underline{\mathbf{R}}_\mathrm{t} = \frac{1}{(\sigma^{(k_\mathrm{i})})^2} \mathrm{E}\left\{\underline{\mathbf{n}}_\mathrm{d}^{(k_\mathrm{i})} \underline{\mathbf{n}}_\mathrm{d}^{(k_\mathrm{i})\ *\mathrm{T}}\right\}, \quad k_\mathrm{i} = 1 \ldots K_\mathrm{i}. \tag{7.19}$$

It is noted that $\underline{\mathbf{R}}_\mathrm{t}$ is identical for all K_i interferers. Let us now define the scalars

$$\underline{r}_{i,j} = \underline{r}_{i,j}^* = \sum_{k_\mathrm{i}=1}^{K_\mathrm{i}} (\sigma^{(k_\mathrm{i})})^2 \mathrm{e}^{\mathrm{j}(\phi^{(k_\mathrm{i},i)} - \phi^{(k_\mathrm{i},j)})}, \quad i,j = 1 \ldots K_\mathrm{a}, \tag{7.20}$$

which depend on the noise powers, see (7.18), and the phase factors, see (7.13), of the interfering signals. Then, the covariance matrix $\underline{\mathbf{R}}^{(i,j)}$, see (7.15), takes the form [Bla98, PFBP99, WPS99]

$$\underline{\mathbf{R}}^{(i,j)} = \underline{r}_{i,j} \cdot \underline{\mathbf{R}}_{\mathrm{t}}, \quad i,j = 1 \ldots K_{\mathrm{a}}, \tag{7.21}$$

and the total intercell MAI covariance matrix $\underline{\mathbf{R}}_{\mathrm{n}}$, see (7.16), is a $K_{\mathrm{a}}(NQ+W-1) \times K_{\mathrm{a}}(NQ+W-1)$ matrix with its (i,j)–th block equal to $\underline{r}_{i,j} \cdot \underline{\mathbf{R}}_{\mathrm{t}}$, see (7.21). If we define the $K_{\mathrm{a}} \times K_{\mathrm{a}}$ spatial intercell MAI covariance matrix with elements $[\underline{\mathbf{R}}_{\mathrm{s}}]_{i,j}$ equal to $ru_{i,j}$, see (7.20), then the intercell MAI covariance matrix $\underline{\mathbf{R}}_{\mathrm{n}}$, see (4.17) takes the simple form [PHFB97]

$$\underline{\mathbf{R}}_{\mathrm{m}} = \underline{\mathbf{R}}_{\mathrm{s}} \otimes \underline{\mathbf{R}}_{\mathrm{t}}, \tag{7.22}$$

where $\underline{\mathbf{R}}_{\mathrm{t}}$ is defined in (7.19). It is noted that the spatial intercell MAI covariance matrix $\underline{\mathbf{R}}_{\mathrm{s}}$ exclusively depends on the DOAs and the noise powers of the K_{i} interfering signals, and, therefore, it is also valid for channel estimation in TD–CDMA, see Section 5.3.2.4 and Section 5.4.2.3. On the other hand, the temporal intercell MAI covariance matrix $\underline{\mathbf{R}}_{\mathrm{t}}$ depends on the length of the part of the received signal which is used. Therefore, when channel estimation is considered, the temporal intercell MAI covariance matrix has vectors $L \times L$, see (5.1), and is denoted by $\underline{\mathbf{R}}_{\mathrm{m,t}}$. Then, (5.10) expresses the total intercell MAI covariance matrix valid for channel estimation in TD–CDMA mobile radio systems.

As mentioned at the beginning of this section, the intercell MAI plays the most important role on the transmission quality and the reliability of TD–CDMA. When applying the ZF–BLE, see (4.21), the performance of TD–CDMA can be improved by using the information about the total intercell MAI covariance matrix $\underline{\mathbf{R}}_{\mathrm{n}}$, see (7.16). In this section, in order to have a relative straightforward measure for assessing the performance of TD–CDMA, the SNR degradation δ_i, $i = 1 \ldots KN$, see (6.26), is used. However, in Section 6.3.2, the SNR degradation is derived for the case that the intercell MAI is modeled as AWGN. For the purpose of this section, if the total intercell MAI covariance matrix $\underline{\mathbf{R}}_{\mathrm{n}}$, see (7.16), is known at the BS receiver, it is easily shown that the SNR degradation of TD–CDMA receivers is expressed as

$$\delta_i = \frac{\mathrm{E}\{\mid \underline{\mathbf{b}}^{(k)} \mid^2\}}{Q} \left[\left(\underline{\mathbf{A}}^{*\mathrm{T}} \underline{\mathbf{R}}_{\mathrm{n}}^{-1} \underline{\mathbf{A}}\right)^{-1}\right]_{i,i}, \; i = 1 \ldots KN, \tag{7.23}$$

see (6.26) and the analysis of Section 6.3.2. In contrast to this situation, if the total intercell MAI covariance matrix $\underline{\mathbf{R}}_{\mathrm{n}}$, see (7.16), is not known at the BS receiver, the SNR degradation takes the form

$$\delta_i = \frac{\mathrm{E}\{\mid \underline{\mathbf{b}}^{(k)} \mid^2}{Q} \left[\left(\underline{\mathbf{A}}^{*\mathrm{T}} \underline{\mathbf{A}}\right)^{-1} \underline{\mathbf{A}}^{*\mathrm{T}} \underline{\mathbf{R}}_{\mathrm{n}} \underline{\mathbf{A}} \left(\underline{\mathbf{A}}^{*\mathrm{T}} \underline{\mathbf{A}}\right)^{-1}\right]_{i,i}, \; i = 1 \ldots KN. \tag{7.24}$$

In the rest of this section, based on (7.23) and (7.24), a systematic study of the influence of the intercell interference on a TD–CDMA mobile radio system is presented.

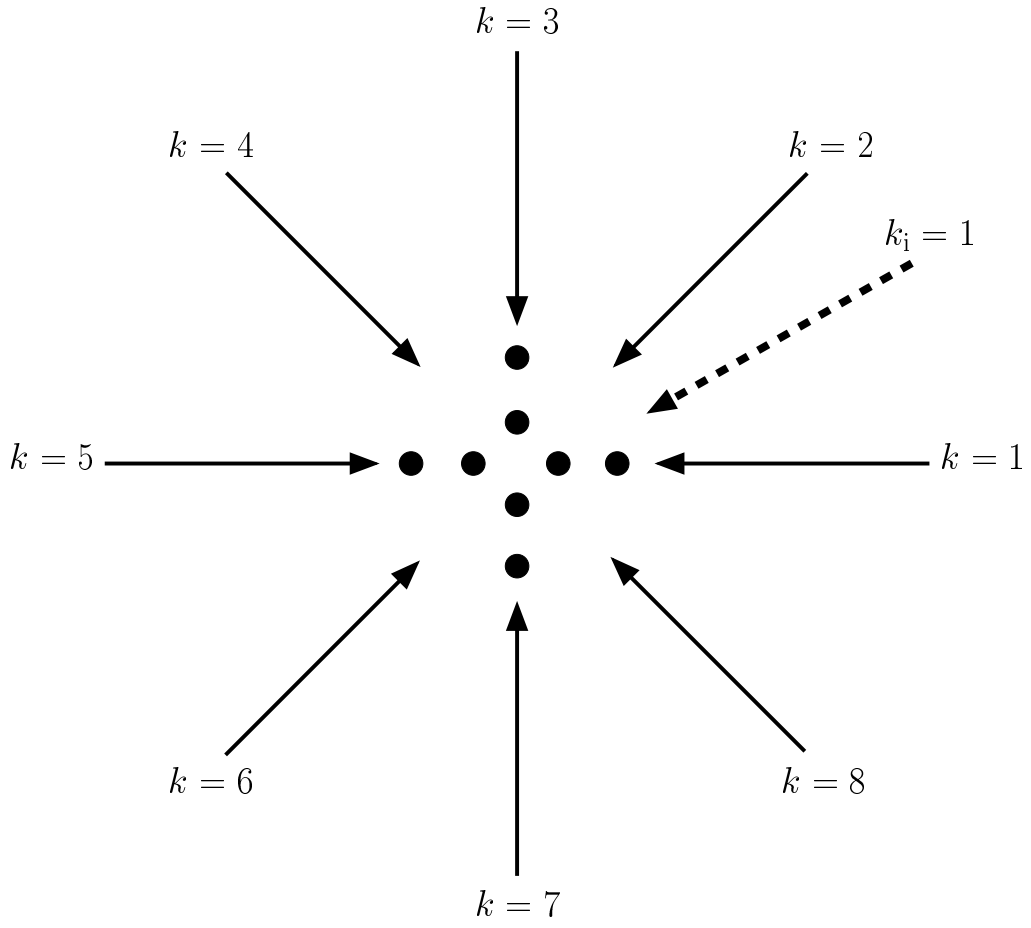

Figure 7.19. Considered spatial scenario; $K = 8$ useful signals; $K_\mathrm{i} = 1$ interfering signal

In the simulations, a cross array configuration with K_a array elements is assumed to be used at the BS receiver. The adopted spatial scenario is depicted in Fig. 7.19. There are K equal to eight users active in the considered time slot, which form the intracell MAI. In order to enable a systematic study of the influence of the intercell MAI on the system performance, the simulation scenario for the $K = 8$ user signals is not changed, i.e., the channel impulse responses, which are created by using the modified COST 207 RA channel model, are kept unchanged for the user signals, whereas the intercell MAI consists of two components:

1. A single interfering signal, $K_\mathrm{i} = 1$, which impinges on the BS array from a single DOA $\gamma^{(1)}$, see also Fig. 5.1. The spatial intercell MAI covariance matrix of this component is denoted by $\underline{\mathbf{R}}_{\mathrm{s,DOA}}$, see (7.20).

2. Omnidirectional intercell MAI, which is created by a very large number of interfering signals with a uniform distribution of their DOAs in the total azimuthal range $[0,\ 2\pi]$. The resulting spatial covariance matrix is termed $\underline{\mathbf{R}}_{\mathrm{s,omni}}$, and is derived analytically in [Bla98].

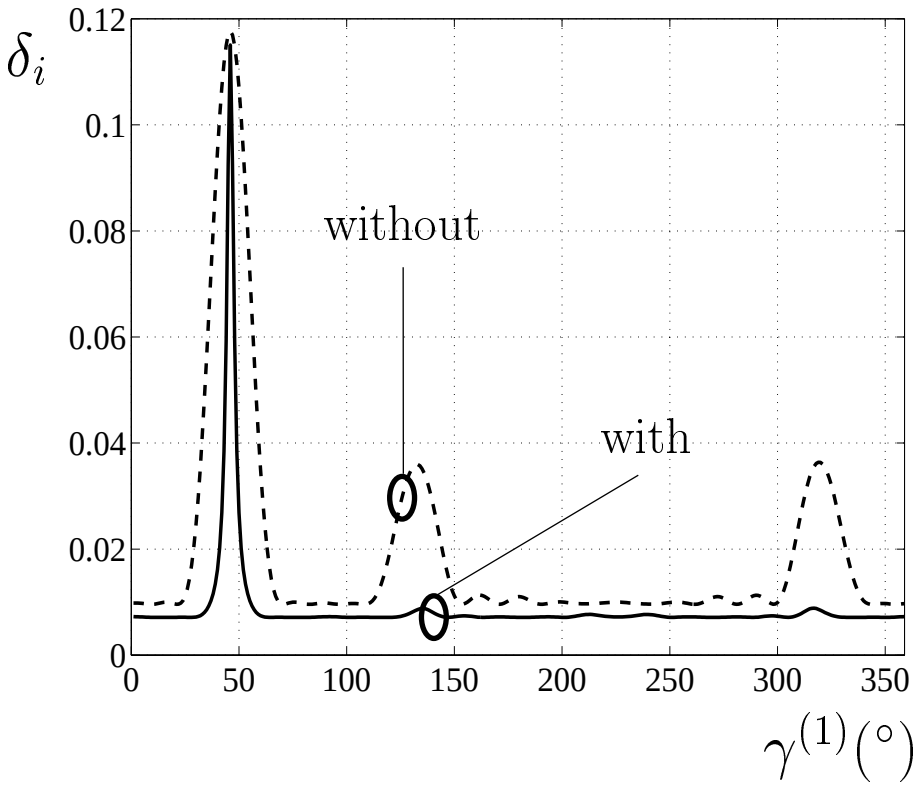

Figure 7.20. SNR degradation δ_i of user $k = 2$ versus the DOA $\gamma^{(1)}$ of the interfering signal for the scenario of Fig. 7.19; $\alpha = 0.5$

Then, the spatial intercell MAI covariance $\underline{\mathbf{R}}_{\mathrm{s}}$ is assumed to be given by

$$\underline{\mathbf{R}}_{\mathrm{s}} = \alpha \cdot \underline{\mathbf{R}}_{\mathrm{s,DOA}} + \beta \cdot \underline{\mathbf{R}}_{\mathrm{s,unif}}, \tag{7.25}$$

where α and β denote the percentage of the total intercell MAI power which pertains to the single interfering signal and the omnidirectional intercell MAI, respectively, i.e.,

$$\alpha + \beta = 1 \tag{7.26}$$

holds. Moreover, the temporal intercell MAI covariance matrix $\underline{\mathbf{R}}_{\mathrm{t}}$, see (7.19), is assumed to be equal to the $(NQ + W - 1) \times (NQ + W - 1)$ identity matrix. Note that, since $\underline{\mathbf{R}}_{\mathrm{s,DOA}}$ is singular, the existence of the omnidirectional interference in the intercell MAI guarantees the regularity of the spatial intercell MAI covariance matrix $\underline{\mathbf{R}}_{\mathrm{s}}$, see (7.25), and, consequently, of the total intercell MAI covariance matrix $\underline{\mathbf{R}}_{\mathrm{n}}$, see (7.16), since $\underline{\mathbf{R}}_{\mathrm{t}}$ equals the identity matrix. Under these assumptions for the simulation scenario, the DOA $\gamma^{(1)}$ of the single interfering signal is varied from 0 to 360° with a step equal to 1°. The simulation results are presented and discussed in the following of the section.

In Fig. 7.20 the SNR degradation δ_i of the symbol transmitted in the middle of the burst from the second user, see Fig. 7.19, is exemplarily plotted as a function of $\gamma^{(1)}$ for two cases:

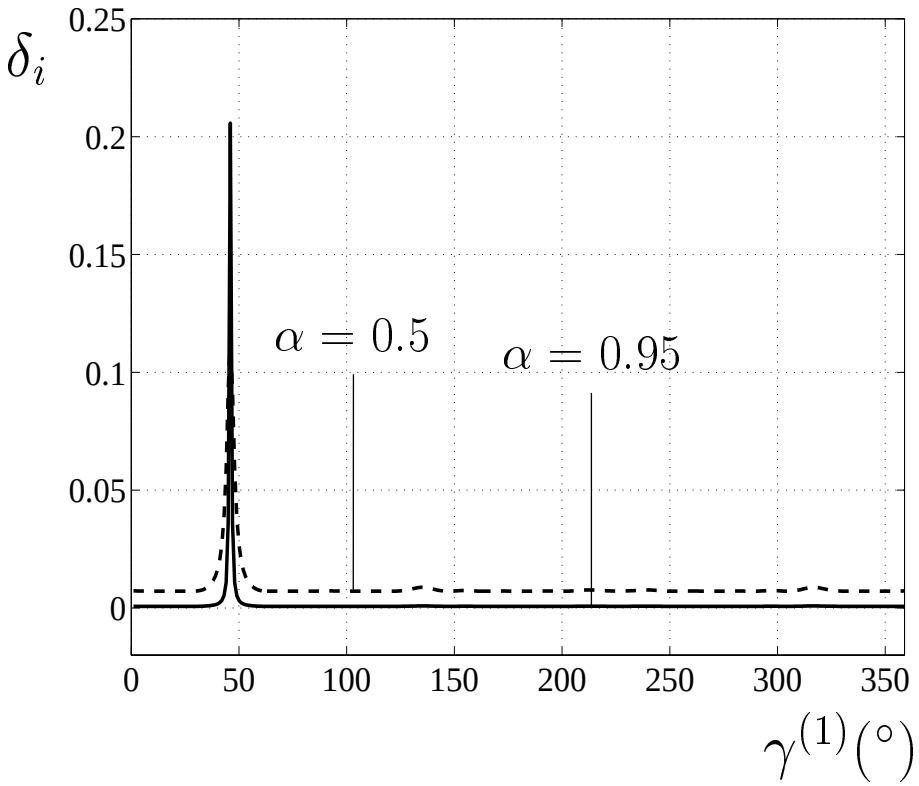

Figure 7.21. SNR degradation δ_i of user $k = 2$ versus the DOA $\gamma^{(1)}$ of the interfering signal for the scenario of Fig. 7.19; influence of α

1. When the information about the intercell MAI covariance matrix $\underline{\mathbf{R}}_{\mathrm{n}}$, see (7.16), is taken into account, i.e., when (7.23) is valid.

2. When the information of the intercell MAI covariance matrix $\underline{\mathbf{R}}_{\mathrm{n}}$, see (7.16), is not used, i.e., when (7.24) holds.

In both cases, α is chosen to be 0.5, see (7.26), and K_{a} is equal to 16. First, it can be observed from Fig. 7.20 that, in both investigated cases, the SNR degradation of the user $k = 2$ takes on big values when the DOA of the interfering signal is close to the DOA from which the user $k = 2$ impinges on the BS array, here 45°, see Fig. 7.19. Furthermore, it can be seen that the use of the information about the intercell MAI covariance matrix $\underline{\mathbf{R}}_{\mathrm{n}}$, see (7.16), improves the system performance over the whole range of the values of $\gamma^{(1)}$. Note that if the BER performance of TD–CDMA is evaluated for the cases of Fig. 7.20, the use of $\underline{\mathbf{R}}_{\mathrm{n}}$, see (7.16), achieves an SNR gain approximately equal to 10 dB at an average coded BER $\bar{P}_{\mathrm{b}} = 10^{-3}$, compared to the case where $\underline{\mathbf{R}}_{\mathrm{n}}$, see (7.16), is not utilized, see for instance the results presented in [PW99, WP99a, WPS99]. Therefore, although the difference between the two cases investigated in Fig. 7.20 does not seem to be large, according to the results presented in [PW99, WP99a, WPS99], the use of $\underline{\mathbf{R}}_{\mathrm{n}}$, see (7.16), is connected with a dramatic improvement of the performance of TD–CDMA.

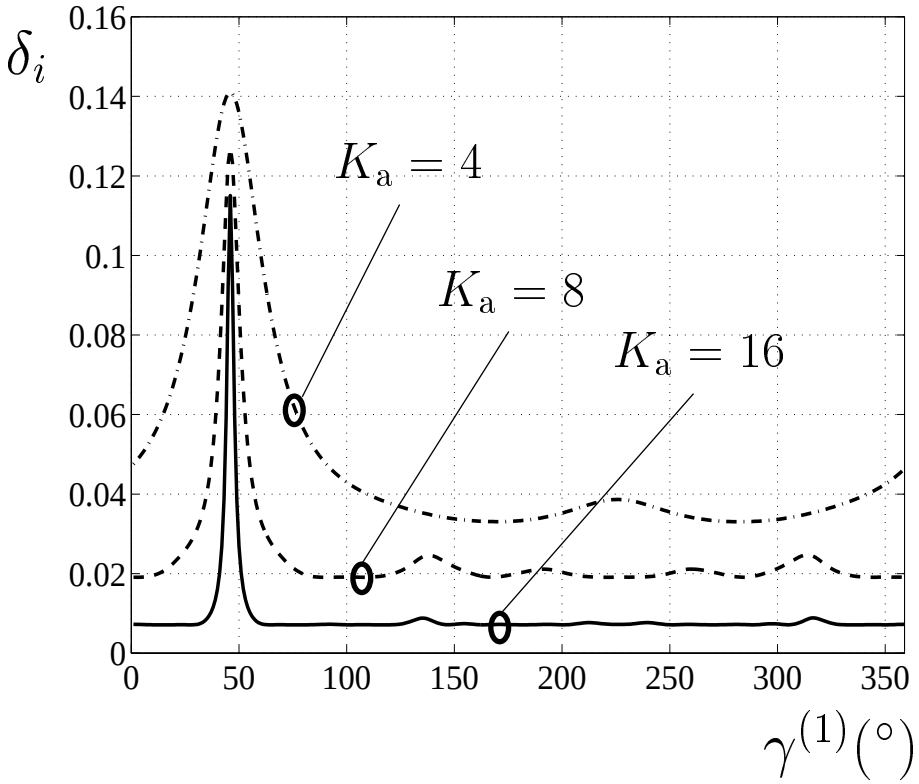

Figure 7.22. SNR degradation δ_i of the user $k = 2$ versus the DOA $\gamma^{(1)}$ of the interfering signal for the scenario of Fig. 7.19; influence of K_a; $\alpha = 0.5$

In Fig. 7.21 the influence of the intensity of the intercell MAI which pertains to the single interfering signal coming from a discrete DOA is investigated by exemplarily showing the SNR degradation δ_i, see (7.23) and (7.24), of the symbol transmitted in the middle of the burst from the second user. K_a is chosen to be equal to 16. From Fig. 7.21 it is obvious that when α takes on big values, e.g., $\alpha = 0.95$, the SNR degradation takes very small values, i.e., the interference can be very efficiently suppressed. Certainly, when the DOA of the second user, which is equal to 45°, see Fig. 7.19, does not differ much from $\gamma^{(1)}$, the SNR degradation increases even in the case where α is relatively high, see also Figure 7.20.

Finally, in Fig. 7.22 the influence of the number of array elements employed at the BS receiver on the SNR degradation δ_i, see (7.23) and (7.24), of the second user is illustrated. As in Fig. 7.20, α is chosen to be equal to 0.5 in each case and the investigated number of array elements is four, eight, and 16, respectively. From 7.20, it can be seen that the larger the number of employed array elements, the smaller the SNR degradation, i.e., the better the system performance, see also [WP99a, WPS99]. Note that when the DOA of the interfering signal $\gamma^{(1)}$ approaches the DOA of the useful signal, which is equal to 45°, the SNR degradation takes on large values independently from the number of the array elements. In this case, though, since only single DOAs are considered for the useful signals,

the array configuration with the largest number of array elements, i.e., when K_{a} equals 16, offers a better spatial resolution and, therefore, the influence of the interfering signal is restricted to a small interval around the value of the DOA of the useful signal, see Fig. 7.22.

As a final remark to this section, it is observed that along with the benefits of adaptive antennas concerning data detection and channel estimation, see Chapters 4 and 5, respectively, adaptive antennas offer the additional advantage of intercell MAI suppression, which leads to an improved system performance, see Figs. 7.20–7.22. A novel technique for estimating the intercell MAI covariance matrix in TD–CDMA and numerous simulation results concerning the improvement of channel estimation and the BER performance of TD–CDMA can be found in [BPW99, WPS99, WP99a, PW99].

8 Spectrum efficiency and capacity

8.1 Preliminaries

The simulation results presented in Chapters 4 to 8 evaluate the link level performance of a TD–CDMA mobile radio system with adaptive antennas. This evaluation illustrates the increased potential of adaptive antennas for performance improvement, compared to the use of single antennas. However, when considering a cellular mobile radio system, the ultimate goal should be the investigation of adaptive antennas with respect to the system efficiency [BBS97, Bla98]. The efficiency of mobile radio systems is evaluated through widely accepted performance measures, such as the spectrum efficiency and capacity, which are closely related [EHV97]. In addition to the possibility of comparing different mobile radio systems, the spectrum efficiency and capacity enable the comparison of different concepts within the same mobile radio system [Ste96, Bla98].

The constantly increasing demand for mobile radio services, on the one hand, and the available frequency spectrum which is a limited resource [Bai94, Bai96a, Bai96c], on the other hand, have an antagonistic influence on the efficiency of a mobile radio system [BBS97, Bla98]. Therefore, an economic utilization of the available frequency spectrum should be pursued. The spectrum efficiency is a measure which enables the assessment of a mobile radio system with respect to the economic utilization of the available frequency spectrum [BBS97, Bla98]. However, when considering a mobile radio system from a commercial point of view, the main objective is to determine the number of subscribers which can be served within the available resources of the system, which are the total available bandwidth and total area of the complete cellular network [EHV97, May99]. The spectrum capacity is a measure which enables the assessment of a mobile radio system with respect to its resources.

In this chapter, based on the definition of the spectrum efficiency [EHV97, BBS97, Bla98] for cellular mobile radio systems, the spectrum efficiency is derived for TD–CDMA according to [BBS97, Bla98]. Then, based on the definition of the spectrum capacity [EHV97, May99], a novel approach is presented, which enables the determination of the spectrum capacity of TD–CDMA by explicitely considering its spectrum efficiency. In the following, the simulation method presented in [BSPJ97, Bla98] for evaluating the spectrum efficiency of TD–CDMA is briefly described, and the modifications concerning its application for the purpose of this thesis are presented. Finally, simulation results of the spectrum efficiency and capacity of TD–CDMA are presented, which compare the use of adaptive and single antennas in different operation situations, which are defined by the channel model, the velocity of the users, and the antenna configuration used at the BS receiver. The goal of the investigations in this chapter is the illustration of the benefits of adaptive antennas with respect to the system level performance of TD–CDMA, compared to the use of single antennas.

8.2 Definitions

8.2.1 Spectrum efficiency

One of the most widely accepted performance measures of a cellular mobile radio system is its spectrum efficiency η [EHV97, BBS97, Bla98]. In order to determine the spectrum efficiency, a single cell of the cellular network is considered. The spectrum efficiency relates the total available information rate within the considered cell to the total available system bandwidth [EHV97, BBS97, Bla98]. With the total available information rate R_{tot} within the considered cell and the total system bandwidth B_{sys}, the spectrum efficiency is defined as [EHV97, Bla98]

$$\eta = \frac{R_{\text{tot}}}{B_{\text{sys}}} \tag{8.1}$$

and measured in bit/(s $\cdot$ Hz) per cell. In what follows, the spectrum efficiency is derived for a TD–CDMA mobile radio system according to [BBS97, BSPJ97, Bla98].

A cellular network of identical hexagonal cells is considered. First, let the total available system bandwidth B_{sys} be divided into N_{par} partial frequency bands each of bandwidth B, i.e.,

$$B_{\text{sys}} = N_{\text{par}} B, \tag{8.2}$$

holds [Bla98], see also Fig. 1.1. Further, let r denote the reuse factor [Ste96, Bla98], so that there are N_{par}/r partial frequency bands per cell. Moreover, due to the TDMA component of TD–CDMA, there are N_{fr} time slots of duration T_{bu} per TDMA frame, see Fig. 1.1 and Fig. 6.2. As already mentioned in Section 1.2, K users are active within each time slot and frequency band in TD–CDMA. Without loss of generality, each user is assumed to be active only in one time slot per TDMA frame, see Figs. 1.1 and 6.2. If R denotes the information rate per user, the total available information rate is given by [Bla98]

$$R_{\text{tot}} = RKN_{\text{fr}} \frac{N_{\text{par}}}{r}, \tag{8.3}$$

where

$$N_{\text{fr}} = \frac{T_{\text{fr}}}{T_{\text{bu}}}, \tag{8.4}$$

see Fig. 1.1 and Fig. 6.2. Then, according to (8.3), (8.2) and (8.4), the spectrum efficiency defined in (8.1) is expressed as [BBS97, BSPJ97, Bla98]

$$\eta = \frac{K\ T_{\text{fr}}\ R}{r\ T_{\text{bu}}\ B}. \tag{8.5}$$

This expression shows that, for given values of T_{fr}, R, T_{bu} and B, η is determined by K and r. Concerning r, the minimum possible value of which is one, it should be chosen to be as small as possible to make η large. Concerning K, it is observed at first glance that η could be made arbitrarily large by increasing K more and more. However, the choice of the values for r and K has an impact on the performance of the system: The smaller r, the more severe the effect of intercell MAI, and the larger K, the larger the SNR degradation experienced when separating the user signals by JD at the receiver [BBS97], see also the analysis of Section 6.3. This means that, when choosing r and K such that η is maximized, the side condition of keeping the system performance sufficiently high has to be simultaneously fulfilled.

To quantify the system performance, a quality of service (QoS) criterion is chosen which is defined as follows [BBS97, Bla98]: The QoS criterion is met if the bit error probability P_{b} exceeds a given upper bound $P_{\mathrm{b}}^{\mathrm{M}}$ with a probability not greater than a given value $P_{\mathrm{o}}^{\mathrm{M}}$. The values $P_{\mathrm{b}}^{\mathrm{M}}$ and $P_{\mathrm{o}}^{\mathrm{M}}$ determine the required QoS. For each pair (r, K), a cumulative distribution function (cdf) $\mathrm{Prob}\{P_{\mathrm{b}} \leq \Gamma\}$ holds. Then, the outage probability P_{o} is defined as [Bla98]

$$P_{\mathrm{o}} = P_{\mathrm{o}}(\Gamma) = \mathrm{Prob}\{P_{\mathrm{b}} > \Gamma\} = 1 - \mathrm{Prob}\{P_{\mathrm{b}} \leq \Gamma\}. \tag{8.6}$$

In order to test whether the QoS criterion specified by $P_{\mathrm{b}}^{\mathrm{M}}$ and $P_{\mathrm{o}}^{\mathrm{M}}$ is met, the value $P_{\mathrm{o}}(P_{\mathrm{b}}^{\mathrm{M}})$ has to be determined. Then the following decision rule holds [BBS97, Bla98]:

$$\begin{array}{ll} P_{\mathrm{o}}(P_{\mathrm{b}}^{\mathrm{M}}) > P_{\mathrm{o}}^{\mathrm{M}}: & \text{QoS criterion not fulfilled,} \\ P_{\mathrm{o}}(P_{\mathrm{b}}^{\mathrm{M}}) \leq P_{\mathrm{o}}^{\mathrm{M}}: & \text{QoS criterion fulfilled.} \end{array} \tag{8.7}$$

If the QoS criterion is not fulfilled, r has to be increased and/or K has to be decreased until the QoS criterion is met. On the other hand, if the QoS criterion is met with a certain pair (r, K), one should try to increase K and/or decrease r with the goal to arrive at another pair (r, K), for which the QoS criterion is still fulfilled, however, with a larger spectrum efficiency η, see (8.5).

The above described procedure to determine η cannot be performed in a closed analytical way [BBS97]. Extensive computer simulations are required to reach this goal. In Section 8.3 the simulation method presented in [BSPJ97, Bla98] for determining the spectrum efficiency η of TD–CDMA is described, and the modifications concerning its application for the purpose of this thesis are presented. Simulation results of the spectrum efficiency are presented in Section 8.4, where single antenna systems are compared to systems with adaptive antennas in macrocellular propagation environments.

8.2.2 Spectrum capacity

The second widely accepted measure considered in this chapter for evaluating the efficiency of TD–CDMA is the spectrum capacity. The spectrum capacity describes the total offered

traffic per total bandwidth and total area of the complete cellular network by regarding it as a queueing system [EHV97, HV99]. With the total offered traffic A_{tot}, measured in Erl [Klein75], the total system area A_{sys} and the total system bandwidth B_{sys} of the complete cellular network, the spectrum capacity is defined as [EHV97, HV99, May99]

$$\kappa = \frac{A_{\mathrm{tot}}}{B_{\mathrm{sys}}\ A_{\mathrm{sys}}} \tag{8.8}$$

and measured in Erl/(MHz $\cdot$ km^2). In the following, the spectrum capacity is determined for a TD–CDMA mobile radio system.

As in Section 8.2.1, a cellular network of identical hexagonal cells is considered, the number of which is denoted by N_{c}. Further, there are N_{par}/r partial frequency bands per cell. If A denotes the offered traffic per cell, the total offered traffic in the cellular network is given by

$$A_{\mathrm{tot}} = A\ N_{\mathrm{c}}\ \frac{N_{\mathrm{par}}}{r}. \tag{8.9}$$

Moreover, if A_{c} denotes the area of a single cell in km^2, the total system area is

$$A_{\mathrm{sys}} = A_{\mathrm{c}}\ N_{\mathrm{c}}. \tag{8.10}$$

Then, according to (8.8), (8.9), (8.2) and (8.10), the spectrum capacity of a TD–CDMA mobile radio system is expressed as

$$\kappa = \frac{A}{r\ B\ A_{\mathrm{c}}}. \tag{8.11}$$

Before elaborating on (8.11), some elementary issues connected with queueing aspects in macrocellular mobile communications systems are addressed. In order to determine the offered traffic per cell A, see (8.9), and, consequently, the spectrum capacity κ of the system, see (8.11), a traffic analysis has to be provided [HV99]. According to the assumptions of [HV99], a mobile radio system operating in macrocellular environments, see Section 2.3.3, is assumed to be a M/M/m/m queueing system. The four–part descriptor M/M/m/m specifies completely the queueing system [Klein75, HV99]:

- The first part describes the interarrival time distribution. The identifier M states that the interarrival times are negative exponentially distributed with mean $1/\lambda$, where λ denotes the constant arrival rate from a Poisson distribution.
- The second part describes the service time distribution. As for the first part, the service times are assumed to have a negative exponential distribution with mean $1/\mu$.
- The third part states that the system has m servers.

- Finally, the fourth part denotes that we deal with an m–server loss system, i.e., if all m servers are occupied and a new call arrives, this call is lost.

According to the above assumptions, the traffic offered to the m–server system is given by [Klein75]

$$A = \frac{\lambda}{\mu} \tag{8.12}$$

and is measured in Erl. In the context of a mobile radio system offering voice services, the interarrival time is the intercall time, and the service time is the call holding time. According to the notation of [May99], a server is denoted as a resource per physical channel. In the case of TD–CDMA, a physical channel is defined by the combination of a frequency band and a time slot [May99]. Thus, a resource per physical channel is a user active in a time slot and frequency band of the cell, to which a single CDMA code is assigned [May99]. Therefore, the total number of resources m per cell of the cellular network is

$$m = K \; N_{\mathrm{fr}}, \tag{8.13}$$

i.e., the product of the number of users K per time slot and the number of time slots N_{fr} per TDMA frame, see Fig. 1.1. Since the mobile radio system is considered to be an m–server loss system, a blocking probability P_{B} is defined as the time share during which all resources are busy [Klein75, HV99]. P_{B} depends on the number m of resources per cell, see (8.13), and the offered traffic A, see (8.12), and is given by the Erlang's loss or Erlang's B formula [Klein75]:

$$P_{\mathrm{B}} = P_{\mathrm{B}}(m, A) = \frac{A^m/m!}{\sum\limits_{i=0}^{m} A^i/i!}. \tag{8.14}$$

P_{B} of (8.14) is tabulated and graphed in many books [Sie70], which means that given two of P_{B}, m and A, the third can be taken from the tables or graphs of such books [Sie70].

Now, let us elaborate on (8.11), which expresses the spectrum capacity of a TD–CDMA mobile radio system. As for the expression of the spectrum efficiency, see (8.5), at a first glance, κ of (8.11) could be made arbitrarily large by setting the reuse factor r to the minimum possible value, i.e., equal to one, and by increasing the offered traffic A more and more. Note that for a given blocking probability P_{B}, e.g., equal to 10^{-2}, A could be made arbitrarily large by increasing the number of active users K within a cell and, consequently, m of (8.13). However, this is not allowed because, then, the QoS criterion demanded for determining the spectrum efficiency, see (8.7), would not be fulfilled. This means that the consideration of a mobile radio system as a queueing system cannot be done by simultaneously neglecting the quality of its connections, which establish the traffic of the queueing system. In other words, the calculation of the spectrum capacity κ of a

mobile radio system should be based on the calculation of its spectrum efficiency η, thus demonstrating that these two widely accepted measures are closely connected [EHV97]. Therefore, when calculating the offered traffic A per cell from (8.14), the total number of resources per cell m is determined by (8.13), where the number of users K per time slot should be the value of the combination (r, K) which maximizes the spectrum efficiency η of (8.5) for the respective operation situation. Certainly, the respective value of r from the considered combination (r, K) should be used when evaluating the spectrum capacity κ from (8.11). As a concluding remark, it is stressed that the consideration of the combination (r, K) which maximizes the spectrum efficiency η of (8.5) when calculating the spectrum capacity κ of (8.11) demonstrates the close relation between η and κ. This important result was first demonstrated in [EHV97], and is used in the context of TD–CDMA in this thesis for the first time.

As a final remark concerning the calculation of the offered traffic per cell A when the spectrum capacity κ is determined according to (8.11), it is assumed that only voice services are offered in the considered TD–CDMA mobile radio system. This assumption is consistent with the approach followed in this thesis for determining the spectrum capacity of TD–CDMA, which explicitely uses the spectrum efficiency η of (8.5) when calculating κ from (8.11), see Section 8.2.1. However, a number of assumptions are made concerning the teletraffic analysis of a mobile radio system:

- First, ideal handover is assumed for all users of the cellular network.
- Second, the information transmitted in the network for signaling purposes is not considered.
- Third, the user distribution within the cellular network is assumed to be identical for all users.

The consideration of handover, signaling aspects, and inhomogeneous user distribution, which achieve a more complete teletraffic analysis of a mobile radio system, is beyond the scope of this thesis. The influence of these three issues on the spectrum capacity of mobile radio systems is studied in detail in [May99, HV99]. As mentioned in Section 8.1, the goal of the investigations in this thesis is the illustration of the differences between single and adaptive antennas in TD–CDMA. Therefore, although the values for the spectrum capacity κ of TD–CDMA obtained in this thesis are somewhat optimistic, the relative difference between the spectrum capacity κ of TD–CDMA with single and adaptive antennas is expected to be affected marginally by the assumptions connected with the method followed for determining κ.

8.3 Simulation method

As already mentioned in Section 8.2.1, the spectrum efficiency η is determined by the combination (r, K) for otherwise fixed system parameters, see (8.5). Further, it is shown

in Section 8.2.2 that the spectrum capacity κ, see (8.11), depends explicitely on the combination (r, K) which determines the spectrum efficiency. In this section the simulation method for determining the spectrum efficiency of a TD–CDMA mobile radio system is described according to [BSPJ97, Bla98], and the modifications concerning its application for the purpose of this thesis are presented. However, due to the close relation between η and κ, the simulation method described in this section enables the investigation of both spectrum efficiency and capacity of TD–CDMA. This investigation depends, on the one hand, on the said combination (r, K), and, on the other hand, on a number of parameters which must be held fixed during the simulations. These parameters are

- the propagation environment established by the used channel model,
- the mobile user velocity, and
- the antenna configuration used at the BS receiver,

and are addressed as the system operation situation in the following.

It is shown in [Par92, Ste96, Bla98] that a model considering separately the fast fading and slow fading is very useful when modeling the mobile radio channel. This is true since the fast and slow fading describe different properties of the mobile radio propagation [Par92]: The fast fading is determined by the small–scale variations or short–term statistics, whereas the slow fading is determined by the large–scale variations or the long–term statistics of the mobile radio channel, see also Section 2.2. Therefore, if a power control algorithm is applied in the cellular network [Zan92a, Zan92b, Ste96], the slow fading can be compensated and is not important for the properties of the transmission channels between the MSs and the BS of a considered cell [Naß95]. In this case, the transmission channels are exclusively determined by the fast fading characteristics of the mobile radio channel. However, the slow fading should be considered when the interference situation is analyzed in a cellular network, since the slow fading constitutes the main factor which critically influences the interference in a considered cell of the cellular network [Naß95, Ste96, Bla98]. In this case, because of the smaller dynamic range of the fast fading compared to the slow fading [Par92], the fast fading needs not be taken into account when analyzing the interference situation in a cellular network [Naß95, Ste96]. Based on the fact that the fast fading and slow fading can be considered separately when modeling the mobile radio channel, the expense of time can be kept within acceptable limits, when investigating the system level performance of mobile radio systems by simulations. The simulation method presented in [BSPJ97, Bla98] is based on this fact, and can be used for the determination of the spectrum efficiency of TD–CDMA as described in the following.

The simulation method presented in [BSPJ97, Bla98] determines the outage probability P_o of (8.6) by Monte–Carlo simulations of data transmission in a reference cell embedded

in a cellular environment. The determination of the outage probability P_o by Monte–Carlo techniques is based on a great number of repeated experiments, e.g., 10^4. Each experiment, which is performed for a certain combination (r, K) and a certain system operation situation, may be split into three steps [Bla98]:

1. First, based on a Hata–like model for slow fading, an inhomogeneous directional distribution of the intercell interference is generated for the reference cell of the cellular network regarding both the average power and the DOA associated with each interferer. The average power and the DOA associated with each interferer are available in the form of databases which contain $1.5 \cdot 10^4$ different interference situations [Bla98]. These databases are created according to the interference analysis of a TD–CDMA mobile radio system presented in [SB96, Ste96, Bla98], and they are distinguished by the combination (r, K), see also Section 8.2.1. Note that the performed analysis in [SB96, Ste96, Bla98] considers only the intercell MAI valid for the reference cell, because the intracell MAI is eliminated by the ZF–BLE which performs JD of the user signals of the reference cell, see Section 4.3.3.2 for a detailed analysis. The main assumptions made when producing the said databases are listed in the following according to [SB96, Ste96, Ste97, Bla98]:

   - The locations of the BSs are chosen to form a regular hexagonal grid and at least two tiers of BSs around the reference cell are considered.
   - Conventional frequency reuse patterns are assumed, leading to regular clusters of size r, i.e., a given carrier frequency is reused in every r–th cell.
   - The locations of the MSs are randomly and uniformly distributed within the cellular network. The locations of any two MSs are statistically independent from each other.
   - The slow fading is described by a simple but widespread Hata–like link gain model which accounts for shadowing effects. Following the notation of [Ste96, Ste97], if $\delta_{b,m}$ denotes the distance between a BS β_b and an MS μ_m and α is the attenuation exponent, which depends on the environment and the antenna heights, the link gain is defined as

     $$g_{b,m} = \frac{\xi_{b,m}}{\delta_{b,m}^{\alpha}}, \tag{8.15}$$

     where $\xi_{b,m}$ denotes a lognormal random variable, which is derived from a Gaussian random variable $\chi_{b,m}$ by the transformation

     $$\xi_{b,m} = \exp\left(\frac{\ln(10)}{10}\chi_{b,m}\right). \tag{8.16}$$

     Note that since $\chi_{b,m}$ is Gaussian distributed, it is fully determined by its expectation $\mathrm{E}\{\chi_{b,m}\}$ and its variance σ^2. For the databases used in the simulations of this thesis, it is assumed that $\chi_{b,m}$ has zero mean and standard deviation σ equal to 6 dB. Further, the attenuation exponent α, see (8.15), is taken to be equal to 3.6.

- A power control algorithm is implemented for the complete cellular network. According to this algorithm, the transmit powers at the MSs are chosen in such a way that the average received carrier powers at the BSs have the same constant value $C = \text{const.}$ for all MSs. This power control algorithm compensates only for large–scale variations of the received signals due to slow fading, see also Section 2.2.
- Handover is assumed to be perfectly power controlled, which means that an MS μ_m is always assigned to that BS β_b to which the link gain $g_{b,m}$ of (8.15) is maximum.
- When considering adaptive antennas, it is assumed that the shadowing conditions are the same for all antennas of the used antenna configuration at the BS. Moreover, concerning the power control algorithm, the received power at an assumed RP of the antenna configuration, see Fig. 5.1, is considered as the received power. Finally, the temporal and spatial correlations of the intercell interference are assumed to be in accordance with the analysis of Section 7.4.

2. Second, based on directional channel models modeling the fast fading characteristics of the mobile radio channel, channel impulse responses are generated for the intracell interference, i.e., the connections between the MSs and the BS of the considered reference cell.

3. Third, data transmission is simulated for a small time duration T_{sim} under consideration of both the intercell interference, see the first step of the method, and the intracell interference, see the second step of the method. It is noted that the time duration of the data transmission should be selected such that, on the one hand, the shadowing conditions do not change significantly within T_{sim} and, on the other hand, the number of counted bit errors is sufficiently large for determining a reliable value of P_{b} for each user active in the reference cell.

The outcome of each experiment is the value of P_{b} for each user from the third step. Then, after a great number of experiments is performed, the values of P_{b} from each experiment can be used for approximating the outage probability P_{o}, see (8.6). Certainly, if the outage probability P_{o} is available, then it can be decided if the QoS criterion, see (8.7), is fulfilled for the considered combination (r, K) and system operation situation. As mentioned in Section 8.2.1, the combination which maximizes η, see (8.5), should be used for determining the spectrum efficiency for the considered system operation situation.

In what follows, the exact modifications concerning the application of this simulation method for the purpose of this thesis are presented.

Concerning the first step of the simulation method of [BSPJ97, Bla98], the databases containing the different intercell interference situations are also used in the simulations performed by the author of this thesis for calculating the spectrum efficiency of TD–CDMA. For each interference situation of the database, the average power $(\sigma^{(k_{\text{i}})})^2$, see

(7.18), and the DOA $\gamma_1^{(k_\mathrm{i})}$, see (7.13), associated with each interferer k_i, $k_\mathrm{i} = 1 \ldots K_\mathrm{i}$, are used for determining the spatial intercell MAI covariance matrix $\underline{\mathbf{R}}_\mathrm{s}$, see (7.16), according to (7.20). Then, by using the temporal intercell MAI covariance matrix $\underline{\mathbf{R}}_{\mathrm{t,m}}$ valid for the channel estimation, or the temporal intercell MAI covariance matrix $\underline{\mathbf{R}}_\mathrm{t}$ valid for the data detection, the total intercell MAI covariance matrix can be determined according to (5.10) or (7.16), respectively. The exact use of the total intercell MAI covariance matrix in the simulations is described during the discussion of the modifications associated with the third step of the simulation method.

Concerning the second step of the simulation method, the simulation results presented in [BSPJ97, Bla98] are produced by using the UKL directional channel models [BBJ95, Bla98]. In this thesis, the UKL 2 directional channel models [SP97, SP98b] are used for generating directional channel impulse responses in the second step of the simulation method, see Section 2.3.3 for a detailed analysis concerning the UKL 2 directional channel models and their comparison with the UKL directional channel models. By using the UKL 2 directional channel models, two goals are achieved: First, the simulation of the movement of users within the reference cell is incorporated. In this way, a more realistic representation of the real world is attained. Second, the simulation time is considerably reduced, which is desired when dealing with extensive simulations of mobile radio systems, see also Section 2.3.3.

In the simulations of [BSPJ97, Bla98], the simulation of the data transmission is performed according to the original simulation concept developed for TD–CDMA [BBNS94, Naß95, Bla98], see also Section 6.2. It is reminded that the original simulation concept does not take advantage of the receiver structure in TD–CDMA. Therefore, it depends exclusively on the user velocity and the used coding, interleaving, and modulation scheme, which lead to high simulation time and complexity. In contrast to the original simulation concept, the novel simulation concept for TD–CDMA including channel estimation errors, see Section 6.2.3.2, is used when the third step of the simulation method is applied in this thesis. This means that for each time duration T_sim required for determining the BER P_b of each user, a database is created with the equivalent output intercell MAI vectors as explained in Section 6.2.3.2. In this way, the investigation of any user velocity multiple of the smallest considered non–zero velocity v_0, see Section 6.2, and any possible linear scheme of coding, interleaving, and modulation is now possible not only for the BER performance, see Section 6.2, but also for the determination of the spectrum efficiency, and consequently, of the spectrum capacity of TD–CDMA. Thus, in contrast to [BSPJ97, Bla98], by incorporating the novel simulation concept presented in Section 6.2.3.2 when applying the third step of the simulation method in this thesis, the flexibility of the simulation method is increased, since the investigation of any user velocity and any linear scheme of coding, interleaving, and modulation can be done without the need for repeating the experiments producing the databases. In addition to this modification associated with the application of the third step of the simulation method, two more modifications are made when investigating adaptive antennas:

- First, 2D array configurations are assumed to be exclusively used at the BS, which achieve a more efficient use of the directional inhomogeneity of the mobile radio channel in real mobile radio scenarios [Haa97a, PFBP99], see also Section 6.6.4.

- Second, the 2D Unitary ESPRIT algorithm is used for estimating the DOAs of signals impinging on the BS array as described in Sections 5.3.2.2 and 5.4.2.2 for the large cell and the small cell channel type , respectively. Thus, a more realistic representation concerning the real world operation of TD–CDMA is obtained.

Further, it should be noted that the simulation results of the spectrum efficiency presented in [BSPJ97, Bla98] for adaptive antennas are produced without taking into account the spatial intercell MAI covariance matrix $\underline{\mathbf{R}}_{\mathrm{s}}$, see (7.16), in the third step of the simulation method. In contrast to this situation, the simulation results presented in this thesis are produced by using the total intercell MAI covariance matrix $\underline{\mathbf{R}}_{\mathrm{m}}$ of (5.10) in channel estimation, and the total intercell MAI covariance matrix $\underline{\mathbf{R}}_{\mathrm{n}}$ of (7.16) in data detection. The exact way $\underline{\mathbf{R}}_{\mathrm{m}}$ is applied is described in Section 5.3.2.3 for the large cell channel type, and in Section 5.4.2.3 for the small cell channel type. The exact way $\underline{\mathbf{R}}_{\mathrm{n}}$ is applied is described in Section 6.2.3.1. The motivation for including the information about the spatial properties of the intercell MAI, when applying the third step of the simulation concept in this thesis, is

- first, the development of concepts, which provide an on–line estimation of the spatial intercell MAI covariance matrix $\underline{\mathbf{R}}_{\mathrm{s}}$, see (5.10) and (7.16), at the BS receiver [WPS99, WP99a], and

- second, the significant performance improvement of TD–CDMA when the information about the spatial interference covariance matrix is used at the BS receiver during channel estimation and data detection [WPS99, WP99a, BPW99, PW99], see also the simulation results presented in Section 7.4.

Moreover, there is a relatively small performance degradation when $\underline{\mathbf{R}}_{\mathrm{s}}$ is estimated at the receiver, compared to the case where $\underline{\mathbf{R}}_{\mathrm{s}}$ is assumed to be perfectly known, especially when no time or frequency hopping is applied to TD–CDMA [WPS99, WP99a]. Therefore, $\underline{\mathbf{R}}_{\mathrm{s}}$ is assumed to be perfectly known in the simulations performed for determining η in this thesis. This assumption keeps the simulation time and complexity as low as possible, whereas simultaneously the BER performance difference compared to the case where $\underline{\mathbf{R}}_{\mathrm{s}}$ is estimated at the receiver is small [WPS99, WP99a]. Thus, this assumption is expected to influence marginally the results on the spectrum efficiency and capacity of TD–CDMA with adaptive antennas presented in the following section.

8.4 Simulation results

8.4.1 Simulation parameters

In this section simulation results for the spectrum efficiency and capacity of TD–CDMA are presented by using the simulation method of Section 8.3. The spectrum efficiency and capacity are determined for different system operation situations, see Section 8.3, whereas the goal of the investigations is the illustration of the difference between single and adaptive antennas in a TD–CDMA mobile radio system.

Concerning the first step of the simulation method of Section 8.3, it is noted that the databases with the different interference situations consider a maximum of eight active users K in the same frequency band and time slot and a maximum of seven for the reuse factor r. Unfortunately, this fact constitutes a restriction, because an even greater value of K may be achieved, especially when adaptive antenna concepts are used at the BS receiver. Further, a new interference situation from the available databases is generated every fourth time slot, i.e., the interference situation remains the same for the duration of four successive transmitted time slots. This choice implies the use of ideal slow frequency hopping, see also [Bla98] for a similar assumption, and is consistent with the application of DOA estimation, which is performed by using the estimated channel impulse responses over four successive time slots, see also [PFBP99]. Further, this choice enables the consideration of a great number of intercell interference situations during the required period for producing the BER P_{b} of a single experiment, see Section 8.3. Thus, the reliability of the BER determined from a single experiment is increased and the required number of experiments for determining the spectrum efficiency and capacity of TD–CDMA can be significantly reduced, see also [BSPJ97, Bla98].

Concerning the second step of the simulation method, see Section 8.3, the UKL 2 rural, urban and dense urban channel models established in Section 2.3.3 are exclusively used in the simulations.

Concerning the third step of the simulation method, see Section 8.3, each user is assumed to be active only in one time slot of the TDMA frame and, without loss of generality, only the user group 0 is considered, see Section 6.2. Further, each user of the user group 0 is assumed to have the same constant velocity v measured in km/h. When the UKL 2 rural channel model is used, v is chosen to be equal to 90 km/h. When the UKL 2 urban and dense urban channel models are employed, v is taken to be equal to 30 km/h. This choice for the user velocity is connected with the increased diversity offered by the respective channel model compared to smaller or greater user velocities, see also Section 6.5.4 and similar results in [Naß95, Bla98]. Finally, it is reminded that if the spatial channel assignment strategy presented in Section 7.3 is implemented, the BER performance of TD–CDMA comes very close to the one achieved by the simple spatial scenario of Figs. 5.2 and 5.5. However, the incorporation of this strategy to the simulation method used in this

thesis, see Section 8.3, would additionally increase the simulation time and complexity. Therefore, in order not to increase the simulation time and complexity when determining the spectrum efficiency and capacity of TD–CDMA, the adopted spatial scenario and the direction of movement for the simultaneously active users within the considered cell are illustrated in Fig 5.2, when the UKL 2 rural channel model is used, and in Fig. 5.5, when the UKL 2 urban and dense urban channel models are employed, respectively. Certainly, according to the simulation results presented in Section 7.3, it is expected that the influence of this assumption on the spectrum efficiency and capacity of TD–CDMA can be neglected.

As already mentioned in Section 8.3, the time duration T_{sim} of a single experiment of P_{b} has to be chosen in such a way that the shadowing conditions do not change significantly within T_{sim} and, simultaneously, the number of counted bit errors is sufficiently large for determining a reliable value of P_{b} from a single experiment. To this end, let N_{bu} denote the number of bursts transmitted for each user within T_{sim}, which is valid for a single experiment of the BER. Then, the relation

$$T_{\mathrm{sim}} = N_{\mathrm{bu}}\ T_{\mathrm{fr}} \tag{8.17}$$

holds, where T_{fr} is the duration of a TDMA frame, see Fig. 1.1. Moreover, since the UKL 2 directional channel models used in the simulations allow the simulation of the movement of users within the considered scenario, see Section 2.3.3, the total length S_{sim} covered by each MS within T_{sim} may be calculated. If ΔS_{sim} denotes the length covered by each MS after the duration of T_{fr}, which is equal to

$$\Delta S_{\mathrm{sim}} = \frac{v}{3.6}\ T_{\mathrm{fr}} \tag{8.18}$$

and measured in m, then the total length S_{sim} is given by

$$S_{\mathrm{sim}} = N_{\mathrm{bu}}\ \Delta S_{\mathrm{sim}} = N_{\mathrm{bu}}\ \frac{v}{3.6}\ T_{\mathrm{fr}} = \frac{v}{3.6}\ T_{\mathrm{sim}}, \tag{8.19}$$

where T_{sim} is defined in (8.17). In the simulations, N_{bu} is chosen to be equal to 240 in accordance with [BSPJ97, Bla98]. In this case, T_{sim} is equal to 1.44 s, see (8.17) and Table 5.1. Then, if v is, e.g., equal to 90 km/h, S_{sim} is equal to 36 m, see (8.19), whereas if v is equal to 30 km/h, S_{sim} is equal to 12 m. Finally, when adaptive antennas are employed at the BS receiver, cross array configurations of K_{a} equal to eight or 16 antennas are assumed to be exclusively used, see Fig. 3.4. Moreover, the choice for the number of antennas of the cross array configuration is in accordance with realtime implementations of adaptive antenna hardware demonstrators, see, e.g., [KTT99]. The rest of the parameters used in the simulations can be taken from Table 5.1.

Finally, concerning the calculation of the spectrum capacity of TD–CDMA according to (8.11), the only quantity required additionally for calculating the system spectrum capacity κ is the area of a single cell A_{c}, see (8.10). If it is assumed that the radius R_{s} which determines the scenario area of the UKL 2 directional channel models, see Section 2.3.3

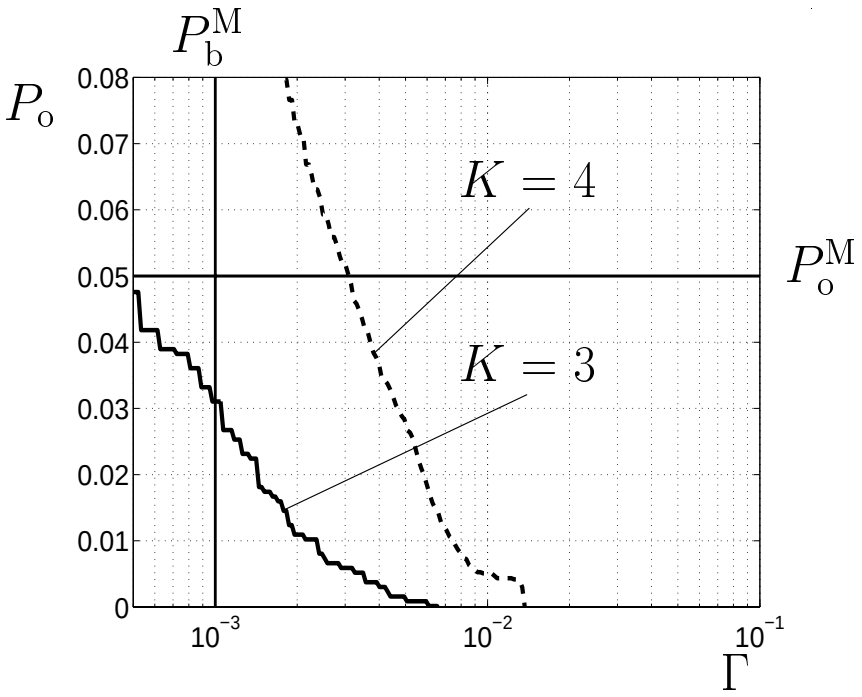

Figure 8.1. P_{o} versus Γ; system operating situation: UKL 2 rural, $v = 90$ km/h, $K_{\mathrm{a}} = 1$; $r = 4$

and Table 2.1, is equal to the radius of a single hexagonal cell of the considered cellular network, then the area of a single cell A_{c}, see (8.10), is given by

$$A_{\mathrm{c}} = \frac{3\sqrt{3}}{2} R_{\mathrm{s}}^2, \tag{8.20}$$

and the spectrum capacity κ of (8.11) is expressed as

$$\kappa = \frac{2\ A}{r\ B\ 3\sqrt{3}\ R_{\mathrm{s}}^2}, \tag{8.21}$$

where B is equal to 1.6 MHz, see Table 5.1, and R_{s} is given in Table 2.1 for the considered UKL 2 directional channel models.

8.4.2 Spectrum efficiency

In this section simulation results for the spectrum efficiency η, see (8.5), of TD–CDMA are presented based on the simulation method of Section 8.3. The parameters of TD–CDMA used in the simulations are given in Section 8.4.1. As already mentioned in Section 8.4.1, goal of the investigations is the illustration of the difference between single and adaptive antennas in TD–CDMA. First, the simulation results for TD–CDMA with single antennas are presented and discussed. Then, the simulation results for adaptive antennas are presented and compared to the ones achieved by the use of single antennas.

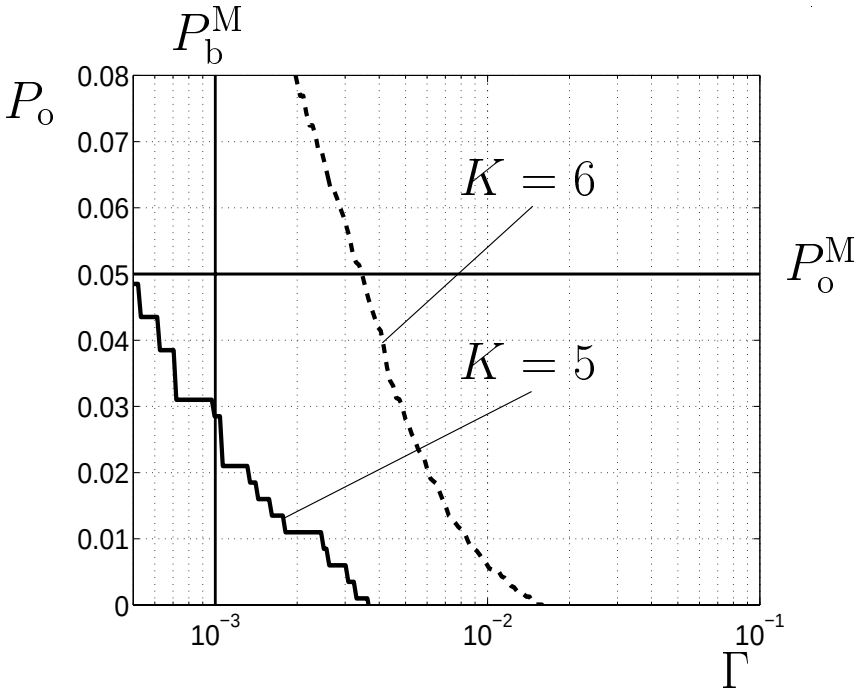

Figure 8.2. P_{o} versus Γ; system operating situation: UKL 2 urban, $v = 30$ km/h, $K_{\mathrm{a}} = 1$; $r = 4$

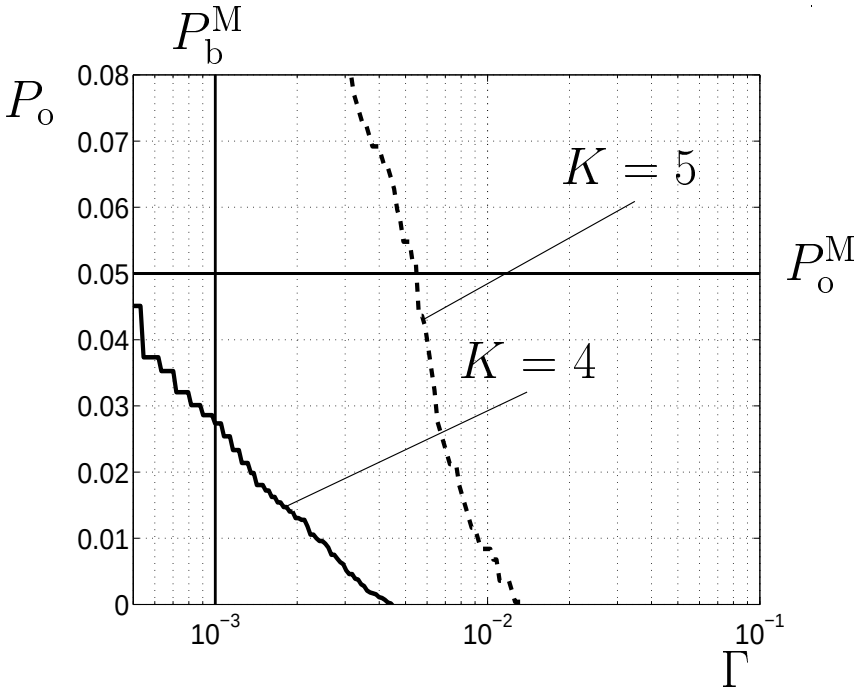

Figure 8.3. P_{o} versus Γ; system operating situation: UKL 2 dense urban, $v = 30$ km/h, $K_{\mathrm{a}} = 1$; $r = 3$

Table 8.1. Spectrum efficiency η of TD–CDMA according to (8.5) for the three investigated system operation situations; single antenna operation

system operation situation	r	K	η in $\frac{\text{bit/s}}{\text{Hz}}$ per cell
UKL 2 rural; $v = 90$ km/h; $K_\text{a} = 1$	4	3	0.045
UKL 2 urban; $v = 30$ km/h; $K_\text{a} = 1$	4	5	0.075
UKL 2 dense urban; $v = 30$ km/h; $K_\text{a} = 1$	3	4	0.08

In Figs. 8.1–8.3 the simulation results for the outage probability $P_\text{o}(\Gamma)$, see (8.6), are shown for the following system operation situations

- UKL 2 rural channel model, $v = 90$ km/h, $K_\text{a} = 1$,
- UKL 2 urban channel model, $v = 30$ km/h, $K_\text{a} = 1$,
- UKL 2 dense urban channel model, $v = 30$ km/h, $K_\text{a} = 1$,

respectively, see also Section 8.3. For specifying a QoS criterion, P_b^M and P_o^M, see Section 8.3, are chosen to be equal to 10^{-3} and $5 \cdot 10^{-2}$, respectively. P_b^M and P_o^M are represented by straight lines in Figs. 8.1–8.3. The chosen values for P_b^M and P_o^M are typical for speech services and are in accordance with [BBS97, BSPJ97, Bla98]. Then, following the rationale of [BSPJ97, Bla98], the QoS criterion, see (8.7), is met if a shown curve for $P_\text{o}(\Gamma)$ crosses the vertical line for P_b^M beneath the horizontal line for P_b^M. It is noted that the combinations (r, K) from Figs. 8.1–8.3 which fulfill the QoS criterion lead to the maximization of the spectrum efficiency η of (8.5) for the considered system operation situations, respectively. Therefore, the simulation results for $P_\text{o}(\Gamma)$ which fulfill the QoS criterion but do not maximize the spectrum efficiency η of (8.5) are not explicitely shown. Fig. 8.1 shows that the combination $r = 4$, $K = 3$ fulfills the QoS criterion for the UKL 2 rural channel model with user velocity $v = 90$ km/h and a single antenna at the BS, leading to the highest possible value for η, see (8.5), equal to 0.045 (bit/s)/Hz per cell. Fig. 8.2 shows that the combination $r = 4$, $K = 5$ fulfills the QoS criterion for the UKL 2 urban channel model with user velocity $v = 30$ km/h and a single antenna at the BS. In this case, η equals 0.075 (bit/s)/Hz per cell. Finally, Fig. 8.3 shows that the combination $r = 3$, $K = 4$ fulfills the QoS criterion for the UKL 2 dense urban channel model with user velocity $v = 30$ km/h and single antenna operation, thus producing a spectrum efficiency equal to 0.08 (bit/s)/Hz per cell. These results show that the spectrum efficiency η of a TD–CDMA mobile radio system with single antennas at the BSs depends critically on the propagation environment where TD–CDMA operates. The greater the frequency diversity of the used channel model, the higher the achievable spectrum efficiency η of a TD–CDMA mobile radio system operating in the respective propagation environment. Therefore, the UKL 2 dense urban channel model offers the

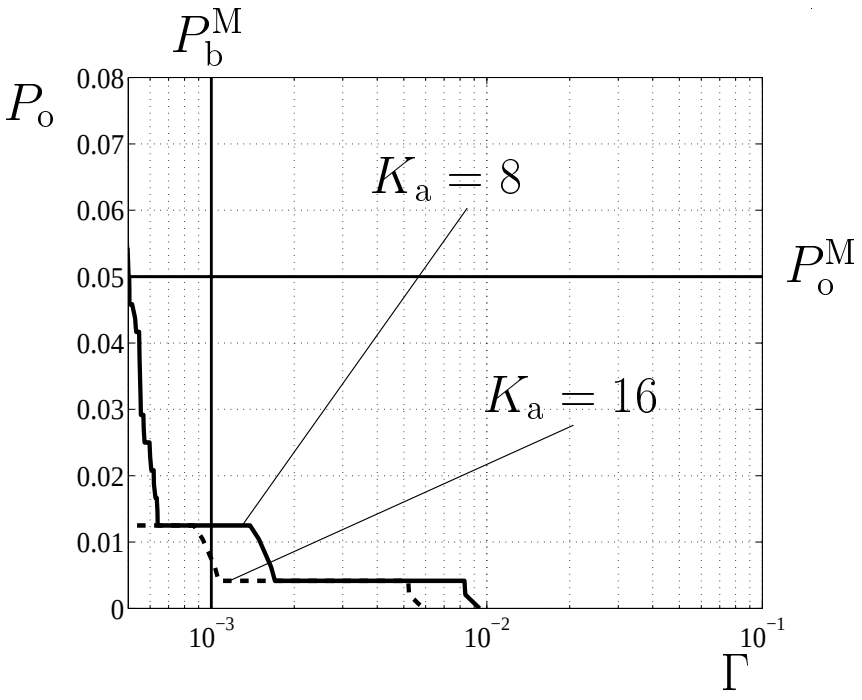

Figure 8.4. P_{o} versus Γ; system operating situation: UKL 2 rural, $v = 90$ km/h; $r = 1$, $K = 8$

highest value for η, see also [Bla98] for a similar result concerning the single antenna operation of TD–CDMA. The values of the spectrum efficiency η for the three investigated system operation situations are summarized in Table 8.1. Note that these values are used as reference for illustrating the benefits of adaptive antennas in TD–CDMA mobile radio systems.

In Figs. 8.4–8.6 the simulation results for the outage probability $P_{\mathrm{o}}(\Gamma)$ of (8.6) are shown for the respective to Figs. 8.1–8.3 system operation situations, when adaptive antennas are used. As for Figs. 8.1–8.3, the QoS criterion is specified by choosing $P_{\mathrm{b}}^{\mathrm{M}}$ and $P_{\mathrm{o}}^{\mathrm{M}}$ to be equal to 10^{-3} and $5 \cdot 10^{-2}$, respectively. From Figs. 8.4–8.6 it is observed that in all system operation situations a combination $r = 1$ and $K = 8$ is achieved when adaptive antennas are used in TD–CDMA. It is noted that the used number of antennas K_{a}, i.e., eight or 16, do not influence the value of the spectrum efficiency, since the curves for both values of K_{a} cross the vertical line for $P_{\mathrm{b}}^{\mathrm{M}}$ beneath the horizontal line for $P_{\mathrm{b}}^{\mathrm{M}}$, see Figs. 8.4–8.6. This fact means that the smaller number of antennas K_{a}, i.e., equal to eight, should be used for achieving the combination $r = 1$ and $K = 8$, because it is connected with reduced implementation costs compared to K_{a} equal to 16. Further, it is noted that even a greater number of users K may be possible for $r = 1$, especially when K_{a} equal to 16 antennas are used at the BS receivers. As already mentioned in Section 8.4.1, the investigation of a greater number of K has not been possible since the databases with the interference situations, see the first step of the simulation method of Section 8.3, consider up to K equal to eight users. Nevertheless, the achieved values of the spectrum efficiency η by using the available databases of the interference situations for the three investigated sys–

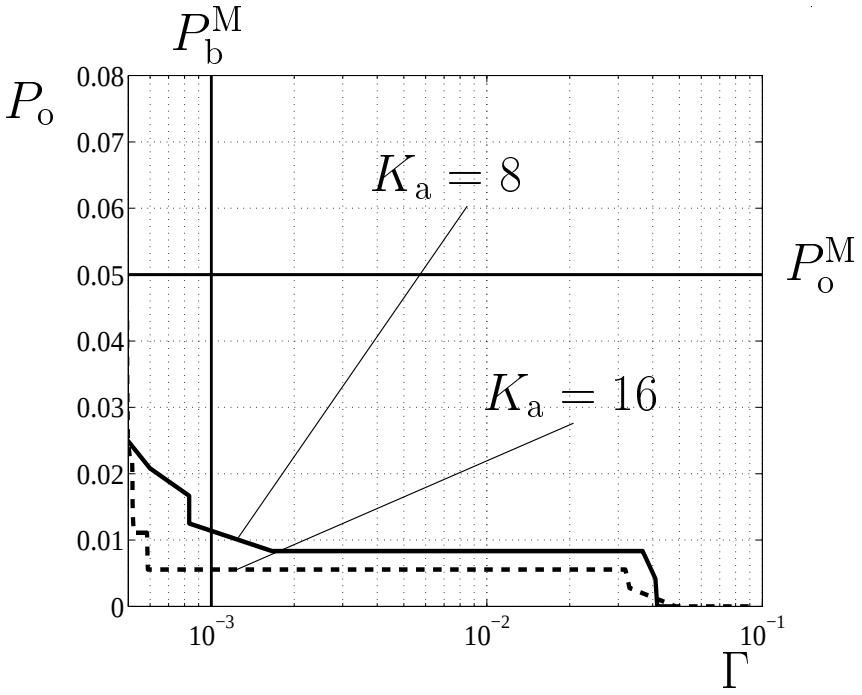

Figure 8.5. P_{o} versus Γ; system operating situation: UKL 2 urban, $v = 30$ km/h; $r = 1$, $K = 8$

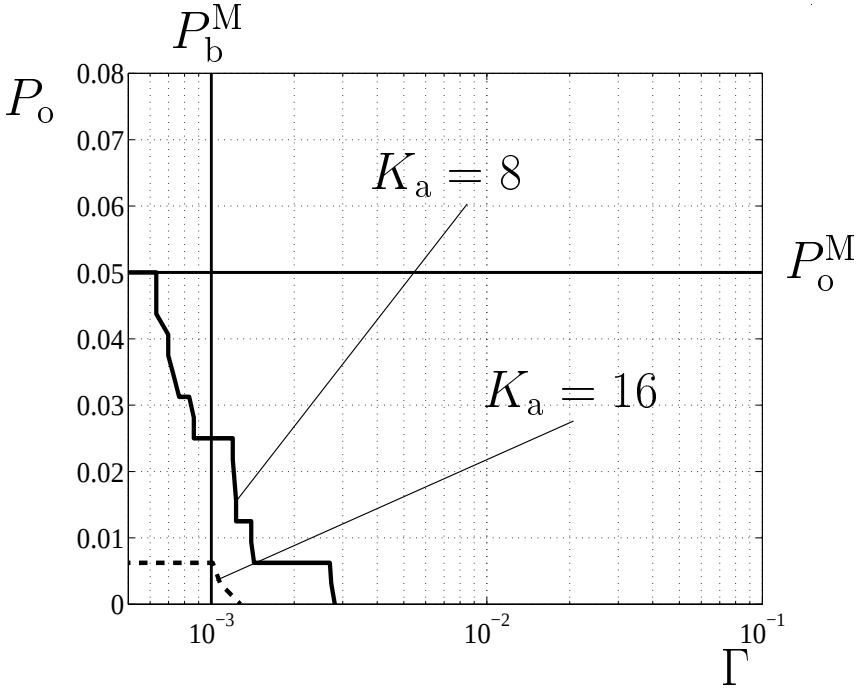

Figure 8.6. P_{o} versus Γ; system operating situation: UKL 2 dense urban, $v = 30$ km/h; $r = 1$, $K = 8$

tem operation situations are summarized in Table 8.2. Compared to the results of the spectrum efficiency η for single antenna operation, see Table 8.1, it is observed from Table 8.2 that an enormous improvement of the system efficiency with respect to bandwidth utilization is achieved when adaptive antennas are used in TD–CDMA mobile radio systems, which is explained in the rest of this section.

In Chapter 5 the improvement of the channel impulse response estimates is illustrated for the UKL 2 directional channel models when adaptive antennas are used at the BS receiver, compared to the case where conventional channel estimation techniques are employed. In Chapter 6 it is shown that the improvement of the channel impulse response estimates, which is achieved by the use of adaptive antennas, leads directly to considerable improvements of the BER behaviour for the UKL 2 directional channel models, compared to systems without adaptive antennas. In Chapters 5 and 6 the simulations have been performed under the assumption that the intercell MAI is modeled as AWGN. In Section 7.4 a rather straightforward analysis is presented which illustrates the additional improvement of the system performance achieved by adaptive antennas when the intercell MAI is not modeled as AWGN, i.e., it has certain temporal and spatial correlation properties described by the intercell MAI covariance matrix, see (5.10) and (7.16), which can be used in both channel estimation and data detection of TD–CDMA receivers. Since the simulation method described in Section 8.3, which is used for determining the

Table 8.2. Spectrum efficiency η of TD–CDMA according to (8.5) for the three investigated system operation situations; adaptive antenna operation

system operation situation	r	K	η in $\frac{\text{bit/s}}{\text{Hz}}$ per cell
UKL 2 rural; $v = 90$ km/h; $K_a = 8$ or 16	1	8	0.48
UKL 2 urban; $v = 30$ km/h; $K_a = 8$ or 16	1	8	0.48
UKL 2 dense urban; $v = 30$ km/h; $K_a = 8$ or 16	1	8	0.48

Table 8.3. Improvement factor of the spectrum efficiency η between single and adaptive antenna operation, $K_a = 8$ or $K_a = 16$, of TD–CDMA for the three investigated system operation situations

channel model	user velocity	improvement factor for η
UKL 2 rural	$v = 90$ km/h	10.7
UKL 2 urban	$v = 30$ km/h	6.4
UKL 2 dense urban	$v = 30$ km/h	6.0

spectrum efficiency of TD–CDMA, combines the above mentioned benefits of adaptive antennas, i.e., the benefits concerning both the intracell and the intercell MAI, an enormous improvement of the spectrum efficiency of TD–CDMA is achieved by adaptive antennas,

compared to single antenna systems, compare Tables 8.1 and 8.2. Similar results for the spectrum efficiency η of TD–CDMA are presented in [BSPJ97, Bla98]. However, the information about the intercell MAI covariance matrix is used neither in channel estimation nor in data detection for the results presented in [BSPJ97, Bla98]. Therefore, compared to the single antenna case, the determined improvement of the spectrum efficiency of TD–CDMA presented in [BSPJ97, Bla98], when adaptive antennas are used, is smaller compared to the improvement achieved by the results presented in this thesis, see Tables 8.1 and 8.2. Concluding the analysis of the section, the improvement factor of the spectrum efficiency η is shown in Table 8.3 for each investigated system operation situation.

8.4.3 Spectrum capacity

In this section simulation results for the spectrum capacity κ of TD–CDMA are presented. As already mentioned in Section 8.2.2, the calculation of κ explicitely depends on the combination (r, K) which maximizes the spectrum efficiency η for a certain system operation situation. Therefore, when the offered traffic A, see (8.9) and (8.12), is calculated, the used resources per cell m, see (8.13), should be based on the number of users K per time slot of the combination (r, K) which maximizes the spectrum efficiency η. Then, by knowing m and requiring a certain blocking probability P_{B}, see (8.14), the offered traffic A per cell can be determined from the tables of the books [Sie70] which tabulate P_{B} of (8.14). As in Section 8.4.2, the spectrum capacity κ is determined in this section according to (8.21) for TD–CDMA with single and adaptive antennas.

In Table 8.4 the offered traffic A and the spectrum capacity κ are shown for the three investigated system operation situations of Section 8.4.2, when TD–CDMA operates with single antennas at the BSs. The blocking probability P_{B} of (8.14) is taken to be equal

Table 8.4. Spectrum capacity κ of TD–CDMA according to (8.21) for the three investigated system operation situations of Section 8.4.2; single antenna operation; $P_{\mathrm{B}} = 10^{-2}$

system operation situation	A in Erl	κ in Erl/(MHz km^2)
UKL 2 rural; $v = 90$ km/h; $K_{\mathrm{a}} = 1$	25.5	0.06
UKL 2 urban; $v = 30$ km/h; $K_{\mathrm{a}} = 1$	46.9	0.71
UKL 2 dense urban; $v = 30$ km/h; $K_{\mathrm{a}} = 1$	36.1	0.72

to 10^{-2}, in accordance with [HV99]. Note that the value for K from Table 8.1 is used for determining A and, additionally, the value for r from Table 8.1 is used for determining κ for each of the investigated system operation situations, respectively. Therefore, an improvement of the spectrum capacity κ of TD–CDMA is achieved in the urban and dense urban channel models, compared to the rural channel model. However, this improvement

Table 8.5. Spectrum capacity κ of TD–CDMA according to (8.21) for the three investigated system operation situations of Section 8.4.2; adaptive antenna operation; $P_{\mathrm{B}} = 10^{-2}$

system operation situation	A in Erl	κ in Erl/(MHz km^2)
UKL 2 rural; $v = 90$ km/h; $K_{\mathrm{a}} = 8$ or 16	80.3	0.77
UKL 2 urban; $v = 30$ km/h; $K_{\mathrm{a}} = 8$ or 16	80.3	4.83
UKL 2 dense urban; $v = 30$ km/h; $K_{\mathrm{a}} = 8$ or 16	80.3	4.83

Table 8.6. Improvement factor of the spectrum capacity κ between single and adaptive antenna operation, $K_{\mathrm{a}} = 8$ or $K_{\mathrm{a}} = 16$, of TD–CDMA for the three investigated system operation situations; $P_{\mathrm{B}} = 10^{-2}$

channel model	user velocity	improvement factor for κ
UKL 2 rural	$v = 90$ km/h	12.6
UKL 2 urban	$v = 30$ km/h	6.9
UKL 2 dense urban	$v = 30$ km/h	6.7

is by a factor seven bigger for κ compared to the respective improvement of η, see Tables 8.1 and 8.4. This is due to the fact that the blocking probability P_{B}, see (8.14), is a nonlinear function of the offered traffic A and the number m of available resources. This nonlinearity results in a certain economy of scale involved in queueing systems, which is called bundling gain in telephone systems [HV99], and can be explained as follows: The larger a bundle of circuits, the number of resources m of (8.13) in the context of TD–CDMA, the more traffic A is carried per single circuit. Thus, a higher resource usage is obtained, which explains the increased improvement of the spectrum capacity of TD–CDMA operating in urban and dense urban propagation environments with respect to the rural propagation environment, compared to the respective improvement achieved for the spectrum efficiency.

In Table 8.5 the results for κ are shown for the respective system operation situations of Table 8.4, when adaptive antennas are used. As for the spectrum efficiency η, compare Table 8.1 with Table 8.2, the spectrum capacity κ of TD–CDMA is considerably improved when adaptive antennas are used, compared to the single antenna system. The improvement factor of η is shown in Table 8.6 for each investigated system operation situation. However, as observed by comparing Table 8.5 with Table 8.2, although η is equal for all propagation environments when adaptive antennas are used, κ is still higher for the urban and dense urban propagation environments, compared to the rural propagation environment. This is due to the fact that the cells in urban and dense urban propagation environments are extended over a smaller area, which is expressed by the different values of R_{s}, see Table 2.1, used for determining κ from (8.21). Therefore, the efficiency

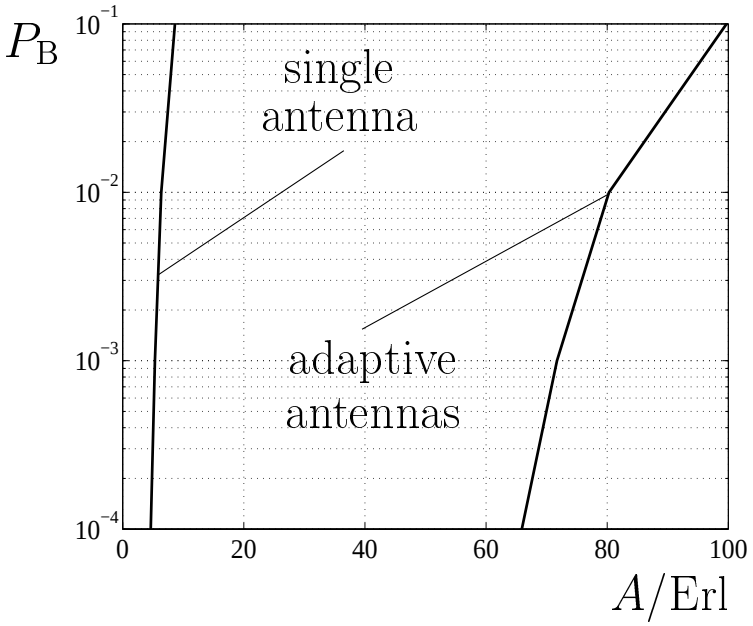

Figure 8.7. Blocking probability P_B versus offered traffic A; single antenna versus adaptive antenna system; UKL 2 rural channel model; $v = 90$ km/h

of TD–CDMA with respect to its resources expressed by κ, see also Section 8.2.2, is still higher in the urban and dense urban propagation environments, compared to the rural propagation environment, even if the respective value of η takes the same value for all propagation environments. This important result justifies the use of the spectrum capacity for evaluating the overall system performance of TD–CDMA, adopted in this thesis.

In a final step in this section, the offered traffic A is calculated according to (8.14) for different values of the blocking probability P_B. The number of servers m, see (8.13), depends only on the value for K valid for the investigated system operation situation, see also the discussion corresponding to Tables 8.4 and 8.5 of this section. In Figs. 8.7–8.9 the P_B is plotted versus the offered traffic A, when TD–CDMA operates in the rural, urban, and dense urban propagation environment, respectively. In each figure, P_B is evaluated for single and adaptive antennas, respectively. It is noted that the illustration of P_B versus A is typical for investigations concerning the teletraffic analysis of mobile radio systems, see [HV99]. From Figs. 8.7–8.9 the enormous improvement of the traffic achieved by adaptive antennas is obvious for all propagation environments, compared to the use of single antennas. However, in the context of a mobile radio system, not only the recourses per physical channel have to be considered, but also the total available system bandwidth and the total area of the cellular network. Therefore, the spectrum capacity defined in (8.8) should be preferred when evaluating the efficiency of a cellular mobile radio system with respect to its resources. In the context of the investigated TD–CDMA mobile radio system, this observation implies that the results for its spectrum capacity presented in Tables 8.4–8.6 should be chosen to the results presented in Figs. 8.7–8.9.

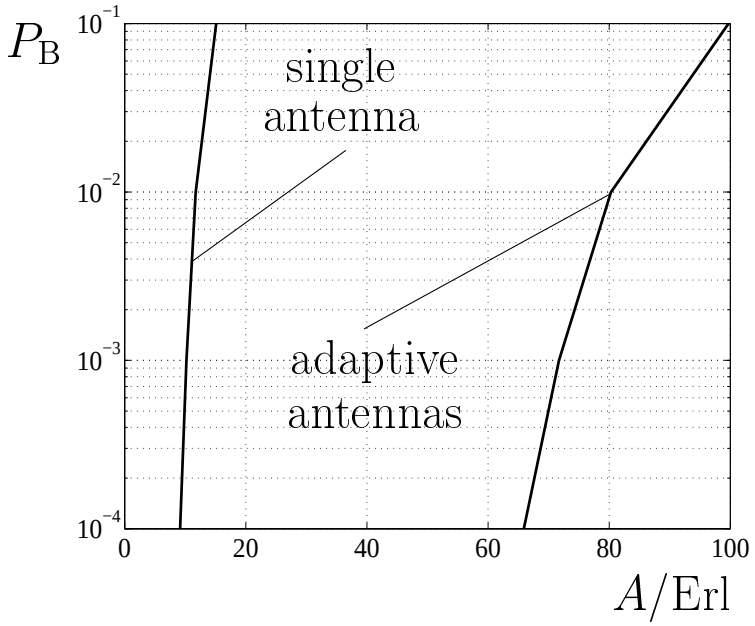

Figure 8.8. Blocking probability P_{B} versus offered traffic A; single antenna versus adaptive antenna system; UKL 2 urban channel model; $v = 30$ km/h

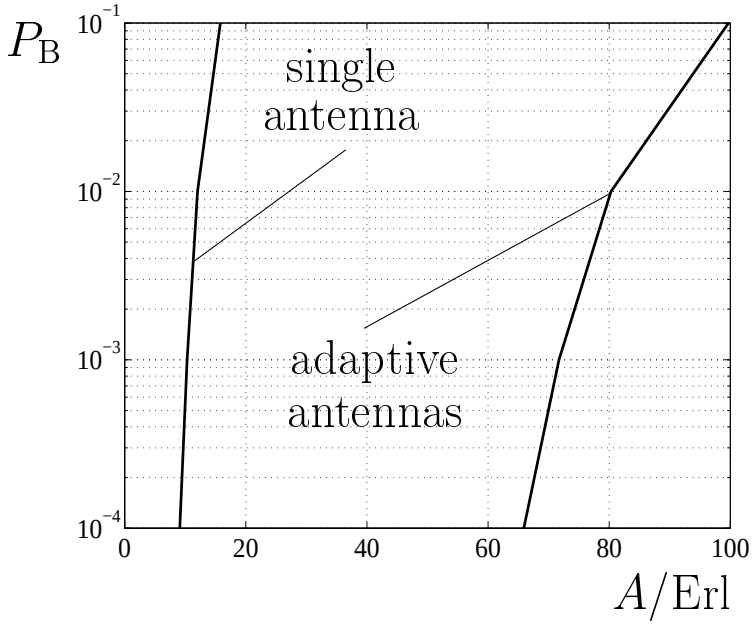

Figure 8.9. Blocking probability P_{B} versus offered traffic A; single antenna versus adaptive antenna system; UKL 2 dense urban channel model; $v = 30$ km/h

9 Comparison between uplink and downlink

9.1 Motivation

In the previous chapters of this thesis, adaptive antennas are considered for the uplink (UL) of a TD–CDMA mobile radio system. The presented analysis contains issues connected with data detection and channel estimation techniques, novel performance assessment methods for TD–CDMA, and techniques for increasing the performance of adaptive antennas in TD–CDMA. However, one of the most important issues for 3G mobile radio systems is the performance evaluation in the downlink (DL) and the comparison with the UL performance [BBS97, SB97a]. Worldwide research and standardization activities are devoted to this issue. The main goal of these activities is the reduction of the performance differences between the UL and the DL, since the use of a single antenna at the MS is connected with a–priori fewer advantages compared to the UL case, where multi–antenna configurations can be used.

Concerning TD–CDMA, the primary duplexing scheme of which is TDD [NTD98], the performance comparison between the UL and the DL is a very important issue, because it will mostly influence the decision for the number of time slots in a TDMA frame which will be assigned to the UL and the DL [NTD98]. If the performance in the DL is worse than the one in the UL and symmetrical data rates are applied, e.g., in voice communications, a greater number of time slots should be assigned to the DL in order to compensate for its worse performance compared to the UL, which is expressed for instance by greater reuse factors, or smaller number of CDMA users within a time slot.

In this chapter the performance between the UL and the DL in TD–CDMA is compared in a rather straightforward manner for single and multi–antenna systems by using the SNR degradation of TD–CDMA receivers, which is the second performance assessment method presented in Chapter 6, see Section 6.3.. As a precondition of this analysis, a novel mathematical model for the DL of TD–CDMA has to be established, which also contains the use of adaptive antenna concepts. Then, the system performance is compared for different operation situations in a TD–CDMA mobile radio system by introducing the definitions of the mean SNR degradation per user and the mean gain per user.

9.2 System model for the downlink

9.2.1 Preliminaries

In this section the system model for the DL in TD–CDMA is established for single and multi–antenna systems. In the case of multi–antenna systems, the application of the space diversity concept, see Section 3.2, and adaptive antennas is treated separately. In

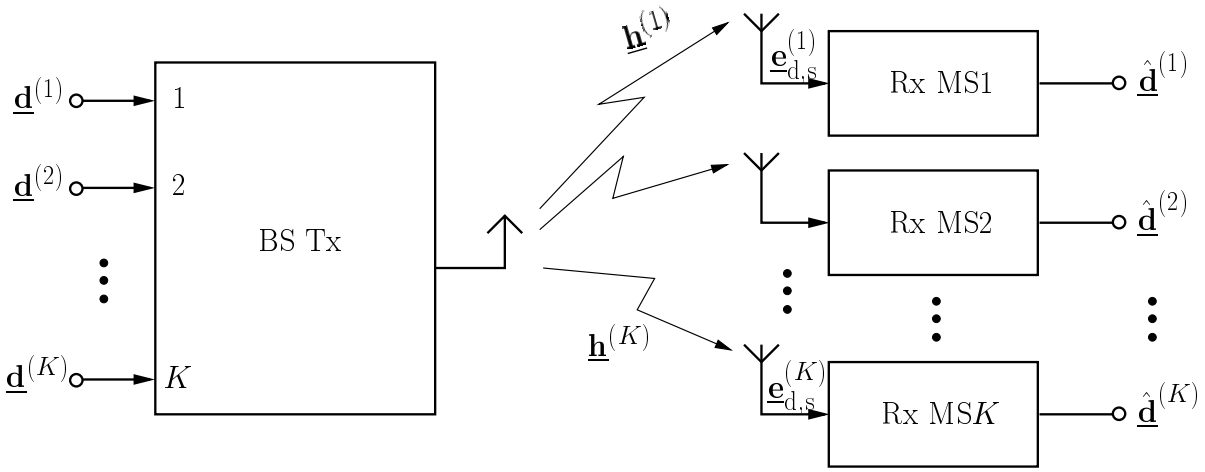

Figure 9.1. System model for single antenna systems in the DL of TD–CDMA

all cases, the system matrix for the DL is derived, which, together with the use of the SNR degradation of TD–CDMA receivers, enables a rather straightforward approach for illustrating the differences between the UL and the DL performance. Finally, it is noted that in every case the received signal at a single MS k, $k = 1 \ldots K$, is considered.

9.2.2 Single antenna systems

When a single antenna is used at the BS, the influence of the mobile radio channel on the received signal for MS k, $k = 1 \ldots K$, can be characterized by a single channel impulse response $\underline{\mathbf{h}}$ of dimension W [Kle96], see Fig. 9.1. With the CDMA codes $\underline{\mathbf{c}}^{(k)}$ the $NQ \times KN$ matrix

$$\underline{\mathbf{C}}_{\mathrm{d}} = \left[\underline{\mathbf{C}}^{(1)} \ldots \underline{\mathbf{C}}^{(K)}\right] \tag{9.1}$$

can be formed, where the matrix $\underline{\mathbf{C}}^{(k)}$, $k = 1 \ldots K$, is defined in (4.2). With the channel impulse response $\underline{\mathbf{h}}$ the $(NQ + W - 1) \times NQ$ matrix $\underline{\mathbf{H}}_{\mathrm{d,s}}$ can be defined, the elements of which are given by the following expression:

$$\left[\underline{\mathbf{H}}_{\mathrm{d,s}}\right]_{n+w-1,n} = \begin{cases} \underline{h}_w & , w = 1 \ldots W, \\ & \quad n = 1 \ldots NQ \\ 0 & , \text{otherwise.} \end{cases} \tag{9.2}$$

According to (9.1) and (9.2), the DL system matrix

$$\underline{\mathbf{A}}_{\mathrm{d,s}} = \underline{\mathbf{H}}_{\mathrm{d,s}}\, \underline{\mathbf{C}}_{\mathrm{d}} \tag{9.3}$$

can be established, when a single antenna is used at the BS receiver. Then, the received signal originating from the K simultaneously transmitted data sections $\underline{\mathbf{d}}^{(k)}$, $k = 1 \ldots K$, is represented by the vector

$$\underline{\mathbf{e}}_{\mathrm{d,s}} = \underline{\mathbf{A}}_{\mathrm{d,s}}\, \underline{\mathbf{d}} + \underline{\mathbf{n}} \tag{9.4}$$

of dimension $NQ + W - 1$, which contains, as in the UL, an additive vector $\underline{\mathbf{n}}$, which represents the received intercell MAI.

An equivalent representation of the DL system model can be obtained by considering the composite channel impulse response $\underline{\mathbf{b}}^{(k)}$, $k = 1 \ldots K$, which is the convolution of the single channel impulse response vector $\underline{\mathbf{h}}$ and the user specific CDMA code $\underline{\mathbf{c}}^{(k)}$:

$$\underline{\mathbf{b}}^{(k)} = \underline{\mathbf{c}}^{(k)} * \underline{\mathbf{h}}, \quad k = 1 \ldots K. \tag{9.5}$$

With $\underline{\mathbf{b}}^{(k)}$, $k = 1 \ldots K$, given by (9.5) the system matrix is defined as

$$\underline{\mathbf{A}}_{\mathrm{d,s}} = \left[\underline{\mathbf{A}}^{(1)}\ \underline{\mathbf{A}}^{(2)} \ldots \underline{\mathbf{A}}^{(K)}\right] \tag{9.6}$$

$$\left[\underline{\mathbf{A}}^{(k)}\right]_{(n-1)Q+l,n} = \begin{cases} \underline{b}_l^{(k)}, & n = 1 \ldots N, \\ & l = 1 \ldots Q + W - 1, \\ 0, & \text{otherwise.} \end{cases} \tag{9.7}$$

The structure of each block $\underline{\mathbf{A}}^{(k)}$, $k = 1 \ldots K$, is the same as the one shown in Fig. 4.4.

9.2.3 Multi–antenna systems applying the space diversity concept

When multi–antenna configurations are used at the BS receiver, the system model illustrated in Fig. 9.2 is valid. First, the well-known space diversity concept is considered [MM80, BBP97, BSPJ97], see also Section 3.2. In this concept, the different antennas are positioned at locations separated by several, e.g. ten, wavelengths. Space diversity has the effect that K_{a} transmission channels between the BS and each MS exist, which experience more or less independent fading processes [MM80, BSPJ97]. In this case, the mobile radio channel for each MS can be characterized by K_{a} channel impulse responses $\underline{\mathbf{h}}^{(k_{\mathrm{a}})}$, $k_{\mathrm{a}} = 1 \ldots K_{\mathrm{a}}$, $k = 1 \ldots K$. With the channel impulse responses $\underline{\mathbf{h}}^{(k_{\mathrm{a}})}$, $k_{\mathrm{a}} = 1 \ldots K_{\mathrm{a}}$, the $(NQ + W - 1) \times NQ$ matrices $\underline{\mathbf{H}}_{\mathrm{d}}^{(k_{\mathrm{a}})}$, $k_{\mathrm{a}} = 1 \ldots K_{\mathrm{a}}$, can be defined, the elements of which are given by

$$\left[\underline{\mathbf{H}}_{\mathrm{d}}^{(k_{\mathrm{a}})}\right]_{n+w-1,n} = \begin{cases} \underline{h}_w^{(k_{\mathrm{a}})} & , w = 1 \ldots W, \\ & \quad n = 1 \ldots NQ \\ 0 & , \text{otherwise.} \end{cases} \tag{9.8}$$

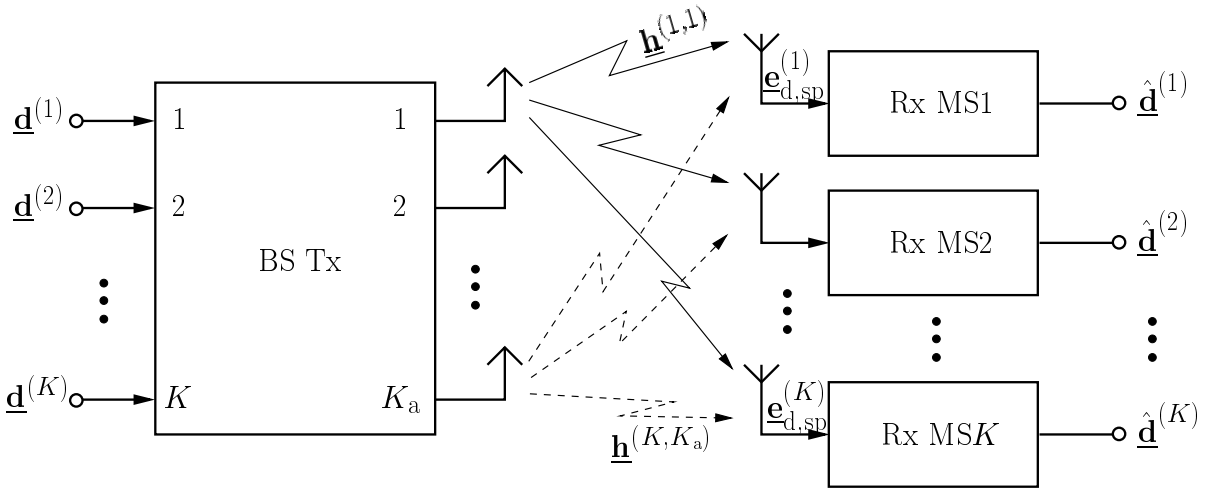

Figure 9.2. System model for multi–antenna systems in the DL of TD–CDMA

Then, the total channel impulse response matrix

$$\underline{\mathbf{H}}_{\mathrm{d,sp}} = \sum_{k_\mathrm{a}=1}^{K_\mathrm{a}} \underline{\mathbf{H}}_{\mathrm{d}}^{(k_\mathrm{a})} \tag{9.9}$$

can be formed, and the DL system matrix

$$\underline{\mathbf{A}}_{\mathrm{d,sp}} = \underline{\mathbf{H}}_{\mathrm{d,sp}}\ \underline{\mathbf{C}}_{\mathrm{d}} \tag{9.10}$$

can be established when the space diversity concept is applied, where $\underline{\mathbf{C}}_{\mathrm{d}}$ is given by (9.1). As in the single antenna system, see (9.4), the received signal is expressed by

$$\underline{\mathbf{e}}_{\mathrm{d,sp}} = \underline{\mathbf{A}}_{\mathrm{d,sp}}\ \underline{\mathbf{d}} + \underline{\mathbf{n}}. \tag{9.11}$$

9.2.4 Adaptive antenna systems

When adaptive antennas are used at the BS, e.g., centro–symmetric array configurations, see Fig. 3.4, prior to transmission the user specific spread signals are weighted by user specific steering vectors $\underline{\mathbf{w}}^{(k)}$, $k = 1 \ldots K$, thus taking advantage of the directional inhomogeneity of the mobile radio channel, see Chapter 2. The system model is illustrated in Fig. 9.3. The vectors $\underline{\mathbf{w}}^{(k)}$, $k = 1 \ldots K$, are chosen to be the complex conjugates of the UL steering vectors [BHP97], see (5.19). If the steering vectors $\underline{\mathbf{w}}^{(k)}$, $k = 1 \ldots K$, are combined to the matrix

$$\underline{\mathbf{W}} = \left[\underline{\mathbf{w}}^{(1)} \ldots \underline{\mathbf{w}}^{(K)}\right], \tag{9.12}$$

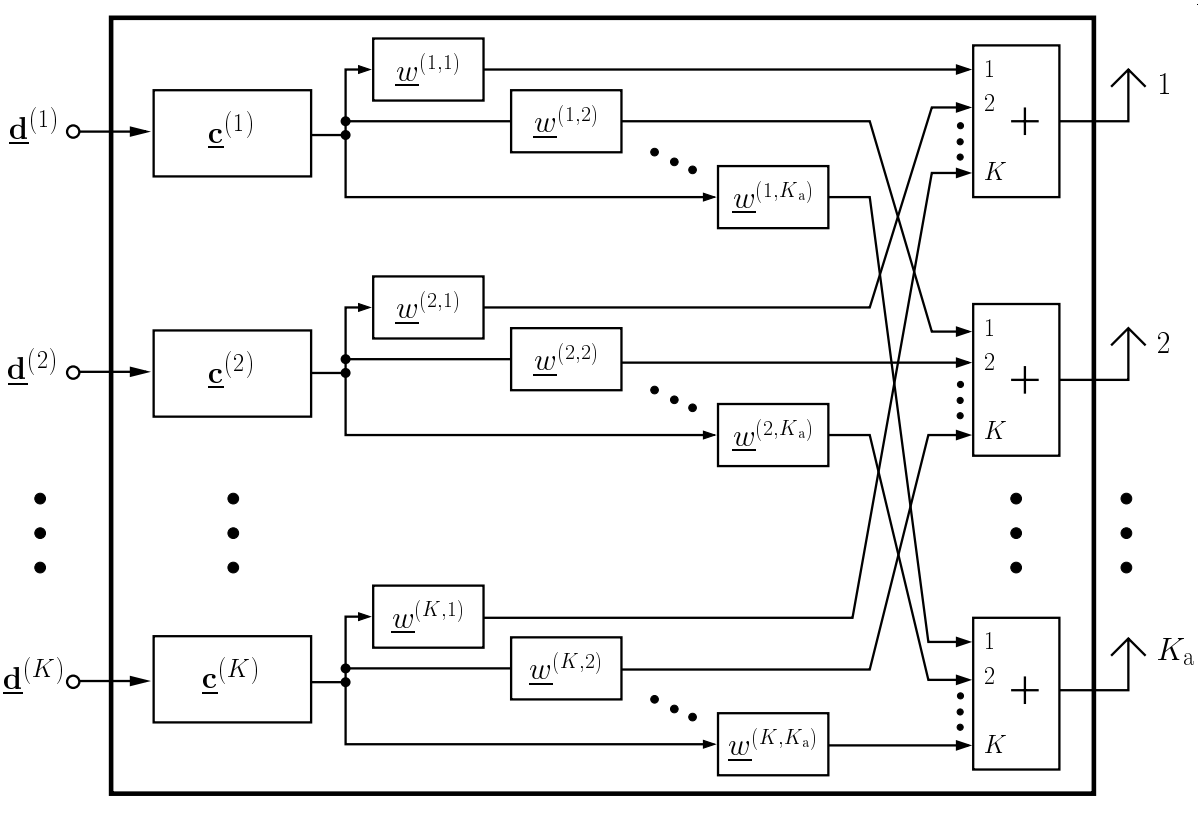

Figure 9.3. Transmitter structure for adaptive antenna systems in the DL of TD–CDMA

the channel impulse response matrix

$$\underline{\mathbf{H}}_{\mathrm{d,arr}} = \left[\underline{\mathbf{H}}_{\mathrm{d}}^{(1)} \ldots \underline{\mathbf{H}}_{\mathrm{d}}^{(K_\mathrm{a})}\right] \left(\underline{\mathbf{W}} \otimes \mathbf{I}^{(NQ)}\right) \tag{9.13}$$

can be formed, where the elements of $\underline{\mathbf{H}}_{\mathrm{d}}^{(k_\mathrm{a})}$, $k_\mathrm{a} = 1 \ldots K_\mathrm{a}$, are defined in (9.8). Then, the DL system matrix

$$\underline{\mathbf{A}}_{\mathrm{d,arr}} = \underline{\mathbf{H}}_{\mathrm{d,arr}}\, \underline{\mathbf{C}}_{\mathrm{u}} \tag{9.14}$$

can be established for the DL when adaptive antennas are used at the BS, where $\underline{\mathbf{C}}_{\mathrm{u}}$ is given by (4.1). Then, the received signal is expressed by

$$\underline{\mathbf{e}}_{\mathrm{d,arr}} = \underline{\mathbf{A}}_{\mathrm{d,arr}}\, \underline{\mathbf{d}} + \underline{\mathbf{n}}, \tag{9.15}$$

see also (9.11).

9.3 Mean SNR degradation and mean gain

In Section 6.3.2 the SNR degradation δ_i, $i = 1 \ldots KN$, see (6.26), is defined. In this section the definitions of the mean SNR degradation per user and the mean gain user user

are introduced in order to have a relatively easy measure for comparing in a straightforward manner the UL with DL performance.

From (6.26) the SNR degradation $\delta_n^{(k)}$, $n = 1 \dots N$, for the N transmitted data symbols from each user k, $k = 1 \dots K$, can be expressed as

$$\delta_{\mathrm{mod}((i)/N)}^{(\mathrm{int}((i-1)/N)+1)} = \delta_i, \quad i = 1 \dots KN, \tag{9.16}$$

where the operator mod$(\cdot)$ gives the remainder after division and the operator int$(\cdot)$ rounds the element in parentheses to the nearest integer towards zero. Then, a mean SNR degradation for the data symbols of each user can be defined as

$$\bar{\delta}^{(k)} = \frac{1}{N} \sum_{n=1}^{N} \delta_n^{(k)}, \quad k = 1 \dots K. \tag{9.17}$$

$\bar{\delta}^{(k)}$, $k = 1 \dots K$, of (9.17) provides the means for directly comparing the performance between UL and DL.

Finally, in order to have a single quantity for the performance gain in the UL compared to the DL case, the mean SNR gain in dB per user is defined as follows:

$$g^{(k)}/\mathrm{dB} = 10\log_{10}\left(\bar{\delta}_{\mathrm{DL}}^{(k)}\right) - 10\log_{10}\left(\bar{\delta}_{\mathrm{UL}}^{(k)}\right), \quad k = 1 \dots K. \tag{9.18}$$

In the following, simulation results are presented which illustrate the performance differences between the UL and the DL in TD–CDMA.

9.4 Simulation results

9.4.1 Introductory remarks

In this section the SNR degradation is calculated for the cases of the UL and the DL transmission considered in Section 9.2. First, the probability density function (pdf) of the mean SNR degradation $\bar{\delta}^{(1)}$ of the user $k = 1$, see (9.17), for the cases considered in Section 9.2 is presented. Then, the UL and the DL performance are compared in a more straightforward manner by the use of the mean SNR gain per user k, $k = 1 \dots K$, see (9.18). It is noted that in both the UL and the DL the same transmission power per user and antenna is used in order to make the comparison fair. In the simulations, the UKL 2 rural channel model, see Section 2.3.3, is used and 10^4 experiments are conducted, i.e., 10^4 bursts are transmitted both in the UL and the DL. The remaining parameters of the TD–CDMA mobile radio system used in the simulations can be found in Table 5.1.

9.4.2 Mean SNR degradation

In Figs. 9.4 and 9.5 the pdf $p(\bar{\delta}^{(1)})$ of $\bar{\delta}^{(1)}$ is shown for the UL and the DL, respectively, when a single antenna is used at the BS and $K = 4$ users are simultaneously active in the same frequency band and time slot. The user velocity v is equal to 3 km/h. The more favourable system performance in the UL is obvious from a direct comparison between Figs. 9.4 and 9.5. It is noted that similar simulation results are observed for the other users as well.

In Figs. 9.6 and 9.7 the pdf $p(\bar{\delta}^{(1)})$ of $\bar{\delta}^{(1)}$ is shown for the UL and the DL, respectively, when $K_{\mathrm{a}} = 4$ antennas are used at the BS and the space diversity concept is applied, i.e., the antennas are spaced 12 λ apart from each other so that the links between each user and each antenna can be considered to be independent [BSPJ97], see also Section 9.2.3. There are $K = 4$ users simultaneously active in the same frequency band and time slot and the user velocity v is 3 km/h. The more favourable system performance of the UL becomes again obvious from a direct comparison of Figs. 9.6. and 9.7.

In Figs. 9.8 and 9.9 the pdf $p(\bar{\delta}^{(1)})$ of $\bar{\delta}^{(1)})$ is shown for the UL and the DL, respectively, when $K_{\mathrm{a}} = 4$ antennas in cross configuration are used at the BS and $K = 4$ users are simultaneously active in the same frequency band and time slot. The spatial scenario is depicted in Fig. 9.10, where the beams serving each MS can be observed. Here, the knowledge of the DOAs of the useful signals are used in the DL transmission for steering beams towards the users of interest, i.e., the vectors $\underline{\mathbf{w}}^{(k)}$, $k = 1 \ldots K$, contained in $\underline{\mathbf{W}}$, see (9.12), are chosen to be equal to the steering vectors $\underline{\mathbf{a}}^{(k)}$, $k = 1 \ldots K$, defined in (5.19). Fig. 9.8 shows that the performance in the DL is enhanced compared to Figs. 9.5 and 9.7, whereas the difference between the UL and the DL is not as severe as in the single antenna case, see Figs. 9.4 and 9.5, or in the space diversity concept, see Figs. 9.6 and 9.7. Certainly, as in the previous cases, the more favourable transmission in the UL is obvious from Figs. 9.8 and 9.9.

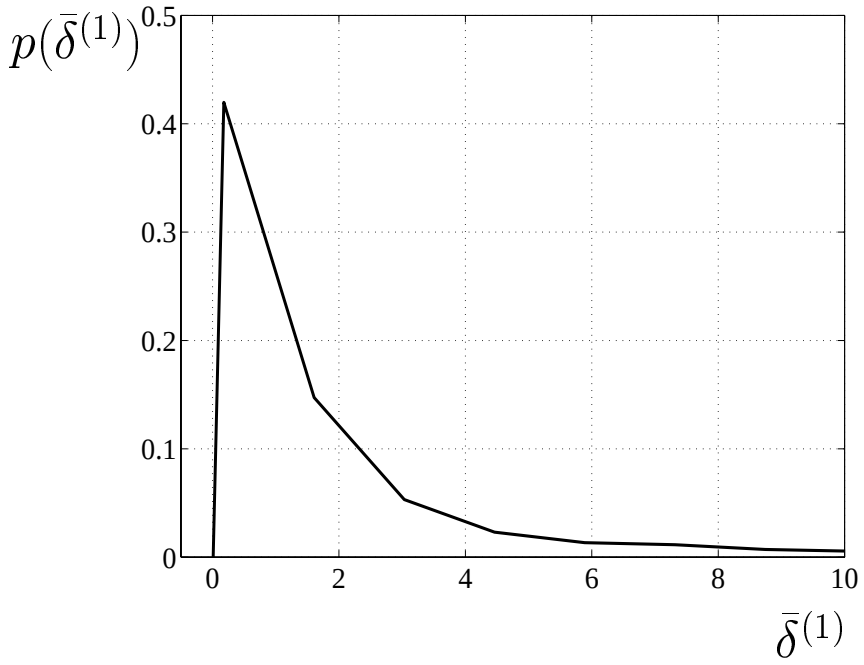

Figure 9.4. UL; single antenna at the BS; pdf of the mean SNR degradation $\bar{\delta}^{(1)}$ of the first user; $K = 4$ users; COST 207 RA channel model

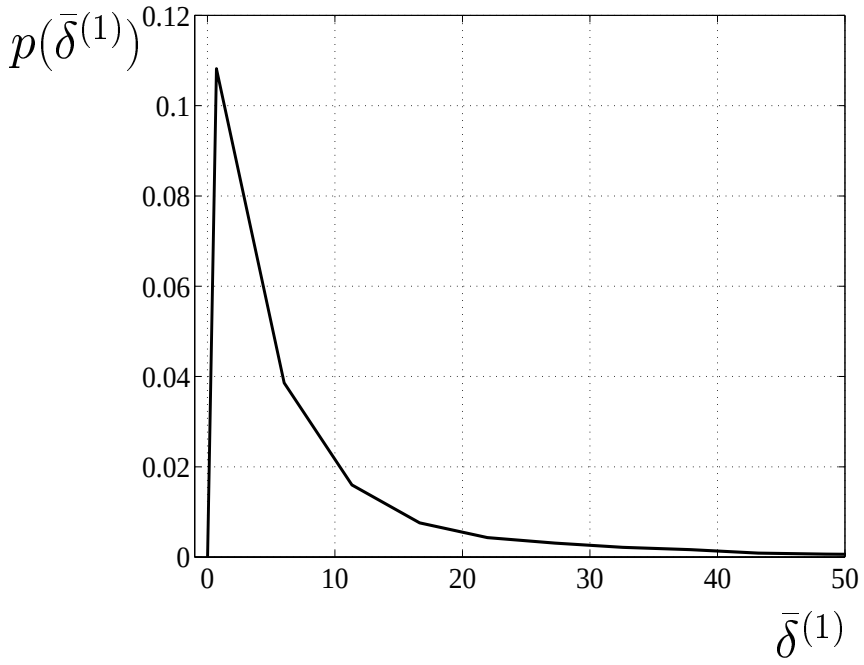

Figure 9.5. DL; single antenna at the BS; pdf of the mean SNR degradation $\bar{\delta}^{(1)}$ of the first user; $K = 4$ users; COST 207 RA channel model

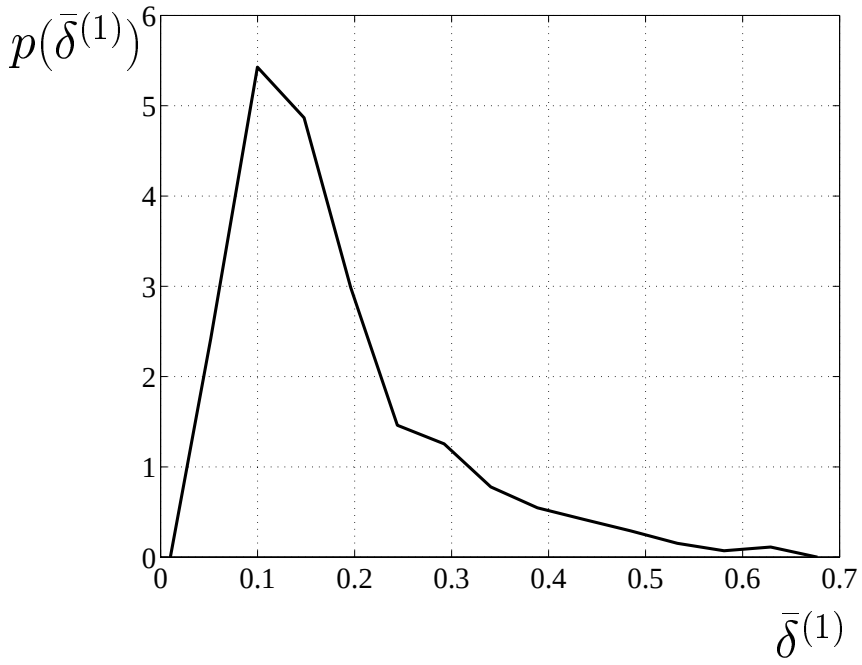

Figure 9.6. UL; $K_a = 4$ antennas at the BS; space diversity concept; pdf of the mean SNR degradation $\bar{\delta}^{(1)}$ of the first user; $K = 4$ users; COST 207 RA channel model

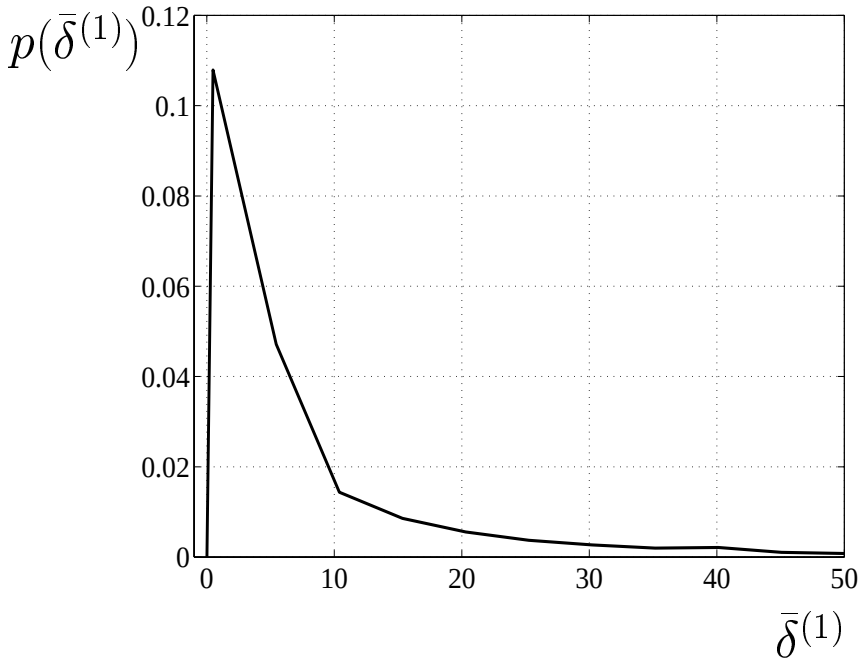

Figure 9.7. DL; $K_a = 4$ antennas at the BS; space diversity concept; pdf of the mean SNR degradation $\bar{\delta}^{(1)}$ of the first user; $K = 4$ users; COST 207 RA channel model

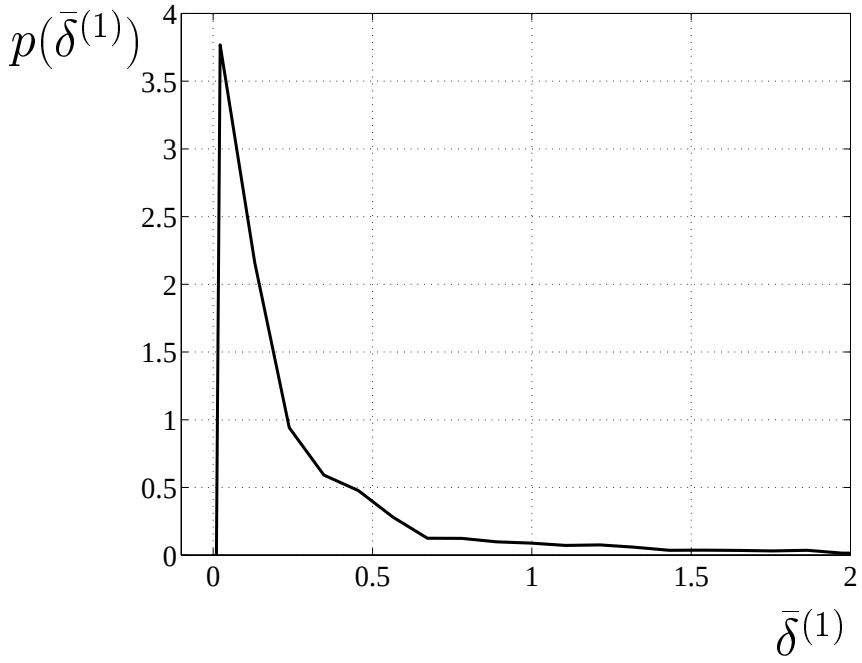

Figure 9.8. UL; $K_{\mathrm{a}} = 4$ antennas in cross configuration at the BS; pdf of the mean SNR degradation $\bar{\delta}^{(1)}$ of the first user; $K = 4$ users; COST 207 RA channel model

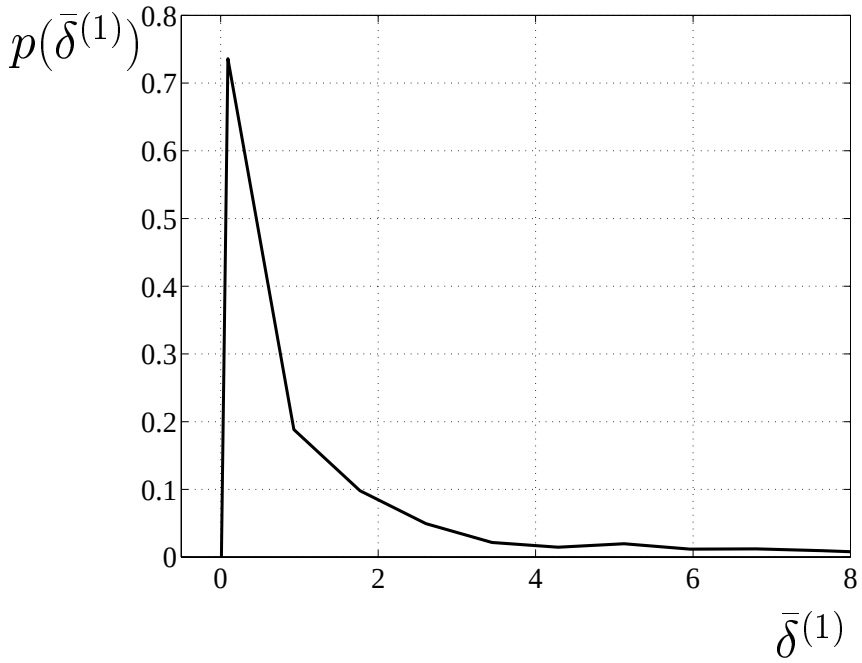

Figure 9.9. DL; $K_{\mathrm{a}} = 4$ antennas in cross configuration at the BS; pdf of the mean SNR degradation $\bar{\delta}^{(1)}$ of the first user; $K = 4$ users; COST 207 RA channel model

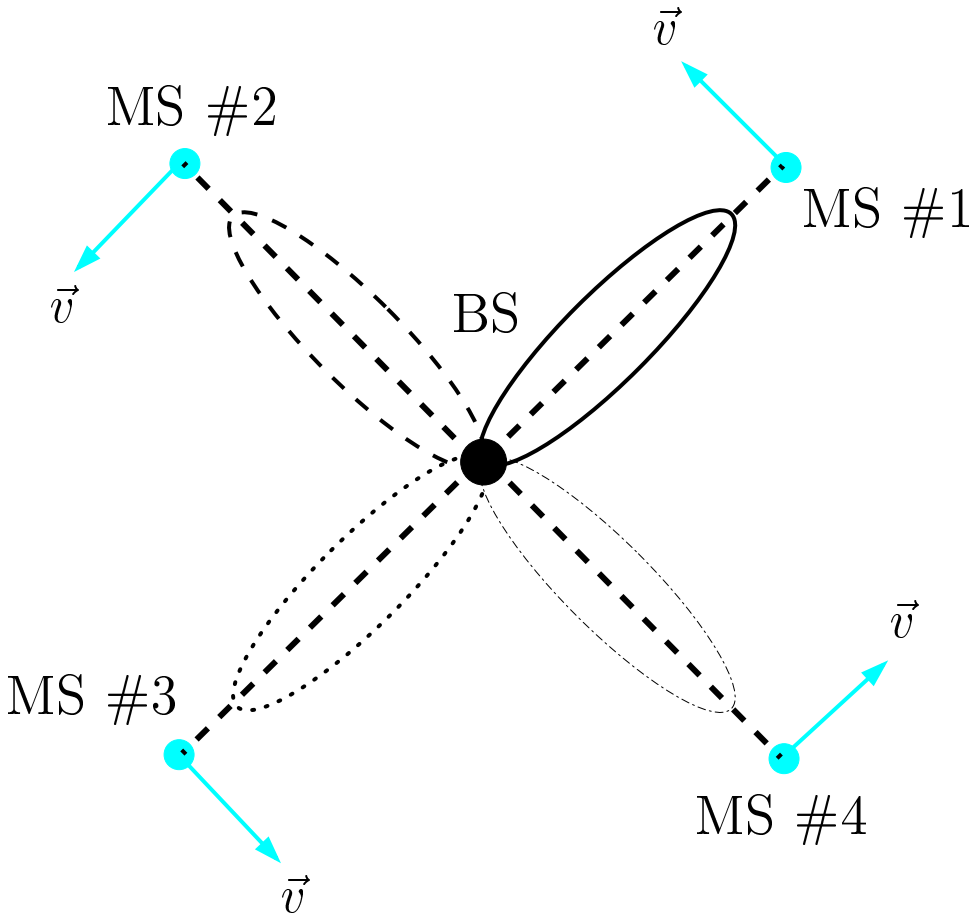

Figure 9.10. Simulation scenario for the Figs. 9.8, 9.9, and 9.10

9.4.3 Mean SNR gain

The UL and DL performance can be compared in a more straightforward manner by the use of the mean SNR gain per user k, $k = 1 \ldots K$, see (9.18). Fig. 9.11 shows the mean SNR gain $g^{(1)}$ versus the number of simultaneously active users within a TDMA burst. This curve is virtually congruent with the curve

$$f(k)/\mathrm{dB} = 10\log_{10}(K), \quad K = 2 \ldots 8, \tag{9.19}$$

see the dashed curve of Fig. 9.11. This result demonstrates the fact that in TD–CDMA the number of simultaneously active users practically determines the difference between the UL and the DL. Certainly, the more favourable structure of the matrix $\underline{\mathbf{A}}^{*\mathrm{T}}\underline{\mathbf{A}}$, see (4.4), in the case of the UL is the reason for its more favourable system performance, compared to the DL case, see (9.3), with the same number of users K.

In Fig. 9.12 $g^{(1)}$ is plotted versus the number K of users for the space diversity concept with $K_\mathrm{a} = 4$ antennas at the BS. Here, the dashed line displays the relation

$$f(k)/\mathrm{dB} = 10\log_{10}(K \cdot K_\mathrm{a}), \quad K_\mathrm{a} = 4, \quad K = 2 \ldots 8. \tag{9.20}$$

The additional gain of approximately 2–3 dB shown by the solid curve of Fig. 9.12 depends again on the more favourable structure of the matrix $\underline{\mathbf{A}}^{*\mathrm{T}}\underline{\mathbf{A}}$, when the space diversity concept is applied, compared to single antenna systems.

Finally, Figs. 9.13 and 9.14 show $g^{(1)}$ versus the number of users K when $K_\mathrm{a} = 4$ and $K_\mathrm{a} = 16$ antennas in a cross configuration are employed at the BS, respectively. It is shown that, independently of the number of antennas used at the BS, there is a gain comparable to single antenna systems, see Fig. 9.11. This result illustrates the increased benefit of adaptive antennas compared to the case where the space diversity concept is applied, see Fig. 9.12. Moreover, the dashed lines in Figs. 9.13 and 9.14 display graphically the relation (9.19). The difference between the solid curves and the dashed curves in Figs. 12 and 13 is smaller than the one in Fig. 9.12, where the space diversity concept is applied. This results shows that the most part of the diversity lost by the space diversity concept compared to single antenna systems is regained by adaptive antennas in TD–CDMA.

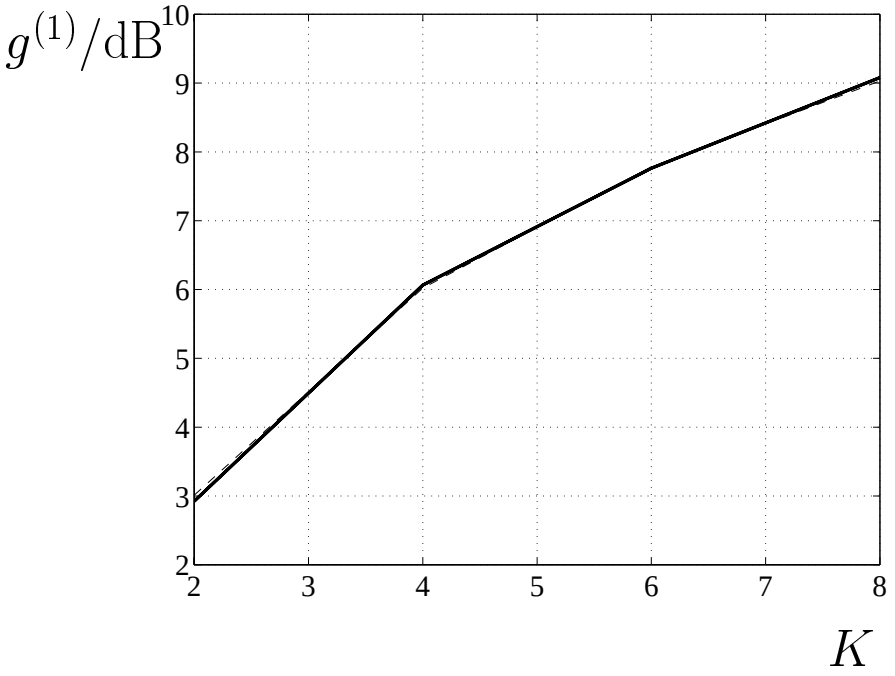

Figure 9.11. Mean gain $g^{(1)}$ in dB versus the number of users K; single antenna at the BS; COST 207 RA channel model

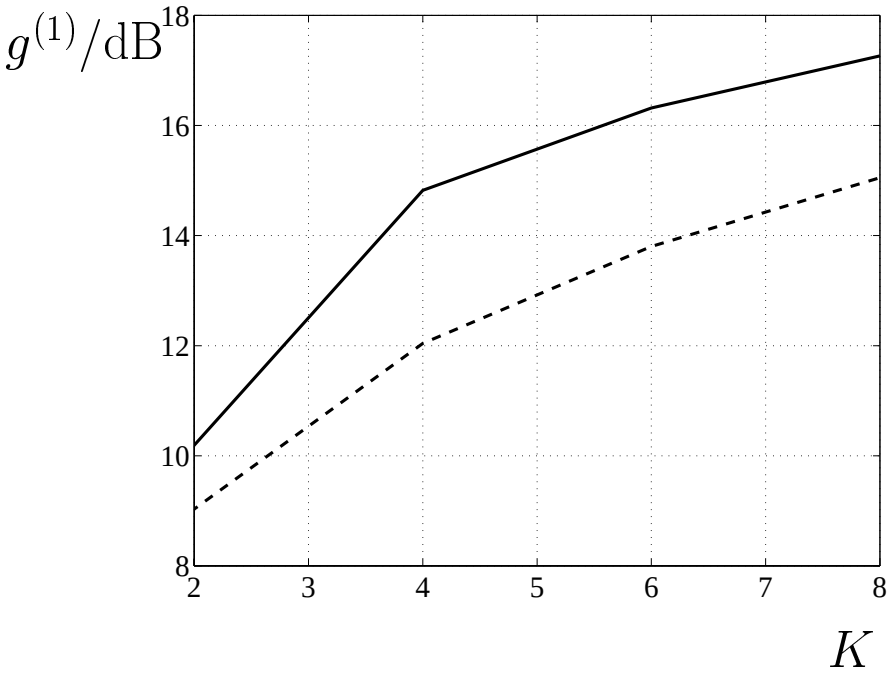

Figure 9.12. Mean gain $g^{(1)}$ in dB versus the number of users K; $K_\mathrm{a} = 4$ antennas at the BS; space diversity concept; COST 207 RA channel model

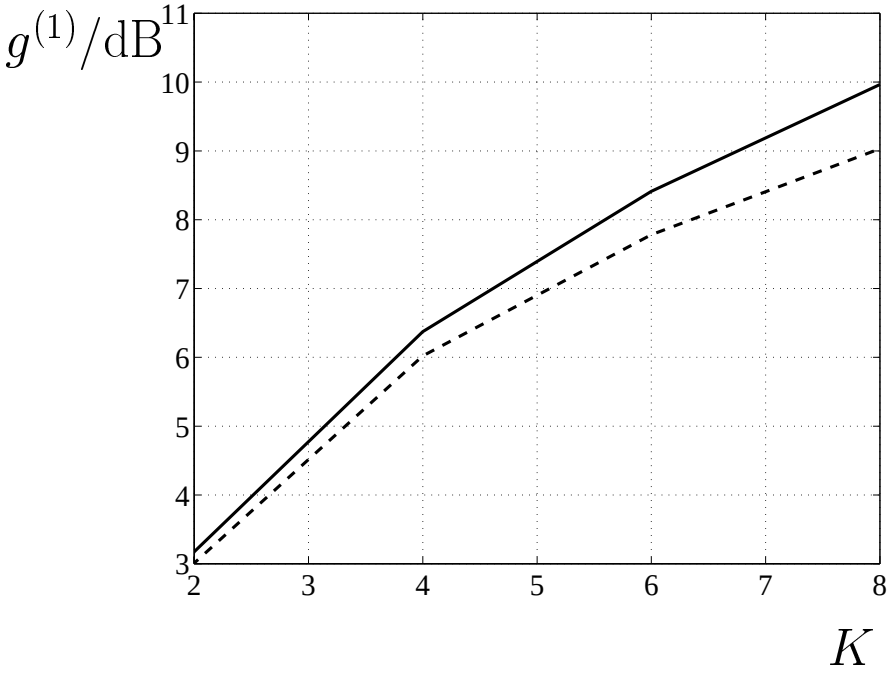

Figure 9.13. Mean gain $g^{(1)}$ in dB versus the number of users K; $K_\mathrm{a} = 4$ antennas in cross configuration at the BS; COST 207 RA channel model

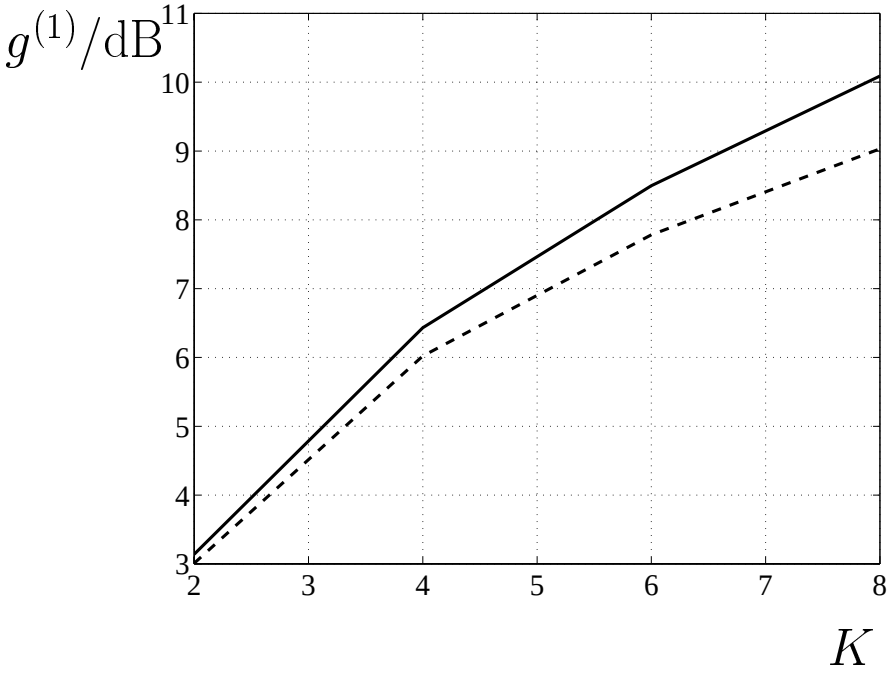

Figure 9.14. Mean gain $g^{(1)}$ in dB versus the number of users K; $K_\mathrm{a} = 16$ antennas in cross configuration at the BS; COST 207 RA channel model

10 Summary

10.1 Summary in English

At present the standardization of third generation (3G) mobile radio systems is the subject of worldwide research activities. These systems will cope with the market demand for high data rate services and the system requirement for flexibility concerning the offered services and the transmission qualities. However, there will be deficiencies with respect to high capacity, if 3G mobile radio systems exclusively use single antennas. Very promising technique developed for increasing the capacity of 3G mobile radio systems the application is adaptive antennas. In this thesis, the benefits of using adaptive antennas are investigated for 3G mobile radio systems based on Time Division CDMA (TD–CDMA), which forms part of the European 3G mobile radio air interface standard adopted by the ETSI, and is intensively studied within the standardization activities towards a worldwide 3G air interface standard directed by the 3GPP (3^{rd} Generation Partnership Project).

One of the most important issues related to adaptive antennas is the analysis of the benefits of using adaptive antennas compared to single antennas. In this thesis, these benefits are explained theoretically and illustrated by computer simulation results for both data detection, which is performed according to the joint detection principle, and channel estimation, which is applied according to the Steiner estimator, in the TD–CDMA uplink. The theoretical explanations are based on well–known solved mathematical problems. The simulation results illustrating the benefits of adaptive antennas are produced by employing a novel simulation concept, which offers a considerable reduction of the simulation time and complexity, as well as increased flexibility concerning the use of different system parameters, compared to the existing simulation concepts for TD–CDMA. Furthermore, three novel techniques are presented which can be used in systems with adaptive antennas for additionally improving the system performance compared to single antennas. These techniques concern the problems of code–channel mismatch, of user separation in the spatial domain, and of intercell interference, which, as it is shown in the thesis, play a critical role on the performance of TD–CDMA with adaptive antennas. Finally, a novel approach for illustrating the performance differences between the uplink and downlink of TD–CDMA based mobile radio systems in a straightforward manner is presented.

Since a cellular mobile radio system with adaptive antennas is considered, the ultimate goal is the investigation of the overall system efficiency rather than the efficiency of a single link. In this thesis, the efficiency of TD–CDMA is evaluated through its spectrum efficiency and capacity, which are two closely related performance measures for cellular mobile radio systems. Compared to the use of single antennas, the use of adaptive antennas allows impressive improvements of both spectrum efficiency and capacity. Depending on the mobile radio channel model and the user velocity, improvement factors range from six to 10.7 for the spectrum efficiency, and from 6.7 to 12.6 for the spectrum capacity of TD–CDMA. Thus, adaptive antennas constitute a promising technique for capacity increase of future mobile communications systems.

10.2 Summary in German

Gegenwärtig wird weltweit an der Standardisierung von Mobilfunksystemen der dritten Generation gearbeitet. Mobilfunksysteme der dritten Generation werden Dienste mit hohen Datenraten und große Flexibilität bezüglich Diensteangebot und Übertragungsqualität bieten. Die Forderung nach hoher Kapazität wird jedoch nicht erreicht werden, wenn der Betrieb von Mobilfunksystemen der dritten Generation ausschließlich auf Einantennensystemen beruht. Eine der allgemein akzeptierten Maßnahmen zur Kapazitätssteigerung von Mobilfunksystemen der dritten Generation ist der Einsatz adaptiver Antennen. In der vorliegenden Arbeit werden adaptive Antennen für ein Mobilfunksystem der dritten Generation untersucht, das auf dem Luftschnittstellenkonzept TD–CDMA (Time Division CDMA) basiert. TD–CDMA ist Bestandteil des von ETSI gewählten Standards für das Luftschnittstellenkonzept von Mobilfunksystemen der dritten Generation in Europa, und TD–CDMA wird bei den Standardisierungsarbeiten von ITU und 3GPP (3^{rd} Generation Partnership Project) in den internationalen Standard des Luftschnittstellenkonzepts für Mobilfunksysteme der dritten Generation eingebracht.

Einer der wichtigsten Gesichtspunkte bei der Anwendung adaptiver Antennensysteme ist die Analyse ihrer Vorteile gegenüber Einantennensystemen. In der vorliegenden Arbeit werden diese Vorteile theoretisch und durch Simulationsergebnisse sowohl für die Datendetektion, die auf dem Prinzip der gemeinsamen Detektion basiert, als auch für die Kanalschätzung, die auf dem Steiner–Schätzer beruht, erläutert. Die theoretischen Erläuterungen basieren auf bereits gelösten mathematischen Problemen. Die Simulationsergebnisse werden mit einem neuen Simulationskonzept für TD–CDMA erzielt, das gegenüber den herkömmlichen Simulationskonzepten die Simulationszeit und –kompexität signifikant reduziert und die Flexibilität bezüglich der Untersuchung verschiedener Systemparameter erhöht. Darüber hinaus werden drei neue Verfahren vorgestellt, die zusätzlich das Verhalten adaptiver Antennensysteme verbessern können. Diese Verfahren betreffen den in der Arbeit gezeigten ungünstigen Einfluß der Fehlanpassung zwischen CDMA–Codes und Kanalimpulsantworten, die Trennung der Teilnehmersignale im räumlichen Bereich und die Unterdrückung der Interzellinterferenz. Schließlich wird eine neue Methode vorgestellt, die einen gerechten Vergleich zwischen der Abwärtsstrecke und der Aufwärtsstrecke von TD–CDMA gestattet.

Da ein zellulares Mobilfunksystem betrachtet wird, sind die von adaptiven Antennen gebotenen Vorteile nicht nur bezüglich einer einzelnen Punkt–zu–Punkt–Übertragungsstrecke, sondern bezüglich der Systemeffizienz eines gesamten Zellnetzes zu untersuchen. In der vorliegenden Arbeit wird die Effizienz von TD–CDMA anhand der Größen spektrale Effizienz und Kapazität bewertet. Der Einsatz adaptiver Antennen erlaubt gegenüber dem Einsatz von Einantennensystemen eine deutliche Steigerung der spektrale Effizienz und Kapazität. Abhängig vom verwendeten Kanaltyp und der Teilnehmergeschwindigkeit ermöglichen adaptive Antennen Verbesserungsfaktoren zwischen sechs und 10,7 für die spektrale Effizienz und zwischen 6,7 und 12,6 für die spektrale Kapazität. Deswegen ist der Einsatz adaptiver Antennen eine vielversprechende Maßnahme zur Kapazitätssteigerung künftiger Mobilfunksysteme.

Appendix A

List of frequently used abbreviations and symbols

A.1 Abbreviations

2D	2–Dimensional
2G	2nd Generation
3G	3rd Generation
3GPP	3G Partnership Project
AWGN	Additive White Gaussian Noise
BER	Bit Error Ratio
BS	Base Station
BU	Bad Urban
cdf	cumulative distribution function
CDMA	Code Division Multiple Access
COST	European COoperation in the Field of Scientific and Technical Research
DFT	Discrete Fourier Transformation
DL	DownLink
DOA	Direction–Of–Arrival
DS	Direct Sequence
ESPRIT	Estimation of Signal Parameters via Rotational Invariance Techniques
ETSI	European Telecommunications Standards Institute
FDD	Frequency Division Duplex
FDMA	Frequency Division Multiple Access
FEC	Forward Error Correction
GMSK	Gaussian Minimum Shift Keying
GSM	Global System for Mobile Communications
IC	Iinterference Cancellation
IMT-2000	International Mobile Telecommunications 2000
ISI	InterSymbol Interference
ITU	International Telecommunications Union
JD	Joint Detection
LOS	Line Of Sight
MAI	Multiple Access Interference
MDL	Minimum Discription Length
ML	Maximum Likelihood
MLSE	Maximum Likelihood Sequence Estimation

MLSSE	Maximum Likelihood Symbol–by–Symbol Estimation
MS	Mobile Station
MUSIC	MUltiple SIgnal Classification
pdf	probability density function
PL	Path Loss
QoS	Quality of Service
RA	Rural Area
RL	Reference Line
RP	Reference Point
SA	Scattering Area
SDMA	Space Division Multiple Access
TDD	Time Division Duplex
TDMA	Time Division Multiple Access
TU	Typical Urban
UKL	University of KaisersLautern
UL	UpLink
ULA	Uinform Linear Array
UMTS	Universal Mobile Telecommunications System
URA	Uinform Rectangular Array
UTRA	UMTS Terrestrial Radio Access
ZF–BLE	Zero Forcing Block Linear Equalizer

A.2 Symbols

α	attenuation exponent
A	offered traffic per cell
A_{c}	area of a single cell of the cellular network
$\underline{\mathbf{a}}^{(k,k_{\mathrm{d}})}$	steering vector for the k_{d}–th DOA of user k, $k_{\mathrm{d}} = 1 \ldots K_{\mathrm{d}}$, $k = 1 \ldots K$, valid for the large cell channel type
$\underline{\mathbf{a}}^{(k,k_{\mathrm{d}})}$	steering vector for the k_{d}–th DOA of the w–th tap of user k, $k_{\mathrm{d}} = 1 \ldots K_{\mathrm{d}}$, $w = 1 \ldots W$, $k = 1 \ldots K$, valid for the large cell channel type
$\underline{\mathbf{A}}_{\mathrm{u,s}}$	uplink system matrix valid for single antennas, which is determined by the CDMA codes $\underline{\mathbf{c}}^{(k)}$, $k = 1 \ldots K$, and the channel impulse responses $\underline{\mathbf{h}}^{(k)}$, $k = 1 \ldots K$
$\underline{\mathbf{A}}_{\mathrm{u,s}}^{(k)}$	k–th block of $\underline{\mathbf{A}}_{\mathrm{u,s}}$
$\underline{\mathbf{A}}_{\mathrm{u,m}}$	uplink system matrix valid for adaptive antennas, which is determined by the CDMA codes $\underline{\mathbf{c}}^{(k)}$, $k = 1 \ldots K$, and the channel impulse responses $\underline{\mathbf{h}}^{(k,k_{\mathrm{a}})}$, $k = 1 \ldots K$, $k_{\mathrm{a}} = 1 \ldots K_{\mathrm{a}}$
$\underline{\mathbf{A}}_{\mathrm{u,m}}^{(k,k_{\mathrm{a}})}$	(k, k_{a})–th block of $\underline{\mathbf{A}}_{\mathrm{u,m}}$
$\underline{\mathbf{A}}$	matrix representing one of the matrices $\underline{\mathbf{A}}_{\mathrm{u,s}}$ or $\underline{\mathbf{A}}_{\mathrm{u,m}}$

$\underline{\mathbf{A}}_{\mathrm{d,s}}$	downlink system matrix of user k valid for single antennas, which is determined by the CDMA codes $\underline{\mathbf{c}}^{(k)}$, $k = 1 \ldots K$, and the channel impulse response $\underline{\mathbf{h}}^{(k)}$
$\underline{\mathbf{A}}_{\mathrm{d,arr}}$	downlink system matrix of user k valid for adaptive antennas, which is determined by the CDMA codes $\underline{\mathbf{c}}^{(k)}$, $k = 1 \ldots K$, the channel impulse responses $\underline{\mathbf{h}}^{(k,k_\mathrm{a})}$, $k_\mathrm{a} = 1 \ldots K_\mathrm{a}$, and the weight vectors $\underline{\mathbf{w}}^{(k)}$, $k = 1 \ldots K$
$\underline{\mathbf{A}}_\mathrm{s}^{(k)}$	matrix valid for the large cell channel type, which contains the steering vectors $\underline{\mathbf{a}}^{(k,k_\mathrm{d})}$, $k_\mathrm{d} = 1 \ldots {K_\mathrm{d}}^{(k)}$
$\underline{\mathbf{A}}_\mathrm{s}^{(k,w)}$	matrix valid for the small cell channel type, which contains the steering vectors $\underline{\mathbf{a}}^{(k,w,k_\mathrm{d})}$, $w = 1 \ldots W$, $k_\mathrm{d} = 1 \ldots {K_\mathrm{d}}^{(k,w)}$
$\beta^{(k)}$	user specific scalar for evaluating the code–channel mismatch
$\beta_1^{(k,k_\mathrm{d})}$	azimuthal angle of the k_d–th wavefront of user k, $k_\mathrm{d} = 1 \ldots {K_\mathrm{d}}^{(k)}$, $k = 1 \ldots K$
$\beta_2^{(k,k_\mathrm{d})}$	elevation angle of the k_d–th wavefront of user k, $k_\mathrm{d} = 1 \ldots {K_\mathrm{d}}^{(k)}$, $k = 1 \ldots K$
$\underline{\mathbf{b}}^{(k)}$	composite channel impulse response of user k, $k = 1 \ldots K$, valid for single antennas
$\underline{\mathbf{b}}^{(k,k_\mathrm{a})}$	composite channel impulse response of user k, $k = 1 \ldots K$, at antenna k_a, $k_\mathrm{a} = 1 \ldots K_\mathrm{a}$, valid for adaptive antennas
B	bandwidth of a partial frequency band
$\underline{\mathbf{B}}$	matrix with $\underline{\mathbf{b}}^{(k)}$, $k = 1 \ldots K$, used for determining $\underline{\mathbf{R}}_\mathrm{b}$
C	carrier received power of a desired signal
$\underline{\mathbf{c}}^{(k)}$	vector with the user specific CDMA code, $k = 1 \ldots K$
$\underline{\mathbf{C}}^{(k)}$	matrix containing $\underline{\mathbf{c}}^{(k)}$
$\underline{\mathbf{C}}_\mathrm{u}$	matrix with all K CDMA codes $\underline{\mathbf{c}}^{(k)}$, $k = 1 \ldots K$, valid for the uplink
$\underline{\mathbf{C}}_\mathrm{d}$	matrix with all K CDMA codes $\underline{\mathbf{c}}^{(k)}$, $k = 1 \ldots K$, valid for the downlink, when single antennas are used
d	distance between BS and MS
$D^{(n_\mathrm{z})}$	diameter of SA n, $n_\mathrm{z} = 1 \ldots N_\mathrm{z}$
$\Delta\phi$	spatial distance in azimuth between two adjacent DOAs within a TDMA burst
$\Delta\underline{\mathbf{A}}$	error matrix pertaining to the system matrix $\underline{\mathbf{A}}$ and depending on the channel estimation errors
$\underline{d}_n^{(k)}$	user specific data symbol, $n = 1 \ldots N$, $k = 1 \ldots K$
$\underline{\mathbf{d}}$	total data vector
$\underline{\mathbf{d}}^{(k)}$	user specific data vector, $k = 1 \ldots K$
$\hat{\underline{\mathbf{d}}}$	estimated total data vector
δ_i	SNR degradation of TD–CDMA receivers, valid for the i–th component of $\underline{\mathbf{d}}$, $i = 1 \ldots KN$
$\delta_{\mathrm{n},i}$	normalized SNR degradation of TD–CDMA receivers, valid for the i–th component of $\underline{\mathbf{d}}$, $i = 1 \ldots KN$
$\bar{\delta}_\mathrm{n}$	mean normalized SNR degradation of TD–CDMA receivers
$\bar{\delta}^{(k)}$	mean SNR degradation of user k, $k = 1 \ldots K$

E_b	average received energy per transmitted bit
$\underline{\mathbf{e}}_\mathrm{u,s}$	received total signal valid for single antennas, which is determined by $\underline{\mathbf{A}}_\mathrm{u,s}$, $\underline{\mathbf{d}}$, and $\underline{\mathbf{n}}$
$\underline{\mathbf{e}}_\mathrm{u,m}$	received total signal valid for adaptive antennas, which is determined by $\underline{\mathbf{A}}_\mathrm{u,m}$, $\underline{\mathbf{d}}$, and $\underline{\mathbf{n}}$
$\underline{\mathbf{e}}$	vector representing one of the vectors $\underline{\mathbf{e}}_\mathrm{u,s}$ or $\underline{\mathbf{e}}_\mathrm{u,m}$
$\underline{\mathbf{e}}_\mathrm{m}$	received total signal valid for channel estimation
$\underline{\mathbf{E}}_\mathrm{m}$	matrix exclusively determined from $\underline{\mathbf{e}}_\mathrm{m}$
η	spectrum efficiency
f	frequency
f_d	Doppler frequency
$\underline{f}_\mathrm{t}^{(\vartheta)}(\vartheta,\varphi)$	characteristic of the transmitter antenna for the ϑ–component
$\underline{f}_\mathrm{t}^{(\varphi)}(\vartheta,\varphi)$	characteristic of the transmitter antenna for the φ–component
$\underline{f}_\mathrm{r}^{(\Theta)}(\Theta,\Phi)$	characteristic of the receiver antenna for the Θ–component
$\underline{f}_\mathrm{r}^{(\Phi)}(\Theta,\Phi)$	characteristic of the receiver antenna for the Φ–component
$\underline{\mathbf{F}}$	matrix exclusively determined by $\underline{\mathbf{b}}^{(k)}$, $k = 1 \ldots K$, and Q, which is used for normalizing $\underline{\mathbf{A}}$
$\underline{\mathbf{F}}^{(k)}$	k–th diagonal block of $\underline{\mathbf{F}}$
$\gamma_1^{(k_\mathrm{i})}$	azimuthal angle of the k_i–th interfering signal, $k_\mathrm{i} = 1 \ldots K_\mathrm{i}$
$\gamma_2^{(k_\mathrm{i})}$	elevation angle of the k_i–th interfering signal, $k_\mathrm{i} = 1 \ldots K_\mathrm{i}$
$\bar{\gamma}_\mathrm{in}$	mean SNR at the input of the receiver
$g^{(k)}$	mean SNR gain per user k, $k = 1 \ldots K$, used for comparing the performance of UL and DL
$\underline{g}_\mathrm{c}{}^{(\mu,\nu)}(\vartheta,\varphi,\Theta,\Phi,\tau,t)$	differential directional channel impulse response, $\mu \in \{\Theta,\Phi\}$, $\nu \in \{\vartheta,\varphi\}$
$\underline{g}_\mathrm{d}(\tau,t,\varphi)$	directional differential channel impulse response valid for the RP of the BS
$\underline{\mathbf{g}}^{(k,w)}$	column of $\underline{\mathbf{G}}$, corresponding to the w–th tap of user k, $w = 1 \ldots W$, $k = 1 \ldots K$
$\underline{\mathbf{G}}$	channel estimation matrix, exclusively determined by the user specific training sequence
$\underline{\mathbf{G}}^{(k)}$	k–th block of $\underline{\mathbf{G}}$, $k = 1 \ldots K$
$\underline{\mathbf{G}}_\mathrm{c}(\vartheta,\varphi,\Theta,\Phi,\tau,t)$	matrix containing all differential directional channel impulse responses $\underline{g}_\mathrm{c}{}^{(\mu,\nu)}(\vartheta,\varphi,\Theta,\Phi,\tau,t)$, $\mu \in \{\Theta,\Phi\}$, $\nu \in \{\vartheta,\varphi\}$
$\underline{\mathbf{G}}_\mathrm{d}$	channel estimation matrix for the large cell channel type, when adaptive antennas are used
$\underline{\mathbf{G}}_\mathrm{d,s}$	channel estimation matrix for the small cell channel type, when adaptive antennas are used
$\underline{\mathbf{h}}(k)$	channel impulse response of user k, $k = 1 \ldots K$, valid for single antennas
$\underline{\mathbf{h}}(k,k_\mathrm{a})$	channel impulse response for the link between user k and antenna k_a, $k = 1 \ldots K$, $k_\mathrm{a} = 1 \ldots K_\mathrm{a}$, valid for adaptive antennas
$\underline{\mathbf{h}}$	total channel impulse response vector containing all channel impulse responses $\underline{\mathbf{h}}(k)$, $k = 1 \ldots K$, or $\underline{\mathbf{h}}(k,k_\mathrm{a})$, $k = 1 \ldots K$, $k_\mathrm{a} = 1 \ldots K_\mathrm{a}$

$\underline{\hat{\mathbf{h}}}$	estimated total channel impulse response vector
$\underline{\mathbf{h}}_{\mathrm{d}}^{(k,k_{\mathrm{d}})}$	directional channel impulse response corresponding to the k_{d}–th DOA of user k, valid for the large cell channel type
$\underline{\mathbf{h}}_{\mathrm{d}}^{(k,k_{\mathrm{d}})}$	directional channel impulse response corresponding to the k_{d}–th DOA of user k, valid for the large cell channel type
$\underline{\mathbf{h}}_{\mathrm{d}}^{(k,w)}$	directional channel impulse response corresponding to the w–th tap of user k, valid for the small cell channel type
$\underline{\mathbf{h}}_{\mathrm{d}}$	vector containing all K_{d} directional channel impulse responses
$\underline{\mathbf{H}}_{\mathrm{u,s}}$	matrix with $\underline{\mathbf{h}}^{(k)}$, $k = 1 \ldots K$, valid for single antennas in the uplink
$\underline{\mathbf{H}}_{\mathrm{u,s}}^{(k)}$	k–th block of $\underline{\mathbf{H}}_{\mathrm{u,s}}$
$\underline{\mathbf{H}}_{\mathrm{u,m}}$	matrix with $\underline{\mathbf{h}}^{(k,k_{\mathrm{a}})}$, $k = 1 \ldots K$, $k_{\mathrm{a}} = 1 \ldots K_{\mathrm{a}}$, valid for adaptive antennas in the uplink
$\underline{\mathbf{H}}_{\mathrm{u,m}}^{(k,k_{\mathrm{a}})}$	(k, k_{a})–th block of $\underline{\mathbf{H}}_{\mathrm{u,m}}$
$\underline{\mathbf{H}}_{\mathrm{d,s}}$	matrix with $\underline{\mathbf{h}}^{(k)}$, valid for single antennas in the downlink
$\underline{\mathbf{H}}_{\mathrm{d,arr}}$	matrix with $\underline{\mathbf{h}}^{(k,k_{\mathrm{a}})}$, $k_{\mathrm{a}} = 1 \ldots K_{\mathrm{a}}$, valid for adaptive antennas in the downlink
i	general burst number
I	received power of interfering signals
$\mathbf{I}^{(M)}$	$M \times M$ identity matrix
j	imaginary unit
κ	spectrum capacity
K	number of users active in a time slot
K_{a}	number of antennas at the BS
$K_{\mathrm{d}}{}^{(k)}$	number of DOAs of user k, $k = 1 \ldots K$, valid for the large cell channel type
$K_{\mathrm{d}}{}^{(k,w)}$	number of DOAs of tap w of user k, $w = 1 \ldots W$, $k = 1 \ldots K$, valid for the small cell channel type
K_{i}	number of interfering signals
K_{tot}	total number of users to be assigned to a TDMA frame
λ	wavelength
l	user group valid for a time slot of the TDMA frame, $l = 0 \ldots T_{\mathrm{fr}}/T_{\mathrm{bu}} - 1$
$l^{(k_{\mathrm{a}})}$	distance of antenna k_{a} from the RP of the array configuration, $k_{\mathrm{a}} = 1 \ldots K_{\mathrm{a}}$
L	dimension of $\underline{\mathbf{e}}_{\mathrm{m}}$
L_{m}	dimension the midamble section of a burst
$\underline{\mathbf{L}}_{\mathrm{n}}$	matrix resulting from the Cholesky decomposition of $\underline{\mathbf{R}}_{\mathrm{n}}$
$l^{(k_{\mathrm{a}})}$	distance of antenna k_{a} to RP
M	size of the data symbol alphabet
$\underline{\mathbf{M}}$	channel matrix, which is exclusively determined from $\underline{\mathbf{A}}$ and $\underline{\mathbf{R}}_{\mathrm{n}}$
N	number of symbols per data block and user
N_{c}	number of cells of the cellular network
N_{par}	number of partial frequency bands

N_p	number of scatterers contained in the scenario area, which is determined by R_s
$\mathbb{N}_\mathrm{p}^{(n_\mathrm{z})}$	number of relevant scatterers of SA n_z, $n_\mathrm{z} = 1 \ldots N_\mathrm{z}$
N_fr	number of time slots per TDMA frame
N_z	total number of SA's
$\underline{n}'_i$	i–th component of $\underline{\mathbf{n}}'$, $i = 1 \ldots KN$
$\underline{\mathbf{n}}$	intercell MAI vector valid for data detection
$\underline{\mathbf{n}}_\mathrm{m}$	intercell MAI vector valid for channel estimation
$\underline{\mathbf{n}}_\mathrm{out}$	output intercell MAI vector exclusively determined from $\underline{\mathbf{M}}$ and $\underline{\mathbf{n}}$
$\underline{\mathbf{n}}'$	intercell MAI vector, the components of which have unit variance
$\underline{\mathbf{n}}^{(k_\mathrm{a})}$	intercell MAI vector valid for antenna k_a, $k_\mathrm{a} = 1 \ldots K_\mathrm{a}$
$\underline{\mathbf{n}}_\mathrm{d}^{(k_\mathrm{i})}$	k_i–th interfering signal impinging from $\gamma_1^{(k_\mathrm{i})}$ and $\gamma_2^{(k_\mathrm{i})}$, $k_\mathrm{i} = 1 \ldots K_\mathrm{i}$
$\underline{\mathbf{N}}_\mathrm{m}$	matrix exclusively determined by $\underline{\mathbf{n}}_\mathrm{m}$
$\underline{\mathbf{N}}^{(k)}$	user specific noise matrix valid for DOA estimation, $k = 1 \ldots K$
$\mathbf{0}$	zero vector
P_b	instantaneous BER, which is used for determining the spectrum efficiency
$\bar{P}_\mathrm{b}$	average BER
P_b^M	upper bound for the BER
P_o^M	maximum allowable outage probability
P_o	outage probability
Q	dimension of $\underline{\mathbf{c}}^{(k)}$, $k = 1 \ldots K$
R	data rate per user k, $k = 1 \ldots K$
R_s	radius determining the scenario area of the UKL 2 directional channel models
R_tot	total available information rate per cell
$\underline{\mathbf{R}}_\mathrm{b}$	covariance matrix of $\underline{\mathbf{B}}$
$\underline{\mathbf{R}}_\mathrm{d}$	covariance matrix of $\underline{\mathbf{d}}$
$\underline{\mathbf{R}}_\mathrm{m}$	total intercell MAI covariance matrix valid for channel estimation
$\underline{\mathbf{R}}_\mathrm{m,t}$	temporal intercell MAI covariance matrix valid for channel estimation
$\underline{\mathbf{R}}_\mathrm{n}$	total intercell MAI covariance matrix valid for data detection
$\underline{\mathbf{R}}_\mathrm{n,out}$	covariance matrix of $\underline{\mathbf{n}}_\mathrm{out}$
$\underline{\mathbf{R}}_\mathrm{s}$	spatial intercell MAI covariance matrix
$\underline{\mathbf{R}}_\mathrm{t}$	temporal intercell MAI covariance matrix valid for data detection
$\underline{\mathbf{R}}_\mathrm{n}^{(i,j)}$	covariance matrix of $\underline{\mathbf{n}}^{(i)}$ and $\underline{\mathbf{n}}^{(j)}$, $i, j = 1 \ldots K_\mathrm{a}$
r	reuse factor
σ^2	noise power, which is assumed to equal for all components of $\underline{\mathbf{n}}$
$\left(\sigma^{(k_\mathrm{i})}\right)^2$	power of the k_i–th interfering signal
τ	delay parameter
T_bu	duration of a time slot
T_c	chip duration
T_fr	duration of a TDMA frame
T_g	duration of the guard interval

T_s	symbol duration
v	user velocity
$\vec{v}$	user velocity vector
v_0	smallest non–zero user velocity, used for developing the novel simulation concept for TD–CDMA
W	dimension of $\underline{\mathbf{h}}^{(k)}$ or $\underline{\mathbf{h}}^{(k,k_\mathrm{a})}$
$\underline{\mathbf{Z}}$	matrix exclusively determined from $\underline{\mathbf{A}}$
$\underline{\tilde{\mathbf{Z}}}$	normalized matrix of $\underline{\mathbf{Z}}$, used to determine the SNR degradation of TD–CDMA receivers
$\underline{\tilde{\tilde{\mathbf{Z}}}}$	normalized matrix of $\underline{\mathbf{Z}}$, with its diagonal elements equal to one
ϑ	elevation angle at the transmitter, used for determining $\underline{g_\mathrm{c}}^{(\mu,\nu)}(\vartheta,\varphi,\Theta,\Phi,\tau,t)$, $\mu \in \{\Theta,\Phi\}$, $\nu \in \{\vartheta,\varphi\}$
φ	azimuthal angle at the transmitter, used for determining $\underline{g_\mathrm{c}}^{(\mu,\nu)}(\vartheta,\varphi,\Theta,\Phi,\tau,t)$, $\mu \in \{\Theta,\Phi\}$, $\nu \in \{\vartheta,\varphi\}$
Θ	elevation angle at the receiver, used for determining $\underline{g_\mathrm{c}}^{(\mu,\nu)}(\vartheta,\varphi,\Theta,\Phi,\tau,t)$, $\mu \in \{\Theta,\Phi\}$, $\nu \in \{\vartheta,\varphi\}$
Φ	azimuthal angle at the receiver, used for determining $\underline{g_\mathrm{c}}^{(\mu,\nu)}(\vartheta,\varphi,\Theta,\Phi,\tau,t)$, $\mu \in \{\Theta,\Phi\}$, $\nu \in \{\vartheta,\varphi\}$
$\psi(k,k_\mathrm{a},k_\mathrm{d})$	phase factor valid for antenna k_a, corresponding to the k_d–th DOA of user k

Appendix B

Special issues concerning the SNR degradation of TD–CDMA receivers

B.1 Proof of Theorem of Section 4.3.3.2

The proof of the Theorem of Section 4.3.3.2 is presented in the following. In order to simplify the analysis, it is assumed that only a single symbol, i.e., N is equal to one, is transmitted by each of the K simultaneously active users. The proof for the case that N is greater than one can be performed by following the same rationale, as the one presented in the rest of this section.

By assuming that N equals one, if $\underline{\mathbf{N}}_{\mathrm{n}}$ denotes a $K \times K$ diagonal matrix with

$$\left[\underline{\mathbf{N}}_{\mathrm{n}}\right]_{k,k} = \sqrt{\sum_{k_{\mathrm{a}}=1}^{K_{\mathrm{a}}} \underline{\mathbf{b}}^{(k,k_{\mathrm{a}})*\mathrm{T}} \underline{\mathbf{b}}^{(k,k_{\mathrm{a}})}}, \tag{B.1}$$

where $\underline{\mathbf{b}}^{(k,k_{\mathrm{a}})}$, $k = 1 \ldots K$, $k_{\mathrm{a}} = 1 \ldots K_{\mathrm{a}}$, is defined in (4.13), $\underline{\mathbf{Z}}$, see (4.28), can be written as

$$\underline{\mathbf{Z}} = \underline{\mathbf{N}}_{\mathrm{n}} \underline{\mathbf{Z}}_{\mathrm{n}} \underline{\mathbf{N}}_{\mathrm{n}}, \tag{B.2}$$

where $\underline{\mathbf{Z}}_{\mathrm{n}}$ is a $K \times K$ matrix with its diagonal elements equal to one and its off–diagonal elements equal to

$$\left[\underline{\mathbf{Z}}_{\mathrm{n}}\right]_{k_1,k_2} = \left[\underline{\mathbf{N}}_{\mathrm{n}}\right]_{k_1,k_1} \left[\underline{\mathbf{N}}_{\mathrm{n}}\right]_{k_2,k_2} \cdot \sum_{k_{\mathrm{a}}=1}^{K_{\mathrm{a}}} \underline{\mathbf{b}}^{(k_1,k_{\mathrm{a}})*\mathrm{T}} \underline{\mathbf{b}}^{(k_2,k_{\mathrm{a}})}, \tag{B.3}$$

where $\left[\underline{\mathbf{N}}_{\mathrm{n}}\right]_{k,k}$ is defined in (B.1). Under these assumptions, the proof consists of two steps:

- In a first step, it is proven that a diagonal element $\left[\underline{\mathbf{Z}}_{\mathrm{n}}^{-1}\right]_{i,i}$, $i = 1 \ldots KN$, of $\underline{\mathbf{Z}}_{\mathrm{n}}^{-1}$, see (B.2) and (B.3), always takes greater values than the corresponding diagonal element $\left[\underline{\mathbf{Z}}_{\mathrm{n}}\right]_{i,i}$, $i = 1 \ldots KN$, of $\underline{\mathbf{Z}}_{\mathrm{n}}$.
- In a second step, it is proven that if the elements of the diagonal blocks of $\underline{\mathbf{Z}}_{\mathrm{n}}$ are multiplied by a constant factor l greater than one, with the resulting matrix denoted by $\underline{\mathbf{Z}}_{\mathrm{n,l}}$, the diagonal elements of $\underline{\mathbf{Z}}_{\mathrm{n,l}}^{-1}$ take lower values than the diagonal elements of $\underline{\mathbf{Z}}_{\mathrm{n}}^{-1}$.

Then, the validity of the Theorem follows in a straightforward manner.

In order to prove the first of said steps, it suffices to prove that the diagonal elements of $\underline{\mathbf{Z}}_{\mathrm{n}}^{-1}$ are greater than one. In the following, only the element $\left[\underline{\mathbf{Z}}_{\mathrm{n}}^{-1}\right]_{1,1}$ is considered. The proof for the remaining $K-1$ diagonal elements of $\underline{\mathbf{Z}}_{\mathrm{n}}^{-1}$ is straightforward.

$\underline{\mathbf{Z}}_{\mathrm{n}}$, see (B.3), may be partitioned as

$$\underline{\mathbf{Z}}_{\mathrm{n}} = \begin{bmatrix} 1 & \underline{\mathbf{x}}_{\mathrm{n}}^{*\mathrm{T}} \\ \underline{\mathbf{x}}_{\mathrm{n}} & \underline{\mathbf{B}}_{\mathrm{n}} \end{bmatrix}, \tag{B.4}$$

where $\underline{\mathbf{x}}_{\mathrm{n}}$ denotes the first column of $\underline{\mathbf{Z}}_{\mathrm{n}}$ without its first element $[\underline{\mathbf{Z}}_{\mathrm{n}}]_{1,1}$, and $\underline{\mathbf{B}}_{\mathrm{n}}$ is a $(K-1)\times(K-1)$ hermitian matrix with ones on its diagonal. Then, according to the matrix inversion lemma [Mar87] for matrices partitioned as in (B.4), $\left[\underline{\mathbf{Z}}_{\mathrm{n}}^{-1}\right]_{1,1}$ is given by

$$\left[\underline{\mathbf{Z}}_{\mathrm{n}}^{-1}\right]_{1,1} = \frac{1}{1-\zeta} \tag{B.5}$$

with

$$\zeta = \underline{\mathbf{x}}_{\mathrm{n}}^{*\mathrm{T}} \underline{\mathbf{B}}_{\mathrm{n}}^{-1} \underline{\mathbf{x}}_{\mathrm{n}}, \tag{B.6}$$

see also (B.4). According to (4.28), $\underline{\mathbf{Z}}$, and consequently $\underline{\mathbf{Z}}_{\mathrm{n}}$, is a positive definite hermitian matrix, since $\underline{\mathbf{A}}$, see (4.14), is assumed to be a non–singular matrix [Gant91]. Then, the diagonal elements of $\underline{\mathbf{Z}}_{\mathrm{n}}^{-1}$ are greater than zero [Mar87]. Therefore,

$$\zeta < 1 \tag{B.7}$$

follows from (B.6). Further, $\underline{\mathbf{B}}_{\mathrm{n}}$, see (B.4), is a positive definite hermitian matrix. Then, the eigenvalue decomposition [Gant91]

$$\underline{\mathbf{B}}_{\mathrm{n}} = \underline{\mathbf{E}}_{\mathrm{n}}^{*\mathrm{T}} \mathbf{\Lambda}_{\mathrm{n}} \underline{\mathbf{E}}_{\mathrm{n}} \tag{B.8}$$

of $\underline{\mathbf{B}}_{\mathrm{n}}$ holds, where $\underline{\mathbf{E}}_{\mathrm{n}}$ denotes the K eigenvectors of $\underline{\mathbf{B}}_{\mathrm{n}}$ satisfying [Gant91]

$$\underline{\mathbf{E}}_{\mathrm{n}}^{-1} = \underline{\mathbf{E}}_{\mathrm{n}}^{*\mathrm{T}}, \tag{B.9}$$

and $\mathbf{\Lambda}_{\mathrm{n}}$ is a diagonal matrix with its diagonal elements λ_i, $i = 1 \ldots K-1$, representing the positive eigenvalues of $\underline{\mathbf{B}}_{\mathrm{n}}$. Then, if the transformation

$$\underline{\boldsymbol{\xi}}_{\mathrm{n}} = \underline{\mathbf{E}}_{\mathrm{n}} \underline{\mathbf{x}}_{\mathrm{n}} \tag{B.10}$$

is introduced, where $\underline{\mathbf{x}}_{\mathrm{n}}$ is defined (B.4),

$$\underline{\mathbf{x}}_{\mathrm{n}}^{*\mathrm{T}} \underline{\mathbf{B}}_{\mathrm{n}} \, \underline{\mathbf{x}}_{\mathrm{n}} = \sum_{i=1}^{K-1} \lambda_i \underline{\xi}_{\mathrm{n},i}^{*} \underline{\xi}_{\mathrm{n},i} \tag{B.11}$$

holds, see also (B.10). Then, by using (B.8), (B.10) and (B.11), (B.6) can be written as

$$\zeta = \sum_{i=1}^{K-1} \frac{1}{\lambda_i} \underline{\xi}^*_{\mathrm{n},i} \underline{\xi}_{\mathrm{n},i}, \tag{B.12}$$

which can be recognized as a positive definite hermitian form [Gant91], which guarantees that

$$\zeta > 0\,. \tag{B.13}$$

Therefore, by combining (B.5) with (B.7) and (B.13), the first of said steps is proven, i.e., a diagonal element $\left[\underline{\mathbf{Z}}_{\mathrm{n}}^{-1}\right]_{i,i}$, $i = 1 \ldots KN$, of $\underline{\mathbf{Z}}_{\mathrm{n}}^{-1}$, see (B.2), always takes greater values than the corresponding diagonal element $[\underline{\mathbf{Z}}_{\mathrm{n}}]_{i,i}$, $i = 1 \ldots KN$, of $\underline{\mathbf{Z}}_{\mathrm{n}}$.

Concerning the second of said steps, it is assumed that the diagonal elements of $\underline{\mathbf{Z}}_{\mathrm{n}}$, see (B.3), are multiplied by a constant factor l greater than zero. The resulting matrix is denoted by $\underline{\mathbf{Z}}_{\mathrm{n,l}}$. By adopting the same partition for $\underline{\mathbf{Z}}_{\mathrm{n,l}}$ as in (B.4), $\underline{\mathbf{Z}}_{\mathrm{n,l}}$ can be written as

$$\underline{\mathbf{Z}}_{\mathrm{n,l}} = \begin{bmatrix} l & \underline{\mathbf{x}}_{\mathrm{n}}^{*\mathrm{T}} \\ \underline{\mathbf{x}}_{\mathrm{n}} & \underline{\mathbf{B}}_{\mathrm{n}} + (l-1)\mathbf{I}^{(K-1)}, \end{bmatrix}, \tag{B.14}$$

where $\mathbf{I}^{(K-1)}$ denotes the $(K-1) \times (K-1)$ identity matrix. In the following, only the element $\left[\underline{\mathbf{Z}}_{\mathrm{n,l}}^{-1}\right]_{1,1}$ is considered. The proof for the remaining $K-1$ diagonal elements of $\underline{\mathbf{Z}}_{\mathrm{n-l}}^{-1}$ is straightforward.

By using the matrix inversion lemma, as it is done for $\underline{\mathbf{Z}}_{\mathrm{n}}$, see (B.5),

$$\left[\underline{\mathbf{Z}}_{\mathrm{n,l}}^{-1}\right]_{1,1} = \frac{1}{l - \zeta_{\mathrm{l}}} \tag{B.15}$$

holds, where

$$\zeta_{\mathrm{l}} = \underline{\mathbf{x}}_{\mathrm{n}}^{*\mathrm{T}} \left(\underline{\mathbf{B}}_{\mathrm{n}} + (l-1)\mathbf{I}^{(K-1)}\right)^{-1} \underline{\mathbf{x}}_{\mathrm{n}}, \tag{B.16}$$

see also (B.6). The eigenvalues of $\underline{\mathbf{B}}_{\mathrm{n}} + (l-1)\mathbf{I}^{(K-1)}$ are simply the eigenvalues of $\underline{\mathbf{B}}_{\mathrm{n}}$ augmented by $(l-1)$ [GvL90]. Therefore, by using (B.10) and (B.11), (B.16) can be written in the form

$$\zeta_{\mathrm{l}} = \sum_{i=1}^{K-1} \frac{1}{\lambda_i + l - 1} \underline{\xi}^*_{\mathrm{n},i} \underline{\xi}_{\mathrm{n},i}\,. \tag{B.17}$$

However, since l is greater than one,

$$\frac{1}{\lambda_i + l - 1} < \frac{1}{\lambda_i}, \quad i = 1 \ldots K-1, \tag{B.18}$$

is always valid, independently of the value of λ_i, $i = 1 \ldots K-1$. Therefore, by comparing (B.17) with (B.12), (B.18) guarantees that

$$\zeta > \zeta_{\mathrm{l}} \,. \tag{B.19}$$

Since (B.19) is valid, the relation

$$\frac{1}{1-\zeta} > \frac{1}{1-\zeta_{\mathrm{l}}} \geq \frac{1}{1-\zeta_{\mathrm{l}}+(l-1)} \tag{B.20}$$

holds as well, and according to (B.5) and (B.15),

$$\left[\underline{\mathbf{Z}}_{\mathrm{n}}^{-1}\right]_{1,1} > \left[\underline{\mathbf{Z}}_{\mathrm{n,l}}^{-1}\right]_{1,1} \tag{B.21}$$

is true, which proves the second of said steps.

Then, since

$$\left[\underline{\mathbf{Z}}^{-1}\right]_{i,i} = \frac{1}{\left[\underline{\mathbf{N}}_n\right]_{i,i}^2} \left[\underline{\mathbf{Z}}_{\mathrm{n}}^{-1}\right]_{i,i}, \tag{B.22}$$

$$\left[\underline{\mathbf{Z}}_{\mathrm{l}}^{-1}\right]_{i,i} = \frac{1}{\left[\underline{\mathbf{N}}_n\right]_{i,i}^2} \left[\underline{\mathbf{Z}}_{\mathrm{n,l}}^{-1}\right]_{i,i}, \tag{B.23}$$

$i = 1 \ldots N$, are valid, according to (B.22) and (B.23)

$$\left[\underline{\mathbf{Z}}^{-1}\right]_{i,i} > \left[\underline{\mathbf{Z}}_{\mathrm{l}}^{-1}\right]_{i,i}, \quad i = 1 \ldots N, \tag{B.24}$$

holds, which proves the Theorem.

B.2 Upper and lower bounds for the SNR degradation of TD–CDMA receivers

In this section, a special issue concerning the SNR degradation of TD–CDMA receivers is considered. As already illustrated in Section 4.3.2.2, in TD–CDMA the intracell MAI is mitigated by applying the ZF–BLE to perform JD. The price to be paid for this benefit is an SNR degradation, which is analyzed in depth in Section 6.3. As shown in Section 6.3, the SNR degradation δ_i, $i = 1 \ldots KN$, depends on the information contained in the system matrix $\underline{\mathbf{A}}$, i.e., the selected CDMA code set and the channel impulse responses. In this section it is shown how upper and lower bounds for the SNR degradation in TD–CDMA can be determined in a rather straightforward manner. These bounds are given by the properties of the mobile radio channel and the selected CDMA codes. Depending on the selected CDMA code set, the actual SNR degradation lies somewhere between these bounds, and these bounds can serve as a guideline on CDMA code optimization.

For the analysis of this section, it is assumed that a single antenna is utilized at the

BS receiver. However, first an alternative representation of the system matrix $\underline{\mathbf{A}}$, see (4.4), is presented, which is more illustrating when deriving bounds for the SNR degradation in TD–CDMA.

With the CDMA code vectors $\underline{\mathbf{c}}^{(k)}$, $k = 1 \ldots K$, of dimension Q, the $(NQ+W-1)\times KNW$ matrix

$$\underline{\mathbf{C}}_{\mathrm{b}} = \left[\underline{\mathbf{C}}_{\mathrm{b}}^{(1)} \ldots \underline{\mathbf{C}}_{\mathrm{b}}^{(K)}\right], \tag{B.25}$$

$$\left[\underline{\mathbf{C}}_{\mathrm{b}}^{(k)}\right]_{i,j} = \begin{cases} \underline{c}_q^{(k)}, & i = (n-1)Q + w + q - 1, \\ & j = (n-1)W + w, \\ & n = 1 \ldots N,\ w = 1 \ldots W,\ q = 1 \ldots Q \\ 0 & \text{otherwise,} \end{cases}$$

can be formed. With the channel impulse response vectors $\underline{\mathbf{h}}^{(k)}$, $k = 1 \ldots K$, the $KNW \times KN$ matrix

$$\underline{\mathbf{H}}_{\mathrm{b}} = \mathrm{blockdiag}\left[\underline{\mathbf{H}}_{\mathrm{b}}^{(1)} \ldots \underline{\mathbf{H}}_{\mathrm{b}}^{(K)}\right] \tag{B.26}$$

$$\underline{\mathbf{H}}_{\mathrm{b}}^{(k)} = \mathbf{I}^{(N)} \otimes \underline{\mathbf{h}}^{(k)}$$

can be established, where $\otimes$ denotes the Kronecker product. Then, the system matrix $\underline{\mathbf{A}}$ can be expressed as

$$\underline{\mathbf{A}} = \underline{\mathbf{C}}_{\mathrm{b}}\ \underline{\mathbf{H}}_{\mathrm{b}}, \tag{B.27}$$

which is an equivalent representation to (4.4).

In the first special case, it is assumed that the CDMA codes $\underline{\mathbf{c}}^{(k)}$, $k = 1 \ldots K$, have the worst possible auto– and cross–correlation properties. This means that the matrix $\underline{\mathbf{C}}_{\mathrm{b}}^{*\mathrm{T}}\underline{\mathbf{C}}_{\mathrm{b}}$ consists of K^2 identical $NW \times NW$ blocks $\underline{\mathbf{Q}}$. The matrix $\underline{\mathbf{Q}}$ consists of N^2 $W \times W$ blocks $\underline{\mathbf{Q}}^{(n_1,n_2)}$, $n_1, n_2 = 1 \ldots N$, and it is block Toeplitz and hermitian. Therefore, it can be fully described by its blocks $\underline{\mathbf{Q}}^{(1,n)}$, $n = 1 \ldots N$. The diagonal block $\underline{\mathbf{Q}}^{(1,1)}$, has elements

$$\left[\underline{\mathbf{Q}}^{(1,1)}\right]_{i,j} = \begin{cases} Q - \mid i - j \mid, & 1 \leq \mid i - j \mid + 1 \leq Q \\ 0 & \text{otherwise.} \end{cases} \tag{B.28}$$

The off-diagonal blocks $\underline{\mathbf{Q}}^{(1,n)}$, $n = 2 \ldots N$, are Toeplitz matrices with their first column being the vector

$$\underline{\boldsymbol{q}}_1 = \left[\mathbf{0}^{\mathrm{T}} \quad \underline{\mathbf{s}}^{\mathrm{T}}\underline{\mathbf{S}}^{\mathrm{T}}\right]^{\mathrm{T}}, \tag{B.29}$$

where $\mathbf{0}$ is the $(n-2)Q + 1$ zero vector,

$$\underline{\mathbf{s}} = [1 \ldots Q-1 \quad Q \quad Q-1 \ldots 1], \tag{B.30}$$

and $\underline{\mathbf{S}}$ is a selection matrix of the form

$$\underline{\mathbf{S}} = \left[\mathbf{I}^{(\rho)} \quad \mathbf{0}^{(\rho,2Q-1-\rho)}\right], \tag{B.31}$$

with

$$\rho = W - (n-2)\,Q - 1, \quad n = 1 \ldots N. \tag{B.32}$$

$\mathbf{I}^{(\rho)}$ in (B.31) denotes the $\rho \times \rho$ identity matrix and $\mathbf{0}^{(\rho,2Q-1-\rho)}$ the $\rho \times (2Q-1-\rho)$ zero matrix. Finally, the first row of $\underline{\mathbf{Q}}^{(1,n)}$, $n = 2 \ldots N$, is the $W \times W$ zero row vector. In this case, the matrix $\underline{\mathbf{A}}^{*\mathrm{T}}\underline{\mathbf{A}}$, see (B.27), consists of K^2 $N \times N$ blocks $\underline{\mathbf{Z}}^{(l,m)}$ of the form $\underline{\mathbf{H}}^{(l)*\mathrm{T}}\underline{\mathbf{Q}}\,\underline{\mathbf{H}}^{(m)}$, $l, m = 1 \ldots K$, where the elements of $\underline{\mathbf{Q}}$ are given in (B.28)–(B.32). This case represents an upper bound on the SNR degradation in TD–CDMA, since a CDMA code set $\underline{\mathbf{c}}^{(k)}$, $k = 1 \ldots K$, has always better auto– and cross–correlation properties than the ones described by the matrix $\underline{\mathbf{Q}}$ defined in (B.28)–(B.32).

The second special case involves the situation, where the used CDMA codes $\underline{\mathbf{c}}^{(k)}$, $k = 1 \ldots K$, exhibit ideal auto– and cross–correlation properties. This means that the matrix $\underline{\mathbf{C}}_{\mathrm{b}}^{*\mathrm{T}}\underline{\mathbf{C}}_{\mathrm{b}}$, see (B.25), takes the form

$$\underline{\mathbf{C}}_{\mathrm{b}}^{*\mathrm{T}}\underline{\mathbf{C}} = Q \cdot \mathbf{I}^{(KNW)}. \tag{B.33}$$

In this case, the SNR degradation defined in (6.26) can be directly expressed as a function of the energy $\underline{\mathbf{h}}^{(k)*\mathrm{T}}\underline{\mathbf{h}}^{(k)}$ of the channel impulse response of each user k:

$$\delta_i = \mathrm{E}\left\{\underline{\mathbf{h}}^{(k)*\mathrm{T}}\underline{\mathbf{h}}^{(k)}\right\} \cdot \frac{1}{\underline{\mathbf{h}}^{(k)*\mathrm{T}}\underline{\mathbf{h}}^{(k)}}, \tag{B.34}$$

$$i = (k-1)N + n, \quad n = 1 \ldots N, \quad k = 1 \ldots K.$$

This case places a lower bound on the SNR degradations, since, in practice, a CDMA code set $\underline{\mathbf{c}}^{(k)}$, $k = 1 \ldots K$, can never have ideal correlation properties.

At this point, we define a random variable δ, which takes all the values of the SNR degradations δ_i, $i = 1 \ldots KN$, see (6.26). In Fig. B.1 the pdf $p(\delta)$ of δ is shown for the two special cases described above. These pdf's are considered as upper and lower bounds, respectively, for the SNR degradation, and, in practice, the actual SNR degradation lies somewhere between these bounds. In the simulations, the COST207 RA channel models [COS89] were used and 10^4 experiments were conducted. Moreover, there are K equal to four users active within the same frequency band and time slot, and the number of symbols N is chosen to be equal to four, see the analysis of Section 6.3.3. The remaining parameters of TD–CDMA used in the simulations can be taken from Table 5.1. In Fig. B.2 the cdf $F(\delta)$ of δ is plotted for the upper and lower bound of the SNR degradation. Finally, in Figs. B.3 and B.4 the respective pdf and cdf are shown when the COST207 BU channel model [COS89] is used.

A direct comparison of the solid curves, i.e., lower bound, with the dashed curves, i.e., upper bound, of Figs. B.1 and B.2 shows the more favourable transmission conditions when the used CDMA codes $\underline{\mathbf{c}}^{(k)}$, $k = 1 \ldots K$, would have ideal correlation properties. The same can be also observed from Figs. B.3 and B.4, where the COST207 BU channel model is used. Now, comparing Figs. B.1 and B.2 with Figs. B.3 and B.4, a more favourable system behaviour is observed when the COST207 BU channel model is used, see Figs. B.3 and B.4, compared to the COST207 RA channel model, see Figs. B.1 and B.2. This is especially true for the case where the codes have the worst possible auto– and cross–correlation properties. In practice, though, codes with ideal correlation properties cannot be found. Moreover, codes have always better correlation properties than the first special case considered in the paper, i.e., for the worst possible correlation properties. Therefore, depending on the properties of the employed CDMA codes $\underline{\mathbf{c}}^{(k)}$, $k = 1 \ldots K$, and the propagation environment, the SNR degradation has a pdf and a cdf somewhere between the upper and lower bounds set by the special cases investigated in this letter and illustrated by the simulation results of Figs. B.1–B.4. As already mentioned above, the results of Figs. B.1–B.4 can serve as a guideline on CDMA code optimization in TD–CDMA mobile radio systems.

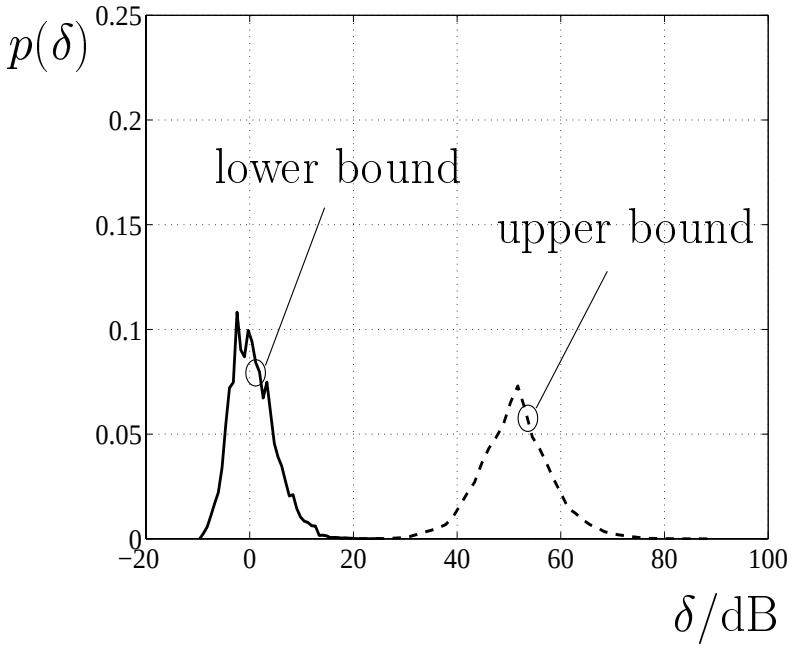

Figure B.1. pdf for the upper and lower bound of the SNR degradation; COST207 RA channel model; $K = 4$ users

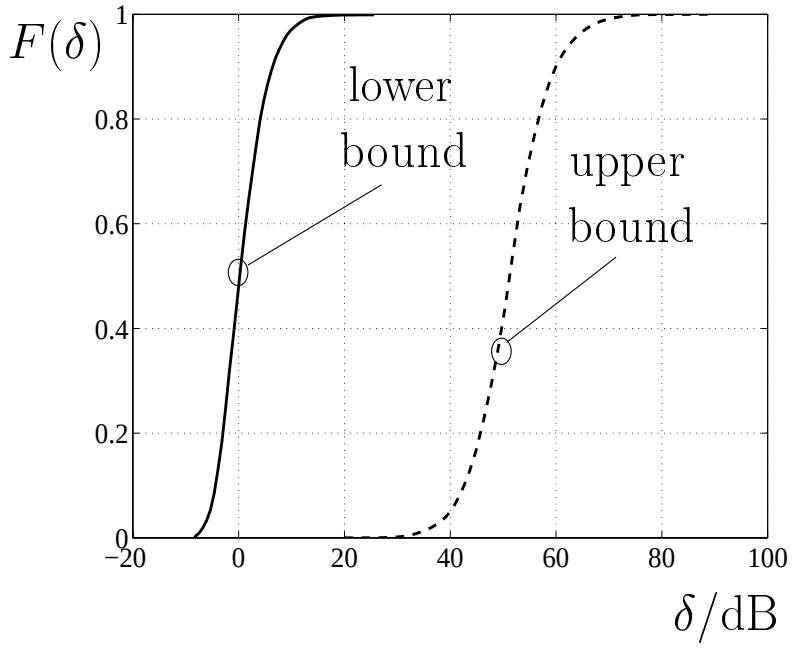

Figure B.2. cdf for the upper and lower bound of the SNR degradation; COST207 RA channel model; $K = 4$ users

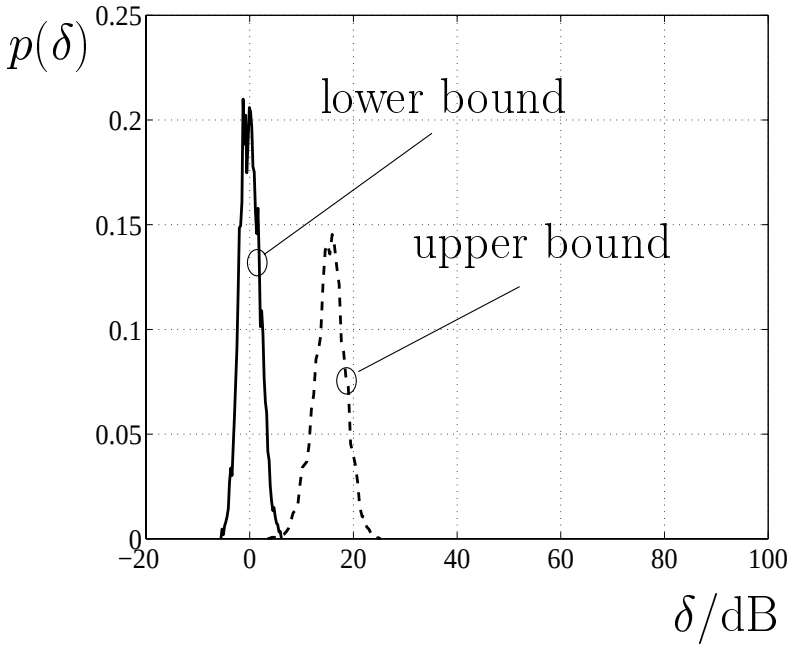

Figure B.3. pdf for the upper and lower bound of the SNR degradation; COST207 BU channel model; $K = 4$ users

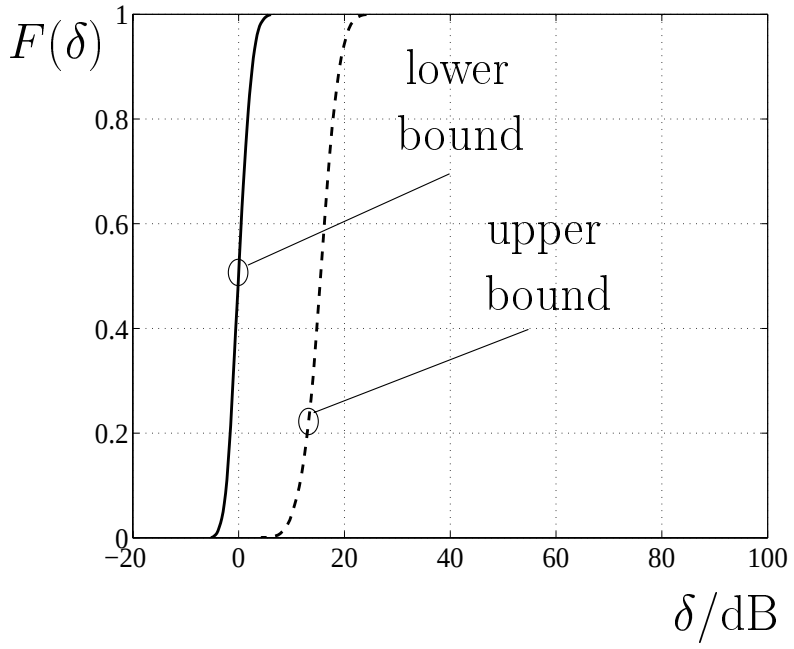

Figure B.4. cdf for the upper and lower bound of the SNR degradation; COST207 BU channel model; $K = 4$ users

Appendix C

Special issues concerning DOA estimation and the SNR degradation

C.1 Summary of 2D Unitary ESPRIT

The following summary of the 2D Unitary ESPRIT [Haa97a] algorithm is based on the covariance approach. The algorithm is used for efficient DOA estimation in the simulations of Chapters 5–8, in order to obtain estimates of the DOAs of each user.

1. Initialization: Form the matrix $\underline{\mathbf{X}} \in C^{M \times N}$ from the available measurements. M is the number of elements of the used 2D array configuration, and N is the number of snapshots.

2. Signal Subspace Estimation: Determine the real matrix

$$\mathrm{T_s}\left(\underline{\mathbf{X}}\right) = \underline{\mathbf{Q}}_{\mathrm{M}}^{*\mathrm{T}} \left[\underline{\mathbf{X}} \;\; \mathbf{\Pi}_{\mathrm{M}} \underline{\mathbf{X}}^{*} \mathbf{\Pi}_{\mathrm{N}}\right] \underline{\mathbf{Q}}_{2\mathrm{N}}, \tag{C.1}$$

   where

$$\underline{\mathbf{Q}}_{2n} = \frac{1}{\sqrt{2}} \begin{bmatrix} \mathbf{I}_n & \mathrm{j}\mathbf{I}_n \\ \mathbf{\Pi}_n & -\mathrm{j}\mathbf{\Pi}_n \end{bmatrix} \tag{C.2}$$

   and

$$\underline{\mathbf{Q}}_{2n+1} = \frac{1}{\sqrt{2}} \begin{bmatrix} \mathbf{I}_n & \mathbf{0} & \mathrm{j}\mathbf{I}_n \\ \mathbf{0}^{\mathrm{T}} & \sqrt{2} & \mathbf{0}^{\mathrm{T}} \\ \mathbf{\Pi}_n & \mathbf{0} & -\mathrm{j}\mathbf{\Pi}_n \end{bmatrix} \tag{C.3}$$

   are left Π–real matrices of even and odd order, respectively, and $\mathbf{\Pi}_{\mathrm{q}}$ is the $q \times q$ exchange matrix with ones on its antidiagonal and zeros elsewhere. Then, form the covariance matrix

$$\underline{\mathbf{R}}_{\mathrm{s}} = \mathrm{T_s}\left(\underline{\mathbf{X}}\right) \;\; \mathrm{T_s}\left(\underline{\mathbf{X}}\right)^{*\mathrm{T}} \tag{C.4}$$

   and compute the eigenvalue decomposition of $\underline{\mathbf{R}}_{\mathrm{s}}$. The d dominant left singular vectors will be called $\mathbf{E}_{\mathrm{s}}$. Estimate the number of sources d, if d is not known a priori [XRK94].

3. Invariance equation: Solve the overdetermined system of equations

$$\boldsymbol{K}_1 \mathbf{E}_{\mathrm{s}} \mathbf{\Upsilon} = \boldsymbol{K}_2 \mathbf{E}_{\mathrm{s}} \tag{C.5}$$

by means of least squares (LS), total least squares (TLS) or structured least squares (SLS) [Haa97b]. The matrices $\boldsymbol{K}_1$ and $\boldsymbol{K}_2$ are defined as follows:

$$\boldsymbol{K}_1 = \underline{\mathbf{Q}}_{\mathrm{m}}^{*\mathrm{T}} \left(\boldsymbol{J}_1 + \boldsymbol{J}_2\right) \underline{\mathbf{Q}}_{\mathrm{M}} = 2 \cdot \mathrm{Re}\left\{\underline{\mathbf{Q}}_{\mathrm{m}}^{*\mathrm{T}} \boldsymbol{J}_2 \underline{\mathbf{Q}}_{\mathrm{M}}\right\}, \tag{C.6}$$

$$\boldsymbol{K}_2 = \mathrm{j}\underline{\mathbf{Q}}_{\mathrm{m}}^{*\mathrm{T}} \left(\boldsymbol{J}_1 - \boldsymbol{J}_2\right) \underline{\mathbf{Q}}_{\mathrm{M}} = 2 \cdot \mathrm{Im}\left\{\underline{\mathbf{Q}}_{\mathrm{m}}^{*\mathrm{T}} \boldsymbol{J}_2 \underline{\mathbf{Q}}_{\mathrm{M}}\right\}. \tag{C.7}$$

The matrices $\boldsymbol{J}_1$ and $\boldsymbol{J}_2$ are the $m \times M$ selection matrices presented in [Haa97a] with $m < M$.

4. Eigenvalue Decomposition: Compute the eigendecomposition of the resulting solution

$$\boldsymbol{\Upsilon} = \boldsymbol{T}\boldsymbol{\Omega}\boldsymbol{T}^{-1}, \tag{C.8}$$

where

$$\boldsymbol{\Omega} = \mathrm{diag}\left\{\omega_k\right\}_{k=1}^{d}. \tag{C.9}$$

5. Reliability test: If all eigenvalues ω_k are real, the estimates will be reliable. Otherwise, start again with more or more reliable measurements.

6. DOA estimation: Determine the estimates of the DOAs from

$$\mu_k = 2 \arctan\left(\omega_k\right), \; k = 1 \ldots d, \tag{C.10}$$

according to (A.9).

C.2 Covariance matrix of the intercell MAI valid for DOA estimation in the large cell channel type

In this section the covariance matrix $\underline{\mathbf{R}}_{\mathrm{N}}^{(k)}$ of the matrix $\underline{\mathbf{N}}^{(k)}$, $k = 1 \ldots K$, see (5.45), is derived. This covariance matrix can be used in the 2–D Unitary ESPRIT algorithm, see Appendix A.1, and can lead to considerable performance improvement. Here, the large cell channel type is considered. The covariance matrix of the intercell MAI used in the DOA estimation process for the small cell channel type is computed in Appendix A.3.

By definition, the covariance matrix $\underline{\mathbf{R}}_{\mathrm{N}}^{(k)}$ of $\underline{\mathbf{N}}^{(k)}$, see (5.47), is given by [Wha71]

$$\underline{\mathbf{R}}_{\mathrm{N}}^{(k)} = \mathrm{E}\left\{\underline{\mathbf{N}}^{(k)} \underline{\mathbf{N}}^{(k)*\mathrm{T}}\right\} \tag{C.11}$$

$$= \mathrm{E}\left\{\underline{\mathbf{N}}_{\mathrm{m}}^{\mathrm{T}} \underline{\mathbf{M}}_{\mathrm{m}}^{\mathrm{T}} \left(\mathbf{u}^{(k)} \otimes \mathbf{I}^{(W)}\right) \left(\mathbf{u}^{(k)\mathrm{T}} \otimes \mathbf{I}^{(W)}\right) \underline{\mathbf{M}}_{\mathrm{m}}^{*} \underline{\mathbf{N}}_{\mathrm{m}}^{*}\right\}, \tag{C.12}$$

where $\underline{\mathbf{M}}_{\mathrm{m}}$ is defined in (5.37). If we define the selection matrix

$$\underline{\mathbf{P}}^{(k)} = \underline{\mathbf{M}}_{\mathrm{m}}^{\mathrm{T}} \left(\mathbf{u}^{(k)} \otimes \mathbf{I}^{(W)}\right) \left(\mathbf{u}^{(k)\mathrm{T}} \otimes \mathbf{I}^{(W)}\right) \underline{\mathbf{M}}_{\mathrm{m}}^{*}, \tag{C.13}$$

(C.12) can be written in the following form:

$$\underline{\mathbf{R}}_{\mathrm{N}}^{(k)} = \mathrm{E}\left\{\underline{\mathbf{N}}_{\mathrm{m}}^{\mathrm{T}} \underline{\mathbf{P}}^{(k)} \underline{\mathbf{N}}_{\mathrm{m}}^{*}\right\}. \tag{C.14}$$

The matrix $\underline{\mathbf{P}}^{(k)}$, $k = 1 \ldots K$, of (C.13) is a hermitian matrix which depends exclusively on the midamble training sequences, see (5.4), with its structure being determined by the selection matrices $\left(\mathbf{u}^{(k)} \otimes \mathbf{I}^{(W)}\right)$, $k = 1 \ldots K$, see (C.13). Therefore, it can be computed off–line and thus not contribute to the receiver realtime processing. Noting that $\underline{\mathbf{N}}_{\mathrm{m}}$ consists of K_{a} column vectors $\underline{\mathbf{n}}_{\mathrm{m}}^{(k_{\mathrm{a}})}$, $k_{\mathrm{a}} = 1 \ldots K_{\mathrm{a}}$, see (5.28) and (5.26), the covariance matrix of (C.14) can be expressed as [Wha71]:

$$\begin{aligned}
\underline{\mathbf{R}}_{\mathrm{N}}^{(k)} &= \mathrm{E}\left\{ \begin{bmatrix} \underline{\mathbf{n}}_{\mathrm{m}}^{(1)\mathrm{T}} \underline{\mathbf{P}}^{(k)} \underline{\mathbf{n}}_{\mathrm{m}}^{(1)*} & \cdots & \underline{\mathbf{n}}_{\mathrm{m}}^{(1)\mathrm{T}} \underline{\mathbf{P}}^{(k)} \underline{\mathbf{n}}_{\mathrm{m}}^{(K_{\mathrm{a}})*} \\ \vdots & & \vdots \\ \underline{\mathbf{n}}_{\mathrm{m}}^{(K_{\mathrm{a}})\mathrm{T}} \underline{\mathbf{P}}^{(k)} \underline{\mathbf{n}}_{\mathrm{m}}^{(1)*} & \cdots & \underline{\mathbf{n}}_{\mathrm{m}}^{(K_{\mathrm{a}})\mathrm{T}} \underline{\mathbf{P}}^{(k)} \underline{\mathbf{n}}_{\mathrm{m}}^{(K_{\mathrm{a}})*} \end{bmatrix} \right\} \\
&= \begin{bmatrix} \mathrm{tr}\left\{\underline{\mathbf{P}}^{(k)\mathrm{T}} \underline{\mathbf{R}}_{\mathrm{m}}^{(1,1)}\right\} & \cdots & \mathrm{tr}\left\{\underline{\mathbf{P}}^{(k)\mathrm{T}} \underline{\mathbf{R}}_{\mathrm{m}}^{(1,K_{\mathrm{a}})}\right\} \\ \vdots & & \vdots \\ \mathrm{tr}\left\{\underline{\mathbf{P}}^{(k)\mathrm{T}} \underline{\mathbf{R}}_{\mathrm{m}}^{(K_{\mathrm{a}},1)}\right\} & \cdots & \mathrm{tr}\left\{\underline{\mathbf{P}}^{(k)\mathrm{T}} \underline{\mathbf{R}}_{\mathrm{m}}^{(K_{\mathrm{a}},K_{\mathrm{a}})}\right\} \end{bmatrix}
\end{aligned} \tag{C.15}$$

where the fact that [Wha71]

$$\begin{aligned}
\mathrm{E}\left\{\underline{\mathbf{n}}_{\mathrm{m}}^{(l)\mathrm{T}} \underline{\mathbf{P}}\, \underline{\mathbf{n}}_{\mathrm{m}}^{(m)*}\right\} &= \mathrm{tr}\left\{\underline{\mathbf{P}}^{(k)\mathrm{T}} \underline{\mathbf{R}}_{\mathrm{m}}^{(l,m)}\right\}, \\
l, m &= 1 \ldots K_{\mathrm{a}},
\end{aligned} \tag{C.16}$$

has been used. The operator $\mathrm{tr}\{\cdot\}$ denotes the trace of a matrix [Wha71]. By using (C.17) and (7.21), (C.15) can be written as follows:

$$\begin{aligned}
\underline{\mathbf{R}}_{\mathrm{N}}^{(k)} &= \begin{bmatrix} \mathrm{tr}\left\{\underline{\mathbf{P}}^{(k)\mathrm{T}} \underline{r}_{1,1} \underline{\mathbf{R}}_{\mathrm{m,t}}\right\} & \cdots & \mathrm{tr}\left\{\underline{\mathbf{P}}^{(k)\mathrm{T}} \underline{r}_{1,K_{\mathrm{a}}} \underline{\mathbf{R}}_{\mathrm{m,t}}\right\} \\ \vdots & & \vdots \\ \mathrm{tr}\left\{\underline{\mathbf{P}}^{(k)\mathrm{T}} \underline{r}_{K_{\mathrm{a}},1} \underline{\mathbf{R}}_{\mathrm{m,t}}\right\} & \cdots & \mathrm{tr}\left\{\underline{\mathbf{P}}^{(k)\mathrm{T}} \underline{r}_{K_{\mathrm{a}},K_{\mathrm{a}}} \underline{\mathbf{R}}_{\mathrm{m,t}}\right\} \end{bmatrix} \\
&= \mathrm{tr}\left\{\underline{\mathbf{P}}^{(k)\mathrm{T}} \underline{\mathbf{R}}_{\mathrm{m,t}}\right\} \otimes \begin{bmatrix} \underline{r}_{1,1} & \cdots & \underline{r}_{1,K_{\mathrm{a}}} \\ \vdots & & \vdots \\ \underline{r}_{K_{\mathrm{a}},1} & \cdots & \underline{r}_{K_{\mathrm{a}},K_{\mathrm{a}}} \end{bmatrix} \\
&= \mathrm{tr}\left\{\underline{\mathbf{P}}^{(k)\mathrm{T}} \underline{\mathbf{R}}_{\mathrm{m,t}}\right\} \otimes \underline{\mathbf{R}}_{\mathrm{s}},
\end{aligned} \tag{C.17}$$

where $\underline{\mathbf{R}}_{\mathrm{s}}$ forms the spatial part of the total covariance defined in (7.22), see also [PHFB97]. Thus, using the user specific matrix $\underline{\mathbf{X}}^{(k)}$, $k = 1 \ldots K$, see (5.45), and the user specific covariance matrix $\underline{\mathbf{R}}_{\mathrm{N}}^{(k)}$, $k = 1 \ \ldots \ K$, see (C.17), as inputs to the 2D Unitary ESPRIT algorithm, DOA estimates and subsequently estimates of the user specific steering matrices $\underline{\mathbf{A}}^{(k)}$, $k = 1 \ldots K$, see (5.21), can be determined. These estimated steering matrices are used for the enhanced joint channel estimation described in Section 5.3.3.3.

C.3 Covariance matrix of the intercell MAI valid for DOA estimation in the small cell channel type

In this section the covariance matrix $\underline{\mathbf{R}}_{\mathrm{N}}^{(k,w)}$ of $\underline{\mathbf{n}}_w^{(k)}$, $w = 1 \ldots W$, $k = 1 \ldots K$, see (5.64), is derived for the small cell channel type. This covariance matrix can be used in the 2–D Unitary ESPRIT algorithm, see Appendix A.1, and can lead to considerable performance improvement as in the case of the small cell channel type.

By definition, the covariance matrix $\underline{\mathbf{R}}_{\mathrm{N}}^{(k,w)}$ is given by [Wha71]

$$\underline{\mathbf{R}}_{\mathrm{N}}^{(k,w)} = \mathrm{E}\left\{\underline{\mathbf{N}}_{\mathrm{m}}^{\mathrm{T}}\underline{\mathbf{M}}_{\mathrm{m}}^{\mathrm{T}}\left(\mathbf{u}^{(k)} \otimes \mathbf{I}^{(W)}\right)\mathbf{u}^{(w)}\mathbf{u}^{(w)\mathrm{T}}\left(\mathbf{u}^{(k)\mathrm{T}} \otimes \mathbf{I}^{(W)}\right)\underline{\mathbf{M}}_{\mathrm{m}}^{*}\underline{\mathbf{N}}_{\mathrm{m}}^{*}\right\}. \tag{C.18}$$

If we define the selection matrix

$$\underline{\mathbf{P}}^{(k,w)} = \underline{\mathbf{M}}_{\mathrm{m}}^{\mathrm{T}}\left(\mathbf{u}^{(k)} \otimes \mathbf{I}^{(W)}\right)\mathbf{u}^{(w)}\mathbf{u}^{(w)\mathrm{T}}\left(\mathbf{u}^{(k)\mathrm{T}} \otimes \mathbf{I}^{(W)}\right)\underline{\mathbf{M}}_{\mathrm{m}}^{*}, \tag{C.19}$$

(C.18) can be written in the following form:

$$\underline{\mathbf{R}}_{\mathrm{N}}^{(k,w)} = \mathrm{E}\left\{\underline{\mathbf{N}}_{\mathrm{m}}^{\mathrm{T}}\underline{\mathbf{P}}^{(k,w)}\underline{\mathbf{N}}_{\mathrm{m}}^{*}\right\}. \tag{C.20}$$

The matrix $\underline{\mathbf{P}}^{(k,w)}$, $w = 1 \ldots W$, $k = 1 \ldots K$ of (C.19) is a hermitian matrix which depends exclusively on the midamble training sequences, see (5.4), with its structure being determined by the selection matrices $\left(\mathbf{u}^{(k)} \otimes \mathbf{I}^{(W)}\right)$, $k = 1 \ldots K$, and the selection vector $\mathbf{u}^{(w)}$, $w = 1 \ldots W$, see (C.19). Therefore, it can be computed off–line and thus not contribute to the receiver realtime processing, as in the case of the large cell channel type, see (C.13). If the relation (C.17) is used, then (C.20) can be brought to the form:

$$\begin{aligned}
\underline{\mathbf{R}}_{\mathrm{N}}^{(k,w)} &= \begin{bmatrix} \mathrm{tr}\left\{\underline{\mathbf{P}}^{(k,w)\mathrm{T}}\underline{r}_{1,1}\underline{\mathbf{R}}_{\mathrm{m,t}}\right\} & \cdots & \mathrm{tr}\left\{\underline{\mathbf{P}}^{(k,w)\mathrm{T}}\underline{r}_{1,K_{\mathrm{a}}}\underline{\mathbf{R}}_{\mathrm{m,t}}\right\} \\ \vdots & & \vdots \\ \mathrm{tr}\left\{\underline{\mathbf{P}}^{(k,w)\mathrm{T}}\underline{r}_{K_{\mathrm{a}},1}\underline{\mathbf{R}}_{\mathrm{m,t}}\right\} & \cdots & \mathrm{tr}\left\{\underline{\mathbf{P}}^{(k,w)\mathrm{T}}\underline{r}_{K_{\mathrm{a}},K_{\mathrm{a}}}\underline{\mathbf{R}}_{\mathrm{m,t}}\right\} \end{bmatrix} \\
&= \mathrm{tr}\left\{\underline{\mathbf{P}}^{(k,w)\mathrm{T}}\underline{\mathbf{R}}_{\mathrm{m,t}}\right\} \otimes \begin{bmatrix} \underline{r}_{1,1} & \cdots & \underline{r}_{1,K_{\mathrm{a}}} \\ \vdots & & \vdots \\ \underline{r}_{K_{\mathrm{a}},1} & \cdots & \underline{r}_{K_{\mathrm{a}},K_{\mathrm{a}}} \end{bmatrix} \\
&= \mathrm{tr}\left\{\underline{\mathbf{P}}^{(k,w)\mathrm{T}}\underline{\mathbf{R}}_{\mathrm{m,t}}\right\} \otimes \underline{\mathbf{R}}_{\mathrm{s}},
\end{aligned} \tag{C.21}$$

see also (C.17). Thus, using the covariance matrix $\underline{\mathbf{h}}_w^{(k)}$, $k = 1 \ldots K$, $w = 1 \ldots W$, see (5.62), and the covariance matrix $\underline{\mathbf{R}}_{\mathrm{N}}^{(k,w)}$, $k = 1 \ \ldots \ K$, $w = 1 \ldots W$, see (C.21), as inputs to the 2–D Unitary ESPRIT algorithm, DOA estimates and subsequently estimates of the user specific steering matrices $\underline{\mathbf{A}}^{(k,w)}$, $k = 1 \ldots K$, see (5.49), can be determined. These estimated steering matrices are used for the enhanced joint channel estimation described in Section 5.4.2.3.

References

[3GPP] 3GPP, "About the Third Generation Partnership Project (3GPP)", published in the Internet under the URL http://www.3gpp.org/ABOUT_3GPP/3gpp.htm, 1999.

[Ada66] R.T. Adams, "An adaptive antenna system for maximizing signal–to–noise ratio", Proc. WESCON Conference, pp. 1–4, Session 24, 1966.

[Aka66] H. Akaike, "A new look at the statistical model identification", IEEE Transactions on Automation Control, vol. 19, pp. 716–723, 1966.

[AMVW91] S. Anderson, M. Millnert, M. Viberg, and B. Wahlberg, "An adaptive array for mobile communication systems", IEEE Transactions on Vehicular Technology, vol. 40, pp. 230–236, 1991.

[And63] T.W. Anderson, "Asymptotic theory for principal components analysis", Ann. Math. Statist., vol. 34, pp. 122–148, 1963.

[App76] S.P. Applebaum, "Adaptive arrays", IEEE Transactions on Antennas and Propagation, vol. 24, pp. 585–598, 1976.

[AS84] E. Ashok and P.M. Schultheiss, "The effect of auxiliary source on the performance of the randomly perturbed array", Proc. IEEE International Conference on Acoustics, Speech, Signal Processing (ICASSP'95), vol. 40.1, San Diego, 1984.

[ASS98] F. Adachi, M. Sawahashi, and H. Suda, "Wideband DS–CDMA for next–generation mobile communications systems", IEEE Communications Magazine, vol. 163, pp. 56–69, 1998.

[Bai94] P.W. Baier, "CDMA or TDMA? CDMA for GSM?", Proc. IEEE 5$^{\text{th}}$ International Symposium on Personal, Indoor and Mobile Radio Communications (PIMRC '94), pp. 1280–1284, The Hague, 1994.

[Bai96a] P.W. Baier, "Evaluating the multiple access options", Proc. IBC Conference Next Generation Mobile — Evolution or Revolution?, London, 1996.

[Bai96b] P.W. Baier, "A critical review of CDMA", Proc. IEEE 46$^{\text{th}}$ Vehicular Technology Conference (VTC '96), pp. 6–10, Atlanta, 1996.

[Bai96c] P.W. Baier, "CDMA, a challenging approach to multiple access", Proc. King's College Workshop on Wireless Multi-Media Communications, pp. 72–76, London, 1996.

[BARY95] J. Bach Andersen, T.S. Rappaport, and S. Yoshida, "Propagation measurements and models for wireless communications channels", IEEE Communications Magazine, vol. 33, pp. 42–49, 1995.

[BBA95] T. Bull, M. Barrett, and R. Arnott, "Technology in smart antennas for universal advanced mobile infrastructure (TSUNAMI R2108) – Overview", Proc. RACE Mobile Telecommunications Summit, pp. 88–97, Cascais, 1995.

[BBJ95] J.J. Blanz, P.W. Baier, and P. Jung, "A flexibly configurable statistical channel model for mobile radio systems with directional diversity", in [Wal95], pp. 93–100.

[BBNS94] P.W. Baier, J.J. Blanz, M.M. Naßhan, and A. Steil, "Realistic simulations of a CDMA mobile radio system using joint detection and coherent receiver antenna diversity", Proc. IEE Colloquium on Spread Spectrum Techniques for Radio Communication Systems, pp. 1/1 – 1/5, London, 1994.

[BBP97] P.W. Baier, J.J. Blanz, and A. Papathanassiou, "Joint detection CDMA and antenna diversity techniques", Proc. IEE Colloquium on CDMA Techniques and Applications for third Generation Mobile Systems, pp. 1/1 – 1/7, London, 1997.

[BBS97] P.W. Baier, J.J. Blanz, and R.M. Schmalenberger, "Fundamentals of smart antennas for mobile radio applications", IEEE 8$^{\text{th}}$ International Symposium on Personal, Indoor and Mobile Radio Communications (PIMRC'97), Helsinki, 1997, in [GL97], pp. 345–376.

[BEM98a] S. Bahrenburg, C. Euscher, J. Mayer, J. Schlee, and T. Weber, "Fading simulator measurements with a TD–CDMA hardware demonstrator", Proc. IEEE 5$^{\text{th}}$ International Conference on Telecommunications (ICT'98), vol. III, pp. 12–16, Chalkidiki, 1998.

[BEM98b] S. Bahrenburg, C. Euscher, J. Mayer, J. Schlee, and T. Weber, "Outdoor measurements with a TD (Time Division)–CDMA hardware demonstrator for UMTS", Proc. IEEE 4$^{\text{th}}$ International Symposium on Spread Spectrum Techniques & Applications (ISSSTA'96), pp. 625–629, Sun City, 1998.

[BH94] J.E. Berg and Holmquist, "An FFT multiple half–screen diffraction model", Proc. IEEE 44$^{\text{th}}$ Vehicular Technology Conference (VTC'94), pp. 195–199, Stockholm, 1994.

[BHP97] J.J. Blanz, M. Haardt, A. Papathanassiou, I. Furió, and P. Jung, "Combined direction of arrival and channel estimation for time-slotted CDMA", Proc. IEEE 4$^{\text{th}}$ International Conference on Telecommunications (ICT'97), pp. 395–400, Melbourne, 1997.

[BJK96] P.W. Baier, P. Jung, and A. Klein, "Taking the challenge of multiple access for third generation cellular mobile radio systems — a European view", IEEE Communications Magazine, vol. 34, pp. 82–89, 1996.

[BJN94] J.J. Blanz, P. Jung, and M.M. Naßhan, "Realistic simulations of CDMA mobile radio systems using joint detection and coherent receiver antenna diversity", Proc. IEEE 3$^{\text{rd}}$ International Symposium on Spread Spectrum Techniques and Applications (ISSSTA '94), pp. 193–197, Oulu, 1994.

[BJSB96] J.J. Blanz, P. Jung, A.J. Steil, and P.W. Baier, "Coherent receiver antenna diversity with directional antennas", Proc. IEEE 3$^{\text{rd}}$ International Conference on Telecommunications (ICT'96), pp. 410–417, Istanbul, 1996.

[BK91] A. Baier and W. Koch, "Potential of CDMA for 3$^{\text{rd}}$ generation mobile radio systems", Proc. Mobile Radio Conference, Nice, 1991.

[BK95] P.W. Baier and A. Klein, "Flexible hybrid multiple access schemes for 3rd generation mobile radio systems", E. Del Re, editor, Proc. Joint COST 227/231 Workshop on Mobile and Personal Communications, Florence, 1995, in [DR95], pp. 31–43.

[BKM96] J.J. Blanz, A. Klein, and W. Mohr, "Measurement-based parameter adaptation of wideband spatial mobile radio channel models", Proc. IEEE 4$^{\text{th}}$ International Symposium on Spread Spectrum Techniques & Applications (ISSSTA'96), pp. 91–97, Mainz, 1996.

[BKNS94a] J.J. Blanz, A. Klein, M.M. Naßhan, and A. Steil, "Capacity of a cellular CDMA mobile radio system applying joint detection", COST 231 TD (94) 2, Lisbon, 1994.

[BKNS94b] J.J. Blanz, A. Klein, M.M. Naßhan, and A. Steil, "Performance of a cellular hybrid C/TDMA mobile radio system applying joint detection and coherent receiver antenna diversity", IEEE Journal on Selected Areas in Communications, vol. 12, pp. 568–579, 1994.

[BKNS94c] J.J. Blanz, A. Klein, M.M. Naßhan, and A.J. Steil, "Cellular spectrum efficiency of a joint detection CDMA mobile radio system", Proc. International Zurich Seminar on Digital Communications, Zurich, 1994, in [Gün94], pp. 184–195.

[Bla98] J.J. Blanz, Empfangsantennendiversität in CDMA–Mobilfunksystemen mit gemeinsamer Detektion der Teilnehmersignale, Fortschrittberichte VDI, series 10, no. 535, VDI–Verlag, Düsseldorf, 1998.

[BM86] Y. Bresler and A. Markovski, "On the number of signals resolvable by a uniform linear array", IEEE Transactions on Acoustics, Speech, and Signal Processing, vol. 34, pp. 1361–1375, 1986.

[BN93] P.W. Baier and M.M. Naßhan, "Recent results concerning the benefit of joint detection in CDMA systems", Proc. IEE Colloquium on Spread Spectrum Techniques for Radio Communication Systems, pp. 5/1 – 5/4, London, 1993.

[BPH00] J.J. Blanz, A. Papathanassiou, M. Haardt, I. Furió, and P.W. Baier, "Smart antennas for combined DOA and joint channel estimation in time–slotted CDMA mobile radio systems with joint detection", IEEE Transactions on Vehicular Technology, vol. 49, pp. 293–306, 2000.

[BPW99] P.W. Baier, A. Papathanassiou, and M. Weckerle, "Recent results on the benefits of adaptive antennas for TD–CDMA mobile radio systems", Proc. IEEE 6$^{\text{th}}$ International Conference on Telecommunications (ICT'99), pp. 399–404, Cheju, 1999.

[BSPJ97] J.J. Blanz, R.M. Schmalenberger, A. Papathanassiou, and P. Jung, "Smart antenna concepts for time-slotted CDMA", Proc. IEEE 47$^{\text{th}}$ Vehicular Technology Conference (VTC'97), pp. 11–15, Phoenix, 1997.

[BSS84] P. Balaban, K.S. Shanmugan, and B.W. Stuck, "Computer–aided modeling, analysis, and design of communication systems: Introduction and issue overview", IEEE Journal on Selected Areas in Communications, vol. 2, pp. 1–8, 1984.

[Bur67] J.P. Burg, "Maximum entropy spectral analysis", 37th Ann. Meeting, Society Exploration Geohysics, Oklahoma City, 1967.

[Cal88] G. Calhoun, Digital cellular radio, Artech House, Inc., Norwood, 1988.

[Cap69] J. Capon, "High–resolution frequency–wave number spectrum analysis", Proc. of the IEEE, vol. 57, pp. 1408–1418, 1969.

[COS89] COST 207, Digital land mobile radio communications, Office for Official Publications of the European Communities, Luxembourg, 1989.

[CZO87] H. Cox, R.M. Zeskind, and M.M. Owen, "Robust adaptive beamforming", IEEE Transactions on Acoustics, Speech, and Signal Processing, vol. 35, pp. 1365–1376, 1987.

[CZO88] H. Cox, R.M. Zeskind, and M.M. Owen, "Effects of amplitude and phase errors on linear predictive array processors", IEEE Transactions on Acoustics, Speech, and Signal Processing, vol. 36, pp. 10–19, 1988.

[DLDMV96] L. De Lathauwer, B. De Moor, and J Vandewalle, "Independent component analysis based on higher–order statistics only", Proc. IEEE SP Workshop on Statistical. Signal Array Processing, pp. 356–359, Corfu, 1996.

[DLR77] A.P. Dempster, N.M. Laird, and D.B. Rubin, "Maximum likelihood from incomplete data via the EM algorithm", Journal Royal Statist. Soc, Ser. B, vol. 39, pp. 477–489, 1977.

[DM80] C.N. Dorny and B.S. Meaghr, "Cohering of an experimental nonrigid array by self–survey", IEEE Transactions on Antennas and Propagation, vol. 28, pp. 902–904, 1980.

[DR95] E. Del Re, editor, Mobile and personal communications, Elsevier, Amsterdam, 1995.

[Edr94] M. Edrich, Einsatz computergestützter Methoden im nachrichtentechnischen Systementwurf, gezeigt an Beispielen aus der Spread–Spectrum–Technik, Fortschrittberichte VDI, series 10, no. 276, VDI–Verlag, Düsseldorf, 1994.

[Egg94] P.C.F. Eggers, "TSUNAMI: Spatial radio spreading as seen by directive antennas", COST 231 TD (94) 119, Darmstadt, 1994.

[Egg95] P.C.F. Eggers, "Angular dispersive mobile radio environments sensed by highly directive base station antennas", Proc. IEEE 6th International Symposium on Personal, Indoor and Mobile Radio Communications (PIMRC '95), pp. 522–526, Toronto, 1995.

[EHV97] J. Eberspächer, C. Hartmann, and H.J. Vögel, Spektrale Effizienz / Spektrale Kapazität, Internal report within the DFG project "Systeme mit intelligenten Antennen (SDMA)", June 1997.

[EJS81] J.E. Evans, J.R. Johnson, and D.F. Sun, "High resolution angular spectrum estimation techniques for terrain scattering analysis and angle of arrival estimation", Proc. ASSP Workshop on Spectral Estimation, pp. 134–139, Hamilton, Ontario, 1981.

[ETO93] P.C.F. Eggers, J. Toftgard, and A.M. Opera, "Antenna systems for base station diversity in urban small and micro cells", IEEE Journal on Selected Areas in Communications, vol. 11, pp. 1046–1056, 1993.

[ETSI88] ETSI/TC GSM Recommendations, Series 01–12, 1988.

[Ett76] W. van Etten, "Maximum likelihood receiver for multiple channel transmission systems", Transactions on Communications, vol. 24, pp. 276–283, 1976.

[Far97] C. Farsakh, Raummultiplex mit intelligenten Antennen in zellularen Mobilfunksystemen, PhD Dissertation, Technical University of Munich, 1997.

[FBB95] J. Fuhl, E. Bonek, P. Balducci, P. Nowak, and H. Garn, "Internal antenna arrangements for personal communication systems", Proc. European Personal and Mobile Communications Conference (EPMCC'95), pp. 62–67, Bologna, 1995.

[FBKM93] T. Felhauer, P.W. Baier, W. König, and W. Mohr, "Optimized wideband system for unbiased mobile radio channel sounding with periodic spread spectrum signals", IEICE Transactions on Communications, vol. E76–B, pp. 1016–1029, 1993.

[FDHT96] B.H. Fleury, D. Dahlhaus, R. Heddergott, and M. Tschudin, "Wideband angle of arrival estimation using the SAGE algorithm", Proc. IEEE 4$^{\text{th}}$ International Symposium on Spread Spectrum Techniques & Applications (ISSSTA '96), pp. 79–85, Mainz, 1996.

[FHNP95] C. Farsakh, M. Haardt, J.A. Nossek, and K. Pensel, "Adaptive antenna arrays in mobile radio systems", in [Wal95], pp. 101–108.

[FL96] B.H. Fleury and P.E. Leuthold, "Radiowave propagation in mobile communications: An overview of European research", IEEE Communications Magazine, vol. 34, pp. 70–81, 1996.

[FN94a] C. Farsakh and J.A. Nossek, "Application of SDMA to mobile radio", Proc. IEEE 4$^{\text{th}}$ International Symposium on Personal, Indoor and Mobile Radio Communications (PIMRC'94), pp. 736–739, The Hague, 1994.

[FN96a] C. Farsakh and J.A. Nossek, "On the spatial separation potential of a uniform linear array", Proc. IEEE 46$^{\text{th}}$ Vehicular Technology Conference (VTC '96), pp. 1477–1480, Atlanta, 1996.

[FN96b] C. Farsakh and J.A. Nossek, "A real time downlink channel allocation scheme for an SDMA mobile radio system", Proc. IEEE 7$^{\text{th}}$ International Symposium on Personal, Indoor and Mobile Radio Communications (PIMRC'96), pp. 1216–1220, Taipei, 1996.

[FN97a] C. Farsakh and J.A. Nossek, "Adaptive antenna arrays in mobile radio systems", Proc. IEEE 47$^{\text{th}}$ Vehicular Technology Conference (VTC'97), pp. 2168–2172, Phoenix, 1997.

[FN97b] C. Farsakh and J.A. Nossek, "Maximizing the capacity of an SDMA mobile radio system", Proc. IEEE 4$^{\text{th}}$ International Conference on Telecommunications (ICT'97), pp. 813–818, Melbourne, 1997.

[For72] G.D. Forney, " Maximum–likelihood sequence estimation of digital sequences in the presence of intersymbol interference", IEEE Transactions on Information Theory, vol. 18, pp. 363–378, 1972.

[FTH99] B.H. Fleury, M. Tschudin, R. Heddergott, D. Dahlhaus, and K.I. Pedersen, "Channel parameter estimation in mobile radio environments using the SAGE algorithm", IEEE Journal on Selected Areas in Communications, vol. 17, pp. 434–450, 1999.

[Fuh97] J. Fuhl, Smart antennas for second and third generation mobile communications systems, PhD Dissertation, Technical University of Vienna, 1997.

[FW88] M. Feder and E. Weinstein, "Parameter estimation of superimposed signals using the EM algorithm", IEEE Transactions on Acoustics, Speech, and Signal Processing, vol. 36, pp. 477–489, 1988.

[Gab76] W.F. Gabriel, "Adaptive arrays – An introduction", Proc. IEEE, vol. 64, pp. 239–272, 1976.

[Gant91] F.R. Gantmacher, The theory of matrices, vol. 1, Chelsea Publishing Company, New York, 1991.

[Gia99] G.B. Giannakis, editor, "Highlights of signal processing for communications", IEEE Signal Processing Magazine, pp. 14–48, March 1999.

[GL97] S.G. Glisic and P.A. Leppänen, editors, Wireless communications, Dordrecht, Kluwer, 1997.

[GM89] G.B. Giannakis and J.M. Mendel, "Identification of nonminimum phase systems using higher order statistics", IEEE Transactions on Acoustics, Speech, and Signal Processing, vol. 37, pp. 360–367, 1989.

[God97a] L.C. Godara, "Applications of antenna arrays to mobile communications, Part I: Performance improvement, feasibility, and system considerations", Proc. of the IEEE, vol. 85, pp. 1031–1060, 1997.

[God97b] L.C. Godara, "Applications of antenna arrays to mobile communications, Part II: Beam–forming and direction–of–arrival considerations", Proc. of the IEEE, vol. 85, pp. 1195–1245, 1997.

[Gol69] G.H. Golub, "Matrix decompositions and statistical calculations", in [MN69], pp. 365–397, 1969.

[GR94] M. Goldburg and R.H. Roy, "The impacts of SDMA on PCS system design", Proc. IEEE International Conference on Universal Personal Communications (ICUPC'94), pp. 242–246, San Diego, 1994.

[Gra81] A. Graham, Kronecker products and matrix calculus with applications, Ellis Horwood, Chichester, 1981.

[GT95] N. Gerlich and M. Tangemann, "Towards a channel allocation scheme for SDMA–based mobile communication systems", in [Wal95], pp. 109–116.

[GTB98] P.M. Grant, J.S. Thompson, and Mulgrew B., "Antenna arrays for cellular CDMA systems", Proc. IEEE 5th International Symposium on Spread Spectrum Techniques & Applications (ISSSTA'96), pp. 404–410, Sun City, 1998.

[Gün94] C.C. Günther, editor, Lecture Notes in Computer Science, vol. 783, Zurich, Springer–Verlag, 1994.

[GVGZ92] S.A. Grandhi, R. Vijayan, D.J. Goodman, and J. Zander, "Centralized power control in cellular radio systems", IEEE Transactions on Vehicular Technology, vol. 42, pp. 466–468, 1992.

[GvL90] G.H. Golub and C.F. van Loan, editors, Matrix computations, The Johns Hopkin University Press, 1990.

[Haa97a] M. Haardt, Efficient one– two– and multidimensional array signal processing, Forschungsberichte, Shaker Verlag, Aachen, 1997.

[Haa97b] M. Haardt, "Structured least squares to improve the performance of ESPRIT–type algorithms", IEEE Transactions on Signal Processing, vol. 45, pp. 792–799, 1997.

[Har97] C. Hartmann, "Dynamic channel allocation in cellular communication systems with SDMA", Proc. 2nd European Personal Mobile Communications Conference (EPMCC'97), Bonn, 1997.

[Hat80] M. Hata, "Empirical formula for propagation loss in land mobile radio services", IEEE Transactions on Vehicular Technology, vol. 29, pp. 317–325, 1980.

[Hay91] S. Haykin, Adaptive filter theory, Prentice–Hall, Inc., Englewood Cliffs, New Jersey, 2nd edition, 1991.

[Hess93] G.C. Hess, Land–mobile radio system engineering , Artech House, Boston, 1993.

[HN95] M. Haardt and J.A. Nossek, "Unitary ESPRIT: How to obtain increased estimation accuracy with a reduced computational burden", IEEE Transactions on Signal Processing, vol. 43, pp. 1232–1242, 1995.

[Höh90] P. Höher, Kohärenter Empfang trelliscodierter PSK–Signale auf frequenzselektiven Mobilfunkkanälen — Entzerrung, Decodierung und Kanalparameterschätzung, Fortschrittberichte VDI, series 10, no. 147, VDI–Verlag, Düsseldorf, 1990.

[Höh92] P. Höher, "A statistical discrete–time model for the WSSUS multipath channel", IEEE Transactions on Vehicular Technology, vol. 35, pp. 461–468, 1992.

[HR90] J. Huber and A. Rüppel, "Zuverlässigkeitsschätzung für die Ausgangssymbole von Trellis–Decodern", IEEE International Journal of Electronics and Communications, vol. 44, pp. 8–21, Jan. 1990.

[HS99] C. Hartmann and R. Steffen, "Dynamische Kanalvergabe in SDMA–Systemen mit unregelmäßigem Zell–Layout", Proc. ITG Diskussionssitzung Systeme mit intelligenten Antennen, Stuttgart, 1999.

[Hsu82] F.M. Hsu, "Square root Kalman filtering for high–speed data received over fading dispersive HF channels", IEEE Transactions on Information Theory, vol. 28, pp. 753–763, 1982.

[HV99] C. Hartmann and H.J. Vögel, "Teletraffic analysis of SDMA systems with inhomogeneous MS location, distribution and mobility", Wireless Personal Communications, vol. 11/1, pp. 45–62, 1999.

[HZMN95] M. Haardt, M.D. Zoltowski, C.P. Mathews, and J.A. Nossek, "2D unitary ESPRIT for efficient 2D parameter estimation", Proc. IEEE International Conference on Acoustics, Speech, Signal Processing (ICASSP'95), pp. 2096–2099, Detroit, 1995.

[IK96] N. Ishi and R. Kohno, "Spatially and temporally joint transmitter–receiver using an adaptive array antenna", IEICE Transactions on Communications, vol. E79–B, pp. 361–367, 1996.

[ITU97] Special Issue, "IMT–2000: Standards efforts of the ITU", IEEE Personal Communications Magazine, August 1997.

[Jak74] W. Jakes, Microwave mobile communications, John Wiley & Sons, New York, 1974.

[JBS92] M.C. Jeruchim, P. Balaban, and K.S. Shanmugan, Simulation of communication systems, Plenum Press, New York, 1992.

[KA97] D. Koulakiotis and A.H. Aghvami, "Evaluation of a DS/CDMA multi–user receiver employing a hybrid form of interference cancellation in Rayleigh fading channels", IEEE Communications Letters, vol. 2, pp. 61–63, 1997.

[KA98] D. Koulakiotis and A.H. Aghvami, "Hybrid interference cancellation, a multiuser detection scheme for W–DS/CDMA systems", Proc. IEEE 5th International Conference on Telecommunications (ICT'98), pp. 318–322, Chalkidiki, 1998.

[Kay93] S.M. Kay, Fundamentals of statistical signal processing: Estimation theory, Prentice Hall, New Jersey, 1993.

[KB92a] A. Klein and P.W. Baier, "Optimum unbiased data estimation in mobile radio systems applying CDMA", COST 231 TD (92) 16, Vienna, 1992.

[KB92b] A. Klein and P.W. Baier, "Simultaneous cancellation of cross interference and ISI in CDMA mobile radio communications", Proc. IEEE 3rd International Symposium on Personal, Indoor and Mobile Radio Communications (PIMRC '92), pp. 118–122, Boston, 1992.

[KB93] A. Klein and P.W. Baier, "Linear unbiased data estimation in mobile radio systems applying CDMA", IEEE Journal on Selected Areas in Communications, vol. 11, pp. 1058–1066, 1993.

[KBJ95] A. Klein, J.J. Blanz, P. Jung, M.M. Naßhan, A. Steil, B. Steiner, and P. W. Baier, "Summarizing review of a JD–CDMA third generation mobile radio system concept developed within COST 231 – Part 2", COST 231 TD (95) 18, Berne, 1995.

[KCW93a] T. Kürner, D. Cichon, and W. Wiesbeck, "Concepts and results for 3D digital terrain–based wave propagation models: An overview", IEEE Transactions on Communications, vol. 41, pp. 1002–1012, 1993.

[KCW93b] T. Kürner, D.J. Cichon, and W. Wiesbeck, "Concepts and results for 3D digital terrain based wave propagation models — an overview", IEEE Journal on Selected Areas in Communications, vol. 11, pp. 1002–1012, 1993.

[KIH82a] R. Kohno, H. Imai, and M. Hatori, "Cancellation techniques of co–channel interference in asynchronous spread spectrum multiple access systems", IECE Technical report, CS82–38, pp. 29–35, 1982.

[KIH82b] R. Kohno, H. Imai, and M. Hatori, "Cancellation techniques of co–channel interference in asynchronous spread spectrum multiple access", IECE Technical Report, vol. CS82-38, pp. 29–35, 1982.

[KIH83] R. Kohno, H. Imai, and M. Hatori, "Cancellation techniques of co–channel interference in asynchronous spread spectrum multiple access systems", Transactions of the IECE Japan, vol. J66–A, pp. 416–423, 1983.

[KKB93] A. Klein, K. Kaleh, and P.W. Baier, "Zero forcing and minimum mean square error equalization for multi–user detection in code division multiple access", IEEE Transactions on Vehicular Technology, vol. 35, pp. 461–468, 1993.

[KKB94] A. Klein, G.K. Kaleh, and P.W. Baier, "Equalizers for multi–user detection in code division multiple access mobile radio systems", Proc. IEEE 44$^{\text{th}}$ Vehicular Technology Conference (VTC '94), pp. 762–766, Stockholm, 1994.

[Kle96] A. Klein, Multi–user detection of CDMA–signals — algorithms and their application to cellular mobile radio, Fortschrittberichte VDI, series 10, no. 423, VDI–Verlag, Düsseldorf, 1996.

[Klein75] L. Kleinrock, Queueing systems, Volume I: Theory , John Wiley & Sons, New York, 1975.

[KLF86] S.Y. Kung, C.K. Lo, and R. Foka, "A Toeplitz approximation approach to coherent source direction finding", Proc. IEEE International Conference on Acoustics, Speech, Signal Processing (ICASSP'86), pp. 193–196, Tokyo, 1986.

[KM96] A. Klein and W. Mohr, "A statistical wideband mobile radio channel model including the directions-of-arrival", Proc. IEEE 4$^{\text{th}}$ International Symposium on Spread Spectrum Techniques & Applications (ISSSTA'96), pp. 102–106, Mainz, 1996.

[KMT96] A. Klein, W. Mohr, R. Thomas, P. Weber, and B. Wirth, "Direction-of-arrival of partial waves in wideband mobile radio channels for intelligent antenna concepts", Proc. IEEE 46$^{\text{th}}$ Vehicular Technology Conference (VTC '96), pp. 849–853, Atlanta, 1996.

[Koh94] R. Kohno, "Spatial and temporal filtering for co–channel interference in CDMA", Proc. IEEE 3rd International Symposium on Spread Spectrum Techniques & Applications (ISSSTA'94), pp. 51–60, Oulu, 1994.

[KP85] S.A. Kassam and H.V. Poor, "Robust techniques for signal processing: A survey", Proc. of the IEEE, vol. 73, pp. 433–481, 1985.

[KPK94] B.H. Khalaj, A. Paulraj, and T. Kailath, "2D RAKE receivers for CDMA cellular systems", Proc. GLOBECOM'94, pp. 400–404, San Francisco, CA, 1994.

[KS95] J. Kennedy and M.C. Sullivan, "Direction finding and smart antennas using software radio architectures", IEEE Communications Magazine, vol. 33, pp. 62–68, 1995.

[KSS95] A. Klein, B. Steiner, and A. Steil, "Known and novel diversity approaches in a JD–CDMA system concept developed within COST 231", Proc. IEEE 6th International Symposium on Personal, Indoor and Mobile Radio Communications (PIMRC '95), pp. 512–516, Toronto, 1995.

[KT82] R. Kumaresan and D.W. Tufts, "Estimation of frequencies of multiple sinusoids: Making linear prediction perform like maximum likelihood", Proc. IEEE, vol. 70, pp. 975–989, 1982.

[KT83] R. Kumaresan and D.W. Tufts, "Estimating the angles of arrival of multiple plane waves", IEEE Transactions on Aerospace and Electronic Systems, vol. 19, pp. 134–139, 1983.

[KTT99] A. Kuchar, M. Taferner, M. Tangemann, C. Hoek, W. Rauscher, M. Strasser, G. Pospischil, and E. Bonek, "Real–time GSM smart antenna demonstrator", Proc. ITG Diskussionssitzung Systeme mit intelligenten Antennen, Stuttgart, 1999.

[KV96] H. Krim and M. Viberg, "Two decades of array signal processing research", IEEE Signal Processing Magazine, pp. 67–94, July 1996.

[Lee82] W.C.Y. Lee, Mobile communications engineering, McGraw–Hill, New York, 1982.

[Lee89] W.C.Y. Lee, Mobile cellular telecommunications systems, McGraw–Hill, New York, 1989.

[LH74] C.L. Lawson and R.J. Hanson, Solving least squares problems, Prentice–Hall, Inc., Englewood Cliffs, New Jersey, 1974.

[LK94] U. Liebenow and P. Kuhlmann, "Theoretical investigations and wideband measurements on wave propagation in hilly terrain", Proc. IEEE 44th Vehicular Technology Conference (VTC'94), pp. 1803–1806, Stockholm, 1994.

[Loe92] K. Loew, "Comparison of urban propagation models with CW measurements", Proc. IEEE 42nd Vehicular Technology Conference (VTC '92), pp. 936–942, Denver, 1992.

[LT83] M.G. Larimore and J.R. Treichler, "Convergence behaviour of the constant modulus algorithm", Proc. IEEE International Conference on Acoustics, Speech, Signal Processing (ICASSP'83), pp. 13–16, 1983.

[LWK92] M. Lebherz, W. Wiesbeck, and W. Krank, "A versatile wave propagation model for the VHF/UHF range considring three–dimensional terrain", IEEE Transactions on Communications, vol. 40, pp. 1121–1131, 1992.

[LZ97] H. Liu and M.D. Zoltowski, "Blind equalization in antenna array CDMA systems", IEEE Transactions on Signal Processing, vol. 45, pp. 161–172, 1997.

[Mar87] S.L. Marple, Jr., Digital Spectral Analysis with Applications, Prentice–Hall, Englewood Cliffs, New Jersey, 1987.

[May93] S. Mayrargue, "Spatial equalization of a radio–mobile channel without beamforming using the constant modulus algorithm (CMA)", Proc. IEEE International Conference on Acoustics, Speech, Signal Processing (ICASSP'93), vol. III, pp. 344–347, 1993.

[May99] J. Mayer, Signalisierungsprotokolle und Verkehrskapazität eines Mobilfunksystems der dritten Generation, PhD Dissertation, University of Kaiserslautern, 1999. ISBN Nr.: 3–925178–31–7.

[MDCM95] E. Moulines, P. Duhamel, J.F. Cardoso, and S. Mayrargue, "Subspace methods for the blind identification of multichannel FIR filters", IEEE Transactions on Signal Processing, vol. 43, pp. 516–525, 1995.

[MG96] U. Martin and M. Grigat, "A statistical simulation model for the directional mobile radio channel and its configuration", Proc. IEEE 4th International Symposium on Spread Spectrum Techniques & Applications (ISSSTA'96), pp. 86–90, Mainz, 1996.

[MJ96] A. Mansour and C. Jutten, "A direct solution for blind separation of sources", IEEE Transactions on Signal Processing, vol. 44, pp. 746–748, 1996.

[MM80] R.A. Monzingo and W.T. Miller, Introduction to adaptive arrays, Wiley & Sons, Inc. , New York, 1980.

[MN69] R.C. Milton and J.A. Nelder, editors, Statistical calculations, Academic Press, New York, 1969.

[MP92] M. Mouly and M.B. Pautet, editors, The GSM–system for mobile communications, 1992.

[MSW97a] J. Mayer, J. Schlee, and T Weber, "Protocol and signaling aspects of joint detection CDMA", Proc. IEEE 8th International Symposium on Personal, Indoor and Mobile Radio Communications (PIMRC '97), pp. 867–871, Helsinki, 1997.

[MSW97b] J. Mayer, J. Schlee, and T. Weber, "Realtime feasibility of joint detection CDMA", Proc. 2nd European Personal Mobile Communications Conference (EPMCC'97), pp. 245–252, Bonn, 1997.

[MSW98] J. Mayer, J. Schlee, and T. Weber, "Handoff protocols in JD–CDMA", Proc. IEEE 9th International Symposium on Personal, Indoor and Mobile Radio Communications (PIMRC '98), pp. 355–359, Boston, 1998.

[Naß95] M.M. Naßhan, Realitätsnahe Modellierung und Simulation nachrichtentechnischer Systeme, gezeigt am Beispiel eines CDMA–Mobilfunksystems, Fortschrittberichte VDI, series 10, no. 384, VDI–Verlag, Düsseldorf, 1995.

[Nit79] R. Nitzberg, "Effects of errors in adaptive weights", IEEE Transactions on Aerospace and Electronic Systems, vol. 12, pp. 369–373, 1979.

[NPK94] A.F. Naguib, A. Paulraj, and T. Kailath, "Capacity improvement with base–station antenna arrays in cellular CDMA", IEEE Transactions on Vehicular Technology, vol. 43, pp. 691–698, 1994.

[NTD98] E. Nikula, A. Toskala, E. Dahlman, L. Girard, and A. Klein, "FRAMES multiple access for UMTS and IMT–2000", IEEE Personal Communications, pp. 16–24, April 1998.

[Pap65] A. Papoulis, Probability, random variables and stochastic processes, McGraw–Hill, Auckland, 1965.

[Par92] J.D. Parsons, The mobile radio propagation channel, Pentech Press, London, 1992.

[PBHP98] A. Papathanassiou, J.J. Blanz, M. Haardt, and P.W. Baier, "Spatial channel assignment considerations in a joint detection CDMA mobile radio system employing smart antennas", Proc. IEEE 5th International Conference on Telecommunications (ICT'98), vol. II, pp. 318–322, Chalkidiki, 1998.

[Pen99] K. Pensel, Signalverarbeitung für Mobilfunksysteme mit intelligenten Antennen, PhD Dissertation, Technical University of Munich, 1999.

[Per94] V. Perez, editor, Final propagation model, No. R2020/TDE/PS/DS/P/040/al, RACE UMTS Code Division Testbed (CODIT), Amsterdam, 1994.

[PFB97a] A. Papathanassiou, I. Furió, J.J. Blanz, M. Haardt, and R. Schmalenberger, "Suboptimum combined direction of arrival and channel estimation for time–slotted CDMA with joint detection", COST259 TD (97) 025, Turin, 1997.

[PFB97b] A. Papathanassiou, I. Furió, and J.J. Blanz, "Link level performance in the uplink of a joint detection CDMA mobile radio system employing multi–antenna array configurations", COST259 TD (97) 051, Lisbon, 1997.

[PFBP99] A. Papathanassiou, I. Furió, J.J. Blanz, and P.W. Baier, "Smart antennas with two–dimensional array configurations for performance enhancement of a joint detection CDMA mobile radio system", Wireless Personal Communications, vol. 11/1, pp. 89–108, 1999.

[PFM94] K. Pedersen, B. Fleury, and P. Mogensen, "High resolution of electromagnetic waves in time–varying radio channels", Proc. IEEE 8th International Symposium on Personal, Indoor and Mobile Radio Communications (PIMRC'94), Helsinki, 1994.

[PGH95] J.E. Padgett, C.G. Günther, and T. Hattori, "Overview of wireless personal communications", IEEE Communications Magazine, vol. 33, pp. 28–41, 1995.

[PH94] P. Patel and J. Holztmann, "Analysis of a successive interference cancellation scheme in a DS–CDMA system", IEEE Journal on Selected Areas in Communications, vol. 12, pp. 796–807, 1994.

[PHFB97] A. Papathanassiou, M. Haardt, I. Furió, and J.J. Blanz, "Multi-user direction of arrival and channel estimation for time-slotted CDMA with joint detection", Proc. IEEE International Conference on Digital Signal Processing (DSP'97), pp. 375–378, Santorini, 1997.

[PHW99] A. Papathanassiou, C. Hartmann, and T. Weber, "Uplink spectrum efficiency and capacity of TD–CDMA with adaptive antennas", COST259 TD (99) 113, Leidschendam, 1999.

[PK89] S.U. Pillai and B.H. Kwon, "Forward/Backward spatial smoothing techniques for coherent signal identification", IEEE Transactions on Acoustics, Speech, and Signal Processing, vol. 37, pp. 8–15, 1989.

[PN97] K. Pensel and J.A. Nossek, "Uplink and downlink calibration of an antenna array in a mobile communication system", COST259 TD (97) 058, Lisbon, 1997.

[PN98] K. Pensel and J.A. Nossek, "Uplink and downlink calibration of smart antennas", Proc. IEEE 5^{th} International Conference on Telecommunications (ICT'98), vol. II, pp. 323–327, Chalkidiki, 1998.

[POB99] A. Papathanassiou, J. Oster, and P.W. Baier, "A novel simulation concept of reduced computational cost for TD–CDMA mobile radio systems with adaptive antennas", Proc. IEEE 50^{th} Vehicular Technology Conference (VTC'99 Fall), pp. 218–222, Amsterdam, 1999.

[Pro89] J.G. Proakis, Digital communications, McGraw–Hill, New York, 2^{nd} edition, 1989.

[PSWB98] A. Papathanassiou, R. Schmalenberger, M. Weckerle, and P.W. Baier, "User angular separation considerations on the uplink performance of a TD–CDMA mobile radio system", COST259 TD (98) 055, Bradford, 1998.

[PSWB99] A. Papathanassiou, R. Schmalenberger, M. Weckerle, and P.W. Baier, "Advances in channel estimation techniques in TD–CDMA mobile radio systems with smart antennas", Proc. International Workshop on Mobile Communications (IWMC'99), pp. 11–20, Chania, 1999.

[PW98] A. Papathanassiou and M. Weckerle, "A spatial channel assignment strategy for improving the performance of TD–CDMA mobile radio systems with smart antennas", Proc. ITG Diskussionssitzung Systeme mit intelligenten Antennen für UMTS und GSM, Karlsruhe, 1998.

[PW99] A. Papathanassiou and M. Weckerle, "Transmission quality enhancement by considering the spatial interference covariance matrix in a TD–CDMA mobile radio system with adaptive antennas", Proc. ITG Diskussionssitzung Systeme mit intelligenten Antennen, Stuttgart, 1999.

[PWBB98] A. Papathanassiou, M. Weckerle, J.J. Blanz, and P.W. Baier, "Influence of user spatial separation on the uplink performance of a TD–CDMA mobile radio system with smart antennas", Proc. IEEE 5$^{\text{th}}$ International Symposium on Spread Spectrum Techniques & Applications (ISSSTA'98), pp. 384–388, Sun City, 1998.

[Rap98] T.S. Rappaport, editor, Smart antennas: adaptive arrays, algorithms, and wireless position location, Published by the IEEE, 1998.

[Ris78] J. Rissanen, "Modeling by shortest data description", Automatica, vol. 14, pp. 465–471, 1978.

[RK89] R.H. Roy and T. Kailath, "ESPRIT — estimation of signal parameters via rotational invariance techniques", IEEE Transactions on Signal Processing, vol. 37, pp. 984–995, 1989.

[RRPR97] Z. Rong, T.S. Rappaport, P. Petrus, and J.H. Reed, "Simulation of multitarget adaptive algorithms for wireless CDMA systems", Proc. IEEE 47$^{\text{th}}$ Vehicular Technology Conference (VTC'97), pp. 1–5, Phoenix, 1997.

[RS87a] Y. Rockah and P.M. Schultheiss, "Array shape calibration using sources in unknown locations – part 1: Far field sources", IEEE Transactions on Acoustics, Speech, and Signal Processing, vol. 35, pp. 286–299, 1987.

[RS87b] Y. Rockah and P.M. Schultheiss, "Array shape calibration using sources in unknown locations – part 2: Near field sources and estimator implementation", IEEE Transactions on Acoustics, Speech, and Signal Processing, vol. 35, pp. 286–299, 1987.

[RTVW95] R. Rheinschmitt, M. Tangemann, J.O. Vallet, and V. Weyl, "Network aspects of the introduction of adaptive arrays in mobile communication systems", Proc. RACE Mobile Telecommunications Summit, pp. 367–371, Cascais, 1995.

[RZ96] J. Ramos and M.D. Zoltowski, "Reduced complexity 2D RAKE receiver for CDMA", Proc. IEEE SP Workshop on Statistical Signal Array Processing, pp. 502–505, Corfu, 1996.

[RZ97] J. Ramos and M.D. Zoltowski, "Blind space–time processor for CDMA to maximize the SNIR", Proc. IEEE SP for Advanced Wireless Communications (SPAWC'97), Paris, 1997.

[SB96] A.J. Steil and J.J. Blanz, "Spectral efficiency of JD-CDMA mobile radio systems applying coherent receiver antenna diversity with directional antennas", Proc. IEEE 4$^{\text{th}}$ International Symposium on Spread Spectrum Techniques & Applications (ISSSTA '96), pp. 313–319, Mainz, 1996.

[SB97a] R. Schmalenberger and J.J. Blanz, "Multi antenna C/I balancing in the downlink of digital cellular mobile radio systems", Proc. IEEE 47$^{\text{th}}$ Vehicular Technology Conference (VTC'97), pp. 607–611, Phoenix, 1997.

[SB97b] R.M. Schmalenberger and J.J. Blanz, "A comparison of two different beamforming algorithms for multi antenna C/I balancing", Proc. European Personal Mobile Communications Conference (EPMCC'97), pp. 483–490, Bonn, 1997.

[SBS66] M. Schwartz, W.R. Bennett, and S. Stein, Communication systems and techniques, McGraw–Hill, New York, 1966.

[Sch78] G. Schwartz, "Estimating the dimension of a model", Ann. Math. Statist., vol. 6, pp. 461–464, 1978.

[Sch79] R.O. Schmidt, "Multiple emitter location and signal parameter estimation", Proc. RADC Spectrum Estimation Workshop, pp. 243–258, Griffiths AFB, NY, 1979.

[Sch86] R.O. Schmidt, "Multiple emitter location and signal parameter estimation", IEEE Transactions on Antennas and Propagation, vol. AP–34, pp. 276–280, 1986.

[Schl99] J. Schlee, Ein Hardware–Demonstrator zur Konzeptverifikation eines JD–CDMA–Mobilfunksystems PhD Dissertation, University of Kaiserslautern, 1999. ISBN Nr.: 3–925178–30–9.

[Sie70] Telephone traffic theory, Tables and charts, Part I, Published by Siemens Aktiengesellschaft, Berlin–München, 1970.

[SIT64] "Special Issue on active and adaptive antennas", IEEE Transactions on Antennas and Propagation, vol. 12, March 1964.

[SIT76] "Special Issue on adaptive antennas", IEEE Transactions on Antennas and Propagation, vol. 24, September 1976.

[SK93] B. Steiner and A. Klein, "Kanal– und Datenschätzung in synchronen CDMA–Mobilfunksystemen mit Interferenzeleminierung ", Kleinheubacher Berichte, vol. 36, pp. 253–268, 1993.

[SOSL85] M.K. Simon, J.K. Omura, R.A. Scholtz, and B.K. Levitt, Spread spectrum communications, vol. 1–3, Computer Science Press, Rockville, 1985.

[SP97] R. Schmalenberger and A. Papathanassiou, "Zwei kompatible Kanalmodelle für Simulationen auf System– und Linklevel", Proc. ITG Diskussionssitzung Modellszenarien für Systeme mit intelligenten Antennen, Kaiserslautern, 1997.

[SP98a] R. Schmalenberger and A. Papathanassiou, "Downlink spectrum efficiency of a JD-CDMA mobile radio system with array transmit antennas", COST 259 TD (98) 094, Duisburg, 1998.

[SP98b] R. Schmalenberger and A. Papathanassiou, "Two compatible channel models for system and link level simulations of mobile radio systems", COST 259 TD (98) 036, Bern, 1998.

[SS90] P. Stoica and K.C. Sharman, "Maximum likelihood methods for direction of arrival estimation", IEEE Transactions on Acoustics, Speech, and Signal Processing, vol. 38, pp. 1132–1143, 1990.

[Ste76] B.D. Steinberg, Principles of apperture and array system design, John Wiley & Sons, New York, 1976.

[Ste95] B. Steiner, Ein Beitrag zur Mobilfunkkanalschätzung unter besonderer Berücksichtigung synchroner CDMA–Mobilfunksysteme mit Joint Detection, Fortschrittberichte VDI, series 10, no. 337, VDI–Verlag, Düsseldorf, 1995.

[Ste96] A. Steil, Spektrale Effizienz digitaler zellulare CDMA–Mobilfunksysteme mit gemeinsamer Detektion, Fortschrittberichte VDI, series 10, no. 437, VDI–Verlag, Düsseldorf, 1996.

[Ste97] A. Steil, "Statistics of the carrier–to–interference ratio in C/TDMA cellular mobile radio systems applying multi–user detection", Wireless Personal Communications, vol. 5, pp. 259–277, 1997.

[Tan94] M. Tangemann, "Introducing adaptive array antenna concepts in mobile communication systems", Proc. RACE Mobile Telecommunications Workshop, pp. 2/714–727, Amsterdam, 1994.

[TBM97] G. Tsoulos, M. Beach, and J. McGeehan, "Wireless personal communications for the 21st century: European technological advances in adaptive antennas", IEEE Communications Magazine, vol. 35, pp. 102–109, 1997.

[TGM96] J.S. Thompson, P.M. Grant, and B. Mulgrew, "Smart antenna arrays for CDMA systems", IEEE Communications Magazine, vol. 3, pp. 16–25, 1996.

[Tho80] T. Thorvaldsen, "Maximum entropy spectral analysis in antenna spatial filtering", IEEE Transactions on Antennas and Propagation, vol. 28, pp. 556–562, 1980.

[THT98] M. Tschudin, R. Heddergott, and P. Truffer, "Validation of a high resolution measurement technique for estimating the parameters of impinging waves in indoor environments", Proc. IEEE 9th International Symposium on Personal, Indoor and Mobile Radio Communications (PIMRC '98), pp. 1411–1416, Boston, 1998.

[TSA97] S. Tanaka, M. Sawahashi, and F. Adachi, "Pilot symbol–assisted decision directed coherent adaptive array diversity for DS–CDMA mobile radio reverse link", IEICE Transactions on Fundamentals, vol. E80–A, pp. 2445–2454, 1997.

[TVP96] S. Talwar, M. Viberg, and A. Paulraj, "Blind estimation of synchronous co–channel digital signals using an antenna array, Part I: Algorithms", IEEE Transactions on Signal Processing, vol. 44, pp. 1184–1197, 1996.

[TX97] M. Torlak and G. Xu, "Blind multiuser channel estimation in asynchronous CDMA systems", IEEE Transactions on Signal Processing, vol. 45, pp. 137–147, 1997.

[UHF90] WG 2 UHF Propagation, "Urban transmission loss models for mobile radio in the 900– and the 180–MHz bands", COST231 TD (90) 119, Rev. 2, 1990.

[Vee97] A.J. van der Veen, "Analytical method for blind binary separation", IEEE Transactions on Signal Processing, vol. 45, pp. 178–182, 1997.

[Ver86] S. Verdú, "Minimum probability of error for asynchronous Gaussian multiple–access channels", IEEE Transactions on Information Theory, vol. 32, pp. 85–96, 1986.

[Ver98] S. Verdú, Multiuser detection, Cambridge University Press, 1998.

[Vit95] A.J. Viterbi, Principles of spread spectrum communications, Addison–Wesley, 1995.

[VOD92] A.J. van der Veen, P.B. Ober, and E.F. Deprettere, "Azimuth and elevation computation in high resolution DOA estimation", IEEE Transactions on Signal Processing, vol. 40, pp. 1828–1832, 1992.

[VPP97] M.C. Vanderveen, C. Papadias, and A. Paulraj, "Joint angle and delay estimation (JADE) for multipath signals arriving at an antenna array", IEEE Communications Letters, vol. 1, pp. 12–14, 1997.

[VTP97] A.J. van der Veen, S. Talwar, and A. Paulraj, "A subspace approach to blind space–time signal processing for wireless communication systems", IEEE Transactions on Signal Processing, vol. 45, pp. 173–190, 1997.

[VVP97] A.J. van der Veen, M.C. Vanderveen, and A. Paulraj, "Joint angle and delay estimation using shift–invariance techniques", IEEE Signal Processing Letters, vol. 4, pp. 142–145, 1997.

[Wal95] B. Walke, editor, ITG-Fachbericht, Mobile Kommunikation, vol. 135, VDE-Verlag, Berlin, 1995.

[Wha71] A.D. Whalen, Detection of signals in noise, Academic Press, New York, 1971.

[WK85] M. Wax and T. Kailath, "Detection of signals by information theoretic criteria", IEEE Transactions on Acoustics, Speech, and Signal Processing, vol. 33, pp. 387–392, 1985.

[WMGG67] B. Widrow, P.E. Mantey, L.J. Griffiths, and B.B. Goode, "Adaptive antenna systems", Proc. IEEE, vol. 55, pp. 2143–2159, 1967.

[WP99a] M. Weckerle and A. Papathanassiou, "Verfahren zum Schätzen der räumlichen Kovarianzmatrix der Störung in einem TD–CDMA–System mit adaptiven Antennen", Proc. ITG Diskussionssitzung Systeme mit intelligenten Antennen, Stuttgart, 1999.

[WP99b] M. Weckerle and A. Papathanassiou, "A novel multi–antenna TD–CDMA receiver concept incorporating the estimation and utilization of spatial interference covariance matrices", COST259 TD (99) 059, Vienna, 1999.

[WPE98] M. Weckerle, A. Papathanassiou, and D. Emmer, "The benefits of intelligent antenna arrays in TD–CDMA — A study based on measured channel impulse responses", Proc. IEEE 9th International Symposium on Personal, Indoor and Mobile Radio Communications (PIMRC '98), pp. 962–966, Boston, 1998.

[WPH99] M. Weckerle, A. Papathanassiou, and M. Haardt, "Estimation and utilization of spatial interference covariance matrices in multi–antenna TD–CDMA systems", Proc. IEEE 10th International Symposium on Personal, Indoor and Mobile Radio Communications (PIMRC '99), pp. 1198–1202, Osaka, 1999.

[WPS99] M. Weckerle, A. Papathanassiou, and R. Schmalenberger, "Consideration of the spatial interference covariance matrix in multi–antenna TD–CDMA systems", COST259 TD (99) 018, Thessaloniki, 1999.

[WWR94] Q. Wu, K.M. Wong, and J.P. Reilly, "Maximum likelihood direction finding in unknown noise environments", IEEE Transactions on Signal Processing, vol. 42, pp. 980–983, 1994.

[XRK94] G. Xu, R.H. Roy, and T. Kailath, "Detection of number of sources via exploitation of centro–symmetry property", IEEE Transactions on Signal Processing, vol. 42, pp. 102–112, 1994.

[YU93] W.S. Youn and C.K. Un, "A linearly constrained beamforming robust to array imperfections", IEEE Transactions on Signal Processing, vol. 41, pp. 1425–1428, 1993.

[Zan92a] J. Zander, "Performance of optimum transmitter power control in cellular radio systems", IEEE Transactions on Vehicular Technology, vol. 41, pp. 57–62, 1992.

[Zan92b] J. Zander, "Distributed cochannel interference control in cellular radio systems", IEEE Transactions on Vehicular Technology, vol. 41, pp. 305–311, 1992.

[ZB86] O. Zinke and H. Brunswig, Lehrbuch der Hochfrequenztechnik, vol. 1–2, Springer–Verlag, Berlin, 3rd edition, 1986.

[ZHM96] M.D. Zoltowski, M. Haardt, and C.P. Mathews, "Closed–form 2–D angle estimation with rectangular arrays in element space or beamspace via unitary ESPRIT", IEEE Transactions on Signal Processing, vol. 44, pp. 316–328, 1996.

[ZS96] Z. Zvonar and M. Stojanovic, "Performance of antenna diversity multiuser receivers in CDMA channels with imperfect fading estimation", Wireless Personal Communications, vol. 3, pp. 91–110, 1996.

[ZW88] I. Ziskind and M. Wax, "Maximum likelihood localization of multiple sources by alternating projection", IEEE Transactions on Acoustics, Speech, and Signal Processing, vol. 36, pp. 1553–1560, 1988.

Mrs E. Bear and Messrs V. Bouziekos, A. Heyduck, I. Jalloh, A. Krzesinski, I. Maniatis, F. Mas Vives, E.A. May, and C. Schnorrenberger have prepared their Studienarbeit or Diplomarbeit under the guidance of the author and thus contributed to this thesis.

Tabellarischer Lebenslauf

Name:	Apostolos Papathanassiou
Adresse:	Hermann–Hesse–Straße 30 67663 Kaiserslautern
Geburtsdatum:	5. Mai 1971
Familienstand:	ledig
Staatsangehörigkeit:	griechisch
Schulausbildung:	September 1977 – Juni 1983 Grundschule in Athen September 1983 – Juni 1986 Gymnasium in Athen September 1986 – Juni 1989 Lyzeum in Athen
Schulabschluß:	Abitur
Hochschulaufnahmenprüfung:	Juni 1989
Studium:	Oktober 1989 – Oktober 1994 Studium der Elektrotechnik an der Technischen Universität Athen
Studienabschluß:	Diplom
Wehrdienst:	Januar 1995 – Juli 1996 in Griechenland
Berufstätigkeit:	Oktober 1996 – Januar 1997 wissenschaftliche Hilfskraft am Lehrstuhl für hochfrequente Signalübertragung und –verarbeitung der Universität Kaiserslautern seit Februar 1997 wissenschaftlicher Mitarbeiter am Lehrstuhl für hochfrequente Signalübertragung und –verarbeitung der Universität Kaiserslautern